

QuakeRecNankai

Paleo-tsunami and earthquake records of ruptures along the Nankai Trough, offshore South-Central Japan

Marc DE BATIST (UGent) – Vanessa HEYVAERT (RBINS-GSB) – Aurelia HUBERT-FERRARI (ULiège) - Osamu FUJIWARA (AIST-GSJ) – Yusuke YOKOYAMA (UTokyo) – Helmut BRÜCKNER (UCologne) – Evelien BOES (UGent) – Ed GARRETT (RBINS-GSB) – Philipp KEMPF (RBINS-GSB) – Laura LAMAIR (ULiège) – Atsunori NAKAMURA (AIST-GSJ) - Masanobu SHISHIKURA (AIST-GSJ) – Yosuke MIYAIRI (UTokyo) – Shinya Yamamoto (MFRI) – Stephen OBROCHTA (Uakita) – Svenja RIEDESEL (UCologne)

Axis 2: Geosystems, universe and climate



NETWORK PROJECT

QuakeRecNankai

Paleo-tsunami and earthquake records of ruptures along the Nankai Trough, offshore South-Central Japan

Contract - BR/121/A2

FINAL REPORT

PROMOTORS: Marc DE BATIST (UGent)
Vanessa HEYVAERT (RBINS-GSB)
Aurelia HUBERT-FERRARI (ULiège)

AUTHORS: Osamu FUJIWARA (AIST-GSJ)
Yusuke YOKOYAMA (UTokyo)
Helmut BRÜCKNER (UCologne)
Evelien BOES (UGent)
Ed GARRETT (RBINS-GSB)
Philipp KEMPF (RBINS-GSB)
Laura LAMAIR (ULiège)
Atsunori NAKAMURA (AIST-GSJ)
Masanobu SHISHIKURA (AIST-GSJ)
Yosuke MIYAIRI (UTokyo)
Shinya Yamamoto (MFRI)
Stephen OBROCHTA (Uakita)
Svenja RIEDESEL (UCologne)



Published in 2021 by the Belgian Science Policy Office
WTC III
Boulevard Simon Bolivar 30 bte 7
Simon Bolivarlaan 30 bus 7
B-1000 Brussels
Belgium
Tel: +32 (0)2 238 34 11
<http://www.belspo.be>
<http://www.belspo.be/brain-be>

Contact person: Martine Vanderstraeten
Tel: +32 (0)2 238 36 10

Neither the Belgian Science Policy Office nor any person acting on behalf of the Belgian Science Policy Office is responsible for the use which might be made of the following information. The authors are responsible for the content.

No part of this publication may be reproduced, stored in a retrieval system, or transmitted in any form or by any means, electronic, mechanical, photocopying, recording, or otherwise, without indicating the reference:

De Batist, M., Heyvaert, V., Hubert-Ferrari, A., Fujiwara, O., Yokoyama, Y., Brückner, H., Boes, E., Garrett, E., Kempf, P., Lamair, L., Nakamura, A., Shishikura, M., Miyairi, Y., Yamamoto, S., Obrochta, S. & Riedesel, S. ***Paleo-tsunami and earthquake records of ruptures along the Nankai Trough, offshore South-Central Japan (QuakeRecNankai)***. Final Report. Brussels: Belgian Science Policy Office 2021 – 142 p. (BRAIN-be - (Belgian Research Action through Interdisciplinary Networks)

TABLE OF CONTENTS

1. INTRODUCTION, STATE OF THE ART AND OBJECTIVES	10
2. TECTONIC CONTEXT	11
3. METHODOLOGY	13
3.1. Compilation and critical review of geological evidence of past earthquakes and tsunamis	13
3.1.1. Literature review	13
3.1.2. Recalibration of radiocarbon ages and age modelling	13
3.2. Field work	14
3.2.1. Geomorphological surveying, vibrocoring and gouge coring in coastal lowlands	15
3.2.1.1. Coastal lowlands around Lake Hamana	15
3.2.1.2. Sagara lowlands	19
3.2.2. Geophysical surveying on coastal and in-land lakes	20
3.2.2.1. Lake Hamana	20
3.2.2.2. Fuji Five Lakes	21
3.2.3. Gravity coring and piston coring in coastal and in-land lakes	22
3.2.3.1. Lake Hamana	22
3.2.3.2. Fuji Five Lakes	23
3.3. Laboratory analyses	24
3.3.1. Sedimentological, geochemical and paleo-ecological analyses	24
3.3.1.1. Whole-core analysis and core scanning	24
3.3.1.2. Sedimentological and geochemical analyses	25
3.3.1.3. Paleo-ecological analyses	26
3.3.2. Geochronology	26
3.3.2.1. Radionuclide dating	26
3.3.2.2. Radiocarbon dating	27
3.3.2.3. Tephrochronology	27
3.3.2.4. OSL-dating	27
4. SCIENTIFIC RESULTS AND RECOMMENDATIONS	29
4.1. Review of geological evidence of earthquakes and tsunamis along the Nankai-Suruga Trough	29
4.1.1. Available geological evidence of earthquakes and tsunamis	29
4.1.1.1. Rupture zones of historical earthquakes	30
4.1.1.2. Intervals between earthquakes	34
4.1.1.3. Maximum earthquake and tsunami size	35
4.1.1.4. Rupture modes, segmentation and supercycles	36

4.1.2. Current problems for assessing seismic hazard from the available geological evidence	37
4.1.2.1. <i>Alternative hypotheses</i>	37
4.1.2.2. <i>Chronological control</i>	38
4.1.2.3. <i>Research design</i>	39
4.1.2.4. <i>Paleoseismic thresholds</i>	40
4.2. A new 7,500-year-long record of extreme wave events from Lake Hamana	40
4.2.1. Results	40
4.2.1.1. <i>Bathymetry/Morphology</i>	41
4.2.1.2. <i>Seismic-stratigraphy</i>	42
4.2.1.3. <i>Stratigraphic sub-division of background sediments</i>	42
4.2.1.4. <i>Allochthonous deposits</i>	46
4.2.1.5. <i>Geochronology</i>	46
4.2.2. Discussion	48
4.2.2.1. <i>Extreme wave event deposits (EWEs)</i>	48
4.2.2.2. <i>Historical and prehistorical events</i>	49
4.2.3. Conclusion	53
4.3. Historical megathrust earthquakes recorded by tsunami and terrestrial mass movement deposits on the Shirasuka coastal lowlands	54
4.3.1. Results	54
4.3.1.1. <i>Stratigraphy and sedimentology</i>	54
4.3.1.2. <i>Microfossils</i>	57
4.3.1.3. <i>Geochronology</i>	58
4.3.2. Discussion	58
4.3.2.1. <i>Age of the sand layers and correlation with the historical record</i>	60
4.3.2.2. <i>Depositional mechanisms of the sand layers</i>	60
4.3.2.3. <i>Earthquake-triggered mass movements?</i>	62
4.3.2.4. <i>Implications for historical rupture zones</i>	63
4.3.3. Conclusion	64
4.4. Single-grain feldspar luminescence chronology of historical extreme wave event deposits on the Shirasuka coastal lowlands	65
4.4.1. Results and discussion	66
4.4.1.1. <i>Comparison with independent age control</i>	66
4.4.1.2. <i>Integration with historical records and previous studies</i>	67
4.4.2. Conclusion	69
4.5. Sedimentary evolution of the Sagara coastal area and its potential to preserve extreme wave deposits	69
4.5.1. Results	69
4.5.1.1. <i>Site 1</i>	69
4.5.1.2. <i>Site 2</i>	70
4.5.2. Conclusion	72

4.6. Sedimentary records of past earthquakes in Lake Motosu during the last ca. 6000 years	72
4.6.1. Results	74
4.6.1.1. <i>Bathymetry/Morphology</i>	74
4.6.1.2. <i>Sedimentology</i>	74
4.6.1.3. <i>Background sedimentation versus sedimentary event deposits in the deep basin</i>	76
4.6.1.4. <i>Age of the event deposits</i>	76
4.6.2. Discussion	77
4.6.2.1. <i>Identifying trigger mechanisms for turbidites</i>	77
4.6.2.2. <i>Lake Motosu's sensitivity threshold</i>	81
4.6.2.3. <i>Prehistorical earthquakes and their implications for regional seismicity</i>	81
4.6.3. Conclusion	82
4.7. Signature of earthquakes and extreme flood events in Lake Sai	82
4.7.1. Results	82
4.7.1.1. <i>Bathymetry/Morphology</i>	82
4.7.1.2. <i>Sedimentology</i>	82
4.7.1.3. <i>Geochronology</i>	84
4.7.2. Discussion	85
4.7.2.1. <i>Interpretation of the sedimentary record</i>	85
4.7.2.2. <i>Lake Sai's sensitivity to earthquake shaking</i>	86
4.7.3. Conclusion	87
4.8. The potential of the Fuji Five Lakes to record natural hazards: a general discussion	87
4.8.1. Results	88
4.8.1.1. <i>Morphology and seismic stratigraphy of Lakes Motosu, Sai, Kawaguchi and Yamanaka</i>	88
4.8.1.2. <i>Sedimentology of Lakes Motosu, Sai, Kawaguchi and Yamanaka</i>	89
4.8.2. Discussion	90
5. CONCLUSIONS AND RECOMMENDATIONS	96
5.1. Reassessment of all existing geological evidence of earthquakes and tsunamis	96
5.2. Newly generated records of past earthquakes and tsunamis	97
5.2.1. Lake Hamana	97
5.2.2. Coastal lowlands near Lake Hamana	98
5.2.3. Coastal lowlands in Sagara	98
5.2.4. The Fuji Five Lakes	99
5.2.4.1. <i>Lake Motosu</i>	99
5.2.4.2. <i>Lake Sai</i>	99
5.2.4.3. <i>Lake Kawaguchi and Lake Yamanaka</i>	100
5.2.4.4. <i>The Fuji Five Lakes</i>	100

6. REFERENCES	101
7. DISSEMINATION AND VALORISATION	118
7.1. Communication to the scientific community - presentations at conferences	118
7.2. Communication to the scientific community - organization of sessions/conferences	118
7.3. Outreach and awareness	118
8. PUBLICATIONS	120
8.1. Publications in SCI Journals	120
8.2. Publications as Abstracts or Proceedings	121
8.3. Theses	126
9. ACKNOWLEDGEMENTS	128
ANNEX I: LAKE HAMANA GRAVITY AND PISTON CORES	129
ANNEX II: FUJI FIVE LAKES GRAVITY AND PISTON CORES	131
ANNEX III: FULL CORE ANALYSES/FULL CORE SCANS	134
ANNEX IV: SEDIMENTOLOGICAL-GEOCHEMICAL ANALYSES	137
ANNEX V: GEOCHRONOLOGICAL AND PALEO-ECOLOGICAL ANALYSES	140

ABSTRACT

Context

The east coast of Japan is prone to tsunamigenic megathrust earthquakes, as tragically demonstrated on 11 March 2011 by the Tōhoku-oki earthquake (M_w 9.0) and tsunami. The Nankai-Suruga Trough subduction zone, to the southwest of the area affected by the Tōhoku-oki disaster and facing the densely populated and heavily industrialized eastern coastline of Central and West Japan, is expected to generate another megathrust earthquake and tsunami in the near future.

Historical data, covering the past ca. 1300 yrs, provide some information about the recurrence rate of the earthquakes and resulting tsunami in this region and reveal a mean recurrence interval of 90-200 yrs. Unfortunately, these data still do not extend far enough in time to provide statistically relevant information necessary for adequate hazard and risk assessments. Moreover, the Nankai-Suruga Trough subduction zone is segmented and is characterized by a variable rupture mode, involving single- as well as multi-segment ruptures, which has immediate implications for their tsunamogenic potential.

Objectives

The main goal of the QuakeRecNankai project is to generate a longer time series of tsunami and megathrust earthquake recurrences, in order to gain a better understanding of the complex recurrence patterns, both in space and in time. To this end, the QuakeRecNankai project investigates the geological record of:

- paleo-tsunami in the coastal region around Lake Hamana and in Lake Hamana itself,
- paleo-earthquakes, using suitable lakes from further inland locations (e.g. selected lakes in the Mount Fuji area).

Conclusions and recommendations

At the start of the QuakeRecNankai project, a critical examination was conducted of the available geological evidence of past earthquakes and tsunamis from 72 sites along the Nankai-Suruga Trough. Of these 72 sites, only a minority provide compelling and well-dated evidence. All other sites suffer from various issues, severely limiting their usefulness in understanding past fault behaviour.

For eleven historical earthquakes, the best available evidence was used to constrain their most likely rupture zones. This emphasized that the Nankai-Suruga Trough is characterized by a high degree of variability in rupture mode, but also that there is currently no evidence for the occurrence of a larger magnitude earthquake or greater tsunami inundation than that experienced in 1707 CE.

- > future assessments should consider thresholds of evidence creation and preservation when assessing the intervals between earthquakes from paleoseismic data;
- > future research efforts should address the question of maximum magnitude through combined field and modelling efforts. Amongst the diverse range of paleoseismic field evidence types available, turbidite records in marine and lacustrine settings and tsunami inundation records from coastal lowlands and lakes, offering preserved evidence of past seismic shaking and deformation and of extreme wave event inundation, are best placed to provide new insights into the dimensions of past fault ruptures.

The QuakeRecNankai project has also generated a series of new geological records of past earthquakes and tsunamis.

1. A new, ~7.5 kyr long sedimentary record from Lake Hamana contains ≥ 22 possible event deposits, resulting from extreme wave events (EWEs), such as tsunamis and typhoons, and from megathrust earthquakes. Several of these event deposits can be linked to historical megathrust

- events; others are more likely to have been caused by storm surges and/or typhoons. Prehistorical event deposits show good agreement with other existing sources of megathrust evidence from the region, and add complementary information when going back to 7.5 ka BP.
- > future research efforts should verify if lateral variability in thickness of event deposits in Lake Hamana might be key to differentiate between a tsunami or a typhoon/flood trigger.
2. In the Shirasuka coastal lowlands, near Lake Hamana, four sand layers, interpreted as event deposits caused by inundation during tsunamis or typhoon-driven storm surges as well as by terrestrial mass movements, were identified, in a record dating back to the 14th century. They could be linked to four historical earthquakes, in part aided by chronological data obtained by infrared-stimulated luminescence dating on coarse grains of alkali-feldspars. The new record highlights both the high degree of lateral variability in the deposits and the potential for geological records to underestimate the frequency of tsunami occurrence.
 - > future studies should consider using terrestrial mass movement deposits as a complementary paleoseismic approach.
 3. In the lowlands at the town of Sagara, a new, long sedimentary record contains a series of potential extreme wave event (EWE) deposits, possibly dating back to the early Holocene. Further analysis (e.g. micropaleontological and geochemical analysis) and radiocarbon dating is, however, required to ascertain the nature and age of these deposits.
 4. The sedimentary records of four of the five Fuji Five Lakes were investigated in the QuakeRecNankai project. The two shallower lakes (i.e. Lake Kawaguchi and Lake Yamanaka) appear to be not sensitive to earthquake shaking and are therefore less suited as a paleo-earthquake archive. The two deep lakes, Lakes Motosu and Sai, are much better suited. In Lake Motosu, 32 sedimentary event deposits, interpreted to have been triggered by earthquake shaking, were identified, interbedded within the background sediments, in a sedimentary record covering the last ca. 6000 years. Not only megathrust earthquakes from the Nankai-Suruga Trough may be recorded in Lake Motosu, but also from the Sagami Trough and a number of crustal faults in the Mount Fuji region. Nearby Lake Sai has also recorded a number of earthquakes, although the lake seems more prone to generate event deposits due to floods, triggered by heavy rains, or by debris flows, triggered by typhoons.
 - > the four investigated lakes clearly have a different sensitivity to earthquake shaking, and future studies should evaluate which parameters determine a lake's sensitivity and hence its usefulness as a paleo-earthquake archive: water depth, proportion of the surface area occupied by underwater slopes, sediment composition (i.e. diatom content,...).

The results of the QuakeRecNankai project have been incorporated in new risk and hazard assessments, have been used to support government policy updates, and have been the subject of active public outreach activities.

Keywords

earthquake, tsunami, Nankai-Suruga Trough, geohazard, coastal lowland, coastal lake, Fuji Five Lakes

1. INTRODUCTION, STATE OF THE ART AND OBJECTIVES

The unexpected magnitude of the 2011 CE Tōhoku-oki earthquake (M_w 9.0) and ensuing tsunami triggered a rapid reassessment of approaches to seismic hazard assessment in Japan (Goto et al., 2014). Acknowledging the failure of hazard assessments to adequately evaluate the potential for earthquakes and tsunamis exceeding the magnitude of those experienced in the region over the last 400 years, like it had been the case for the Tōhoku-oki earthquake and tsunami, the Central Disaster Management Council (CDMC) of the Japanese Cabinet Office issued revised hazard assessment guidelines. These call for all available evidence to be used to define the maximum possible magnitude of earthquake and the largest potential tsunami for any given coastline (Central Disaster Management Council, 2011; 2012).

These new guidelines pay close attention to the **Nankai-Suruga Trough** subduction zone, which faces the densely populated and highly industrialized coastline of south central Japan, and is **expected to generate another megathrust earthquake and tsunami in the near future**. The largest possible class of earthquake on the subduction interface could exceed M_w 9.0, with tsunami travel times to the closest shorelines of less than 30 minutes, making reliable hazard assessments of vital and imminent importance.

Historical evidence of earthquakes and tsunamis along the Nankai-Suruga Trough dates back to as early as the 7th century (Ando, 1975b; Ishibashi, 1999; 2004). These historical data provide some information about the recurrence of earthquakes and resulting tsunamis in this region and reveal a mean recurrence interval of 90-200 yrs (Komatsubara et al., 2008). **Geological records** of past earthquakes and tsunamis can generally provide additional lines of evidence, complementing the historical records.

Reviews by Komatsubara et al. (2006a) and Komatsubara & Fujiwara (2007) summarized the spatial and temporal distribution of proposed paleoseismic evidence along the Nankai-Suruga Trough, and concluded that **geological evidence is generally consistent with historical data**, but also note the difficulties in accurately dating evidence and in reconstructing prehistorical earthquake or tsunami characteristics from individual sites. Further field studies undertaken after the publication of these reviews, and particularly since the 2011 Tōhoku earthquake, has **fueled continued discussion of rupture modes and recurrence intervals** (e.g. Satake, 2015; Seno, 2012).

The main goals of the QuakeRecNankai project are i) to **reassess all existing historical and geological evidence** of past earthquakes and tsunamis along the Nankai-Suruga Trough, and ii) to **generate a series of new and reliable records** of past earthquakes and tsunamis, from a number of key sites, in order to contribute to the production of an **improved hazard assessment for the region**.

To this end, the QuakeRecNankai project will investigate the geological record of:

- paleo-tsunamis in the coastal region around Lake Hamana and in Lake Hamana itself, a key site for reconstructing earthquake and tsunami recurrence along the Nankai-Suruga Trough,
- paleo-earthquakes, using suitable lakes from further inland locations (e.g. selected lakes in the Mount Fuji area).

The QuakeRecNankai project combines:

- i) extensive geophysical, geological and geomorphological fieldwork, in the coastal plain areas and on the lakes (i.e. Hamana lake and the Fuji lakes),
- ii) advanced sedimentological and geochemical analyses,
- iii) innovative dating techniques.

2. TECTONIC CONTEXT

The Nankai-Suruga Trough marks the subduction of the northwestward moving Philippine Sea Plate beneath the Eurasian Plate. In the center of the subduction zone the plates converge at a rate of 40–55 mm/year (Loveless & Meade, 2010). At its eastern end, the Fujikawa-Kako Fault Zone constitutes an on-land extension of the interface between the Philippine Sea and Eurasian Plates (Figure 1). The western extremity of the Nankai-Suruga Trough meets the Ryukyu Trench, where the Philippine Sea Plate subducts beneath the Ryukyu Arc.

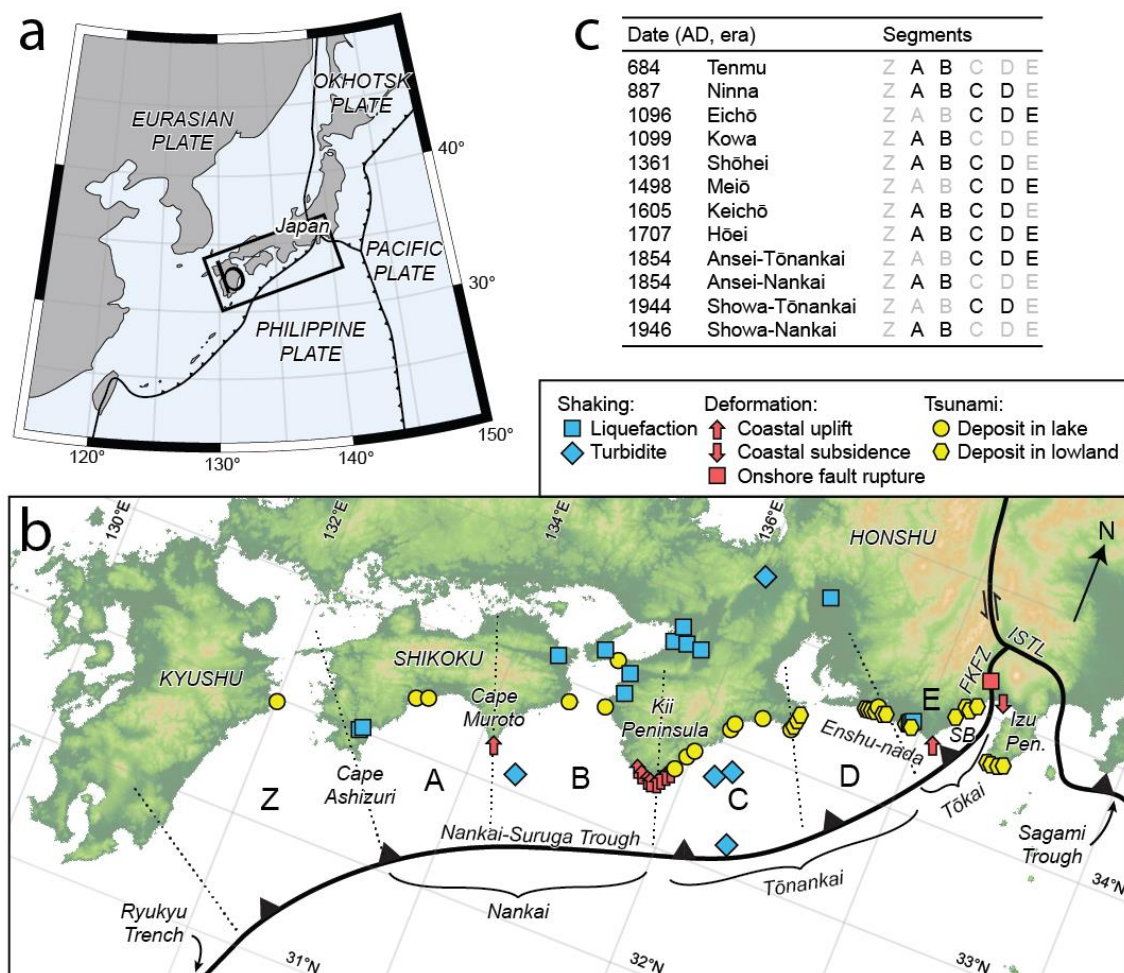


Figure 1: a) Tectonic setting of Japan, including the location of b) The Nankai-Suruga Trough, with the annotation of sites with evidence of past megathrust earthquakes and tsunamis. Abbreviations: SB: Suruga Bay, FKFZ: Fujikawa-Kako Fault Zone, ISTL: Itoigawa-Shizuoka Tectonic Line; letters Z, A, B, C, D and E refer to subduction-zone segments. Segments A and B are collectively referred to as “Nankai”; segments C and D as “Tōnankai”; segment E as “Tōkai”. c) Summary of historical earthquakes, including calendar year, era name (nengō) and proposed rupture zone segments from historical records (Ando, 1975b; Ishibashi, 2004). From Garrett et al. (2016).

The geometry and structure of the Nankai subduction is well constrained by seismic reflection surveys (e.g. Bangs et al., 2004; Park et al., 2010), hypocenter location studies (e.g. Hashimoto et al., 2004), seismic tomography studies (e.g. Nakajima & Hasegawa, 2007; Hirose et al., 2008; Liu & Zhao, 2014), receiver function analysis (e.g. Shiomi et al., 2008) and wide-angle seismic surveys (e.g. Kodaira et al., 2000; Kodaira et al., 2002; Nakanishi et al., 2002; Takahashi et al., 2002). The depth of the slab varies and its geometry is complicated. Thermal modelling is consistent with a seismogenic zone extending from 8 km to 25 km depth, with transitional zones down to 33 km and up to the trench (Hyndman et al., 1995; Mazzotti et al., 2000). At the deep transition zone, low-

frequency earthquakes located on the plate boundary occur (e.g. Ohta & Ide, 2011). The subduction process is also influenced by anomalously thickened oceanic crust interpreted as a subducted seamount (Kodaira et al., 2002) and by the extent of contact between the Neogene Quaternary accretionary prism and the oceanic crust (Nakanishi et al., 2002; Takahashi et al., 2002).

Geodetic data suggests the plate interface is highly coupled, with accumulated strain episodically released through major and great earthquakes with magnitudes exceeding 7 and 8 respectively (Aoki & Scholz, 2003; Mazzotti et al., 2000; Ozawa et al., 1999; Sagiya, 1999). Splay faults, subsidiary faults within the overriding plate that branch off the main interface, may slip concurrently with rupture of the plate boundary (Cummins et al., 2001; Moore et al., 2007; Park et al., 2002), contributing to tsunami genesis. The earliest historical records of seismic activity along the Nankai-Suruga Trough describe the occurrence of an earthquake in 684 CE which caused widespread damage and was accompanied by landslides, vertical land-level changes and tsunami inundation, particularly along coastlines of the western region of the subduction zone (Ando, 1975b; Ishibashi, 2004; Sangawa, 2009; Usami, 1996). This, and eleven subsequent earthquakes, are generally accepted as magnitude 8-class megathrust earthquakes, with part or all of the plate boundary rupturing in 684 CE, 887 CE, 1096 CE, 1099 CE, 1361 CE, 1498 CE, 1605 CE, 1707 CE, 1854 CE (twice), 1944 CE and 1946 CE (Figure 1). Additional undocumented great earthquakes may have occurred during the historical period; this is less likely from the 17th century onwards due to good documentary preservation and the detailed records produced at the domain and village level in Tokugawa society. Japan's classical and medieval periods (c.700–1185 CE and 1185–1600 CE) are relatively well represented documentarily, though periods of civil war such as the late 14th and 16th centuries are more sparsely represented.

Instrumental records and the long historical catalogue suggest the subduction zone is characterized by along-strike segmentation, with a series of persistent seismic segments that may rupture individually or in a range of multi-segment combinations (Ando, 1975b; Ishibashi, 2004). Hyodo & Hori (2013) suggest that, in addition to along-strike segmentation, the subduction zone is characterised by variability in slip depth, with larger megathrust earthquakes featuring slip up-dip of the main seismogenic zone.

The most recent pair of great Nankai-Suruga Trough earthquakes occurred on adjacent but not overlapping rupture zones possibly separated by a change in dip or a tear in the downgoing Philippine Sea Plate in the vicinity of the Kii Peninsula (Baba et al., 2002; Baba & Cummins, 2005; Cummins et al., 2002; Tanioka & Satake, 2001a; 2001b). While the 1946 CE rupture was confined to segments A and B (the Nankai region), the 1944 CE earthquake ruptured segments C and D (the Tōnankai region; Figure 1). Unlike the preceding 1854 CE earthquake, the 1944 CE rupture did not extend east into segment E, the Tōkai region (Ando, 1975a; Baba & Cummins, 2005). The complex ruptures of the 1944 CE and 1946 CE earthquakes may have been related to the occurrence of a subducted seamount and of locally trapped water between the plates; both factors would change the coupling between the plates (e.g. Kodaira et al., 2002).

3. METHODOLOGY

3.1. Compilation and critical review of geological evidence of past earthquakes and tsunamis

3.1.1. *Literature review*

We conducted a critical examination of all published geological evidence for past earthquakes and tsunamis along the Nankai-Suruga Trough, which includes 75 papers, doctoral theses and professional reports, including 52 Japanese language and 23 English language publications. These publications derive evidence for the occurrence of past earthquakes from a range of different types of sites, which fall into three categories, focusing on evidence for i) intense shaking (through liquefaction or turbidite deposits), ii) deformation (through identifying biotic, facies or geomorphic changes in coastal locations or rupture of onshore faults), or iii) tsunami occurrence (through evidence for erosion and/or deposition at coastal sites).

The aims of this review were to:

- i) summarize the current state of knowledge concerning geological evidence for Holocene great earthquakes and tsunamis along the Nankai-Suruga Trough,
- ii) constrain the rupture zones of earthquakes occurring during the historical period,
- iii) assess the contribution of paleoseismic records to defining earthquake occurrence intervals over longer intervals,
- iv) discuss maximum magnitude and variability in rupture modes,
- v) outline the major issues involved with the interpretation of paleoseismic records from the Nankai-Suruga Trough,
- vi) make recommendations on how further geological studies may better contribute to understanding future seismic hazards.

3.1.2. *Recalibration of radiocarbon ages and age modelling*

We recalibrated radiocarbon ages of past earthquakes and tsunamis reported in literature in order to take advantage of the latest radiocarbon calibration curves, IntCal13 and Marine13 (Reimer et al., 2013). Dates from marine samples must be corrected for the marine radiocarbon reservoir effect; however, appropriate corrections for locations along the southern coast of Japan remain uncertain at present. The Kuroshio Current provides water that is well mixed with the atmosphere, resulting in low ΔR values (Nakamura et al., 2016). Hideshima et al. (2001) and Yoneda et al. (2007) report values ranging between 135 ± 48 and -15 ± 64 years for the Ryukyu Islands, southwest of Kyushu. On coastlines facing the Nankai-Suruga Trough, Nakamura et al. (2007) report ΔR values of -11 ± 103 years from Yoshigo and -201 ± 77 years from Kuzubasama, while Yoneda et al. (2000) report a ΔR value of -7 ± 0 years for the Kii Peninsula. Shishikura et al. (2007) propose a ΔR value of 82 ± 33 years for the Miura Peninsula, east of the Nankai-Suruga Trough. As it remains the best estimate from the Nankai-Suruga Trough region and is consistent with a well-mixed Kuroshio Current, we follow Yoneda et al. (2000) and use a ΔR value of -7 ± 0 years to correct all marine samples. We report calibrated dates as 2σ age ranges in years before present (cal yr BP), rounded to the nearest 10 years, and additionally in years CE where beneficial for comparison with historical dates.

Where appropriate, Bayesian age modelling approaches further constrain the timing of past earthquakes and tsunamis. We develop P_sequence (Bronk Ramsey, 2008; 2009) and Sequence (Bronk Ramsey, 1995; Lienkaemper & Ramsey, 2009) models using the OxCal program v.4.2 (Bronk Ramsey, 2009).

3.2. Field work

In order to achieve the goals of the project, new field work was conducted and important new data were acquired in:

- the lowlands around Lake Hamana (i.e. the Shirasuka coastal lowlands, the Shinjo lowlands and on the Murakushi Peninsula), as well as at the town of Sagara,
- coastal Lake Hamana, and
- the in-land Fuji Five Lakes (i.e. Lakes Motosu, Sai, Kawaguchi and Yamanaka), located around Mount Fuji (Figure 2).

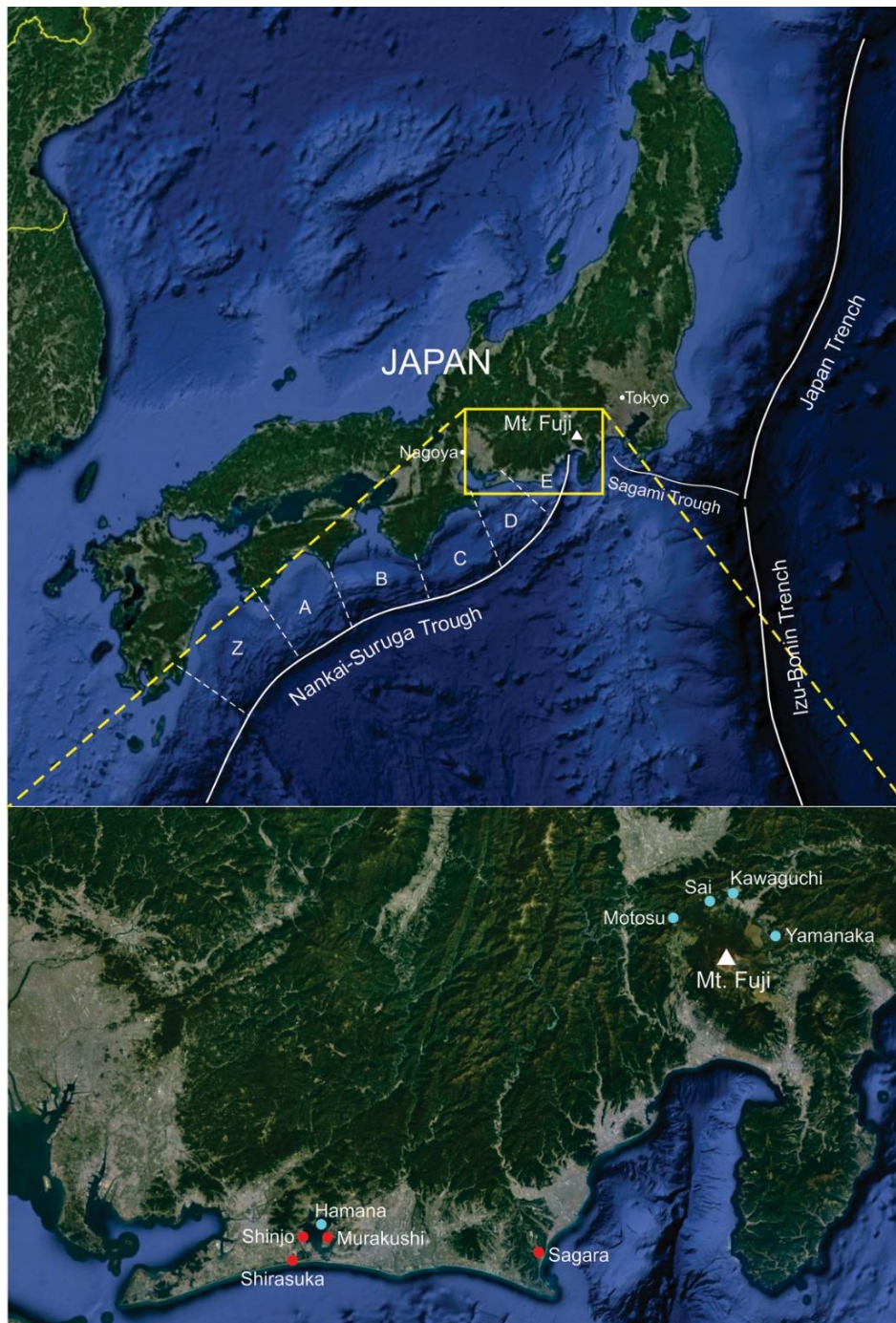


Figure 2: Location of the study areas in which new field work was conducted and field data were collected in the course of the project, plotted relative to the main tectonic features of the region (see also Figure 1). Blue markers: lakes. Red markers: coastal lowlands.

3.2.1. *Geomorphological surveying, vibrocoreing and gouge coring in coastal lowlands*

3.2.1.1. *Coastal lowlands around Lake Hamana*

Potential study sites were identified in concertation with the Japanese partners, based on previous work in the area by AIST. These study sites are located in the Shirasuka coastal lowlands, the Shinjo lowlands and on Murakushi Peninsula (Figure 3). Fieldwork at these study sites was conducted during the period of 21.10.2014-08.11.2014.



Figure 3: Location of the study areas in and around Lake Hamana (see also Figure 2).
Blue marker: lake. Red markers: coastal lowlands.

Shinjo lowlands

The Shinjo lowlands (34°44.22'N, 137°32.20'E) encompass a series of paddy fields on the western margin of Lake Hamana. The lowlands are intensively cultivated and are located behind an embanked area and sea wall approximately 2-3 m high. Much of the site lies at an elevation of ca. 1 m above mean sea level.

Previous work at the site by Sato (2014), focused on the northern branch of the lowlands and based on eight gouge cores, suggested a sedimentary sequence characterized by several peat layers interbedded with mud and overlying silts or clays containing shell fragments. Radiocarbon ages suggested organic accumulation from approximately 6500 cal yr BP.

Our investigations focused on the southern branch of the Shinjo lowlands. We obtained a 1100 cm long vibrocore from site JSL1, using an Atlas Copco Cobra TT vibrocorer and hydraulic core extractor, and gouge cores of up to 550 cm length from sites JSL2-6.

The cores obtained at the Shinjo lowlands (Figure 4) did not reveal stratigraphic units that could be attributed to extreme wave events or abrupt episodes of vertical coseismic deformation.



Figure 4: Location of the vibrocores and gouge cores (red markers) retrieved from the Shinjo lowlands.

Murakushi Peninsula North

The Murakushi Peninsula is a continuation of the fluvial Mikatagahawa terrace, which is found extensively to the east of Lake Hamana. The northern end of the Murakushi Peninsula ($34^{\circ}45.13'N$, $137^{\circ}36.41'E$) is dissected by a low-lying area of land currently used from agriculture, particularly rice cultivation. Our investigations focused on fields close to the village of Shonai. The land surface lies at ca. 1 m above mean sea level. Apart from elevated roads, there are no topographic highs between the site and the lake to the south.

We obtained a 900 cm long open vibrocore, JMN1, and two immediately adjacent closed vibrocores, JMN2 and JMN3, using the same vibrocorer system as mentioned above. Impenetrable gravel repeatedly thwarted attempts to investigate the stratigraphy of areas further to the north using gouge cores, although a maximum depth of 3 m was achieved at JMN10 and JMN11.

The cores obtained at the northern end of the Murakushi Peninsula (Figure 5) did not reveal stratigraphic units that could be attributed to extreme wave events or abrupt episodes of vertical coseismic deformation.



Figure 5: Location of the vibrocores and gouge cores (red markers) retrieved from Murakushi Peninsula North.

Murakushi Peninsula South

The southern end of the Murakushi Peninsula (34°42.88'N, 137°35.49'E) represents artificial land reclamation, mainly during the 20th century. The contemporary land surface lies at an altitude of 2-4 m above mean sea level.

At two sites, JMP1 and JMP2, our attempts to vibrocore through the artificial fill to the lake deposits anticipated beneath were unsuccessful, despite reaching depths of between 500 and 600 cm (Figure 6). Impenetrable sand prevented deeper coring.



Figure 6: Location of the vibrocores and gouge cores (red markers) retrieved from Murakushi Peninsula South.

Shirasuka coastal lowlands

The site of Shirasuka (34°40.68'N, 137°30.29'E) lies 8.5 km west of the mouth of Lake Hamana. Here, paddy fields occupy a narrow strip of low-lying land between the ~60-70 m high riser of the Tenpakubara terrace (a middle Pleistocene marine terrace) to the north and an approximately 9 m high beach ridge (topped by a highway) to the south. The elevation of the site is ca. 4 m.

Previous investigations at Shirasuka (Fujiwara et al., 2006b; Komatsubara et al., 2006b; 2008) suggested the site has been accumulating fine-grained organic silts and clays since the 13th century, with a number of coarse-grained overwash layers reflecting tsunami or typhoon inundation. In part due to the plateau in the radiocarbon calibration curve, the precise correlation between sand layers and historical storms and tsunamis remained unclear.

We obtained 6 vibrocores, from within a ca. 1 m radius, at location JSH1-3 (i.e. JSH1/F, JSH1b/F, JSH2/F, JSH3/F, JSH3/O and JSH1/O), using the same vibrocorer system as mentioned above (Figure 7). Maximum length retrieved was 480 cm.



Figure 7: Location of the vibrocores (red markers) retrieved from the Shirasuka coastal lowlands.

We also recovered six surface samples from locations close to the coring site. These samples allow us to provide an initial characterization of sediments from the modern beach (two samples), dune ridge (two samples), paddy field (one sample) and mid-Pleistocene terrace (one sample).

3.2.1.2. Sagara lowlands

The Sagara lowlands (34°41'N, 138°12'E) form the floodplain of the Hagima River, adjacent to the town of Sagara. The site lies at an altitude of ca. 1 to 5 m and is within the anticipated inundation zone of future worst-case tsunami scenarios (Shizuoka Prefecture, 2016). The area of interest, between 0.2 and 1.5 km inland from the current coastline, is a ~1.5 km wide floodplain. Paddy fields cover the area to the northeast of the river, while the southwestern side is urbanized. The site was previously cored by a contractor employed by AIST, and all cores were shipped to Belgium. The initial survey recovered eighteen oriented continuous cores of between 2 and 11 m (Figures 8 and 9).

New fieldwork in this study area was conducted on 17.10.2016 (Figures 8 and 9). It involved the selection of locations of fourteen additional coring sites, for subsequent recovery by the contracted coring company. Twelve of these cores form three rough transects perpendicular to the initial transect on the northeastern side of the river. The remaining two cores lie close to the previously collected cores on the southwestern side of the river. Most of these cores were then also shipped to Belgium.

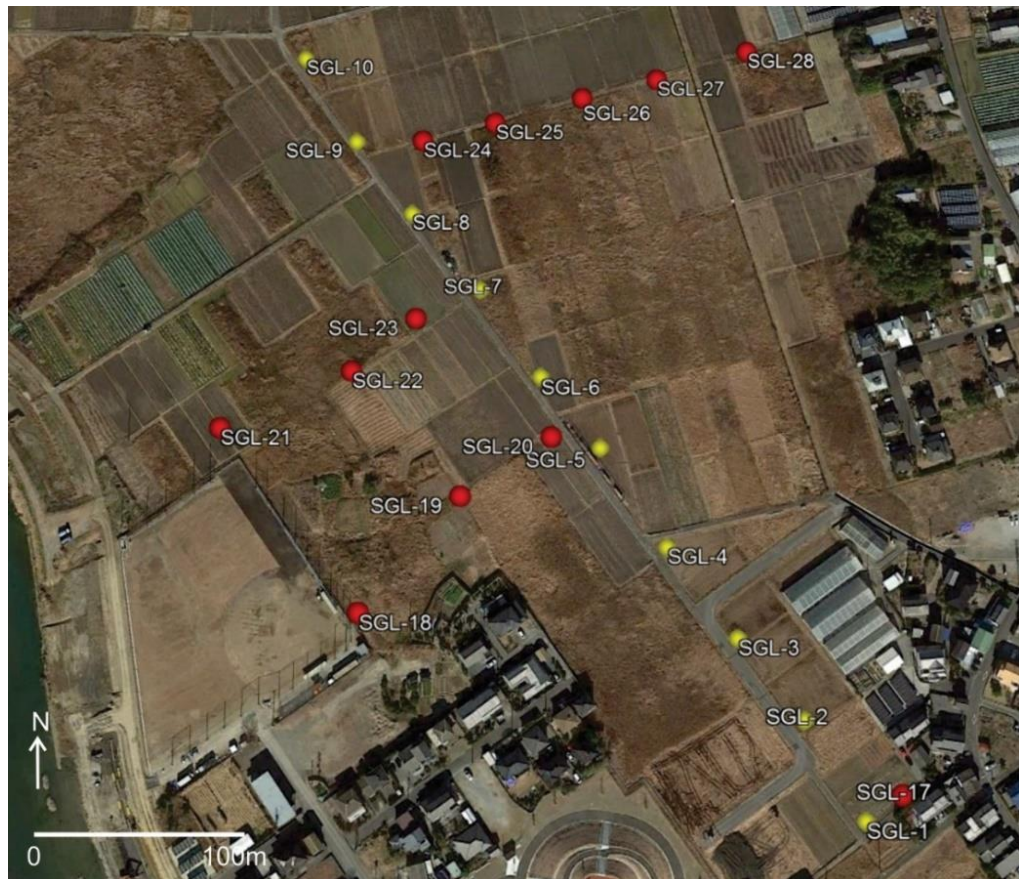


Figure 8: Location of the vibrocores retrieved from the Sagara lowlands, to the northeast of the Hagima River. Yellow markers: cores from before the start of the project. Red markers: cores retrieved during the project.



Figure 9: Location of the vibrocores retrieved from the Sagara lowlands, to the southwest of the Hagima River. Yellow markers: cores from before the start of the project. Red markers: cores retrieved during the project.

3.2.2. Geophysical surveying on coastal and in-land lakes

3.2.2.1. Lake Hamana

Lake Hamana (34°45'N, 137°35'E) is a brackish, eutrophic, coastal lake, located along the Enshū-nada coast in central Japan (Itoh et al., 2003a; 2003b; Taguchi & Nakata, 1998). Its origin has been estimated to date back to around 18 ka BP (Kai & Ikeya, 1989). The lake occupies a surface area of 68.8 km² and possesses maximum and average depths of 12 and 4.8 m, respectively. It is currently connected to the Pacific Ocean through the 200 m wide Imagire-guchi Channel, through which tidal currents drive the exchange of salt water (Itoh et al., 2003a; Kai & Ikeya, 1989). This channel was formed as a result of beach ridge breaching by the tsunami wave following the 1498 CE Meio earthquake (M_w 8.4) (Fujiwara et al., 2013a). Freshwater is supplied mainly by the Miyakoda River, which enters the northeast sub-basin of the lake and secondarily by a series of other smaller streams and gullies (Itoh et al., 2003a; 2003b).

The lake basin is considered to be a good recorder of (pre)historic tsunamis affecting the Enshū-nada coast. Tsunami-triggered deposits in and around Lake Hamana were previously already described by several authors (e.g. Fujiwara et al., 2013a; Komatsubara & Fujiwara, 2007; Kumagai, 1999).

During a first fieldwork season, in the period between 20.10.2014 and 31.10.2014, a grid of high-resolution reflection-seismic profiles (total length of ~150 km) was shot on Lake Hamana (Figure 10). The data were collected using a Geopulse sub-bottom profiler (pinger), mounted on a catamaran that was towed behind a survey vessel. The data were recorded on an iXblue-Delph Seismic system and converted to SEG-Y file format, for digital processing and analysis using IHS Markit Kingdom (version 2016.1). The acoustic signal, with a central frequency of 3.5 kHz, provides an average horizontal resolution of 20-25 cm when moving at a speed of ~6 km/h, and a theoretical vertical resolution of 10-20 cm (Rayleigh criterion).

A bathymetric map was constructed by interpolation of calculated water depths along

the high-resolution reflection-seismic profiles. A time-to-depth conversion factor of ~ 1495 m/s (brackish water with 25 S‰ at ~ 15 °C; Chen & Millero, 1977) was used.

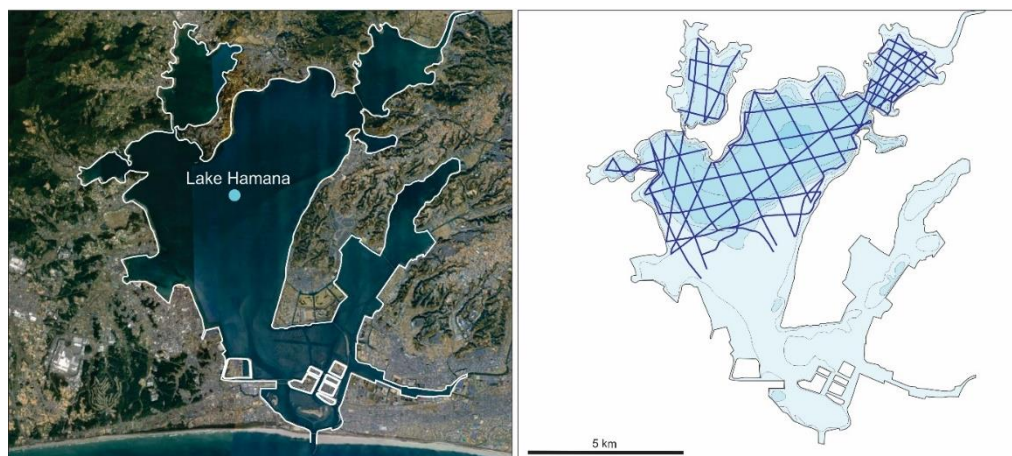


Figure 10: Grid of high-resolution reflection seismic profiles collected on Lake Hamana. Bathymetry background map was constructed by interpolation of calculated water depths along the seismic profiles.

3.2.2.2. Fuji Five Lakes

The “Fuji Five Lakes” comprise Lake Motosu, Lake Shōji, Lake Sai, Lake Kawaguchi and Lake Yamanaka (Figure 11). They are located at the foot of Mount Fuji in south central Honshu. They were formed as a result of natural damming by lava flows and do not have natural draining rivers, with the exception of Lake Yamanaka. Previously collected sediment cores from Lakes Kawaguchi, Yamanaka and Motosu suggest that they formed prior to the Holocene (Aramaki et al., 2007). The Fuji Five Lakes are characterized by annual and inter-annual water-level fluctuations (Nagasaka et al., 2002) and show a diverse range of depths and trophic states (Table 1).

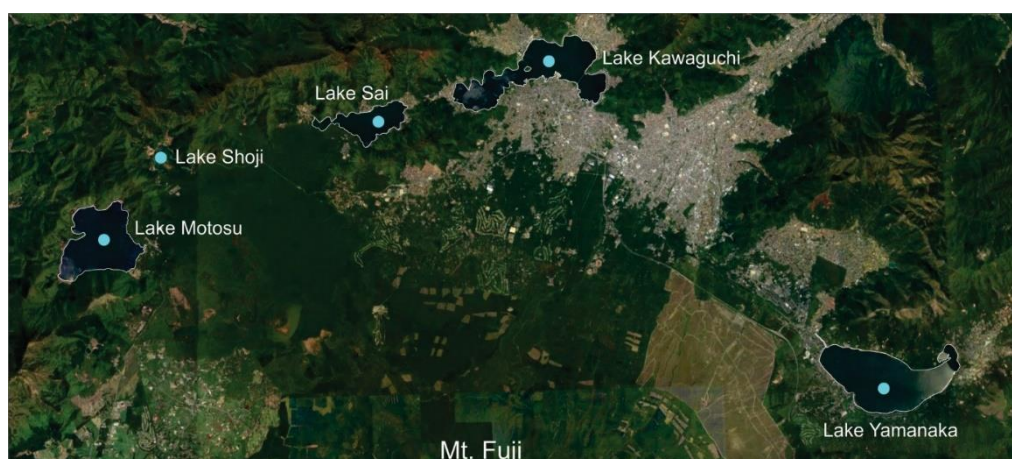


Figure 11: Location of the Fuji Five Lakes (see also Figure 2).

Initially, Lakes Motosu, Shoji and Sai were connected and formed Lake Senoumi. The lakes were separated by lava flows during the 800 CE and 864 CE eruptions of Mount Fuji (Obata & Umino, 1999). Due to ground water interchange through the porous lava, the water levels of Lakes Motosu, Sai and Shoji are similar and fluctuate together

(Aramaki et al., 2007). Lake Yamanaka is closest to Mount Fuji and highly exposed to pyroclastic flows from Mount Fuji.

Table 1: Morphometric parameters and trophic state of the Fuji Five Lakes (Adhikari, 2011; Hirabayashi et al., 2012; Yamanashi Prefecture, 1993).

Lake	Surface area (km ²)	Mean depth (m)	Maximum depth (m)	Trophic state
Yamanaka	6.9	Unknown	14.3	Mesotrophic
Motosu	5.6	Unknown	121.6	Oligotrophic
Sai	2.17	38.5	73.2	Oligotrophic
Kawaguchi	5.96	9.3	16.1	Eutrophic
Shoji	0.5	7	16.2	Eutrophic

During the first fieldwork season, between 06.10.2014 and 18.10.2014, high-resolution reflection-seismic profiles were shot on Lakes Motosu (35°28'N, 138°35'E), Sai (35°30'N, 138°41'E), Kawaguchi (35°31'N, 138°45'E) and Yamanaka (35°25'N, 138°52'E). The data were collected using the same Geopulse sub-bottom profiler, the same acquisition system and layout and they have the same characteristics as mentioned above.

Grids of seismic profiles with total lengths of 39 km, 24 km, 31 km and 28 km were collected from Lakes Motosu, Sai, Kawaguchi and Yamanaka, respectively (Figure 12).

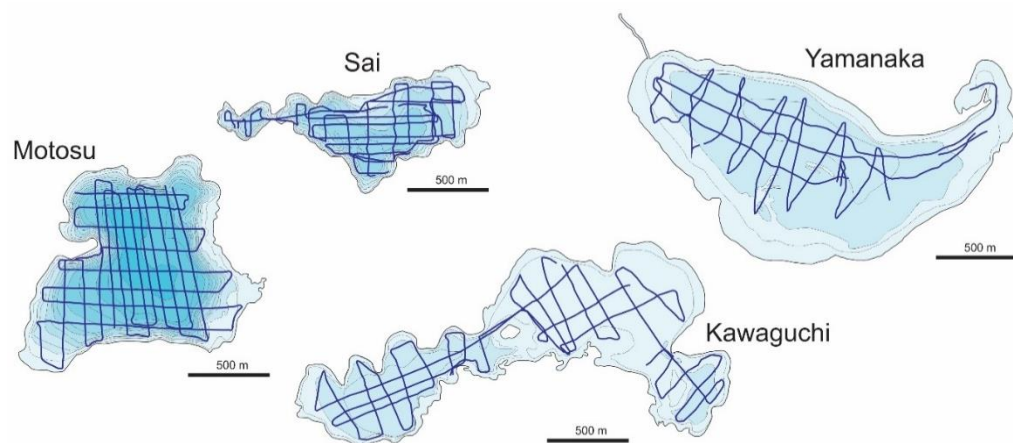


Figure 12: Grids of high-resolution reflection seismic profiles collected on Lakes Motosu, Sai, Kawaguchi and Yamanaka. Bathymetry background maps were constructed by interpolation of calculated water depths along seismic profiles.

3.2.3. Gravity coring and piston coring in coastal and in-land lakes

3.2.3.1. Lake Hamana

During the first fieldwork season, in the period between 20.10.2014 and 31.10.2014, short gravity cores were retrieved at 14 locations in Lake Hamana (i.e. HAM14-01 up to HAM14-14), using a UWITEC gravity corer from ULiège. The 14 coring sites had been selected based on the preliminary analysis of the seismic data that were acquired just before. Duplicate cores were taken on every site, which allowed one core to be taken to Belgium and one to remain in Japan (at AIST). Lengths of the cores vary between 50 and 115 cm. Sediment from the core catchers was put in separate boxes.

During a second fieldwork season, in the period between 01.10.2015 and 31.10.2015, several long piston cores were collected as well, on locations that had been carefully

selected following the analysis of the seismic data and of the short gravity cores. In total 6 coring sites had been identified along a N-S transect through the central, deep lake basin. Piston cores were collected with a UWITEC piston-coring system, deployed from a UWITEC coring platform (borrowed from the British Antarctic Survey). The initial plan was to retrieve nine cores at every site: one gravity core (to recover the sediment-water interface) and eight overlapping piston sections, each 2 m long, in two parallel holes. Due to time restrictions, only four sites could be cored as planned. Two of these sites are entirely finished (i.e. HAM15-01 and HAM15-02), whereas three of the overlapping sections are missing from the other two sites (i.e. HAM15-03 and HAM15-04). All cores were taken to Belgium for further analyses.

A complete list of all collected cores and core sections is provided in Annex I. The coring locations are presented in Figure 13.

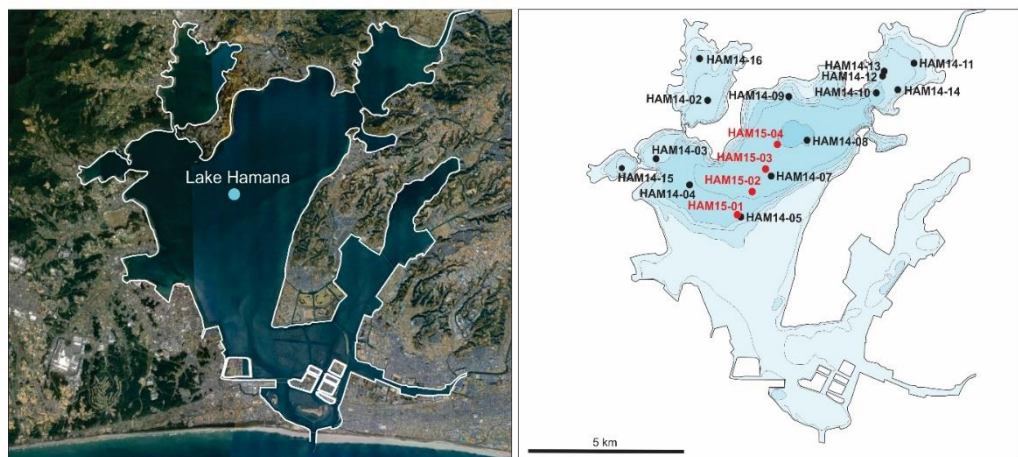


Figure 13: Location of the gravity cores (black) and the piston cores (red) that were collected in Lake Hamana. Bathymetry background map was constructed by interpolation of calculated water depths along seismic profiles.

3.2.3.2. Fuji Five Lakes

During the first fieldwork season, in the period between 06.10.2014 and 18.10.2014, short gravity cores were taken in Lake Motosu, Lake Sai, Lake Kawaguchi and Lake Yamanaka, using the same gravity corer as mentioned above (Figure 14). Coring locations had been selected based on preliminary analysis of the seismic data that were collected just before. Six different locations were cored in both Lake Motosu (i.e. MOT14-01 up to MOT14-06) and Lake Sai (i.e. SAI14-01 up to SAI14-06); five and seven cores were collected in Lake Yamanaka (i.e. YAM14-01 up to YAM14-05), and Lake Kawaguchi (i.e. KAW14-01 up to KAW14-07), respectively. Cores were duplicated at every location (except YAM14-01A), which allowed one core taken to Belgium and one to remain in Japan (at the Mount Fuji Research Institute). Core YAM14-01A was split in two and half of the core sent to Belgium.

During the second fieldwork season, in the period between 01.11.2015 and 30.11.2015, a few long piston cores were collected as well, on locations that had been carefully selected following the analysis of the seismic data and of the short gravity cores. In total six coring sites had been identified: i.e. two in Lake Motosu, two in Lake Sai and two in Lake Kawaguchi. Piston cores were collected with the same piston-coring system and coring platform as mentioned above. Whenever possible, the cores were duplicated so that one core could be taken to Belgium and one could remain in

Japan (at the Mount Fuji Research Institute). Due to time restrictions, not all of the cores could be duplicated, especially the deepest sections. The non-duplicate cores were opened and split at Mount Fuji Institute, so that one half could be shipped to Belgium while the other half could remain in Japan.

A complete list of all collected cores and core sections is provided in Annex II. The coring locations are presented in Figure 14.

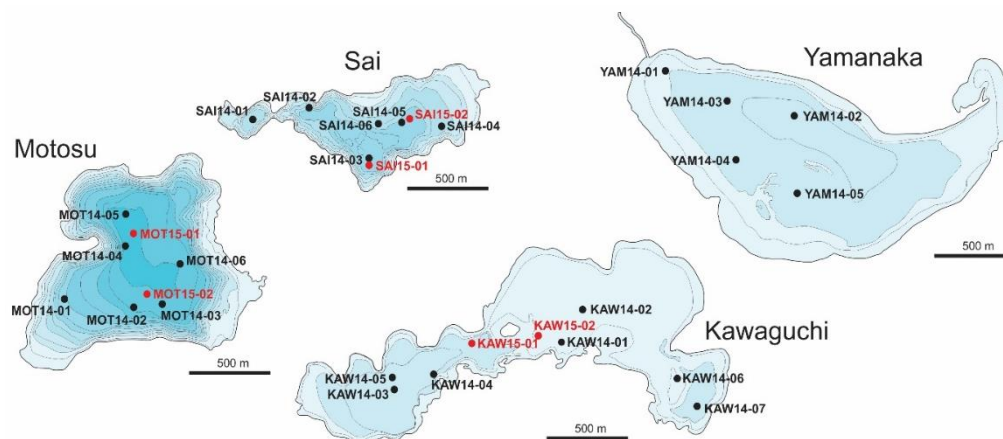


Figure 14: Location of the gravity cores (black) and the piston cores (red) that were collected in Lakes Motosu, Sai, Kawaguchi and Yamanaka (only gravity cores). Bathymetry background maps were constructed by interpolation of calculated water depths along seismic profiles.

3.3. Laboratory analyses

The collected sediment cores (i.e. short gravity and long piston cores from the lakes and vibrocores from onshore sites) and sediment samples were analyzed both in Japan and Europe. A broad spectrum of laboratory analyses was applied in order to characterize the sediment cores and samples in terms of sedimentology, geochemical composition and paleo-ecology and to determine their age.

A complete overview of which analyses were conducted on which samples, is provided in Annexes III, IV and V.

3.3.1. Sedimentological, geochemical and paleo-ecological analyses

3.3.1.1. Whole-core analysis and core scanning

The gravity and piston cores from Lake Hamana and the vibrocores from the onshore sites were imaged –prior to opening and splitting– with a Siemens SOMATOM Definition Flash medical **X-ray computed tomography** (CT) scanner at the Ghent University Hospital (UZGent). The scans were reconstructed into a DICOM image stack, representing a volume with voxel sizes of ~0.15 mm x ~0.15 mm x 0.60 mm. Each DICOM image stack was imported into the VG Studio v3.0 software package to generate digital volume cross-sections for analysis.

All cores were subsequently opened, split and cleaned. Clean sediment surfaces were then **described macroscopically**, with special attention for structures, textures, components and features that are characteristic of event deposits caused by either earthquake shaking (i.e. Fuji Five Lakes) or of tsunami inundation (i.e. Lake Hamana or coastal lowlands).

X-ray radiography was performed at ULiège on all split cores from the Fuji Five Lakes.

Core surfaces were also photographed, using a Geoscan V **colour line-scan camera**, mounted on a GEOTEK multi-sensor core logger (MSCL) at UGent.

The GEOTEK MSCL was also used to produce continuous, along-core records of **magnetic susceptibility** values (with a Bartington MS2E point sensor), **gamma-density** values and **spectrophotometric properties** (with a Konica Minolta CM-2600d spectrophotometer) at a resolution of 2 mm.

Some cores were selected for **XRF scanning**, using different systems:

- the Avaatech XRF Core Scanner at MARUM was used to scan the piston cores from Lake Hamana, at 10 mm resolution, and Lake Motosu, at 2 mm resolution,
- the Avaatech XRF Core Scanner at the University Savoie-Mont-Blanc was used to scan the gravity cores from the Fuji Five Lakes and piston cores from Lake Sai and Lake Kawaguchi, all at 2 mm resolution,
- the ITRAX XRF Core Scanner at UCologne was used to scan some of the vibrocores from Sagara, at 2 mm resolution.

XRF scanning generates semi-quantitative elemental composition data, expressed in counts per second (cps).

3.3.1.2. *Sedimentological and geochemical analyses*

In order to make a first, rapid sediment classification (i.e. mineralogy, provenance, form, size) and assessment of the presence of e.g. microfossils, **smear slides** were prepared of selected samples from the vibrocores from Sagara (at GSB) and gravity cores from Lake Yamanaka (at ULiège).

Grain-size distributions were measured by laser diffraction, using different systems:

- a Malvern Mastersizer 2000 at ULiège was used to analyze several of the gravity and piston cores from the Fuji Five Lakes, at 5 mm (and sometimes 20 mm) along-core intervals,
- a Malvern Mastersizer 3000 at UGent was used to analyze one of the piston cores from Lake Hamana, at a resolution of 50-100 mm for intervals with background deposits and of 10-20 mm for intervals that deviated from background,
- a Beckman Coulter LS 13 320 particle size analyser with aqueous liquid module at UDurham was used to analyze the six surface samples and sand-rich intervals in vibrocores from the Shirasuka coastal lowlands.

Grain-size distribution parameters were calculated according to Folk & Ward (1957), or using the Gradistat 8.0 Excel software (Blott & Pye, 2001).

Water content, organic-matter content and carbonate content of the sediments were measured using the loss-on-ignition (LOI) procedure, by heating sediment samples in a muffle furnace and measuring weight loss after heating at 105°, 550° and 950°, respectively. The analysis was conducted at ULiège for gravity cores from the Fuji Five Lakes and piston cores from Lake Sai, all at a resolution of 10 mm.

To identify the source of the organic matter in the cores of Lake Motosu and Lake Yamanaka, the **C/N ratio** was measured on selected samples using an elemental analyzer (Elementar) coupled with a mass spectrometer ISOPRIME 100 at ULiège.

To validate the elemental variations obtained by XRF scanning and to obtain a **quantitative elemental composition**, selected samples of lacustrine sediment and scoria deposits from the Fuji Five Lakes were analyzed using a Thermo Scientific ARL PERFORM'X Sequential X-Ray Fluorescence Spectrometer at ULiège.

The **bulk and clay mineralogical composition** of sediments from the Fuji Five Lakes was investigated on selected samples. The XRD spectra were acquired on a PANalytical Empyrean XRD, at GSB, for bulk mineralogy, and on a Bruker D8 ADVANCE diffractometer equipped with CuK α radiation ($\lambda = 1.518 \text{ \AA}$), at ULiège, for clay mineralogy. The mineral identification was done using the DIFFRACT software.

SEM images were produced from selected samples to characterize and image the composition of sediments from the Fuji Five Lakes and from Sagara, using the ESEM Philips XL-30 at ULiège and/or the QUANTA 200 at GSB.

In order to identify some of the tephra encountered in the sediments of Lake Motosu, **major element analyses of tephra glass shards** were performed with a CAMECA-SX 100 Electron Microprobe (EPMA CAMPARIS) at UParisVI. Ten elements were analyzed (Na, Mg, Si, Al, P, K, Ca, Ti, Mn and Fe).

3.3.1.3. *Paleo-ecological analyses*

In order to identify transport and deposition by tsunamis (or storm surges) in the vibrocores from the Shirasuka coastal lowlands, diatoms, pollen and non-pollen palynomorphs were used.

Samples from vibrocores JSH3/F and JSH3/O were prepared for **diatom analysis** using standard procedures (Palmer & Abbott, 1986). Focus was on sand layers and the immediately overlying and underlying sediments, and samples were taken at intervals of 20 to 50 mm. At least 250 diatoms were identified per sample. Nomenclature followed Kobayasi (2006), Hartley et al. (1996), Sawai & Nagumo (2003) and Chiba et al. (2016).

Pollen and non-pollen palynomorphs were analyzed from a total of 15 samples from vibrocores JSH3/F and JSH3/O and the contemporary surface of the paddy field. Samples were processed using standard techniques for pollen analysis (Moore et al., 1991). Identifications are based on Beug (2004) and Demske et al. (2013) for pollen and Van Geel (1978; 2001) for other palynomorphs.

3.3.2. *Geochronology*

3.3.2.1. *Radionuclide dating*

In order to calculate sediment accumulation rates and ages of recent sediments (ca. 150 years) measurements of **short-lived radionuclide** activity (i.e. ^{210}Pb , ^{226}Ra and ^{137}Cs) can be used (Oldfield & Appleby, 1984). Pb/Cs radionuclide dating was performed at UBordeaux on freeze-dried samples from gravity cores from Lake Hamana and from the Fuji Five Lakes and from a vibrocore from the Shirasuka coastal lowlands, utilizing a low-background, high-efficiency, well-shaped gamma-ray detector (CANBERRA) (Schmidt & De Deckker, 2015). Excess ^{210}Pb ($^{210}\text{Pb}_{\text{xs}}$) was calculated as the difference of the total ^{210}Pb activity measured in the sediment and the activity supported by its parent isotope ^{226}Ra . The most widely used models for calculating sedimentation rates or ages from $^{210}\text{Pb}_{\text{xs}}$ profiles are Constant Initial Concentration, Constant Rate of Supply or Constant Flux–Constant Sedimentation

(CF:CS) (Appleby & Oldfield, 1978). Considering the generally low $^{210}\text{Pb}_{\text{xs}}$ activities, the CF:CS model was used here, which has the effect of smoothing minor variability (Appleby, 1998). The ^{137}Cs profile was used as an independent time marker. Anomalies in ^{137}Cs activity in sediments are commonly used to identify three events: i.e. 1963 (related to the maximum intensity of nuclear weapon testing), 1986 (related to the Chernobyl nuclear disaster) and 2011 (related to the Fukushima Dai-ichi nuclear disaster, caused by the Tōhoku-oki earthquake and tsunami). In Japan, only the 1963 and 2011 anomalies in ^{137}Cs are recorded.

3.3.2.2. Radiocarbon dating

A total of 94 samples, taken from lake cores as well as coastal lowland cores and mostly consisting of macroscopic plant remains, such as leaf fragments, pieces of wood and twigs, but occasionally also of bulk sediment, were used for **AMS- ^{14}C dating**, at different facilities:

- the National Electrostatics Corporation (NEC) 250 kV single-stage accelerator mass spectrometer at UTokyo,
- the Mini radioCarbon Dating System (MICADAS) accelerator mass spectrometer, with acceleration fields in tandem configuration (Synal et al., 2007), at ETHZürich,
- the Mini radioCarbon Dating System (MICADAS) accelerator mass spectrometer at RICH.

Dates are reported as ^{14}C yr BP and calibrated to calendar years prior to 1950 CE using OxCal v.4.2 (Bronk Ramsey, 2009) and the IntCal13 calibration curve (Reimer et al., 2013). All calibrated ages are expressed as 2σ ranges in years CE.

3.3.2.3. Tephrochronology

Some of the sedimentary sequences contained one or more distinct tephra layers that could be used for **tephrochronology**.

Mineralogy of tephra samples, refractive index and chemical composition of volcanic glasses from a scoria layer and a pumice layer, encountered in the piston cores from Lake Hamana and expected to represent the Osawa scoria (Osw) and the Kawagodaira pumice (Kg), respectively, were analyzed at the Paleo Labo (Japan). Identification and counting of light minerals, heavy minerals and volcanic glasses was done according to Machida & Arai (2003). The refractive index of volcanic glasses was measured according to Yokoyama et al. (1986), using the temperature changing refractometer. EDS analysis was executed using a scanning electron microscope (SEM; Keyence Corp.) and energy dispersive X-ray spectrometer (EDS, Oxford Instruments Corp. AZtecOne system). Samples of Kawagodaira pumice (Kg) and Osawa scoria (Osw) were collected from Kokushi Pass and measured for comparison.

The refractive index and the major element composition of volcanic glasses from tephra layers, encountered in the piston cores from Lake Motosu, and expected to represent either the Kozushima-tenjosan tephra (KT), the Kawagodaira pumice (Kg) or the Kikai-Akahoya tephra (K-Ah), were analysed at UParisVI. The refraction index was measured using the oil immersion method. Wavelength-dispersive X-ray spectroscopic (WDS) analysis of major elements of glass shards was performed with a CAMECA-SX 100 Electron Microprobe (EPMA CAMPARIS).

3.3.2.4. OSL-dating

In order to obtain independent ages from a series of sand layers recorded in the vibrocores from the Shirasuka coastal lowlands, their quartz and alkali-feldspar fractions were sampled for OSL dating at UCologne and UAberystwyth. Tests of the

quartz material indicated that, in accordance with other studies on Japanese quartz (e.g. Tsukamoto et al., 2003; Tamura et al., 2015), it shows inappropriate luminescence properties, which renders it unsuitable for quartz OSL dating.

For determining dose rates, U, Th and K contents were measured by high-resolution gamma spectrometry with an Ortec Profile MSeries GEM Coaxial P-type high-precision Germanium Gamma-Ray detector at UCologne. The stratigraphy of the Shirasuka lowlands is complex and shows abrupt changes in grain size, which may cause variations in the gamma dose rate. Layer-to-layer variations in gamma dose rate were calculated according to Aitken (1985). DRAC v1.1 (Durcan et al., 2015) was used to calculate internal and external alpha and beta dose rates, and to correct them for water content. Conversion factors for gamma and beta dose rates are based on Adamiec & Aitken (1998). Alpha and beta grain size attenuation factors of Bell (1980) and Guerin et al. (2012, for feldspars), respectively, were applied. The cosmic dose rate was determined in accordance with Prescott & Hutton (1994).

Luminescence measurements were made using single-aliquot regenerative dose (SAR) protocols on Risø TL/OSL readers equipped with $^{90}\text{Sr}/^{90}\text{Y}$ beta sources. Fading measurements were conducted according to Auclair et al. (2003). Ages were corrected for fading using the correction model of Huntley & Lamothe (2001) implemented in the R-package 'Luminescence' (Kreutzer et al., 2012; Kreutzer, 2016).

4. SCIENTIFIC RESULTS AND RECOMMENDATIONS

4.1. Review of geological evidence of earthquakes and tsunamis along the Nankai-Suruga Trough

This section comprises *capita selecta* from Garrett et al. (2016). For more comprehensive information, please refer to Garrett et al. (2016).

4.1.1. Available geological evidence of earthquakes and tsunamis

The combined evidence from the 72 sites included in our literature review (for some of which the available chronological data were recalibrated and harmonized, and new age models were produced) constituted the state of knowledge regarding geological records of past earthquakes and tsunamis along the Nankai-Suruga Trough at the onset of the QuakeRecNankai project (Figure 15).

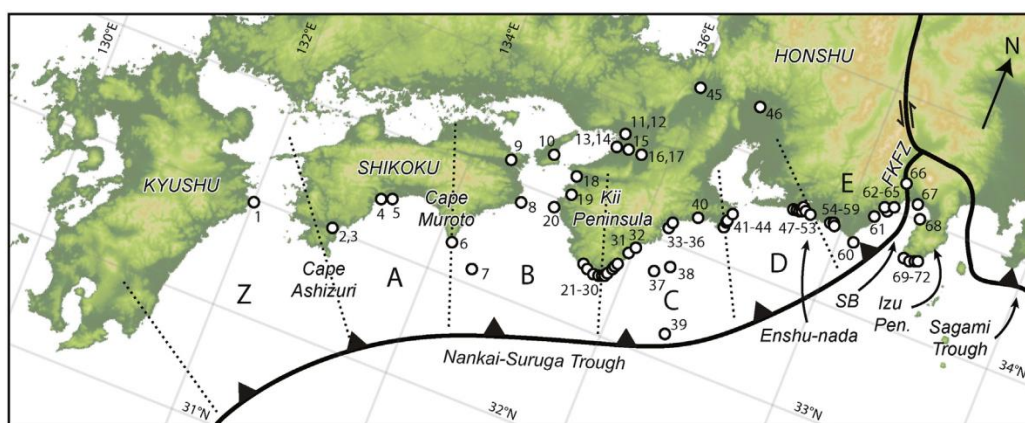


Figure 15: Summary map of proposed sites with evidence for past megathrust earthquakes along the Nankai-Suruga Trough. Site numbers: 1 Ryūjin pond*; 2 Azono*; 3 Funato*; 4 Tadasu pond†; 5 Kani pond*; 6 Cape Muroto; 7 Tosabae Trough‡; 8 Kamoda Lake*; 9 Itanochō*; 10 Shimonaizen*; 11 Kosaka-tei-ato*; 12 Ikeshima Fukumanji*; 13 Iwatsuta Shrine*; 14 Sakai-shi Shimoda*; 15 Tainaka*; 16 Hashio*; 17 Sakafuneishi*; 18 Kawanabe*; 19 Fujinami*; 20 Hidaka Marsh§; 21 Kuchiwabuka†; 22 Ameshima†; 23 Shionomisaki†; 24 Izumozaki†; 25 Arafunezaki†; 26 Ikeshima†; 27 Yamamibana†; 28 Taiji†; 29 Suzushima†; 30 KiiSano§; 31 Atawa§; 32 Shihara§; 33 Ōike pond†‡; 34 Umino pond§; 35 Suwa pond†; 36 Katagami pond§; 37 Kumano Trough W*†; 38 Kumano Trough E†‡; 39 IODP core C0004†; 40 Kogare pond§; 41 Funakoshi pond§; 42 Shijima lowlands§; 43 Kō§; 44 Ōsatsu Town†; 45 Lake Biwa*; 46 Tadokoro*; 47 Nagaya Moto-Yashiki†; 48 Shirasuka†; 49 Arai†; 50 Goten-ato*; 51 Lake Hamana†; 52 Rokken-gawa lowlands†; 53 Hamamatsu lowlands§; 54 Ōtagawa lowlands†; 55 Fukuroi-juku*; 56 Sakajiri*; 57 Tsurumatsu*; 58 Harakawa*; 59 Yokosuka lowlands†; 60 Omaezaki; 61 Yaizu Plain§; 62 Agetsuchi*; 63 Kawai*; 64 Ōya lowlands†‡; 65 Shimizu Plain†; 66 Fujikawa-Kako Fault Zone; 67 Ukishima-ga-hara†; 68 Ita lowlands†‡; 69 Iruma§; 70 Minami-Izu§; 71 Kisami§; 72 Shimoda†. Sites with calibrated ages taken from original publications marked *, sites with ages recalibrated in this review marked †, sites with ages modelled in this review marked ‡, sites with no chronological data or where chronological data cannot be related to paleoseismic evidence marked §. Abbreviations: SB: Suruga Bay, FKFZ: Fujikawa-Kako Fault Zone, letters Z, A, B, C, D and E refer to seismic segments. Modified from Garrett et al. (2016).

Remarkably, only a limited sub-set of these sites has turned out to provide really unequivocal evidence for coseismic deformation, shaking or tsunami inundation. Below, we highlight those sites with the best available geological evidence for earthquakes and tsunamis for the last ~1350 years, summarize the rupture zones of historical earthquakes and discuss occurrence intervals and variability in rupture modes.

4.1.1.1. Rupture zones of historical earthquakes

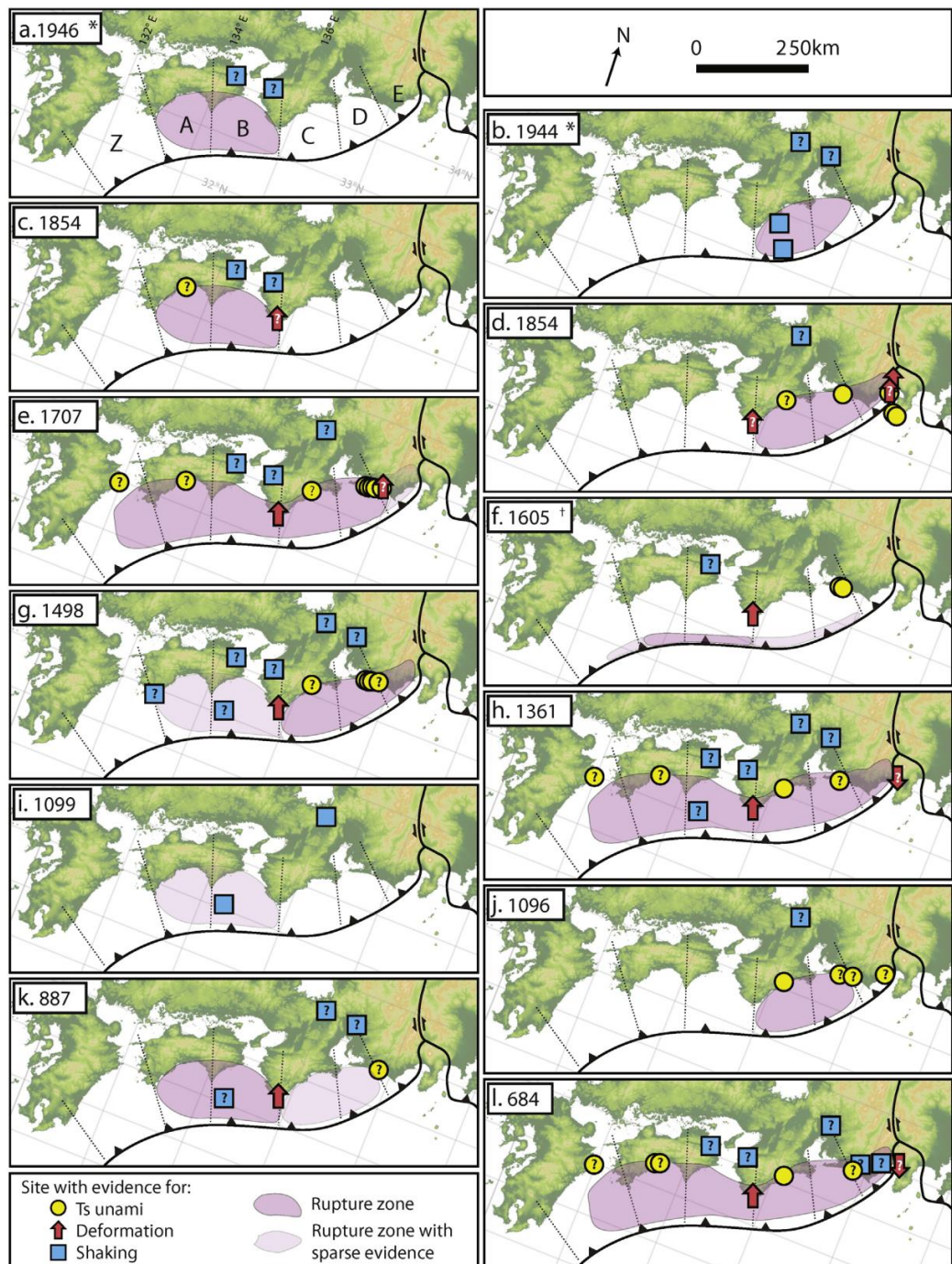


Figure 16: Summary of inferred rupture zones of historical great Nankai-Suruga Trough earthquakes and the distribution of associated geological evidence. Question marks indicate uncertainty over the chronology or the origin of evidence at a site. *Rupture zones of the 1946 CE and 1944 CE earthquakes are approximated from Baba & Cummins (2005) and Tanioka & Satake (2001a; 2001b). †Rupture zone of the 1605 CE earthquake is following Ando & Nakamura (2013) and Park et al. (2014). From Garrett et al. (2016).

The 1944 CE Shōwa-Tōnankai and 1946 Shōwa-Nankai earthquakes

Slip during the 1944 CE earthquake occurred to the east of the Kii Peninsula (segments C and D), but did not extend to segment E (Figure 16b). In 1946 CE, two years later, a non-overlapping rupture released strain in segments A and B to the west of the Kii

Peninsula (Figure 16a).

- > Geological records are sparse for both earthquakes, although shaking in 1944 CE may have been recorded in turbidite and mud-breccia records from the Kumano Trough (Sakaguchi et al., 2011; Shirai et al., 2010) and in liquefaction deposits at Tadokoro (Sangawa, 2009). Archaeological sites on the western side of the Kii Peninsula and in eastern Shikoku record liquefaction possibly resulting from the 1946 CE earthquake (Sangawa, 2009). Published records of sedimentary and geomorphological evidence for tsunami deposition or coseismic deformation are scarce and this may reflect anthropogenic reworking on heavily cultivated and industrialized coastlines.

The 1854 CE Ansei-Tōkai and Ansei-Nankai earthquakes

Separated by just 32 h, these two earthquakes together ruptured segments A to E (Figure 16c). The first earthquake ruptured the three segments east of the Kii Peninsula (Figure 16d). The following day, the second earthquake ruptured segments A and B (Ando, 1975b; Ishibashi, 2004).

- > Tsunami deposits at Shirasuka (Komatsubara et al., 2008) as well as potential evidence for boulder transport at Shimoda (Kitamura et al., 2014), rupture of the Fujikawa-Kako Fault Zone (Lin et al., 2013) and uplift at Shimizu (Kitamura & Kobayashi, 2014) provide compelling evidence for the Ansei-Tōkai event.
- > Paleoseismic evidence for this second event is limited (Figure 16d), with Okamura & Matsuoka (2012) proposing a sand layer at Kani pond as evidence of tsunami inundation and Sangawa (2009) making reference to liquefaction at Itano-chō. Uplifted sessile organisms reported by Shishikura et al. (2008) at three locations on the southern tip of the Kii Peninsula may also reflect coseismic deformation during either of the 1854 CE earthquakes.

The 1707 CE Hōei earthquake

Historical records suggest the 1707 CE Hōei earthquake included both of the regions that ruptured in the two 1854 CE earthquakes (Ando, 1975b; Ishibashi, 2004). The inferred rupture zone, comprising segments A to E, exceeds 600 km in length (Figure 16e).

- > Geological evidence for the earthquake and accompanying tsunami also spans much of the length of the Nankai-Suruga Trough, with possible evidence for tsunami inundation at Ryūjin pond in segment Z (Okamura & Matsuoka, 2012) and at Nagaya Moto-Yashiki and Shirasuka in segment D (Komatsubara et al., 2008; Takada et al., 2002). Also in segment D, uplift may be recorded by a change in facies on the Yokosuka lowlands (Fujiwara et al., 2007a), while in the centre of the subduction zone, sessile organisms suggest coseismic uplift of the southern Kii Peninsula (Shishikura et al., 2008).
- > Furumura et al. (2011) argue that evidence from Ryūjin pond favours the westwards extension of the rupture zone to include at least part of the Hyūganada segment (Z). Modelled tsunami run-up heights from ruptures excluding this segment are insufficient to inundate the pond or to match documented run-up heights in eastern Kyushu and western Shikoku. No geological evidence for the 1707 CE earthquake has yet been proposed from segment E.

The 1605 CE Keichō earthquake

Historically records of effects of the 1605 CE Keichō earthquake are notably scarce (Ando, 1975b; Ishibashi, 2004). Yamamoto & Hagiwara (1995), however, report documentary evidence for tsunami run-up heights exceeding 5 m at locations in

segments A to D. Reports suggest the occurrence of a tsunami earthquake, with Ando & Nakamura (2013) consequently suggesting a rupture zone located along a shallow portion of the plate interface, up-dip of the main seismogenic zone in segments A to D (Figure 16f).

- > Geological evidence for tsunami inundation and vertical land-level change is scarce, but consistent with this rupture zone. Potential tsunami deposits are reported from coastal lowlands at Shirasuka (Komatsubara et al., 2008) and Nagaya Moto-Yashiki (Takada et al., 2002), both in segment D. Age ranges from emerged sessile organisms at Yamamibana (Shishikura et al., 2008) and liquefaction features at Itano-chō (Sangawa, 2001) also overlap with this earthquake.

The 1498 CE Meiō earthquake

The 1498 CE Meiō earthquake is thought to have ruptured segments C to E (Figure 16g).

- > Along the Enshū-nada coastline, sand sheets at Nagaya Moto-Yashiki (Takada et al., 2002) and Shirasuka (Komatsubara et al., 2008) and environmental change recorded at Arai (Fujiwara et al., 2013a) and Lake Hamana (Honda & Kashima, 1997) support historical records of a damaging tsunami (Fujiwara et al., 2013a). Emerged sessile organisms at Shionomisaki may indicate coseismic uplift of the southern Kii Peninsula at this time (Shishikura et al., 2008).
- > Proposed liquefaction features from segments A and B (Sangawa, 2001; 2009) could imply a rupture zone extending further west than previously suggested, however further historical and geological evidence is required to test this hypothesis.

The 1361 CE Shōhei earthquake

With evidence proposed from all six segments of the Nankai-Suruga Trough, the distribution of sites recording the 1361 CE Shōhei earthquake and tsunami is similar to that of the 1707 CE Hōei earthquake (Figure 16h).

- > Okamura & Matsuoka (2012) suggest inundation of coastal lakes in segments Z and A, with potential tsunami inundation also recorded at Ōike pond in segment C (Tsuji et al., 2002).
- > Subsidence at Ukishima-ga-hara in segment E may relate to the 1361 CE earthquake (Fujiwara et al., 2007b; 2016), while Shishikura et al. (2008) document evidence for uplift of the Kii Peninsula at the boundary between segments B and C. As in 1707 CE, this episode of uplift was not followed by reoccupation of sessile organism encrustations, suggesting a larger magnitude of uplift or a lack of subsequent interseismic subsidence. Turbidite occurrence in Lake Biwa (Inouchi et al., 1996) and liquefaction at sites on the western side of the Kii Peninsula and at Tadokoro (Sangawa, 2001; 2009) has also been linked to shaking during this earthquake.

While the similarity in the distribution of evidence with the 1707 CE earthquake and the comparable permanent uplift of the Kii Peninsula (Shishikura et al., 2008) points towards a single large rupture, the potential for two smaller temporally closely spaced ruptures of segments east and west of the Kii Peninsula (cf. Ishibashi, 2004) cannot be conclusively discounted on the basis of geological evidence alone.

Ishibashi (1999; 2004) suggests the occurrence of one or more great earthquakes during the 13th century. While Ishibashi (1998) dismisses an earthquake in 1233 CE reported by Usami (1996) as fictitious, evidence of liquefaction from archaeological

sites in segments B and E (Sangawa, 2001) does support the occurrence of intense shaking in the interval between the historically documented earthquakes in 1099 CE and 1361 CE. While other processes cannot be discounted for their deposition, sand layers at Nagaya Moto-Yashiki could reflect tsunami deposition during this time (Takada et al., 2002). The number, timing and rupture zones of earthquakes occurring during the 12th and 13th centuries remain unknown and should be the focus of further historical and geological investigation.

The 1099 CE Kowa earthquake

Despite the lack of a historically documented tsunami, Ando (1975b), Ishibashi (1999; 2004) and others list the 1099 CE Kowa earthquake as a megathrust earthquake rupturing segments A and B (Figure 16i). The absence of a tsunami and restricted evidence for intense shaking suggests the rupture zone may not have been analogous to the later 1854 CE and 1946 CE Nankai earthquakes. Instead, the 1099 CE earthquake may have ruptured a smaller area of the plate interface or an upper plate fault.

- > Geological evidence for this earthquake is severely limited. While turbidites are proposed from the Tosabae Trough (Iwai et al., 2004) and Lake Biwa (Inouchi et al., 1996), neither site is underpinned by a chronology that is robust enough to discount other possible earthquakes. Consequently, there is currently insufficient evidence to consider the 1099 CE Kowa earthquake as a magnitude 8-class subduction megathrust earthquake.

The 1096 CE Eichō earthquake

The rupture zone of the 1096 CE Eichō earthquake, derived from historical records, incorporates segments C and D (Ishibashi, 1999; 2004).

- > Evidence for potential tsunami inundation at Ōike and Suwa ponds in segment C (Tsuji et al., 2002), Nagaya Moto-Yashiki in segment D (Takada et al., 2002) and the Ōtagawa lowlands (Fujiwara et al., 2013a) and Ōya lowlands (Kitamura et al., 2013) in segment E support this interpretation (Figure 16j).

The 887 CE Ninna earthquake

Historical records suggest the 887 CE Ninna earthquake ruptured segments A and B (Ando, 1975b; Ishibashi, 1999).

- > Paleoseismic evidence from these segments is limited (Figure 16k). Turbidite emplacement in the Tosabae Trough in segment B may have occurred around this time, while ages from sessile biota at Ameshima and Suzushima on the Kii Peninsula are also consistent with coseismic uplift in 887 CE (Shishikura et al., 2008).

Ishibashi (2004) suggests concurrent rupture of segments C and D based on historical records.

- > Evidence for shaking at Tadokoro (Sangawa, 2009) could support this eastwards extension. Further dating is required to confirm the association of a proposed tsunami deposit on the Ōtagawa lowlands in segment E with this earthquake (Fujiwara et al., 2008).

The 684 CE Tenmu earthquake

Ando (1975b) maps the 684 CE Tenmu earthquake as a rupture of segments A and B, with Ishibashi (1999; 2004) tentatively extending the rupture zone into segments C, D and E (Figure 16l).

- > Paleoseismic evidence supports this larger rupture zone, with possible evidence

for coseismic subsidence of the Ukishima-ga-hara lowlands at the eastern end of the subduction zone (Fujiwara et al., 2007b; 2016). Sangawa (2001; 2009) additionally attributes liquefaction features in segments D and E to this earthquake, while Shishikura et al. (2008) provide evidence for the abrupt uplift of the southern tip of the Kii Peninsula. To the west of the peninsula, sand sheets in Ryūjin, Tadasu and Kani ponds suggest tsunami inundation (Okamura & Matsuoka, 2012). As in 1707 CE and 1361 CE, inundation of Ryūjin pond may support rupture of at least part of segment Z during the 684 earthquake, however further shoreline reconstructions and modelling efforts are required (Furumura et al., 2011).

Temporally closely spaced ruptures of more limited spatial extent provide an alternative hypothesis for the evidence that has been linked to the 684 CE earthquake.

4.1.1.2. *Intervals between earthquakes*

Historical records suggest earthquakes ruptured part or all of the Nankai-Suruga Trough twelve times between 684 CE and 1946 CE, yielding an average interval ($\pm 1 \sigma$) for major or great earthquakes occurring anywhere along the subduction zone of 115 ± 89 years. An average belies the variability in occurrence, with individual intervals ranging from 32 h between the two 1854 CE earthquakes to 262 years between the 1099 CE and 1361 CE earthquakes. Looking at the intervals between ruptures of the same area of the plate interface (rather than the subduction zone as a whole), the shortest intervals are 92 years for the Hyūga-nada and Nankai segments (Z, A and B) and 90 years for the Tōnankai and Tōkai segments (C, D and E). Rejecting the 1099 CE earthquake as a great interplate earthquake due to the lack of records of tsunami occurrence and the paucity of geological data, the longest interval between two ruptures of the same segment is the 474 years that separated the 887 CE Ninna and 1361 CE Shōhei earthquakes. If the 1605 CE earthquake occurred solely at the shallowest portion of the interface (Ando & Nakamura, 2013), the main seismogenic zone may not have ruptured for the 209 years between 1498 CE and 1707 CE. Furthermore, if the 1498 CE earthquake did not extend into the Nankai region (segments A and B), this interval may be extended further back to encompass the 376 years between 1361 CE and 1707 CE. Shorter intervals may, however, be inferred if additional great earthquakes occurred during periods with fragmentary and incomplete documentary records. Further geological and historical research is required to resolve these uncertainties.

Paleoseismic records have the potential to yield information on intervals between earthquakes over timescales longer than the historical record. However, only a few sites along the Nankai-Suruga Trough display suitably long, well-dated sequences. Okamura & Matsuoka (2012) suggest Tadasu pond records 14 tsunamis at consistent intervals averaging 270 years, while Ryūjin pond records longer and more variable intervals of between 300 and 700 years. The authors note that later tsunamis may erode sedimentary evidence for earlier inundations, resulting in longer apparent intervals. Modelling of the timing of sand sheet emplacement on the Ōsatsu lowlands (Okahashi et al., 2005) suggests the eight intervals average 400–600 years (2σ). P_{sequence} modelling of the Tosabae Trough record (Iwai et al., 2004) indicates an average interval between turbidites of 200–230 years over the last 5500 years. Sequence modelling of the timing of five episodes of coseismic subsidence on the Ukishima-ga-hara lowlands (Fujiwara et al., 2016) suggests intervals of < 100 years, with an average of 180–200 years. The occurrence intervals for each site reflect both the true intervals between megathrust earthquakes and also site-specific thresholds.

A site's paleoseismic record only includes the earthquakes or tsunamis that exceed both creation and preservation thresholds (Nelson et al., 2006; McCalpin & Nelson, 2009). Consequently, a single site may underrepresent the number of earthquakes or tsunamis within a given period if a sub-set of these events fail to exceed the site's thresholds. A site may also potentially overestimate earthquake frequency due to misidentification of features of a non-seismic origin as paleoseismic evidence.

4.1.1.3. Maximum earthquake and tsunami size

The historical records suggest that the six proposed segments of the Nankai-Suruga Trough ruptured together during a single great earthquake in 1707 CE. No geological evidence for this earthquake has yet been proposed from segment E; whether the rupture extended this far east remains equivocal and future investigations should focus on the coastal lowlands fringing Suruga Bay and on the Fujikawa-Kako Fault Zone to resolve this question. Geological evidence suggests that the earthquakes of 1361 CE and 684 CE may have been of similar rupture length. There is no published geological evidence that currently suggests that earthquakes with longer rupture lengths have occurred along the Nankai-Suruga Trough; however, few attempts have been made to use geological evidence to compare the absolute or relative magnitudes of different historical or prehistorical earthquakes in this region (Komatsubara & Fujiwara, 2007; Komatsubara et al., 2006a).

Several attempts have been made to address the related question of the relative sizes of tsunamis to have impacted coastlines facing this subduction zone. Investigating records of tsunami deposition in coastal lakes, Okamura & Matsuoka (2012) link the presence or absence of sand layers and their characteristics to variation in the height of tsunamis striking western Kyushu and southern Shikoku. While Ryūjin pond preserves evidence for the 1707 CE tsunami, the absence of sand layers relating to the subsequent 1854 CE and 1946 CE tsunamis suggests they were not of comparable height and did not inundate the lake. The presence of deposits related to the 1361 CE and 684 CE tsunamis at Ryūjin and Kani ponds, suggests that these tsunamis may have been of comparable size to the 1707 CE tsunami in this location. The potential for variation in the threshold for evidence creation must be considered, with changing relative sea level, shoreline progradation, the height of the tide at the time of tsunami impact and the availability of erodible sediment also important factors.

The compilation of assessments of the maximum inland extent of tsunami deposits with detailed reconstructions of shoreline positions over time may facilitate comparison of the relative inundation distances of past tsunamis. While further chronological and stratigraphic information is required, initial findings suggest no tsunami during the historical period has inundated the most landward regions of the lowlands to the east of Lake Hamana (Fujiwara, 2013; Fujiwara et al., 2013b). On the Rokken-gawa and Hamamatsu lowlands, swales 3–5 km inland from the present coastline only preserve evidence for tsunamis older than 3150 cal yr BP. More recent tsunami deposits are confined to swales closer to the current coastline, suggesting that over the last few thousand years, no tsunami has inundated the whole of the Hamamatsu coastal plain (Fujiwara, 2013). The continued development of this approach and its replication in other regions along the Nankai-Suruga Trough may provide additional constraints on the largest inundation distances associated with past tsunamis. Such studies and associated modelling of source fault ruptures must, however, acknowledge that true inundation distances may considerably exceed the inland extent of identifiable coarse-grained deposits (Abe et al., 2012; Goto et al.,

2011; Shi et al., 1995).

While the maximum amplitude of tsunami waves in far-field locations (those located separated by ocean basins from their source earthquakes) correlates with earthquake magnitude, this relationship breaks down in locations close to the source (Abe, 1979). Consequently, the largest tsunamis to have struck locations along the Nankai-Suruga Trough may not have been generated by the largest earthquakes. Further field evidence for maximum tsunami run-up heights, inundation distances and their along-strike distribution should be sought to address the question of the maximum size of Holocene tsunamis.

4.1.1.4. Rupture modes, segmentation and supercycles

Historical records, supported by geological data, suggest the Nankai-Suruga Trough is characterized by six segments, with earthquakes rupturing the subduction zone in a range of different multi-segment combinations. The occurrence of full-length ruptures in 1707 CE, 1361 CE and 684 CE, with earthquakes of lesser magnitude rupturing smaller areas of the fault during the intervening periods, suggests the existence of supercycle behavior (cf. Cisternas et al., 2005; Goldfinger et al., 2013; Herrendörfer et al., 2015; Sieh et al., 2008). Such fault behaviour is currently difficult to identify over the longer timescales afforded by geological evidence. Nevertheless, the repeated reoccupation of sessile biotic encrustations on the southern tip of the Kii Peninsula before final, permanent abandonment, could support this hypothesis (Shishikura et al., 2008; Shishikura, 2013). Within each encrusting mass, up to three or four mortality events are each followed by colony reoccupation, before a final uplift episode with no subsequent reoccupation. Shishikura et al. (2008) suggest this could reflect a series of moderate episodes of coseismic uplift, each followed by interseismic subsidence, before a final episode of oversized coseismic uplift. Whether such oversized uplift is associated with a larger earthquake incorporating a greater number of segments and/or variation in the depth of slip on the plate interface remains unresolved. Hyodo & Hori (2013) provide a potential mechanism for variation in coseismic deformation between different earthquakes, with their numerical model suggesting that larger earthquakes could feature slip to the trench, while smaller ruptures are restricted to the main seismogenic zone.

The 1605 CE earthquake stands out as dissimilar from other Nankai-Suruga Trough ruptures, with historical records suggesting an extensive and damaging tsunami despite a lack of strong ground motion (Ando, 1975b; Ishibashi, 2004). As discussed above, these characteristics are consistent with a tsunami earthquake, with slip restricted to the shallowest portion of the interface. With a plate convergence rate of 50 mm/year, just 100 years are required to accumulate sufficient slip to explain the historically documented tsunami run-up heights (Ando & Nakamura, 2013). The lack of other records of such tsunami earthquakes (Ando, 1975b; Ishibashi, 2004) suggests that shallow slip typically occurs simultaneously with ruptures of the main seismogenic zone or that the shallow portions of the interface are only partially locked. There is currently insufficiently geological evidence to identify the occurrence of prehistorical tsunami earthquakes along the Nankai-Suruga Trough.

Ando (1975a) and Ishibashi (1976; 1981) identified the Tōkai region (segment E) as a mature seismic gap, a finding that contributed to the implementation of the 1978 Large Scale Earthquake Countermeasures Act by the Japanese Government and the intensive and ongoing monitoring of the region by the Japanese Meteorological

Agency (Rikitake, 1979). The frequency of ruptures of the Tōkai segment and the simultaneity with ruptures of the Tōnankai region (segments C and D) remain poorly understood. Geological or historical records support rupture of both regions in 1854 CE, 1707 CE, 1361 CE and 684 CE, while instrumental records suggest the 1944 CE earthquake ruptured only the Tōnankai segments and did not extend eastwards into the Tōkai segment. An episode of coseismic subsidence identified from the Ukishima-ga-hara lowlands does not correlate with any major historically documented earthquake (Fujiwara et al., 2007b; 2016) and could reflect an undocumented rupture of the Tōkai segment or of the Fujikawa-Kako Fault Zone. A lack of further paleoseismic evidence for independent rupture of segment E could reflect the magnitudes of coseismic deformation, shaking and tsunami inundation being insufficient to surpass thresholds for evidence creation, rather than the absence of single segment earthquakes in this location.

4.1.2. Current problems for assessing seismic hazard from the available geological evidence

Despite the breadth of sites included in this review and the length of some of the resulting paleo-earthquake records, a complete and coherent picture of the timing, occurrence intervals, rupture zones and magnitudes of past earthquakes along the Nankai-Suruga Trough cannot currently be derived from geological data. This is in contrast to other subduction zone settings, where the integration of records from multiple sites has yielded a more comprehensive understanding of prehistorical great earthquakes, including in Alaska (Shennan et al., 2014a; 2014b), Cascadia (Goldfinger et al., 2012; Nelson et al., 2006) and Chile (Moernaut et al., 2014).

Four key issues currently limit the contribution of paleoseismic records to understanding seismic hazards along the Nankai-Suruga Trough:

- alternative hypotheses for proposed paleoseismic evidence;
- insufficient chronological control to correlate between evidence at different sites;
- research designs insufficient to address maximum earthquake and tsunami magnitudes; and
- incomplete appreciation of the variation in paleoseismic thresholds over time and between sites.

These issues are not unique to the Nankai-Suruga Trough and the identified difficulties and subsequent recommendations presented below have implications for paleoseismic research globally.

4.1.2.1. Alternative hypotheses

Geological records may over-represent the frequency of earthquakes or tsunamis when features of a non-seismic origin are incorrectly identified as paleoseismic evidence. Misidentification arises from equifinality, the principle that dissimilar processes can produce similar sedimentary or geomorphic signatures (Chorley, 1962; McCalpin & Nelson, 2009). Along the Nankai-Suruga Trough, this typically also affects the most widely investigated lines of evidence: i) turbidites, ii) liquefaction features, and iii) tsunami deposits.

- i) Marine and lacustrine sediment sequences have the potential to preserve long, continuous records of intense shaking during multiple great earthquakes. While Lake Biwa records turbidites at closely spaced intervals, storms, hyperpycnal river discharge and shaking during smaller, more local crustal earthquakes may also induce turbidity currents (Talling, 2014; Shirai et al., 2010). Such alternative hypotheses are yet to be conclusively discounted for either the Lake Biwa record

or offshore turbidite records from the Kumano and Tosabae Troughs. Indeed, the presence of turbidites in the Kumano Trough that cannot be linked to recent historical earthquakes indicates that local seismicity or non-seismic processes must also be active (Shirai et al., 2010). The issue of equifinality affects turbidite paleoseismology globally and key ways forward include establishing site sensitivity through calibration of deposits with the historical record, correlation of multiple cores using independent marker horizons (e.g. tephtras), sedimentary provenance analysis, and confluence tests (Goldfinger et al., 2012; Moernaut et al., 2014; Pouderoux et al., 2014; Van Daele et al., 2015).

- ii) Similarly considered a record of intense shaking during great earthquakes, liquefaction features may also suffer from overrepresentation caused both by shaking during smaller earthquakes and the misidentification of similar sedimentary features of non-seismic origin (Obermeier, 1996; 2009). As earthquakes with $M_s \geq 5$ are capable of generating peak ground accelerations large enough to cause liquefaction (Ambraseys, 1988), the occurrence of local upper-plate earthquakes could explain some liquefaction features at sites along the Nankai-Suruga Trough. Particularly in sediments with very high liquefaction susceptibility, rapid sedimentation, landsliding, permafrost and artesian springs may also generate analogous sedimentary features. Along with judicious site selection to avoid the influence of some of these processes, the identification of liquefaction features at multiple locations within a few kilometers, combined with geotechnical testing, can assist in determining a seismic origin (Green et al., 2005; Olson et al., 2005).
- iii) While the papers discussed in this review frequently invoke tsunamis to explain sand sheets found in coastal lakes and lowlands adjacent to the Nankai-Suruga Trough, storm surges may also deposit coarse-grained sand sheets with similar features to the sedimentary imprints of tsunamis. Typhoon-driven storm surges occur along the Nankai-Suruga Trough and there are few seismically active regions where major storms do not occur, at least on geological timescales. The consistent and reliable differentiation between storm and tsunami deposits remains an ongoing issue for the community (Engel & Brückner, 2011; Kortekaas & Dawson, 2007; Morton et al., 2007; Shanmugam, 2012). Careful application of detailed sedimentological criteria (e.g. Komatsubara et al., 2008; Fujiwara & Tanigawa, 2014) and multi-proxy approaches (e.g. Chagué-Goff et al., 2011; Goff et al., 2012; May et al., 2015a) may assist in avoiding misidentification. Further in-depth characterization and comparison of the deposits left by recent tsunamis (e.g. Abe et al., 2012; Brill et al., 2012; Goto et al., 2014; Szczuciński et al., 2012) and storms (e.g. Hawkes & Horton, 2012; May et al., 2015a; 2015b; Williams, 2009) in a wide range of depositional settings remains crucial. Novel methods of sedimentary analysis, such as micro-computed tomography (May et al., 2015a), anisotropy of magnetic susceptibility (Schneider et al., 2014; Wassmer et al., 2010) and microfossil analysis (Uchida et al., 2010) may also assist in discriminating between the origins of different extreme wave event deposits.

4.1.2.2. *Chronological control*

The issues surrounding the use of ^{14}C to discriminate between closely-spaced events are well-documented (Atwater & Yamaguchi, 1991; Nelson et al., 1995). The short intervals between Nankai-Suruga earthquakes, known from the historical record to include periods of just hours to a few years, prevent the use of ^{14}C dating to establish unequivocal correlations between paleoseismic evidence at different sites. Such issues are less often encountered where intervals exceeding several centuries

separate recorded paleo-earthquakes, as appears to be the case in Alaska (Shennan et al., 2014b), and where earthquake timing is constrained by very high resolution chronologies, such as those based on annual varves (e.g. Moernaut et al., 2014). More precise constraints on the timing of paleoseismic evidence are clearly desirable, particularly to assist with characterizing the sedimentary fingerprint of historical earthquakes. Komatsubara & Fujiwara (2007) highlight the issue of ambiguous relationships between ^{14}C -dated samples and proposed paleoseismic evidence. We advocate for this information, including sample depth, context, material, conventional ^{14}C age and isotopic fractionation, to be routinely reported in future. Advances in radiocarbon analyses can be gained through the use of age modelling, particularly when combined with strategically planned sampling approaches (e.g. Bronk Ramsey, 2009; Lienkaemper & Ramsey, 2009). Additionally, the use of alternative dating methods, including annual varves, short lived radionuclides (^{137}Cs and ^{210}Pb), luminescence dating techniques, tephrochronology and other chronohorizons (pollen, pollution markers), may help to improve correlations between sites and between paleoseismic evidence and historically recorded earthquakes. Both age modelling and the application of a diverse suite of complementary dating approaches may serve to enhance chronological control on the sedimentary evidence for earthquakes and tsunamis along the Nankai-Suruga Trough and in other seismically impacted regions around the world.

4.1.2.3. *Research design*

The Central Disaster Management Council of the Japanese Cabinet Office emphasizes the need for greater understanding of the maximum magnitude of earthquakes and the largest possible tsunamis (Central Disaster Management Council, 2011; 2012). This deterministic approach to hazard assessment provides an alternative and complementary approach to probabilistic assessments. Nevertheless, the majority of currently published research has not been designed with questions of magnitude as a central focus. Accurate assessment of the run-up and inland extent of past tsunamis depends on detailed mapping and characterization of tsunami deposits, as well as comprehensive understanding of paleo-shorelines and sea levels (Fujiwara, 2013). At present, these complementary data are not consistently explored when interpreting tsunami deposits. While the extent of identifiable deposits may remain a minimum estimate of inundation distance, this still constitutes a valuable constraint for testing models of tsunami inundation and fault rupture (e.g. Sugawara, 2014; Witter et al., 2012). Future coastal studies should, therefore, seek to better understand paleoshoreline positions and coastal evolution and combine mapped tsunami deposit distributions with inundation and fault slip models.

Turbidite records also have the potential to provide information on the rupture extents and magnitudes of past earthquakes (e.g. Goldfinger et al., 2003; Howarth et al., 2014; Moernaut et al., 2014; Poudroux et al., 2014). While existing publications identify both lacustrine and marine basins as having the potential to hold records of shaking during past Nankai-Suruga Trough earthquakes, these sites have not been exploited to their full extent and reanalysis, combined with investigations of new locations, could yield additional insights into the largest magnitude earthquakes that have struck this subduction zone. As discussed in the preceding paragraphs, the current lack of high resolution chronologies and issues over the differentiation between seismoturbidites and those generated by other processes currently limits the utility of turbidite records. Renewed efforts should attempt to fingerprint the sedimentary record of known historical earthquakes, establish the defining

characteristics of seismoturbidites and use this understanding to exploit longer sedimentary records in marine and lacustrine settings.

Additional paleoseismic approaches, used successfully elsewhere but previously only rarely if at all along the Nankai-Suruga Trough, may supplement existing methods and provide further insights into past earthquake and tsunami occurrence. Sugawara & Goff (2014), for example, propose that beach ridges may respond to seismic forcing and could provide a geomorphic record of the timing of past earthquakes along the Japan Trench. The presence of beach ridge systems on coastal plains facing the Nankai-Suruga Trough (Matsubara, 2005) raises the possibility for the application of analogous approaches along this subduction zone.

4.1.2.4. *Paleoseismic thresholds*

The presence of evidence for past earthquakes and tsunamis depends on thresholds of both creation and preservation (Nelson et al., 2006; McCalpin & Nelson, 2009). For example, for a tsunami-deposited sand sheet to be discovered in the sub-bottom stratigraphy of a coastal lake, the tsunami must have been of sufficient height to overtop the lake's sill with sufficient energy to transport sand (a creation threshold) and the sand layer must have withstood subsequent taphonomic alteration, for instance through bioturbation (a preservation threshold). The sensitivity with which a site preserves evidence for earthquakes or tsunamis should be explicitly assessed, principally through calibrating historic earthquake and tsunami deposits with their causal events (cf. Moernaut et al., 2014; Van Daele et al., 2015). At present, few studies from the Nankai-Suruga Trough have addressed site sensitivity and corresponding paleoseismic thresholds. Furthermore, such thresholds may vary over time, for example the relative elevation of a lake's sill decreasing or increasing due to sea-level rise or fall, complicating the relationship between the initial process and the resulting stratigraphic or geomorphic evidence. When comparing evidence for repeated tsunamis or earthquakes, the impact of changes in these thresholds must be considered if the relative magnitude of each event is to be discerned.

4.2. A new 7,500-year-long record of extreme wave events from Lake Hamana

The newly collected field data from Lake Hamana allow characterizing its sedimentary infill and assessing the record it may contain of past earthquakes and/or tsunami. This section is based on Boes et al. (submitted). For more comprehensive information, please refer to Boes et al. (submitted).

4.2.1. Results

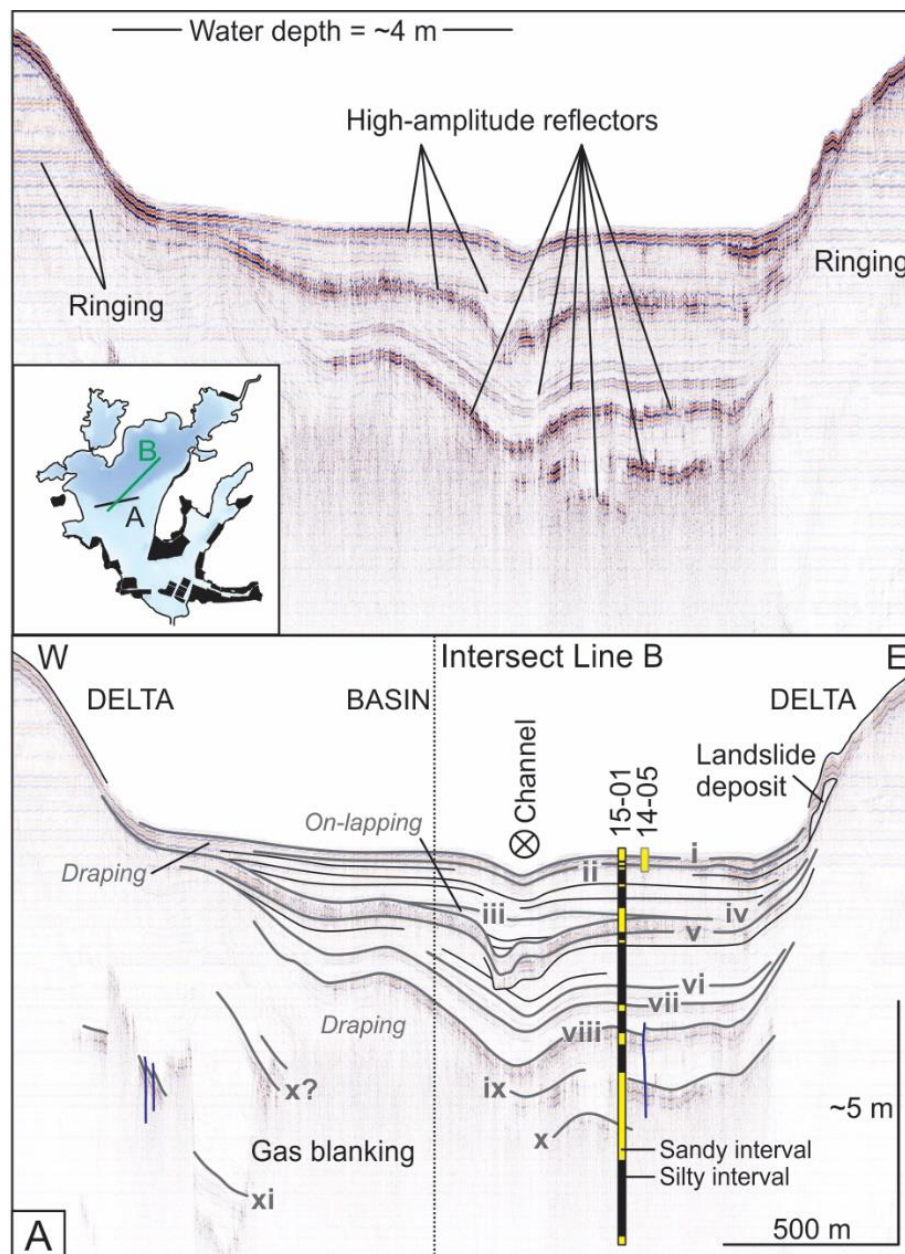
Morphologically, Lake Hamana can be divided into three parts:

- 1) shallow tidal delta (max. ~4 m) and Shōnai sub-basin (max. ~6 m) in the south;
- 2) 'deep' central basin (max. ~12 m), and
- 3) northern sub-basins Miyakoda and Inohana (max. ~6 m), fed by the Miyakoda and Tsuribashi rivers, respectively.

The lateral continuation of the Imagire-Guchi channel stretches across the delta into the central basin. It has a channel width of ~100 m and bank depths varying between 0.3 and 0.5 m. The basin reaches its max. depth in the NE, close to the connection with the Miyakoda sub-basin. In the Miyakoda and Inohana sub-basins, rivers built out shallow deltas.

4.2.1.1. Bathymetry/Morphology

Across the tidal delta, the high-resolution reflection-seismic signals barely penetrate, due to the high acoustic impedance of the coarse sandy delta deposits. Acoustic penetration in the central basin is also limited to < 2.5 ms two-way travel time (TWT) (< 2 m), due to gas blanking (Ikeya et al., 1987; Hovland & Judd, 1988). However, some acoustic windows are present in which the sedimentary infill can be imaged down to 10 ms TWT (~ 8 m). One such acoustic window occurs at the foot of the tidal delta (Figure 17). Here, a series of around 11 strong reflectors or strongly reflecting intervals interrupt layers with weaker reflectivity: i to xi (from top to bottom). Horizon i coincides with the current lake floor. Visibility and lateral continuity of the reflections decrease at greater depths.



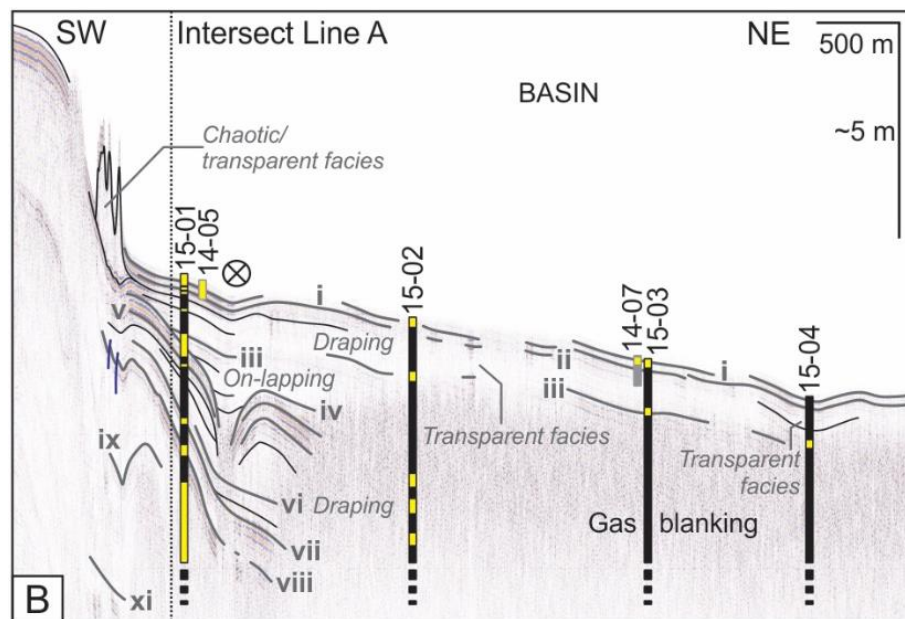


Figure 17: [A, previous page] W-E seismic profile (upper panel: uninterpreted; lower panel: with seismic-stratigraphic interpretation), running north of the tidal delta (see inset for location). A local acoustic window reveals the sedimentary infill of the basin, which displays a series of strong(er) reflectors, i to xi. Coring sites of HAM15-01 and HAM14-05 are projected on the profile and show that sandy layers (yellow) match strong reflectors. [B, this page] SW-NE profile (with seismic-stratigraphic interpretation), running from the tidal delta towards the deepest part of the central basin, approximately along the piston coring transect. This profile displays the same strong reflectors as observed on Line A. Modified from Boes et al. (submitted).

iv Reflector identity 14-07 Piston/gravity core

4.2.1.2. Seismic-stratigraphy

Despite their fragmentary appearance, layers xi-vi seem draped across the basin, preserving underlying topography (Figure 17). Sediment draping comes to an abrupt end at the lower boundary of interval v, which sharply cuts into the underlying facies. This unconformity is especially prominent within the paleochannel. Reflector iv directly overlies v, together defining one acoustic entity. On top of iv, deposits are confined to topographic lows of the former lake bottom, which they fill in gradually, thereby generating on-lapping contacts between reflector iv and the overlying strata. Upward, this ponding geometry gradually transforms back into a draping configuration, as observed for reflectors ii and i. Hiatuses can thus be identified at all unconformable contacts caused by incision and localized deposition (onlap). On seismic Line B (Figure 17B), west of the tidal channel, 3-4 m high piles of sediment with a transparent to chaotic facies are wedged underneath horizon ii at the foot of the delta slope. A much smaller deposit with a similar facies and stratigraphic position is visible on the eastern slope of Line A (Figure 17A). More seismically transparent sediment bodies occur in between horizons iii and ii, downslope site HAM15-01. Gas blanking in the deeper basin limits penetration to horizon iii, making confident correlation between reflectors in the central basin and those in the northern sub-basins near to impossible.

4.2.1.3. Stratigraphic sub-division of background sediments

Cored sediments mainly consist of beige-brown to dark grey silt with admixture of clay and sand, finely distributed organic fibers and few larger fragments, shell hash

and some complete bivalve and gastropod specimens. Bedding varies between homogenous, layered, laminated and bioturbated, depending on coring site and depth. These typical lacustrine deposits are interrupted by two types of layers: type α are sandy deposits with a sharp, truncated base and a fining-upward grain-size trend, and type β are silty deposits that display hints of deformation or reworking. Both types are considered 'allochthonous' compared to the lacustrine deposits in which they are embedded, by virtue of their composition and architecture, and were first defined and numbered in piston coring site HAM15-01, where they are best developed: Layers A1 to A15 (from top to bottom)(Figure 18). Also on site HAM15-01, autochthonous deposits were divided into seven successive structural, textural and compositional entities or units: Unit I to Unit VII (from top to bottom):

- Unit VII (755-588 cm): is composed of very poorly sorted silt and sandy silt. Sediment color changes from yellow-beige to brown-beige in the middle section. CT images show that deposits are structurally uniform and nearly homogenous to very faintly layered. Numerous shell fragments and few organic macro-remains were observed. Layer A15 is partly recovered at the bottom of the core.
- Unit VI (588-405 cm): represents a sand interval, that can be sub-divided into a lower (588-500 cm) and an upper (500-405 cm) section, separated by a ~0.5 cm thick, organic layer. The brown-grey colored lower section is coarsest and contains a primary grain-size mode of ~90 μm , accompanied by a secondary silt fraction with a mode of ~12 μm . The upper section of Unit VI is composed of beige-grey sandy silt with equal modes of ~60 μm and ~12 μm . Centimeter-scale layering occurs throughout Unit VI and displays an alternate semi-parallel and cross-bedded architecture. In contrast to allochthonous type α layers, Unit VI has no truncated, but only gradual contacts. Organic macro-remains and shell hash are abundant. Several complete, however strongly abraded, gastropod specimens of *Umbonium moniliferum* or *Umbonium costatum* occur at 480 cm and one *Circe scripta* bivalve was observed at 460 cm; these species are indicative for an intertidal, shallow marine environment (Habe, 1977; Okutani, 2000).
- Unit V (405-178 cm): mainly consists of brown-beige mud beds with a lighter beige-grey interval at 325-268 cm, which encompasses the allochthonous layer A13 and is delimited by layers A14 and A12 at the bottom and top. Below 268 cm, mean grain size is similar to Unit VII, but better sorted, with slightly coarse-skewed distributions and a pronounced ~12 μm mode. Above 268 cm, mean grain size makes a small drop, however modes stay within the medium silt fraction. Changes in sediment color and variations in X-ray attenuation on a cm-scale reveal a faint semi-horizontal banded to layered structure. Shell fragments and macro-organics can be observed, but are much less prominent than in Unit VI. Within the bottom 5 cm of this Unit, which is a transition zone between units VI and V, a single valve of a juvenile *Scapharca broughtonii* is embedded; this indicates an inner bay, sandy mud environment (Habe, 1977).
- Unit IV (178-130 cm): consists of moderately to poorly sorted, medium to coarse silt with an upward increasing fine sand fraction and average grain-size modes of ~20 μm . Depositional structures resemble Unit V. From a composite depth of 145 cm upward, sediment color changes from grey to brown-beige. This change accompanies a shift in sedimentology, going from mostly lacustrine silt deposits to frequently interbedded sand lenses, identified as layers A11-A9, which provide the deposit with a chaotic appearance. Shell and organic fragments are sparse in Unit IV.

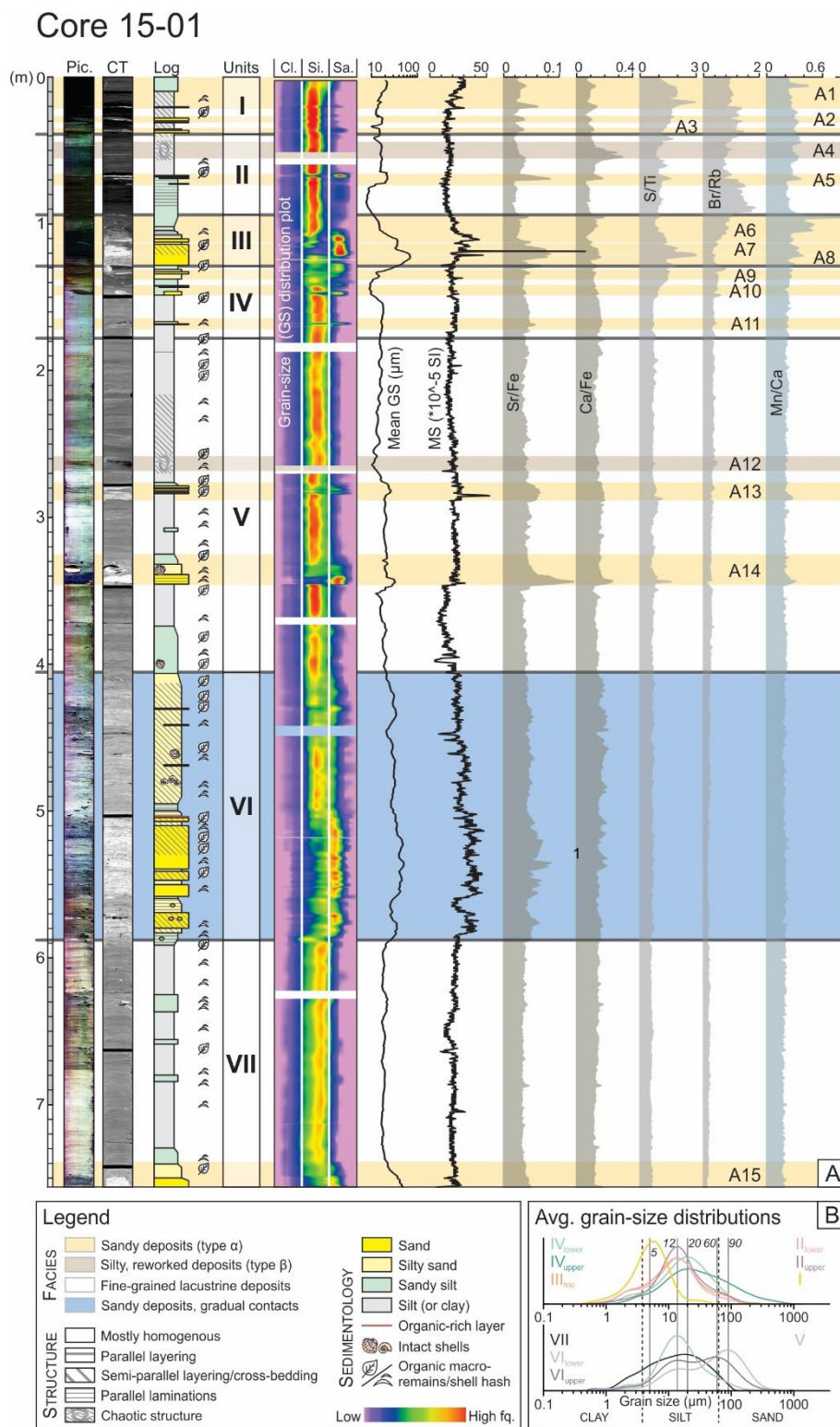


Figure 18: [A] Detailed plot and proxy records of piston core HAM15-01 (~7.5 m). From left to right: contrast-enhanced composite core photograph, CT-image, schematic lithology, division in lithological units, grain-size frequency distribution, mean grain size (GS), MS and several XRF element ratios that mark geochemical variations related to environmental changes and short-term impacts. Allochthonous layers of type α (yellow) and β (beige) are numbered from the top down, A1-A15. [B] Average grain-size distributions of each background unit, sometimes with division in lower and upper part. Black, vertical lines indicate modes of regularly recurring grain-size populations. Modified from Boes et al. (submitted).

- **Unit III (130-94 cm):** represents (in core HAM15-01) a condensed section composed of stacked, allochthonous layers A8-A6, separated by silty drapes. Especially A8 cuts sharply into the underlying deposits of Unit IV. From a depth of 100 cm upward, the top of A6 merges with background deposits, and grain size reduces to a medium silt fraction with a mode of 12 μm .
- **Unit II (94-40 cm):** can be sub-divided into two intervals of each ~ 27 cm based on sediment color and appearance on CT images. The lowermost 27 cm is a continuation of Unit III and consists of dark olive-brown, sandy mud laminations that cause very limited X-ray attenuation. The transition from the lower to the upper section is defined by layer A5. On top of A5, dark beige-grey, faintly layered, silt deposits are present, interrupted by layer A4. As in the lacustrine sediments of Unit IV, shell and organic fragments are sparse.
- **Unit I (40 cm - top):** consists of dark brown, highly organic mud. Grain-size modes vary between 5 and 10 μm . Deposits contain few shell fragments and display sharp, truncated contacts with the three successive allochthonous layers, A3-A1.

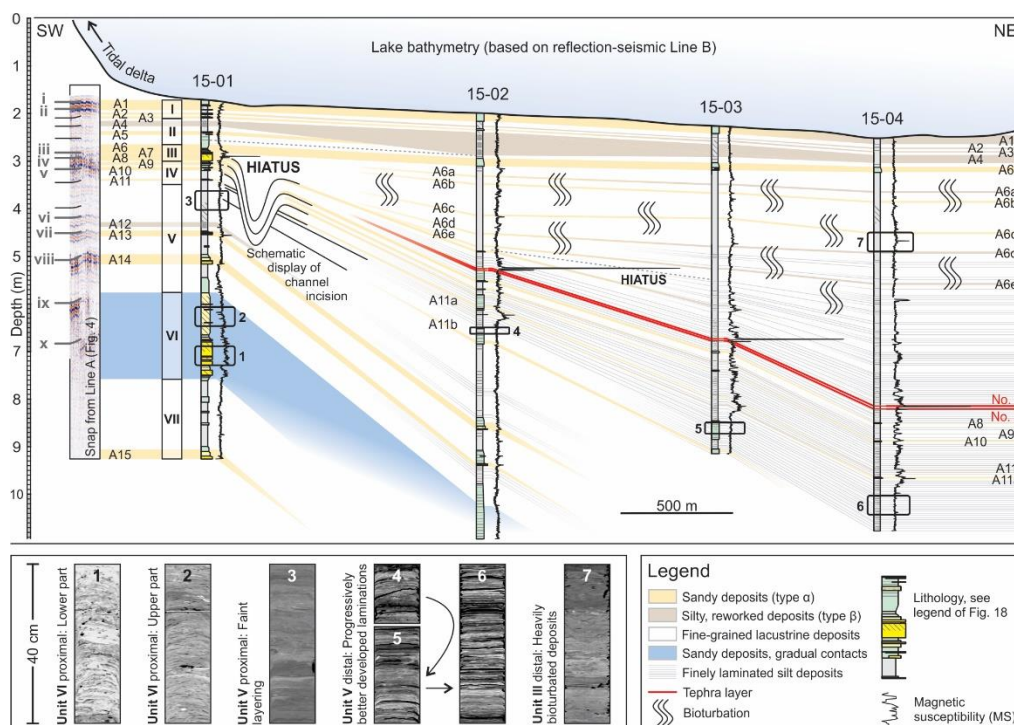


Figure 19: Piston core correlation and lateral distribution of layers A1-A15. Most allochthonous deposits thin and become less sandy from site HAM15-01 to HAM15-04, while background sequences generally become thicker and develop regular laminations in the deeper basin. Upward, laminations turn into heavily bioturbated sediment, masking layers A6a-A6e. MS curves support the correlation, as they highlight the position of two closely-spaced tephra layers in cores HAM15-02 to HAM15-04. Core HAM15-01 contains a large depositional hiatus at the stratigraphic level of both tephras and layers A6a-A6e; smaller hiatuses in HAM15-01 are implied by missing layers A11a and A11b. Enlarged CT images (bottom) include the lower and upper parts of sandy Unit VI. An interval of Unit V in core HAM15-01 is traced further down the basin to show that laminations become increasingly better developed, and contrast with the overlying bioturbation. Modified from Boes et al. (submitted).

Along the piston-core transect (Figure 19), the lacustrine deposits (Units I-VII) change from ocean-proximal to ocean-distal positions when moving further down the lake basin. Overall, grain size decreases towards deeper and less energetic waters, going

from medium to coarse silt in core HAM15-01 to very fine silt with an important clay fraction in core HAM15-04. Barely any sand admixture or scattered shell fragments can be observed in the ocean-distal sites.

Interpretation of seismic profiles, combined with sedimentary facies analysis, allows for correlating seismic-to-core as well as core-to-core. Sandy intervals are associated with strong reflectors on seismic images. However, not every single cm-scale layer is acoustically resolved, given the limited vertical resolution of 10-20 cm. Correlation shows that the identified hiatus between A7 (reflector iv) and A6 (reflector iii) in HAM15-01 gradually shrinks towards distal sites, and completely disappears in HAM15-03. This lateral change is bound to the progressive thickening of background depositional sequences in deeper water with growing accommodation space and decreasing environmental energy. On sites HAM15-02, HAM15-03 and HAM15-04, a sediment package of several meters is wedged in between the A7/A6 hiatus, and comprises five more layers with allochthonous properties (i.e. A6a-A6e), even though identification within this interval is strongly reduced due to bioturbation. The bioturbated interval in core HAM15-04 runs from A6 down to A6e (intensely bioturbated) and 160 cm below A6e (moderately bioturbated). Structurally, it stands in sharp contrast with the underlying deposits that are regularly and continuously laminated. Laminations do not fully resume on top of A6, but deposits become vaguely laminated or even layered, similar to units I-II at site HAM15-01. Apart from the obvious A7/A6 hiatus, units III and IV in HAM15-01 have an overall condensed character and comprise more undefined (smaller) hiatuses, as they laterally spread to much thicker sequences with additional type α layers, A11a and A11b, and two tephra.

4.2.1.4. *Allochthonous deposits*

A total of 22 to 23 allochthonous deposits were identified and classified as type α or type β . Type α deposits can evolve laterally into type β deposits and vice versa, as a result of changing depositional structure and texture. In most cases, erosivity, layer thickness and grain size decrease from HAM15-01 to HAM15-04, and type α deposits at site HAM15-01 tend to gradually evolve into type β deposits in distal sites.

4.2.1.5. *Geochronology*

- Short core HAM14-09: the profile of ^{137}Cs displays two clear peaks, at depths of 0.5 and 22.5 cm, which logically correspond to periods with increased fallout after the Fukushima nuclear disaster in 2011 and atomic bomb experiments in 1963, respectively. The CF:CS model was fitted to the $^{210}\text{Pb}_{\text{xs}}$ measurements, providing a mean sedimentation rate of 0.45 cm/yr for the first 40 cm of the core. ^{137}Cs peaks and the CF:CS $^{210}\text{Pb}_{\text{xs}}$ model agree and support each other.
- Piston core HAM15-01: the radionuclide age model from short core HAM14-09 can be correlated to the upper part of piston core HAM15-01, using the top of A4 as a marker. ^{14}C ages (BP) with 1σ SD and calibrated 95.4 % (2σ) age ranges (BP) reach up to ~ 7 ka BP for the oldest sediment in piston core HAM15-01, at a composite depth of 7.3 m.
- Piston core HAM15-03: ^{14}C ages (BP) with 1σ SD and calibrated 95.4 % (2σ) age ranges (BP) reach up to ~ 5 ka BP for the oldest dated sample from piston core HAM15-03, at a composite depth of 5.6 m. Tephra analysis confirmed that the two tephra deposits represent the Ōsawa scoria (Osw) and the Kawagodaira pumice (Kg), corroborating the ^{14}C age model.

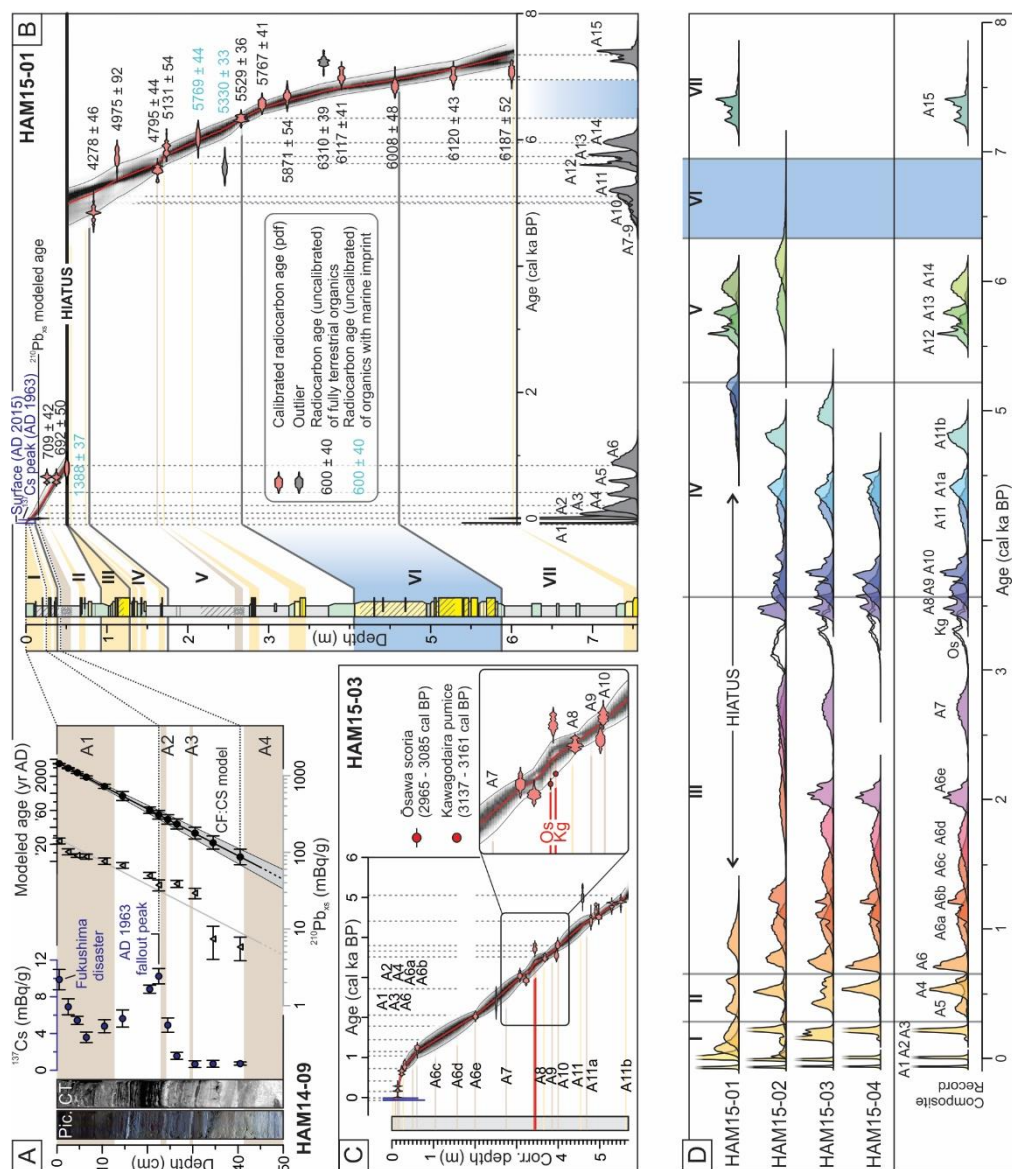


Figure 20: [A] ^{210}Pb and ^{137}Cs profiles in core HAM14-09. Layers A2, A3 and A4 were identified for correlation with other (piston) cores. [B] Bacon age-depth model of piston core HAM15-01, taking into account the presence of a large depositional hiatus in between A7 and A6. The model includes Pb/Cs and radiocarbon ages. Pdf's of allochthonous layers are extracted. [C] Example age-depth model of core HAM15-03, with a zoom-in on the position of the two tephra layers, i.e. Ōsawa (Os) scoria and Kawagodaira (Kg) pumice. [D] Extraction of a composite record (bottom) of allochthonous strata from different age-depth-modeled piston cores, taking time intervals from cores where models are considered most trustworthy. Modified from Boes et al. (submitted).

Age-depth models are presented in Figure 20. Given the drastic facies changes from coring site HAM15-01 towards the deeper basin, radiocarbon dating executed on HAM15-01 was not used to construct models for the other piston cores. The depositional hiatus in between layers A7 and A6, as visible on reflection-seismic images, was taken into account for site HAM15-01. From the bottom upward, sedimentation rates decrease in two subsequent steps: at the top of Unit VI (~6.5 ka BP) and at top of Unit III (~0.9 ka BP).

Probability density functions (pdf's) of allochthonous layer ages were extracted from

each age-depth model and used to create a composite record combining the most reliable sections of each model: A15-A12 and A5 from HAM15-01, A11b-A11 from HAM15-02, A10-A7 from HAM15-03, and A6e-A1 from HAM15-04. Model sections are considered reliable when (1) dated material is of good quality (e.g. pristine leaves and wood), (2) multiple calibrated radiocarbon ages line up without many outliers and (3) pdf's of calibrated ages have limited confidence intervals.

4.2.2. Discussion

4.2.2.1. Extreme wave event deposits (EWEs)

Allochthonous layers A1-A15 all possess characteristics that have been previously linked with tsunamis, or in a broader context, with EWEs. In order to ascertain their EWE-origin, all layers were evaluated against ten criteria:

- Criterion 1: Lateral extent - Considerable lateral extent of a deposit reflects the large-scale nature of its trigger (Morton et al., 2007; Shiki et al., 2008; Sawai, 2012). It should thus be identified on multiple locations with sufficient spacing. Piston cores in Lake Hamana are ~1 km separated from one another along a straight profile and hence provide a good framework for evaluating lateral extent and continuity of the event deposits.
- Criterion 2: Basal erosion - A sharp, erosive contact with the underlying background sediment evidences the high energy of the environment in which the event deposit formed (e.g. Shanmugam, 2012; Hansom et al., 2015; Shinozaki et al., 2015). Prominent basal erosion is a key criterion to distinguish event deposits (Bondevik et al., 1998; Switzer et al., 2005).
- Criterion 3: Coarse-grained (sandy) base - Extreme ocean waves entrain and redeposit large quantities of beach, dune and tidal delta sands, soil material etc., generating an anomalously coarse layer on top of lacustrine silt (e.g. Komatsubara et al., 2008; Goto et al., 2015). Here, this criterion mostly applies to type α layers, which typically contain an important sand fraction at their base. Sand modes in type α event deposits overlap grain-size distributions of surface samples from the beach, dunes, terrace and paddy field, showing that allochthonous components found within the lake must come from these sources, or indirectly from the delta.
- Criterion 4: Characteristic internal structure - After a tsunami or storm wave inundates a lake basin, a multitude of flow conditions arise, which then induce another range of possible depositional mechanisms (Shanmugam, 2012). As a result, EWE deposits can display many bedforms, varying from fining-upward sequences and internal layering (~type α), over homogeneity to chaotic deformation (~type β) (e.g. Morton et al., 2007; Tappin, 2007; Shiki et al., 2008; Engel & Brückner, 2011).
- Criterion 5: High(er) magnetic susceptibility - MS typically reaches higher values in clastic event deposits, as a result of their mineralogy and often coarser grain size (e.g. Thompson et al., 1975; Engel et al., 2013; Chagué-Goff et al., 2016; Kempf et al., 2017). Also, MS signal dilution by organic content in event deposits is minor when compared to autochthonous background sediment. In the given case, biotite (Fe-mica) in beach sands bears the main MS signal in EWE deposits with a marine source.
- Criterion 6: Stronger CT attenuation - The combined effect of anomalous mineralogy, geochemistry and density of the grain packing in EWE deposits, causes X-ray attenuation on CT images to increase (e.g. May et al., 2016; Kempf et al., 2017). A strong contrast between event deposit and background allows CT scans to efficiently resolve allochthonous sediment.
- Criterion 7: Geochemical signature - Geochemistry helps to pinpoint events

during which inundation by ocean water and deposition of marine sediment took place (e.g. Nichol et al., 2010; Goto et al., 2011; Chagué-Goff et al., 2012). In Lake Hamana, Sr/Fe and Ca/Fe mark the presence of marine carbonates, shell hash and microfossils with a CaCO₃ composition, while S/Ti and Br/Rb indicate the respective enrichment in seawater sulfate (i.e. water soluble salts) and marine organobromine (Leri et al., 2010; Chagué-Goff et al., 2017). Mn/Ti is linked to post-depositional redox processes (Chagué-Goff et al., 2017) and could play a role after oxygenation of lake bottom waters following overturning during an EWE.

- Criterion 8: Thinning landward - Landward-thinning and -tapering is characteristic for EWE deposits (e.g. Dawson et al., 1991; Engel & Brückner, 2011).
- Criterion 9: Fining landward - During and after inundation, coarsest grains settle first and finer material settles in a later phase. Also, finest grains get transported furthest away from the ocean as they require less energy to be moved and spend more time as suspended load. Accordingly, EWE deposits tend to become finer grained in a landward direction (e.g. Morton et al., 2007; Goto et al., 2015).
- Criterion 10: Background change - The impact of an EWE can be as strong as to impose a significant shift in the background depositional regime (e.g. Kempf et al., 2017). For example, the sudden input of large quantities of salt water can cause a salt water lens to form on the basin bottom and to generate a density stratification, which, in turn, limits overturning and oxygen supply to the lake floor where oxidation reactions lose importance and organics are no longer decomposed at the same pace (Sanukida et al., 1985). In addition to that, extreme wave action often results in important geomorphological changes, which then influence the nature and quantity of sediment that gets deposited in the lake during calm phases.

Given the absence of rip-up clasts and obvious, interbedded mud drapes in any of the observed event deposits, these criteria were not included here.

4.2.2.2. *Historical and prehistorical events*

Below, the EWE deposits encountered in the piston cores of Lake Hamana are discussed in terms of their possible origin. Ages have been obtained from the composite event record:

- Event layer A1 (2005-2015 cal CE) is consistently erosive and is present in both the central basin and the Miyakoda sub-basin where it has a terrestrial signature (peaking MS) and grows into a thicker, coarser deposit compared to site HAM14-09. This suggests that sediment was delivered from both the ocean and the Miyakoda River at the time of the EWE. Such distribution can be explained by marine inundation and coeval river flooding during typhoon-induced extreme ocean waves as well as heavy rainfall. As the deposit's age does not agree with any possible megathrust event, it is therefore more likely that results from an extreme storm/precipitation event. An appropriate candidate for deposition of A1 is Typhoon Phanfone, a category 4 super typhoon which struck the Enshū-nada coastline in early October 2014 and made landfall near the city of Hamamatsu.
- Event layers A2 (1930-1950 cal CE) and A3 (1710-1790 cal CE) are very similar. They are thin layers, but remain 2-3 cm thick throughout the entire basin. Age-wise, these deposits coincide with historical tsunami events in 1944 CE (Shōwa-Tōnankai) and 1707 CE (Hōei). However, height of the 1944 CE tsunami around Benten-jima was only 0.9 m (Watanabe, 1998; Komatsubara et al., 2008) and evidence of shaking is limited to few traces of sand liquefaction (Sangawa, 2001) and a mass-transport deposit in Shirasuka (see chapter 4.1 and 4.4). Hence, A2 is more likely related to a storm surge, e.g. Typhoon Mary in 1974 CE, Grace & Lorna

in 1954 CE or Tess in 1953 CE, all of which caused significant flooding and coastal damage (Mazda, 1984; Yuk & Aoki, 2008). The 1707 CE Hōei tsunami, on the other hand, is anticipated to have left traces in the Lake Hamana record, as claimed before by Tsuji et al. (1998) and Okamura et al. (2000) (recalculated ages in Garrett et al. (2016)) in the central basin and tidal delta. Archeological and geological evidences along the Enshū-nada coastline (e.g. Kumagai, 1999; Takada et al., 2002; Fujiwara et al., 2006b, 2007a; Komatsubara et al., 2008; Kitamura & Kobayashi, 2014; Sato & Fujiwara, 2017; Riedesel et al., 2018) bear witness of the extent and scale of the 1707 CE event (Figure 21). Even though the Hōei tsunami could have deposited A3, its strong similarity to A2 implies that a storm trigger, such as the 1680 CE and 1699 CE typhoons, should at least be considered. These storm surges were associated with high ocean waves (~3 m), severe flooding, damage and many victims (History of Asaba town editing committee, 2000).

- Event layer A4 (1360-1490 cal CE) is not characteristically sandy, displays chaotic deformation instead of a structured grading, and has an unusual lateral distribution. Mass-transport deposits (MTD's) on the delta slopes or right at the foot of the slopes are coupled with the seismic horizon of A4, which is largely transparent in the deeper basin. A4 is therefore likely the result of slope failure induced by earthquake shaking rather than inundation during an EWE. The absence of the underlying A5 sand layer in cores HAM15-02, HAM15-03 and HAM15-04 suggests that the depositional mechanism of A4 included (1) an erosive turbidity current or slurry flow following slope failure and/or (2) intense coseismic soft-sediment deformation. Event layer A4 is strongly enriched in Ca and distinguishes itself on CT images, indicating that part of the sediment mixture comes from the tidal delta, which carries a diluted marine signature. Megathrust earthquakes in 1498 CE (Meiō) or 1361 CE (Shōhei) are likely triggers. Evidence of earthquake shaking (Sangawa, 2001; 2009) and coseismic uplift (Kitamura et al., 2015; 2016), as well as tsunami inundation (e.g. Kumagai, 1999; Komatsubara et al., 2008; Fujiwara et al., 2010b; Fujino et al., 2008; 2018; Garrett et al., 2018; Riedesel et al., 2018) and documented population migration (Yata, 2005) have been extensively reported along the Enshū-nada coastline for the Meiō and Shōhei events.
- Event layer A5 (1320-1610 cal CE) has a broad modeled age range, which entails that several historical megathrust tsunamis and storm surges could have generated it. However, in case layer A4 was formed by Meiō shaking, only Shōhei and a tropical storm in 1370 CE are remaining possibilities. Based on the available, ambiguous evidence, it is difficult to deduce what type of EWE deposit A5 might be.
- Event layer A6 (1150-1270 cal CE) is present throughout the central basin. It looks very similar to layer A1, but has a slightly coarser base and a less chaotic but more pronounced fining-upward pattern, which makes it more likely to have been deposited by a tsunami. Layer A6 deposit has an age range during which no historical megathrust tsunami nor typhoon have been reported. Hence, layer A6 represents either a historical EWE that has not yet been documented, or it is the product of a reported historical event, but has been incorrectly dated, e.g. by dating reworked, older organics. If layer A6 would be dated younger, e.g. 1500 cal CE, it would make a perfect match for the 1498 CE Meiō tsunami, or the 1498 CE and 1499 CE typhoons. Supporting this assumption is the instantaneous increase in Br/Rb throughout layer A6, but especially on top of A6, which highlights a strong increase in marine organobromine. The Meiō tsunami is thought to have implemented drastic environmental and geomorphological alterations in 1498 CE,

by closing off the Hamana River mouth, which used to be the connection between ocean and lake, and by breaching the until then completely closed coastal ridge (Fujiwara et al., 2010b; 2013a). This breach was followed by the emergence of a new waterway connecting the ocean with Lake Hamana, i.e. Imagire-Guchi channel, and caused a lake water salinity spike, as shown by diatom analyses (Honda & Kashima, 1997; Kashima et al., 1997; Morita et al., 1998; Sato et al., 2016b). Higher background values of S/Ti are also witness of increased marine sulfate concentrations in units II and I, after beach ridge breaching. Of course, when assuming that ^{14}C -dating of A6 is faulty, other event ages shift as well.

To conclude, event deposits A1 to A6 can be associated with different historical events.

- Event layers A6a (730-1080 cal CE), A6b (650-850 cal CE), A6c (260-670 cal CE), A6d (1490-1910 cal yr BP) and A6e (1930-2130 cal yr BP) cover the transition from historical to prehistorical events. Possible correlations exist between A6a and the tsunamis of 1096 CE Eichō or 887 CE Ninna, between A6b and 887 CE Ninna or 684 CE Tenmu, and between A6c and 684 CE Tenmu.
- Event layer A7 (2500-2870 cal yr BP) overlaps in age with the youngest of a series of sand layers, that were identified on Shima Peninsula (Fujino et al., 2018) and attributed to multiple prehistorical tsunamis in ~2180-2670 cal yr BP (Sand F), ~2750-3870 cal yr BP (Sand G), ~3080-4370 cal yr BP (Sand H), before ~3850 cal yr BP (Sand I) and after ~4400 cal yr BP (Sand J).
- Event layers A8 (3400-3590 cal yr BP), A9 (3510-3760 cal yr BP) and A10 (3660-3890 cal yr BP) may have been recovered in previously retrieved cores from the Hamana delta (Tsuji et al., 1998), which contain two prehistorical gravel deposits, the ages of which overlap those of events A7-A10. They were formed after 3050-3530 and 3600-4060 cal yr BP. The Rokken-gawa lowland, east of Lake Hamana, recorded a sand sheet that was deposited c. 3410-3790 cal yr BP (Fujiwara et al., 2013b); thus, it can possibly be linked with A9. This sand sheet marks the transition from a brackish to freshwater marsh environment, suggesting the closure of the tidal inlet during an EWE – most likely a tsunami as derived from the deposit's properties (Sato et al., 2011; Fujiwara et al., 2013b). Along the Suruga Bay coastline, the Shizuoka Plain bears witness of prehistorical tsunami deposits aged 3486-3565 and 3900-4080 cal yr BP that coincide with traces of coseismic uplift during which quick environmental changes from marine to freshwater were imposed (Kitamura et al. 2011; 2013). These deposits may be correlated with A8 and A10 (or A11). In addition, Kitamura & Kobayashi (2014) report tsunami deposits at Shimizu from 3360-3500 to 3540-3670 cal yr BP, coincident with the formation of layer A8 and A9. The third of four uplifted marine terraces at Cape Omaezaki emerged before 2140-2310 cal yr BP (Azuma et al., 2005; Fujiwara et al., 2010a), most likely during the megathrust earthquake that consequently produced tsunami deposit A7, or maybe A6e. While interseismic subsidence and coseismic uplift prevails in the region of Suruga Bay, coseismic subsidence is held responsible for the formation of sharp peat-mud contacts around Lake Hamana (Sato et al., 2011; 2016a; Sato, 2012). Peat-mud contacts dating back to c. 3800 cal yr BP in the Rokken-gawa lowland (Sato et al., 2011; Sato, 2012) may be associated with the same seismic event that formed layer A10. In view of the characteristics of layers A7-A10 and ample correlations with other evidence of megathrust events along the Enshū-nada coastline, A7-A10 are most likely the result of tsunami inundation.

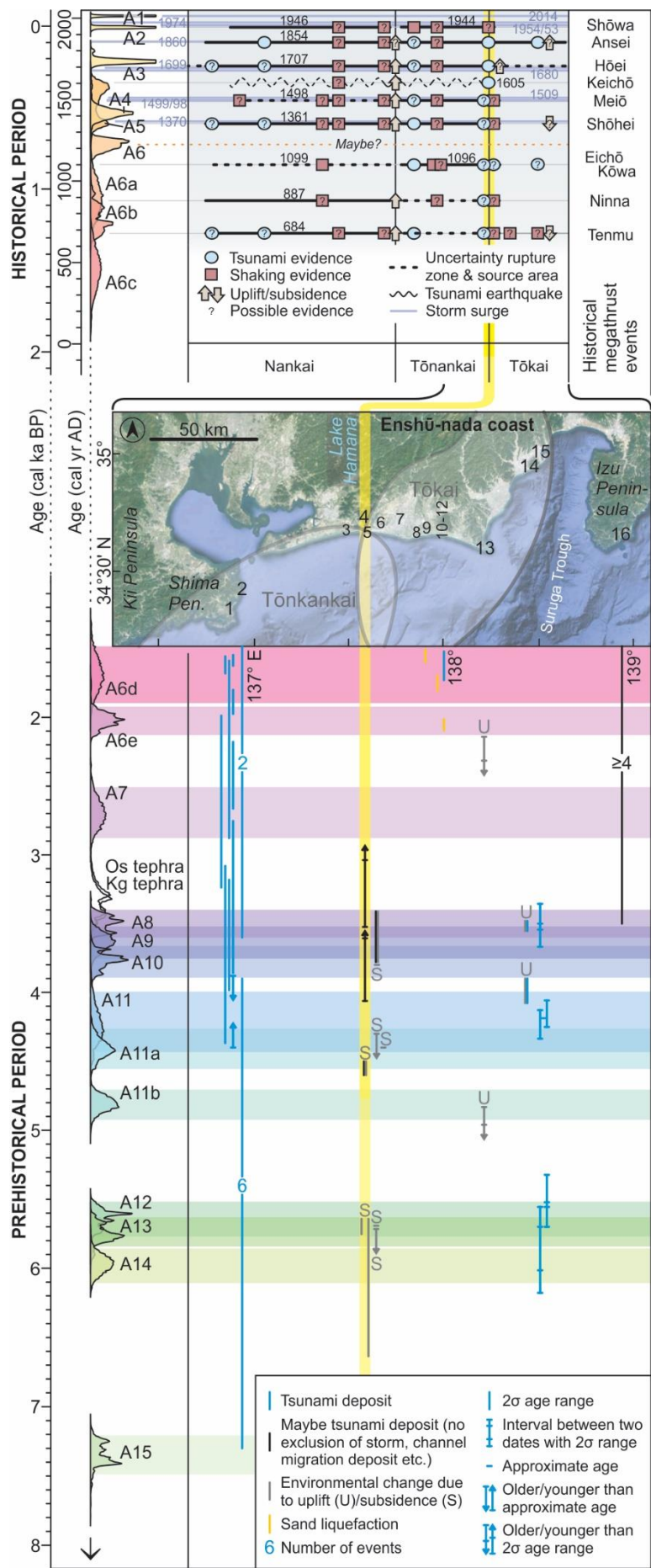


Figure 21: Comparison between the event record from this study (left, vertical) and other existing records from the Nankai-Suruga Trough, in historical and prehistorical times. Top: Locations with evidence of tsunamis, shaking and uplift/subsidence, related to historical megathrust events, with the extent of their respective rupture zones (see also chapter 4.1). Important historical storm surges that (may have) affected the lake area are marked too, with horizontal violet lines. A bright yellow vertical lines gives the position of Lake Hamana, on the boundary between Tōnankai and Tōkai zones. Centre: Zoom-in on the D and E segments, which border Lake Hamana. Numbers on the map correlate with the following locations: (1) Shima Peninsula & Osatsu coastal lowland, (2) Shijima lowland, (3) Shirasuka coastal lowland, (4) Lake Hamana, (5) Benten-jima, (6) Rokken-gawa, Miyakodagawa & Higashi-Kandagawa lowlands, (7) city of Hamamatsu, E of Hamana and the intermediate lowlands, (8) Ōtagawa lowland with Ōta River, (9) Ōsuga lowland/city of Kakegawa, (10) - (12) Sakajiri, Tsurumatsu and Harakawa, (13) Cape Omaezaki, (14) Shizuoka Plain/Ōya lowland, (15) Shimizu, and (16) Shimoda. Modified from Boes et al. (submitted).

- Evidence of abrupt subsidence and uplift was also reported concurrent with event layers A11 (4000-4460 cal yr BP), A11a (4250-4540 cal yr BP) and A11b (4700-4910 cal yr BP). Sato et al. (2011; 2016a) and Sato (2012) discuss coseismic subsidence in the Rokken-gawa and Higashi-Kandagawa (~3.5 km east of Rokken-gawa) lowlands before 4300 cal yr BP and c. 4400 cal yr BP. From around the same period, 4067-4250 to 4125-4335 cal yr BP, tsunami evidence was found at Shimizu (Kitamura & Kobayashi, 2014), and is possibly related to event layer A11. Furthermore, Sato et al. (2016b) describe a tsunami or storm surge deposit in the central basin of Lake Hamana, dated to ~4500-4600 cal yr BP, likely correlated with layer A11a. A11b, in turn, could be associated with the emergence of the fourth marine terrace level at Cape Omaezaki before 4830-4960 cal yr BP (Azuma et al., 2005; Fujiwara et al., 2010a).
- Event layer A12 (5520-5780 cal yr BP) resembles event layer A4, which could point to an earthquake trigger. However, based on its limited thickness and poor representation (only in core 15-01), this layer could be considered a local, insignificant artefact of background processes. If significant, A12, together with event layer A13 (5610-5880 cal yr BP) and A14 (5850-6080 cal yr BP) may be linked with the clustered prehistorical subsidence events that triggered the formation of peat-mud contacts c. 5645-6635 and 5700 cal yr BP in the Shinjo lowland (Sato & Fujiwara, 2017) and c. 5700 cal yr BP and before ~5700 cal yr BP in the Higashi-Kandagawa lowland (Sato et al., 2016a), as well as with evidence of tsunami inundation at Shimizu in 5320-5520 to 5580-5700 and 5580-5700 to 6010-6180 cal yr BP (Kitamura & Kobayashi, 2014)
- No other evidence of a megathrust or EWE as old as event layer A15 (7210-7440 cal yr BP), has been reported before along the Enshū-nada coastline, suggesting that the presented record adds complementary new information to the existing dataset.

4.2.3. Conclusion

Understanding variability of megathrust events remains problematic along the Nankai-Suruga Trough, where a variable rupture mode determines the magnitude and spatial extent of the impact. The long record of coastal Lake Hamana embodies one of the pieces to complete the existing data gaps for the Tōnankai and Tōkai zones. Our analysis of newly acquired geophysical data and sediment cores led to the following insights:

- The collected cores from the lake basin contain a ~7.5 kyr long record of mostly silty background deposits with variable bedding and sand admixture. A total of ≥ 22 possible event deposits, interpreted as products of EWEs (tsunamis and typhoons)

- and megathrust earthquakes are discerned in this study.
- Event deposits vary in thickness between 1 and 50 cm. They often have a sharp and erosive basal contact, a coarser grain size, increased X-ray CT attenuation and magnetic susceptibility (MS), a marine geochemistry (e.g. high Sr/Fe and Ca/Fe ratios), and a thinning and fining landward trend. They can be divided in type α deposits, which are typically sandy, erosive and fining-upward, and type β deposits, which are mostly silty and display deformational structures. Type α deposits are inferred to be triggered by marine inundation during a tsunami or typhoon, while type β deposits are much more likely to be the result of earthquake shaking.
 - Some event deposits are associated with historical megathrust events, such as the 1707 CE Hōei earthquake and/or tsunami, and the 1498 CE Meiō and 684 CE Tenmu tsunamis. Several storm surges are likely to have left deposits too. The top surface sand sheet is attributed to the 2014 category 4 Phanfone Typhoon. Prehistorical event deposits in Lake Hamana do not only show good agreement with other existing sources of megathrust evidence from the same region, but also add complementary information when going back to 7.5 ka BP.
 - Diversity in lateral thickness distribution of event deposits in Lake Hamana might be key to differentiate between a tsunami or typhoon trigger, as storm surges will also cause river flooding and form turbidites in northern sub-basins (e.g. Phanfone deposit), while tsunamis will only affect sedimentation in the central basin.

4.3. Historical megathrust earthquakes recorded by tsunami and terrestrial mass movement deposits on the Shirasuka coastal lowlands

The newly collected field data from the Shirasuka coastal lowlands allow refining previous studies that reported the presence of deposits resulting from past earthquakes and/or tsunamis. This section is based on Garrett et al. (2018). For more comprehensive information, please refer to Garrett et al. (2018).

4.3.1. Results

4.3.1.1. Stratigraphy and sedimentology

The six newly acquired and closely spaced cores from the Shirasuka coastal lowlands reveal four sand layers interbedded with organic muds: Sands 1 to 4 (from top to bottom; Figure 22). The sequence of sand and organic mud layers is underlain by cross-stratified medium to very coarse sand (referred to as the basal sand as it could not be cored beneath).

Sand 4 is brown-grey in color with silt-rich intervals. In core JSH3/F, Sand 4 can be subdivided into five sub-units: (1) a 10 cm thick upper unit of well-sorted medium sand, (2) a 3 cm thick drape of very poorly sorted sand-rich silt, (3) a 10 cm thick middle unit of poorly sorted fine to medium sand, (4) a 4 cm thick layer of very poorly sorted sand-rich medium to coarse silt, and (5) a 1.5 cm thick lower unit of very poorly sorted fine sand (Figure 23D). Grain-size data from core JSH3/F indicate the upper sand sub-unit fines upwards, while the middle sand sub-unit coarsens upwards. Visual inspection and X-ray CT scans of core JSH3/F suggest that sub-unit 4 is a large and rounded mud clast. The lower contact dividing Sand 4 from the underlying organic silt is abrupt in all of the cores, while the upper contact is moderate to abrupt.

Sand 3 consists of brown-grey silt-rich sand (Figure 23C). In the one core that spans both the lower and upper contacts, JSH3/O, the layer is 10 cm thick. Grain-size data indicate a median size of 220-250 μm for the lower 8 cm, which does not display

grading and is very poorly sorted, with a 2 cm thick cap of coarser, poorly sorted material. The lower and upper contacts are abrupt in all cores and centimeter-scale mud clasts are present within the lowermost 2 cm.

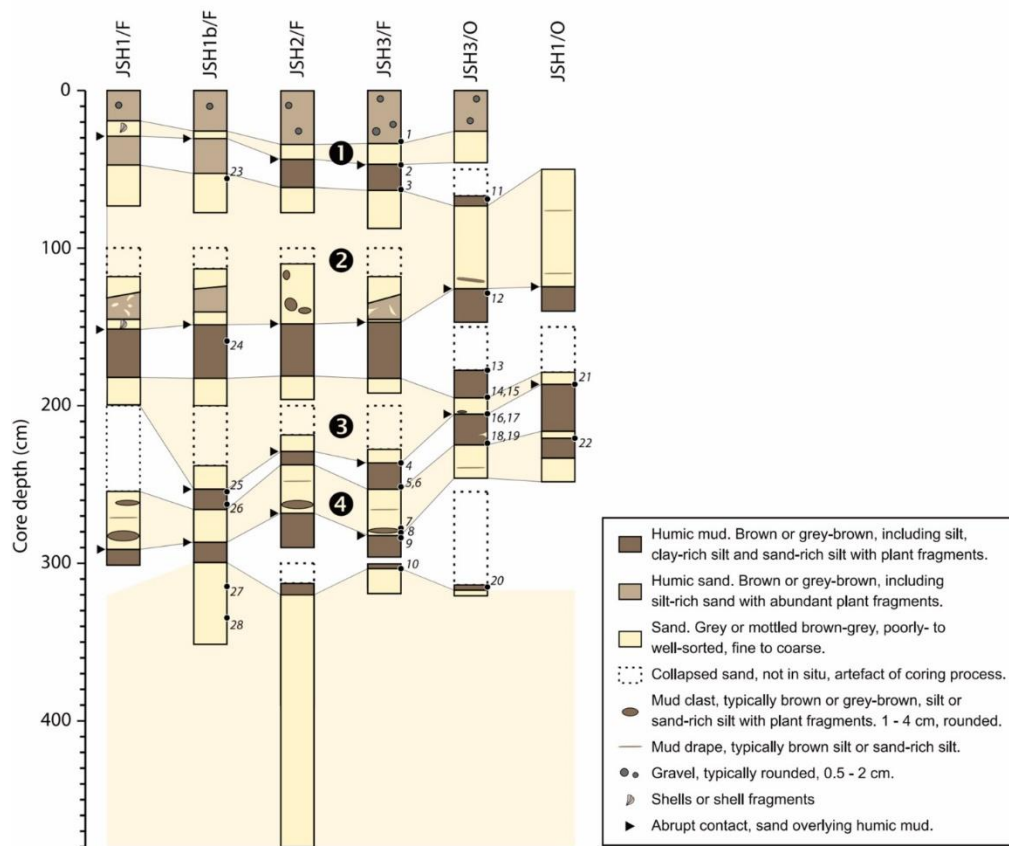


Figure 22: Stratigraphy of the six piston cores from the Shirasuka coastal lowlands. Numbers in circles refer to the four identified sand layers. Italicised numbers refer to radiocarbon samples. Modified from Garrett et al. (2018).

Sand 2 consists of brown-grey sand, with local siltier and more organic sub-units (Figure 23B). Only core JSH3/O includes a single section encompassing both the lower and upper contacts of this sand layer; in this section, the layer is 50 cm thick. Grain-size data from core JSH1/F indicate Sand 2 consists of medium sand with silt-rich medium sand intervals. The layer displays no vertical grading and consistently poor or very poor sorting. The contact with the underlying organic silt is abrupt in all cores, while the upper contact is typically gradual. X-ray CT scans of core JSH3/O reveal complex and chaotic structures within the deposit, including sub-horizontal layering (Figure X) and intervals of finer, more poorly sorted grain-size distributions indicate the presence of mud-rich layers.

Sand 1 consists of brown-grey medium sand (Figure 23A). Its thickness ranges from 5 to 14 cm. The lower contact with the underlying dark brown sand- and organic-rich silt is abrupt in all cores. The upper contact with the overlying dark brown silt- and organic-rich fine to medium sand is also identifiably abrupt through visual analysis, but less distinct in CT scans. Grain-size data from core JSH3/F reveal a slight coarsening-upwards trend. The layer is moderately to moderately well sorted. While no mud clasts or drapes are apparent, CT scans of core JSH3/F show that the deposit is not entirely homogeneous with several regions displaying weak centimeter-scale

layering. This may reflect grain-size variations missed by the coarser sampling resolution of the grain-size analysis or variations in density or mineralogy.

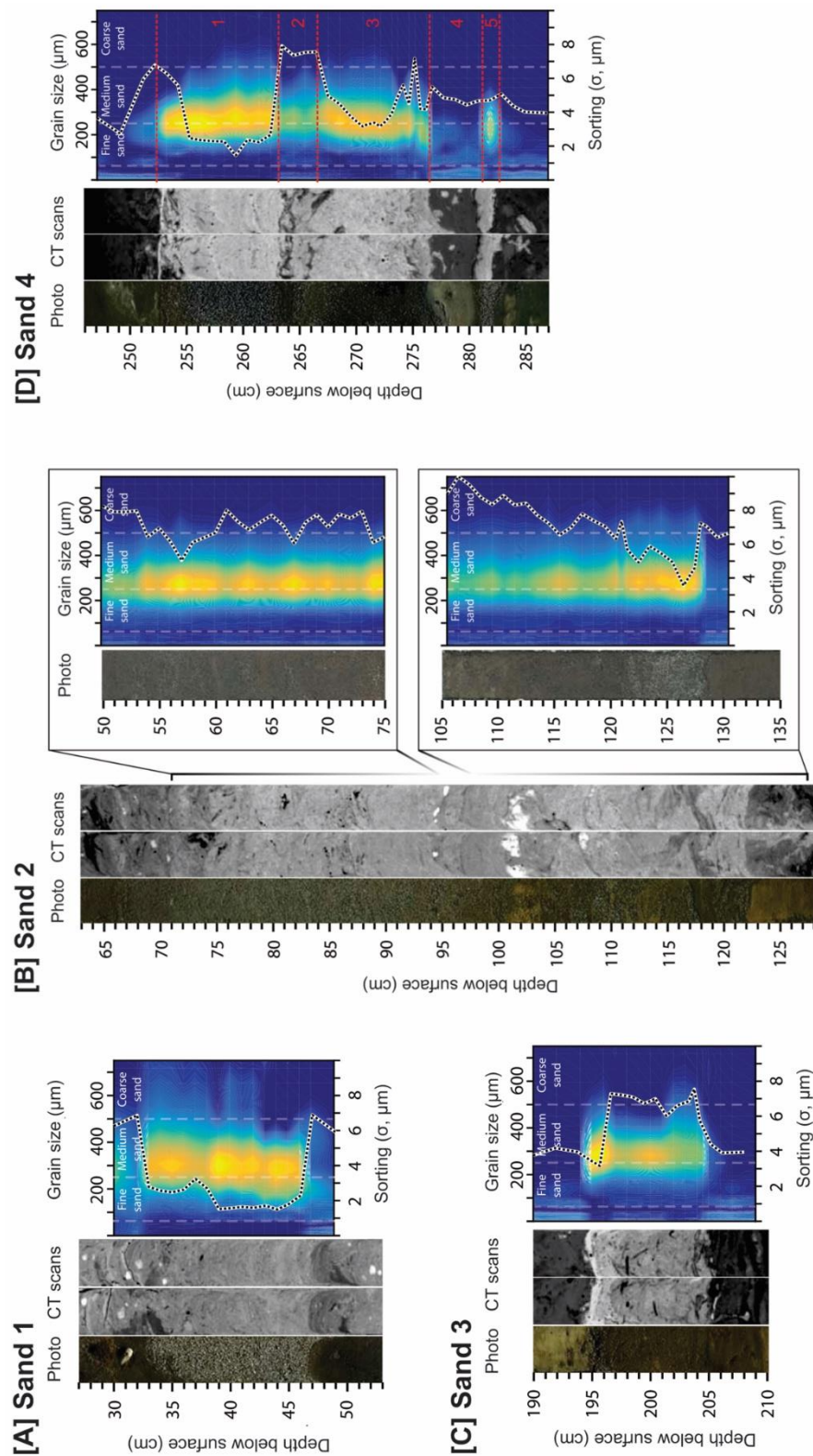


Figure 23: Linescan photographs, frontal and sagittal X-ray CT views, and grain-size distributions for Sand 1 (A; core JSH3/F), Sand 2 (B; CT from core JSH3/O and grain size from core JSH1/F), Sand 3 (C; core JSH3/O) and sand 4 (D; core JSH3/F; red numbers mark sub-units). Modified from Garrett et al. (2018).

Surface samples. The four samples from the contemporary beach and dune consist of moderately well-sorted medium sand (Figure 24). The lower beach and upper dune samples share median grain sizes of $\sim 365 \mu\text{m}$, while the upper beach and lower dune samples are finer. The minerogenic component of the paddy field sample consists of very poorly sorted medium silt. The paddy field sediment also contains abundant plant fragments and humified plant remains. The terrace displays a diverse range of grain sizes and sedimentary structures, including imbricated rounded gravels to 5 cm and cross-bedded coarse sand units. The single available terrace sample consists of poorly sorted medium silt.

[E] Modern samples

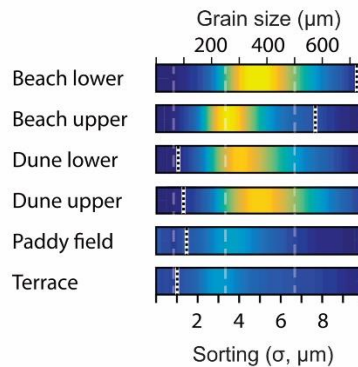


Figure 24: Grain-size distributions for modern surface samples.
Modified from Garrett et al. (2018).

4.3.1.2. Microfossils

Diatoms. Our diatom analysis identified 165 species in 41 samples taken from the four sand layers and the immediately overlying and underlying organic mud units. Salt-tolerant freshwater species dominate the assemblage in every sample. Sands 4, 3 and 2 contain *Pseudostaurosira elliptica* at abundances frequently in excess of 50 % and, in the case of samples from Sand 2, in excess of 95 % of the total diatom count. *P. elliptica* occurs in Sand 1 at lower abundances, with other salt-tolerant freshwater species, including *Staurosira construens* and *S. construens* var. *venter*, also present. The latter is the most commonly encountered species in one sample from this sand layer. In Sand 4, the contribution of marine and brackish taxa peaks at $\sim 9 \%$, with *Fallacia tenera* and *Ctenophora pulchella* the most frequently identified higher salinity species. The percentage of marine and brackish species is consistently less than 3 % in Sands 3, 2 and 1, and no diatoms from these salinity groups are encountered in seven of the 15 samples from these layers. The organic mud units between the sand layers are dominated by salt-tolerant freshwater species, including *P. elliptica* at abundances of between 20 % and 65 %.

No diatoms were found in the five surface samples from the beach, dune and terrace. The sample from the surface of the paddy field contains 39 species, of which 31 are also found in the fossil samples. The three freshwater categories include over 96 % of the modern assemblage, with the remaining 4 % brackish and no marine species encountered. Only one species, *Achnanthes exigua*, exceeds 10 % of the assemblage, with the dominant fossil species, *P. elliptica*, contributing less than 3 %.

Pollen and non-pollen palynomorphs. Exploratory pollen analysis focused on Sands 4, 3 and 1 and the organic silt units above and below Sand 3. Fifteen fossil samples

yielded 20 arboreal and 20 non-arboreal pollen taxa, eight freshwater aquatic taxa, five non-pollen palynomorphs and five green algal taxa. None of the taxa encountered are indicative of marine environments.

Sand 4 features Cyperaceae and grasses (Poaceae and Cerealiatype), with elevated arboreal pollen percentages (mainly *Pinus*, *Corylus* and *Quercus*) found particularly in the large mud clast. The middle and upper sand sub-units of Sand 4, along with the internal silt drape, display elevated abundances of aquatic taxa, particularly *Myriophyllum*, and algae, including *Spirogyra* and *Zygnema*. In Sand 3, *Pinus* and Cyperaceae are found alongside cultivated and wild varieties of grass. Spores of the mycorrhizal fungus *Glomus* peak in abundance in this layer, while aquatic taxa, particularly *Sagittaria*, and algae, principally *Zygnema*, are also encountered at low abundances. Sand 1 contains abundant arboreal and non-arboreal pollen, including *Pinus* and grasses, but few aquatic taxa, non-pollen palynomorphs or algae.

The fine-grained sediment accumulation, typified by the organic silt units above and below Sand 3 and the sample from the contemporary paddy field surface, displays similar pollen assemblages to the sand layers. The silt layers in core JSH3/F contain *Pinus*, Cyperaceae and grass pollen, alongside occasional aquatic taxa, *Zygnema* and rare non-pollen palynomorphs. The surface sample contains *Cryptomeria*, *Pinus*, Cyperaceae and grass pollen; however, aquatic taxa, non-pollen palynomorphs and algae are rare, with *Myriophyllum*, *Sagittaria*, *Glomus*, *Spirogyra* and *Zygnema* absent.

4.3.1.3. Geochronology

A Bayesian age model incorporating 11 of the 12 ^{14}C ages from macrofossil samples constrains the timing of the deposition of our sand layers (Figure 25). We do not include the AIO ^{14}C dates in age model development because of highly variable offsets between paired macrofossil and AIO dates. We also reject ^{14}C dates from bulk samples, as these are inconsistently between 100 and 600 years older than macrofossil dates from the same stratigraphic context. The inconsistent bias towards older ages associated with the use of bulk samples is well-established (Nakamura et al., 2012; 2016; Törnqvist et al., 1992). ^{14}C ages deduced from AIO fractions are also predominantly older than macrofossil dates as well as compound specific radiocarbon ages from the same horizons, depending on the residence time of carbon in the hinterlands (e.g. Ishiwa et al., 2016; Yokoyama et al., 2016). Finally, we do not incorporate one macrofossil sample because of its placement within a mud clast in Sand 4.

The ^{14}C age model constrains the timing of the emplacement of Sand 4 to 1154-1378 CE, Sand 3 to 1491-1610 CE, Sand 2 to 1601-1831 CE and Sand 1 to 1730-1950 CE. Profiles of $^{210}\text{Pb}_{\text{xs}}$ and ^{137}Cs provide further information on the depositional age of Sand 1 (Figure 6b). The CF:CS model indicates a mean sedimentation rate of 0.54 ± 0.10 cm/yr; extrapolation of this rate suggests a depositional age for Sand 1 of 1942-1964 CE. The appearance of detectable levels of ^{137}Cs just below Sand 1 corroborates this estimate; the onset of ^{137}Cs in the environment occurs around 1950 CE.

4.3.2. Discussion

Previous studies established that the stratigraphic record at the Shirasuka coastal lowlands preserves evidence for EWEs and terrestrial mass movements (Fujiwara et al., 2006b; Komatsubara et al., 2006b; 2008). Komatsubara et al. (2008) encountered between one and seven sand layers in each of their 11 geoslicer locations. Our six cores

contain four abruptly emplaced sand layers at a location within 25 m of Komatsubara et al.'s (2008) most comprehensive core. Comparison of the relative positioning and depth of each of these sand layers suggests that our two lowermost sand layers, Sands 4 and 3, can be correlated with the two lowermost sand layers reported by the previous study. Sand 1 can similarly be correlated with the uppermost sand layer. Correlation of the thick Sand 2 is, however, problematic, with the equivalent interval in Komatsubara et al.'s (2008) profile SRL4 featuring at least four sand layers deposited by EWEs. The substantial thickness of Sand 2 and the chaotic structures revealed by X-ray CT scans raise the possibility that, in our cores, successive EWEs are overprinted and the layer relates to multiple events.

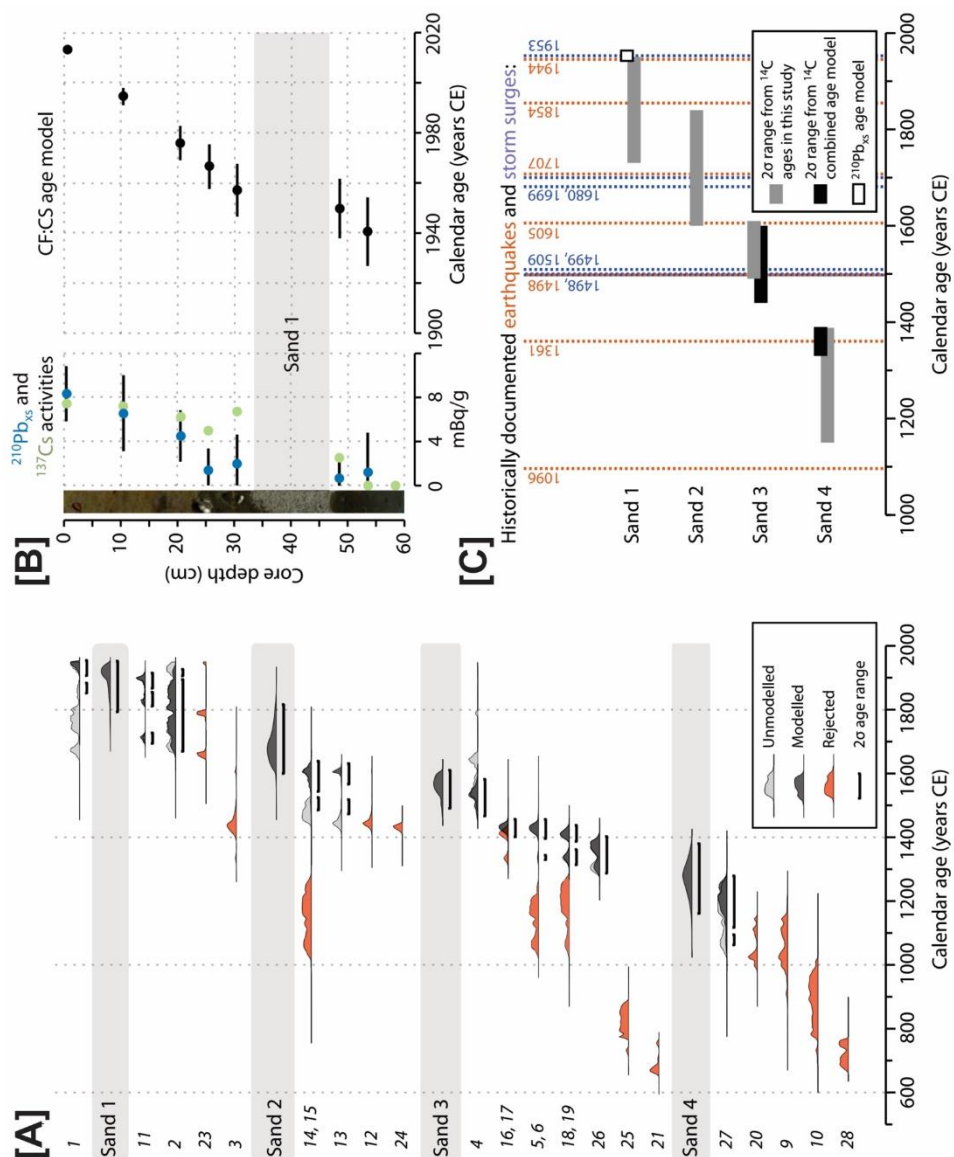


Figure 25: Timing of sand layer deposition at the Shirasuka lowlands. [A] ^{14}C Sequence model displaying prior and posterior probability density functions (italicised numbers refer to sample numbers; see also Figure 22). Paired AIO and macrofossil samples aligned to facilitate comparison. [B] Radionuclide activity profiles and CF:CS age model used to determine the age of Sand 1 in core JSH3/F. [C] Comparison of age ranges from panels [A] and [B] with age ranges from a combined age model incorporating ^{14}C dates from Komatsubara et al. (2008) and historically documented earthquakes and storm surges along the eastern Nankai-Suruga Trough. Modified from Garrett et al. (2018).

4.3.2.1. *Age of the sand layers and correlation with the historical record*

The ages of the four sand layers identified in the present study are consistent with historically documented earthquakes and EWEs occurring over the last ~800 years (Figure 25).

The modelled age range for Sand 4, 1154-1378 CE, includes the 1361 CE Shōhei earthquake and tsunami. Komatsubara et al. (2008) interpreted this layer as resulting from a mass movement because of the finer grain-size distribution, presence of mica and landward thickening of the deposit, but did not discuss the timing of deposition. Reanalysis of radiocarbon ages from the earlier study suggests an age consistent with an earthquake in 1361 CE (see chapter 4.1). A combined model incorporating ^{14}C data from Komatsubara et al. (2008) and from this study provides an age range of 1330-1390 CE, further corroborating our proposed correlation with an earthquake during this era. Single-grain infrared stimulated luminescence ages are also consistent with this hypothesis, with three ages constraining deposition to $1291 \text{ CE} \pm 78$, $1364 \text{ CE} \pm 72$ and $1390 \text{ CE} \pm 64 \text{ CE}$ (see chapter 4.4).

The modelled timing of the deposition of Sand 3, 1491-1610 CE, overlaps with the 1498 CE and 1605 CE tsunamis and storm surges in 1498 CE, 1499 CE and 1509 CE (Figure 25). Komatsubara et al. (2008) attributed the second oldest sand layer to the 1498 CE Meiō tsunami, with reanalysis of their ^{14}C data suggesting an age range of 1390-1460 CE (see chapter 4.1). A combined age model incorporating ^{14}C dates from the previous and current studies provides a 2σ range of 1442-1600 CE, while luminescence approaches yield a 1σ age of $1516 \text{ CE} \pm 49$ (see chapter 4.4). With extensive and well-documented evidence along the Enshū-nada coastline, including estimated wave heights of 6-8 m at the mouth of Lake Hamana (Hatori, 1975), the 1498 CE Meiō tsunami provides the most likely candidate for the origin of this sand layer.

The age model provides a long interval, 1601-1831 CE, for the deposition of Sand 2. This range overlaps with historically documented tsunamis in 1605 CE and 1707 CE and storm surges in 1680 CE and 1699 CE (Figure 25). The 1854 CE Ansei-Tōkai tsunami also lies just outside the 2σ range. The long interval may partly relate to a plateau in the radiocarbon calibration curve, but could also support our suggestion of the deposition and overprinting of multiple sand layers over an extended period of time. Luminescence ages support this interpretation, with the age of the lower part of the deposit consistent with the 1605 CE Keichō tsunami and the upper part dating to the mid to late 18th century (see chapter 4.4). Komatsubara et al. (2008) identified four sand layers within this interval, attributing them to tsunamis in 1605 CE, 1707 CE and 1854 CE and either the 1680 CE or 1699 CE storm surge.

The age range for the uppermost sand layer, constrained to 1942-1964 CE by ^{14}C and radionuclide approaches, overlaps with the 1944 CE Shōwa-Tōnankai earthquake and the storm surge accompanying Typhoon Tess in 1953 CE (Figure 25). Luminescence ages provide further corroboration, dating Sand 1 to $1948 \text{ CE} \pm 8$ (1σ) (see chapter 4.4). Komatsubara et al. (2008) suggested a terrestrial origin for this sand layer and did not discuss the timing of deposition.

4.3.2.2. *Depositional mechanisms of the sand layers*

Komatsubara et al. (2008) interpreted the lowermost sand layer as being derived from the terrace cliff based on its finer grain-size distribution, mica content and landward

thickening. In our study, the sedimentary structures identified in Sand 4 support the alternative hypothesis of tsunami inundation following the 1361 CE Shōhei earthquake. Sand 4 exhibits numerous features frequently linked with tsunami deposition, including abrupt contacts, rip-up clasts, inverse and normally graded beds and an internal mud drape, suggesting the repeated occurrence of waning and reactivation of sediment flows. Furthermore, the grain-size distributions are similar to both Sands 3 and 2 and the modern upper beach sample. The presence of well-preserved marine and brackish diatoms, found at higher percentages in Sand 4 than in any other layer, supports a marine contribution. The presence of freshwater diatoms, pollen from submerged aquatic plants and aquatic green algal taxa indicates sediment was also entrained from freshwater environments. The findings of Komatsubara et al. (2008) and of this study are not mutually exclusive; tsunamis may be accompanied by mass movements triggered by intense shaking. At Shirasuka, intense shaking may have destabilized the steep slopes above the lowland, with tsunami waves, particularly return flows, redistributing mass-movement deposits.

Sand layer 3 displays some notable sedimentary features, including abrupt contacts, multiple beds, entrained vegetation and rip-up clasts. While these structures may be consistent with deposition during tsunamis, they may also characterize storm surge deposits (Engel & Brückner, 2011; Morton et al., 2007; Shanmugam, 2012). Sand 3 displays grain-size distributions most closely reflecting the modern samples from the upper beach and lower dune. While Sand 3 may thus have been derived from beach and dune environments, diatom and palynomorph assemblages suggest a predominantly freshwater source. As none of the contemporary beach or dune samples yielded any diatoms, we suggest the 1498 CE Meiō tsunami may have eroded material from a range of saline and freshwater environments. Tsunami waves may have entrained and mixed diatom-poor beach or dune sand with freshwater marsh sediments rich in diatoms, aquatic pollen and green algae. The increased abundance of *Glomus* spores indicates redistribution of sediment from terrestrial environments. The presence of this mycorrhizal fungus may be associated with erosion of soils (Silva-Sánchez et al., 2014; Van Geel et al., 1989) and has been employed as a marker of erosion in coastal marsh environments (Kouli, 2012).

As discussed in relation to Sand 3, grain-size distributions in Sand 2 most closely resemble the modern beach and dune samples, with the presence freshwater diatom assemblages explained by mixing of different sediment sources. We suggest overprinting of multiple EWE deposits during the 17th and 18th centuries could explain the substantial thickness of Sand 2 and the difficulties in correlating this interval with the four sand layers identified by Komatsubara et al. (2008). The thickness of the deposit in our cores, the lack of grading or identifiable characteristic sedimentary structures and the long age range provided by age modelling suggest the possibility of post-depositional modification and homogenization in this particular location.

Komatsubara et al. (2008) identified a terrestrial origin for the uppermost sand layer based on the presence of mica, which dominates the terrace sediment matrix but is not found in modern foreshore samples. Our results agree with the terrestrial source of this layer. Sedimentation associated with the 1944 CE Shōwa-Tōnankai tsunami can be ruled out as it did not overtop the dune ridge; Watanabe (1998) reported wave heights of 0.9 m at the entrance to Lake Hamana. A landslide or debris flow originating from the mid-Pleistocene terrace appears the most likely origin. Sand 1 is similar to the other sand layers, with a comparable thickness, a marginally coarser grain-size

distribution and an abrupt lower contact. The deposit is inversely graded; while this has been recorded in deposits from both storm surges (e.g. Williams, 2009) and tsunamis (e.g. Naruse et al., 2010), normal grading is more commonly reported during such events (Morton et al., 2007). Optically stimulated luminescence overdispersion values of single-grain feldspars are higher than expected, potentially indicating a different transport mechanism than that associated with the other sand layers (see chapter 4.4). The prevalence of freshwater diatom species in Sand 1, as seen in the underlying sand layers, again points towards redistribution of material from terrestrial environments. Nevertheless, the near absence of aquatic pollen, non-pollen palynomorphs and algae suggests a lack of erosion of freshwater marshes, in contrast to the other sand layers.

4.3.2.3. Earthquake-triggered mass movements?

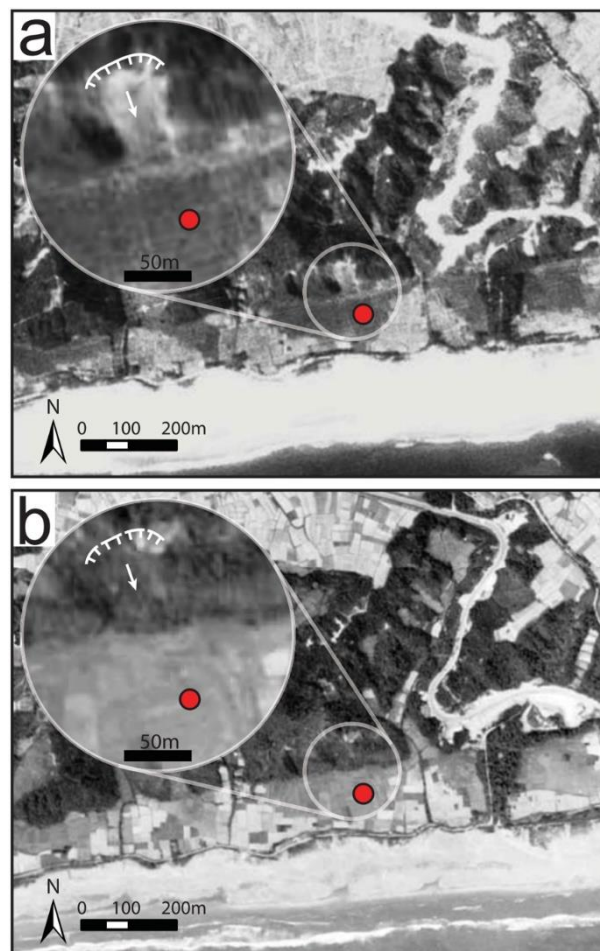


Figure 26: Orthorectified aerial photographs of the Shirasuka coastal lowlands from (a) August 1947, ~2.5 years after the December 1944 CE Shōwa-Tōnankai earthquake and (b) May 1959, ~14.5 years after the 1944 CE earthquake. Circles indicate the location of the cores used in this study and white hachured lines indicate the active scarp. Aerial photographs provided by the Geographical Survey Institute (<http://maps.gsi.go.jp>). From Garrett et al. (2018).

Sand 1, constrained to 1942-1964 CE by radionuclide dating, is consistent with a mass movement from the landward terrace. Shaking during the 1944 CE earthquake or intense rainfall associated with the 1953 CE typhoon provide two plausible triggers. Aerial photographs from 1947 CE confirm the occurrence of a mass movement, with

a fresh scarp and exposed bare soil visible on the steep terrace slope above the coring location (Figure 26). The slope rises at an angle of more than 30° to a height of 45 m above the coastal lowland. The date of this photograph discounts the typhoon as the trigger, but is consistent with the timing of the Shōwa-Tōnankai earthquake. The high rate of vegetation growth, highlighted by revegetation of the slope by 1959 CE, further suggests the mass movement occurred shortly before 1947 CE.

While secondary ground failures may provide evidence of seismic shaking (Keefer, 1984; 2002), field investigations along the Nankai-Suruga Trough have mainly focused on liquefaction features (Sangawa, 2009; 2013), or turbidites in marine and lacustrine settings (Inouchi et al., 1996; Iwai et al., 2004). Hatori (1975) suggested landslides accompanied the 1498 CE earthquake, and Usami (2003) listed landslides associated with the 1361 CE, 1707 CE and 1854 CE earthquakes; however, sub-aerial mass movement deposits have not received extensive study in this region. Nevertheless, our findings suggest they could provide a valuable and complementary coastal paleoseismic approach. Extensive uplifted marine terraces located above coastal lowland depocentres along the southern and eastern coasts of Japan (Koike & Machida, 2001) indicate that this could be a viable approach in Japanese subduction zone settings. As with turbidite-based paleoseismic investigations, the potential for mass movements triggered by typhoons rather than earthquakes would need to be assessed (cf. Shirai et al., 2010). Analysis of mass movement inventories associated with recent historical earthquakes, further development of inventories of typhoon-triggered mass movements (e.g. Saito et al., 2010) and regional correlation of coeval mass movement deposits may provide helpful steps towards developing this approach.

4.3.2.4. *Implications for historical rupture zones*

Komatsubara et al. (2008) correlated sand layers at Shirasuka with tsunami inundation in 1498 CE, 1605 CE, 1707 CE and 1854 CE, alongside storm surge inundation in the late 17th century. Here, we have additionally established the presence of sand layers consistent with tsunami inundation in 1361 CE and a seismically triggered mass movement in 1944 CE.

Evidence from historical records and liquefaction features at archaeological sites suggests that the Shōhei earthquake ruptured the Nankai region, the western half of the Nankai-Suruga megathrust, on 26 July 1361 CE (Ishibashi & Satake, 1998; Sangawa, 2013). Ishibashi (2004) and Seno (2012) raised the possibility of an eastwards extension of coseismic slip into the Tōnankai region, based on historical and geoarchaeological data. Ishibashi & Satake (1998) and Ishibashi (2014) provided an alternative hypothesis, suggesting a separate earthquake in the Tōnankai region in the early morning of 24 July, 2 days before the rupture of the Nankai region. While documentary evidence supports intense shaking around Kyoto and the Kii Peninsula at this time, there is no record of a concurrent tsunami along the Pacific coast. Garrett et al. (2016) summarized geological records and suggested that the wide distribution of possible evidence supported a rupture incorporating the Nankai, Tōnankai and Tōkai regions. Nevertheless, the paucity of well-constrained chronologies and unequivocal evidence for tsunami deposition limited the confidence of this assertion. Furthermore, either the eastwards extension of coseismic slip on 26 July 1361 CE or the occurrence of a separate rupture of the Tōnankai region on 24 July 1361 CE could explain the mapped distribution of geological evidence. In the absence of well-dated and comprehensively reported evidence from other paleoseismic sites, Sand 4 at

Shirasuka currently provides the most compelling evidence for tsunami inundation in 1361 CE from any site along the Nankai-Suruga megathrust. This finding is consistent with either a single larger rupture of both the Nankai and Tōnankai regions or two smaller ruptures separated by 2 days. While the identification of tsunami deposits at Shirasuka does not necessarily imply a rupture of the adjacent region of the megathrust, more recent ruptures of just the Nankai region in 1854 CE (Ansei-Nankai) and 1946 CE (Shōwa-Nankai) did not generate significant wave heights along the coastlines of the Tōnankai region (Watanabe, 1998). Intense shaking implied by the possible coeval occurrence of a mass movement at Shirasuka (Komatsubara et al., 2008) further supports the inferred rupture of the Tōnankai region in 1361 CE. With the 1361 CE Shōhei earthquake proposed as the start of a supercycle that culminated with the 1707 CE Hōei earthquake (Furumura et al., 2011; Garrett et al., 2016; Seno, 2012), further efforts to constrain the rupture zone or zones are clearly warranted.

The correlation of Sand 3 with the 1498 CE Meiō tsunami reaffirms the findings of Komatsubara et al. (2008). Proposed evidence for this tsunami is widespread in the Tōnankai region, including at Shijima (Fujino et al., 2008; Komatsubara & Okamura, 2007) and along the Enshū-nada coastline at Arai (Fujiwara et al., 2013a), Lake Hamana (Honda & Kashima, 1997) and Nagaya Moto-Yashiki (Takada et al., 2002). Historical, archaeological and geological records are in agreement, suggesting a rupture of the Tōnankai region (Garrett et al., 2016; Ishibashi, 2004; Sangawa, 2009; Seno, 2012). Liquefaction features at archaeological sites may imply a second earthquake or a westwards extension of the 1498 CE rupture zone into the Nankai region (Sangawa, 2009).

The difficulties encountered in attributing Sand 2 to particular EWEs prevent further analysis based on the findings presented here. If the site does record tsunami inundation in 1605 CE, 1707 CE and 1854 CE, as asserted by Komatsubara et al. (2008), this is in keeping with current understanding of the rupture zones of these earthquakes (Garrett et al., 2016; Ishibashi, 2004; Satake, 2015; Seno, 2012). The substantial differences in sand layer thickness between our work and the previous study at Shirasuka reinforce the high degree of variability in the stratigraphy and sedimentology of tsunami deposits on a very fine spatial scale. Furthermore, the overprinting of multiple EWEs highlights the potential for geological records to underestimate the frequency and overestimate the recurrence interval between events.

While inversion of geodetic and tsunami wave form data confidently places the 1944 CE Shōwa-Tōnankai rupture zone in the Tōnankai region (Ando, 1975a; Baba & Cummins, 2005; Tanioka & Satake, 2001), sedimentary evidence for this earthquake is limited. Intense shaking may be recorded by turbidite and mud breccia deposits from the Kumano Trough (Sakaguchi et al., 2011; Shirai et al., 2010) and liquefaction features at Tadokoro (Sangawa, 2009). Evidence for a mass movement at Shirasuka may provide a rare terrestrial record of seismic shaking in 1944 CE.

4.3.3. Conclusion

In this study we analyzed abruptly emplaced sand layers on the Shirasuka coastal lowlands using a rigorous multi-proxy approach in order to assess, reinterpret and build on the earlier work of Fujiwara et al. (2006b) and Komatsubara et al. (2006b; 2008). Thanks to a combination of new stratigraphic investigations, X-ray CT scanning and analyses of particle size, diatoms, pollen and non-pollen palynomorphs, we have

identified four sand layers that reflect not only inundation during tsunamis or typhoon-driven storm surges but also the occurrence of a terrestrial mass movement.

The oldest sand layer is consistent with the 1361 CE Shōhei tsunami; the presence of this deposit and possible evidence for coeval shaking support the latest interpretation of the Shōhei earthquake constituting a full-length rupture equivalent to the 1707 CE Hōei earthquake (Furumura et al., 2011; Garrett et al., 2016; Seno, 2012). We cannot discount an alternative hypothesis of two closely spaced ruptures of the Nankai and Tōnankai regions (Ishibashi, 2014; Ishibashi & Satake, 1998), but emphasize that either hypothesis implies slip in the Tōnankai region at this time.

With Bayesian age models, incorporating 11 new ^{14}C dates, we verify evidence for inundation during the 1498 CE Meiō tsunami deposit. While Komatsubara et al. (2008) identified four discrete sand layers associated with tsunamis in 1605 CE, 1707 CE and 1854 CE and a storm surge in 1680 CE or 1699 CE, we encountered a single 50-cm-thick sand at our coring locations. The probable overprinting of evidence previously attributed to multiple EWEs highlights both the high degree of lateral variability in the deposits and the potential for geological records to underestimate the frequency of tsunami occurrence.

By combining radionuclide dating with analysis of aerial photographs, we have demonstrated that the 1944 CE Shōwa-Tōnankai earthquake is the likely trigger for the mass movement responsible for depositing the youngest sand layer. Previously identified as of terrestrial origin (Komatsubara et al., 2008), we suggest this deposit constitutes a rare geological record of the most recent great earthquake in the region. The occurrence of earthquake-triggered failures of uplifted marine terraces supports the development of terrestrial mass movement deposits as a complementary paleoseismic approach in this and other regions

4.4. Single-grain feldspar luminescence chronology of historical extreme wave event deposits on the Shirasuka coastal lowlands

In this section, an assessment was made of the suitability of luminescence dating to constrain the age of young (< 1000 years) EWE deposits from the Shirasuka coastal lowlands (see chapter 4.3). Unsurprisingly, and in accordance with other studies on Japanese quartz (e.g. Tsukamoto et al., 2003; Tamura et al., 2015), quartz was found to be unsuitable for dating. Coarse grains of alkali-feldspar were tested and subsequently used for dating. The IRSL₅₀ signal measured as part of a post-IR₅₀ IRSL₁₃₀ protocol was found to be most suitable for dating these deposits.

The degree of bleaching of the Shirasuka sediment samples taken for luminescence dating was assessed by examining single coarse-grains of alkali-feldspars. The IRSL₅₀ (pre-IR₁₃₀) single-grain distributions were surprisingly well-bleached, suggesting that these were indeed taken from EWE deposits. Nevertheless, each sample contained a small proportion of grains with larger-than-expected D_e values, and for each sample the overdispersion values typically scaled with the D_e value. The unlogged minimum age model was therefore applied to the D_e data from these young sediments, using a novel iterative method for estimating the absolute overdispersion value (in Gy). This approach enabled a single method of D_e distribution analysis to be applied to all samples in this study, and resulted in fading-corrected IRSL₅₀ (pre-IR₁₃₀) ages that were both internally consistent, and that could also be correlated to other evidence for EWEs in this region, including the historical record and independent dating evidence.

As a detailed discussion about the methodology developed and applied for this study falls outside the scope of the QuakeRecNankai project, this section will focus on the results of the study in terms of geochronology. It is based on Riedesel et al. (2018). For more comprehensive information, please refer to Riedesel et al. (2018).

4.4.1. Results and discussion

4.4.1.1. Comparison with independent age control

Figure 27 shows the fading-corrected IRSL₅₀ (pre-IR₁₃₀) ages determined for the 10 samples collected from cores JSH1b/F and JSH1/O in the Shirasuka coastal lowlands. The equivalent dose (D_e) values underpinning all of these IRSL₅₀ (pre-IR₁₃₀) ages were obtained using a single method of D_e distribution analysis, as outlined by Riedesel et al. (2018). All data were corrected for anomalous fading using the average g_{2days} -value (2.48 ± 0.52 %/decade) (Riedesel et al., 2018). Buylaert et al. (2011) have shown that there is no improvement in precision by using aliquot-specific, or sample-specific fading rates. This approach is particularly appropriate in a geological setting where one would expect a similar provenance for all dated samples, as we interpret for the sediments in the cores studied here.

The luminescence ages generated cover the age range from the 13th century until the mid-20th century (Figure 27) and are all in stratigraphic order. Although the central values for the ages of samples JSH1-6 and JSH1-7 (taken 15 cm apart in core JSH1/O, from within the same sand unit) are inverted, these samples are in agreement within the 1σ uncertainties shown, indicating rapid deposition and demonstrating the reproducibility of the luminescence analyses within this sand unit.

The accuracy of the luminescence results can be assessed by comparing the ages with those obtained from ¹⁴C dating of wood, and with aerial photography (see chapter 4.3).

- A first comparison is made with wood samples that were obtained from just above and just below the sedimentary unit from which OSL-sample JSH1-20 was taken in sediment core JSH1b/F. These wood samples yielded calibrated radiocarbon ages of 1282-1399 CE (above) and 1040-1262 CE (below). The IRSL₅₀ (pre-IR₁₃₀) age of 1390 CE (± 64) for JSH1-20 is consistent with these age estimates (Figure 27).
- A second comparison is made with sample JSH1-2, which was taken from a sand layer interpreted to result from a landslide from the terrace immediately behind the coring site, triggered by intense earthquake shaking in 1944 CE. The landslide is recorded on aerial photography of the region in 1947 CE (see chapter 4.3). The IRSL₅₀ (pre-IR₁₃₀) age of 1950 CE (± 8) would support this interpretation. It is interesting to note that this sample has an overdispersion that is higher than would be expected; this too is consistent with a landslide origin.

The agreement of the luminescence ages with independent age estimates, and the low residual doses seen in two beach samples (0.03 ± 0.01 Gy for JSH-MOD3 and 0.12 ± 0.02 Gy for JSH-MOD4) implies that when using the IRSL₅₀ (pre-IR₁₃₀) signal from single grains, residual signals and thermal transfer are not major impediments (cf. Li et al., 2017).

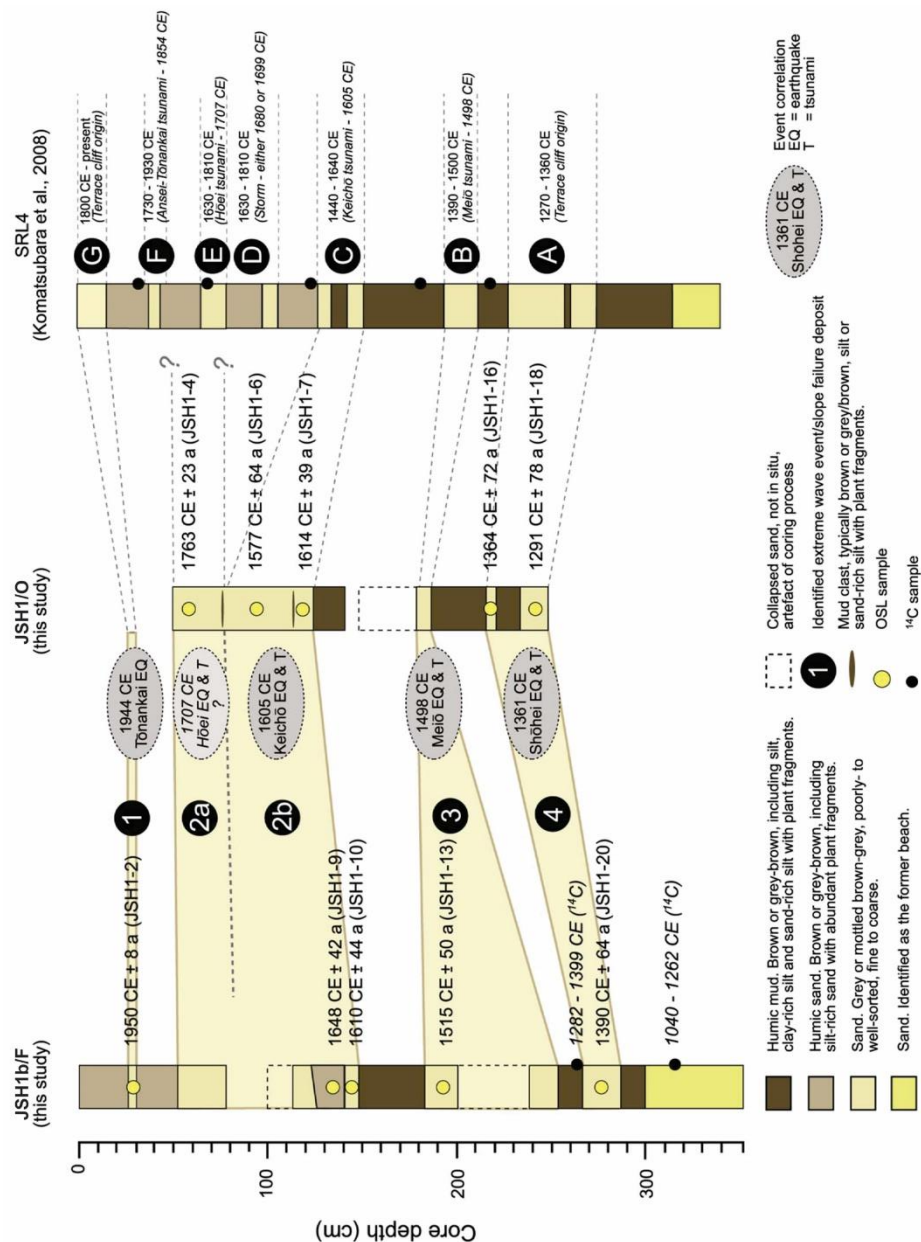


Figure 27: Stratigraphy and chronology based on IRSL₅₀ (pre-IR₁₃₀) ages for the Shirasuka coastal lowlands, in comparison to previous results by Komatsubara et al. (2008). Sand layers 1, 2, 3 and 4 are shown. Letters A to G are sands related to events identified by Komatsubara et al. (2008). The radiocarbon ages of core JSH1b/F are from Garrett et al. (2018) (see also chapter 3.4). Modified from Riedesel et al. (2018).

4.4.1.2. Integration with historical records and previous studies

The sedimentary record of the Shirasuka lowlands reveals a complex stratigraphy with laterally discontinuous sand sheets, reflecting deposition by EWEs. Radiocarbon dates published by Komatsubara et al. (2008) and Fujiwara et al. (2006b) constrain the EWE sedimentary record of the Shirasuka lowlands to be younger than 1200 CE. From 1200 CE onwards, at least six earthquakes and subsequent tsunamis occurred in segments C, D and E of the Nankai-Suruga Trough (see chapter 4.1). Additionally, large storm surges have inundated the lowlands several times (Komatsubara et al., 2008).

Lateral discontinuity between the sand layers recorded in cores taken from this site

has previously been described by Komatsubara et al. (2008), and this lateral discontinuity is also noted in cores JSH1b/F and JSH1/O even though they are only 0.5 m apart. However, correlation between the two cores in the present study, and potential links to the record of Komatsubara et al. (2008), can be aided by the luminescence ages generated (Figure 27).

- The lowermost sand unit in JSH1b/F (Figure 27) is ^{14}C dated to 1040-1262 CE and is identified as the former beach (see chapter 4.3).
- Sand 4. A minimum age for Sand 4 in JSH1b/F is given by the ^{14}C age (1282-1399 CE) of plant macrofossils (see chapter 4.3), and IRSL₅₀ (pre-IR₁₃₀) ages of 1291 CE \pm 78 (sample JSH1-18, core JSH1/O), 1364 CE \pm 72 (sample JSH1-16, core JSH1/O) and 1390 CE \pm 64 (sample JSH1-20; core JSH1b/F) overlap within 1-2 σ uncertainties. Sand 4 in each core can be correlated on the basis of age with unit A of Komatsubara et al. (2008), which they date to 1270-1360 CE using ^{14}C dating, and which they interpret to be derived from terrace material based upon the mica content. The luminescence ages for Sand 4 are consistent with the 1361 CE Shōhei earthquake and tsunami. Based on historical documents, this earthquake has so far been interpreted as a rupture of the western segments of the Nankai-Suruga Trough (segments A and B). Ishibashi (2004) mentioned the possibility of a synchronous rupture of the eastern and western segments of the Nankai Trough in 1361 CE, or even the possibility of a separate rupture of the eastern segments two days prior to the earthquake of the segments A and B (Ishibashi & Satake, 1998; Ishibashi, 2014). No tsunami deposits in the eastern Nankai region have been reported from this event, but this sand sheet could give the first evidence for tsunami inundation in this region.
- Sand 3. Sand 3 has little chronological control from this study, making correlation between cores on the basis of chronology impracticable. However, sample JSH1-13 from core JSH1/F yields a date of 1515 CE (\pm 50), which correlates well with the 1498 CE Meiō tsunami. Komatsubara et al. (2008) also correlated their Unit B with the Meiō tsunami on the basis of radiocarbon dating of their core (Figure 27; 1390-1500 CE). Inundation of the Enshū-nada coastline by the Meiō tsunami has already been demonstrated (e.g. Fujiwara et al., 2013a), making it a reasonable assumption to find some evidence of this event preserved in the Shirasuka lowlands stratigraphy.
- Sand 2. Sand 2 contains samples JSH1-10 (from core JSH1/F) and JSH1-6 and JSH1-7 (from core JSH1/O). The three luminescence ages obtained (1610 CE (\pm 44), 1577 CE (\pm 64) and 1614 CE (\pm 39), respectively) are tightly clustered, and can be correlated with unit C of Komatsubara et al. (2008), which was associated by them with the 1605 CE Keichō tsunami. The three luminescence ages provide a much more precise association with this event than the ^{14}C ages of Komatsubara et al. (2008), which yielded a wide envelope ranging from 1440 CE to 1640 CE. Sample JSH1-9 comes from the finer deposit that caps this sand unit in core JSH1/full, but was later interpreted to be a rip-up clast. The date of 1648 CE (\pm 42) is also consistent with the underlying sand originating from the 1605 CE tsunami. The age of JSH1-9, and the presence of this fine unit between two sand units in core JSH1/F, also implies that the overlying sand units probably relate to a different event. Indeed, the date of 1763 CE (\pm 23) for JSH1-4, taken from the uppermost part of sand unit 2, is statistically distinct from the ages obtained for the lower part of sand unit 2 (which contains JSH1-6 and JSH1-7), suggesting that unit 2 records two discrete events (labelled 2a and 2b on Figure 27). It is not immediately obvious what historical event unit 2a correlates with, or which unit of Komatsubara et al. (2008) it might correspond to (i.e. Unit D, E or F), if any. The

EWE closest in time is the 1707 CE Hōei tsunami, although the luminescence age is ~ 2.5 standard deviations from this event. Interestingly, the 1751 CE Concepción (Chile) tsunami also lies within the age range from luminescence dating (1763 CE ± 23), and is known to have crossed the Pacific and inundated parts of the Japanese coastline (e.g. at Sendai and Wakayama; Atwater et al., 2015); however, there is no historical evidence for inundation along the Enshū-nada coast at this time (Watanabe, 1998).

- **Sand 1.** Sand 1, the uppermost sand unit in core JSH1/full, with sample JSH1-2, gave a luminescence age of 1950 CE (± 8) and this correlates well with the 1944 CE Shōwa-Tōnankai earthquake that affected this region. Although this 1944 CE earthquake caused a tsunami, its wave height (~ 0.9 m) was too small to overwash the coastal dune. Komatsubara et al. (2008) used radiocarbon dating to constrain their Unit G with which this correlates, describing it as being derived from terrace material, but a radiocarbon plateau at this time meant that the age constraints were very limited (younger than 1800-1930 CE). The luminescence age in the present study (Figure 27) provides a much tighter constraint on the timing of emplacement of this sand unit.

4.4.2. Conclusion

The fading-corrected $IRSL_{50}$ (pre- IR_{130}) ages demonstrate that cores JSH1b/F and JSH1/O span the historical record of EWE deposits in this region. The luminescence ages also demonstrate that it is possible to differentiate between individual events that occurred within the past 800 years. These $IRSL_{50}$ (pre- IR_{130}) ages can be linked to the presence and impact of tsunamis in 1361 CE, 1498 CE, and 1605 CE, and also to a slope failure triggered by the 1944 CE Shōwa-Tōnankai earthquake. The absence of sand layers caused by other known EWEs in this region, such as the 1707 CE Hōei tsunami and the 1854 CE Ansei-Tōkai earthquake and tsunami events, is potentially due to issues of preservation such as lateral discontinuity of the sand sheets.

In some cases, the luminescence dates generated in this study constrain the EWE units more precisely than the radiocarbon dating, due to the plateau within the ^{14}C -calibration curve around the time of interest. This study highlights the great potential for using luminescence dating, including using a signal from feldspars, to date even young EWE deposits in both this region, and potentially elsewhere.

4.5. Sedimentary evolution of the Sagara coastal area and its potential to preserve extreme wave deposits

4.5.1. Results

In the Sagara lowlands, cores were retrieved from a series of paddy fields on the northeastern side of the Hagima River (Site 1), and a more urbanized location on the southwestern side of the river (Site 2) (Figure 28).

4.5.1.1. Site 1

The cores from Site 1 are organized in four cross-sections, one cross-shore (A-A*) and three long-shore (B-B*, C-C* and D-D*) (Figure 28). The cores are typically 2 to 3 m in length and depict a complex stratigraphic record with fluvial and coastal sediments (Figure 29). The sedimentary record in Sagara started in the Holocene as an estuarine environment that transitioned into a more deltaic complex. Long-shore coastal currents and riverine input are the two dominant sediment supplies in the greater sedimentary system. The four transects show that fluvial processes dominated in the

early part of the sequence and evolved towards mostly mixed and mud-dominated floodplain sub-environments.



Figure 28: Location map of the core transects A-A*, B-B*, C-C* and D-D* in Site 1, and of core SGB-4 in Site 2 of the Sagara lowlands.

Three potential EWE deposits were identified in cores SGL21, SGL25, SGL26, SGL27 and SGL28. However, their occurrence is rather erratic and in general such EWE deposits are not abundant in the record. This contrasts expectations, as historical documents give evidence for numerous large tsunamis in the area. For unclear reasons the preservation potential of EWE deposits in these lowlands appears to be low. XRF-scanning data show low abundance of sulphur (S) in the upper record, which is hence interpreted to have little marine influence. The sulphur count across suspected EWE deposits remains low, too, which may indicate that they are not of marine origin. Manganese (Mn) is abundant in the top ~50 cm, which are intervals interpreted to be anthropogenically altered.

4.5.1.2. Site 2

On Site 2, focus has been on the interpretation of the stratigraphy and sedimentary record of the 20 m long core SGB-4:

- 0-0,3 m: Anthropogenically impacted sequence
Sagara has been populated since at least c. 700 CE, with construction of a castle less than 1 km away from the coring site. Repetitive ploughing or building and rebuilding houses or infrastructure impacted the upper c. 30 cm of the sedimentary record.
- 0.3-2 m: Late Holocene muddy and sandy sequence
Highly abundant rootlets and charcoal. Reflecting an environment that changes frequently between high and low energy, like a river floodplain.
- 2-6 m: Middle Holocene rather homogenous muddy sequence
Lack of marine macrofossils and sandy sequences. Reflecting a stable low-energy environment, like a barrier-locked estuary.
- 6-10 m: Early to Middle Holocene muddy sequence

High abundance of marine macrofossils and charcoal, and lack of sandy deposits. Reflecting a stable, low-energy marine environment, like a nearshore bay or fjord.

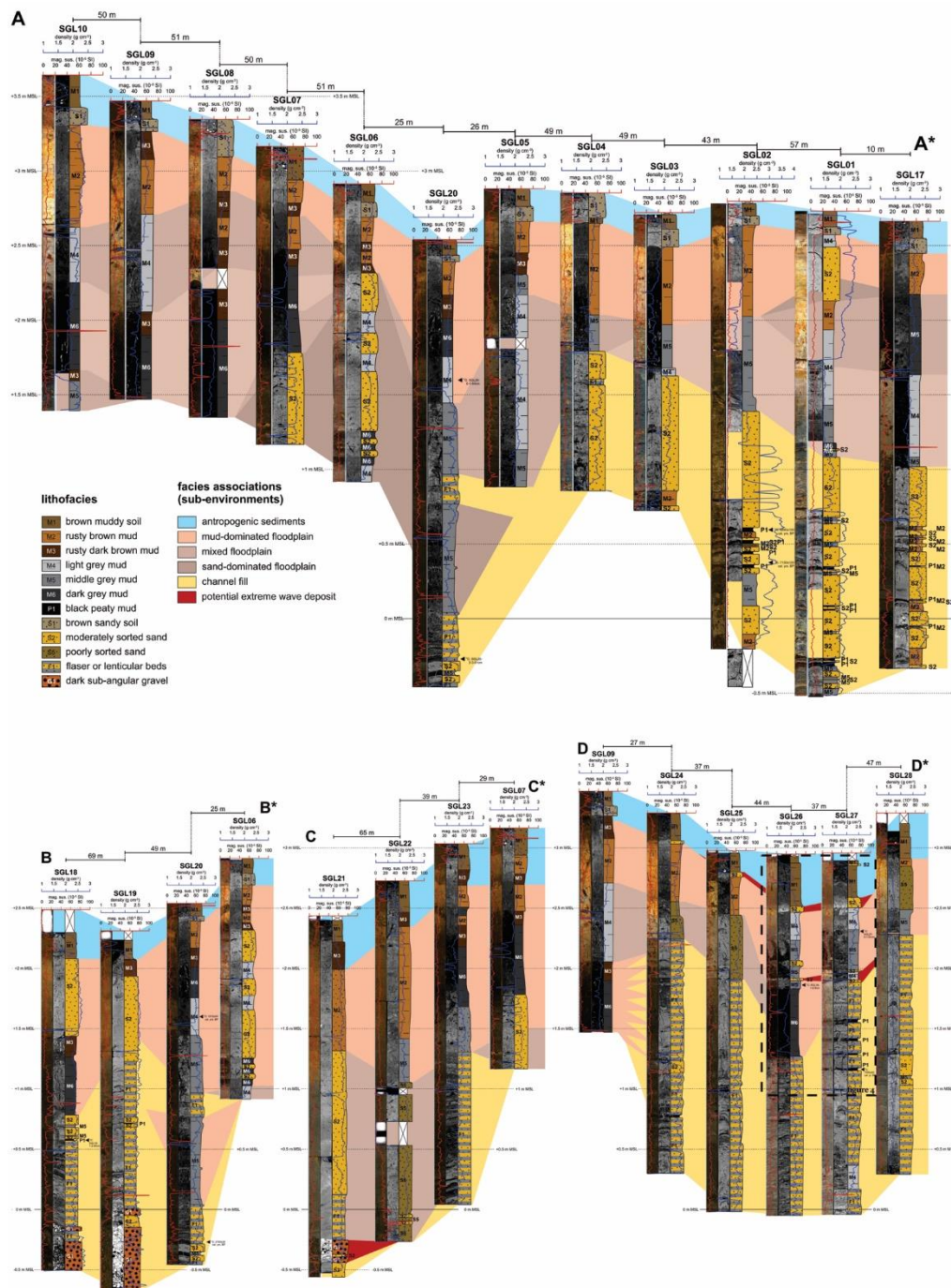


Figure 29: Detailed plot and proxy records of cores along transects A-A*, B-B*, C-C* and D-D*. For each core is shown: contrast-enhanced composite core photograph, CT-image, schematic lithology with division in lithological units, MS and gamma-density. Potential EWE deposits are highlighted in red.

- 10-16 m: Early Holocene muddy and sandy sequence
Shallow bay mud with high abundance of marine macrofossils. Several sandy sequences with muddy layers and some gravel content, up to ~50 cm thick. Reflecting a stable low-energy environment, like an open marine bay, but with

- sporadic, highly energetic episodes.
- 16-16.5 m: Late Pleistocene/Early Holocene sand sequence
Medium to fine shoreface sand with no sedimentary structures. Reflecting the rapid Late Glacial transgression.
 - 16.5-17.5 m: Late Pleistocene coarse gravel sequence
Erosional base and coarse gravel river bed facies. Reflecting a near-coast landscape and forming a Cenozoic/Quaternary unconformity at highly variable depths.
 - 17.5-20 m: Late Miocene mudstone sequence
Continental slope mudstone with intercalated turbidites, representing folded and uplifted accretionary prism deposits of the Nankai-Suruga Trough. These sediments build the base to study area.

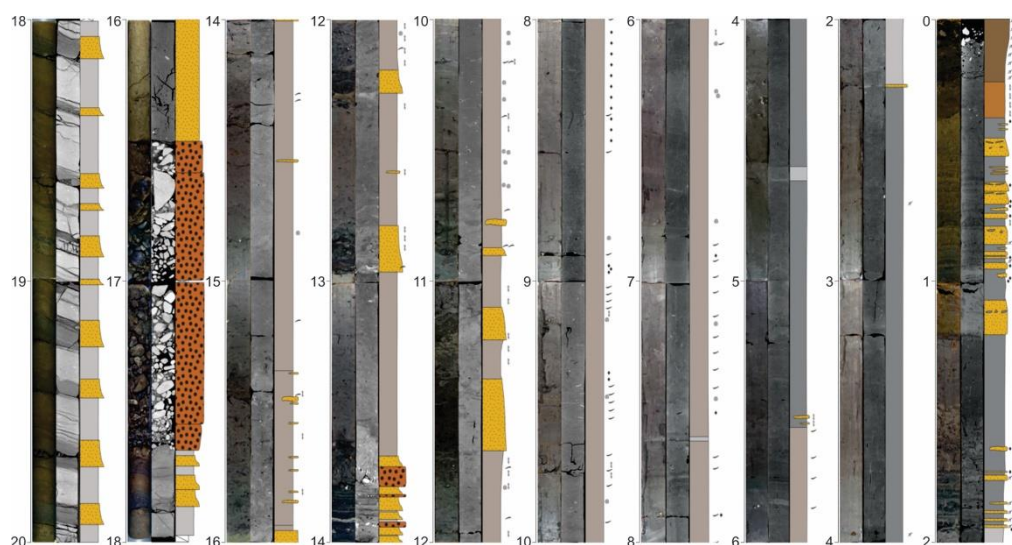


Figure 30: Individual 2 m sections of core SGB-4. For each section is shown: core photograph, CT-image, schematic lithology with division in lithological units.

Repeated fining-up sandy deposits, embedded within Early Holocene shallow-marine mud, characterized by sharp erosional horizons and containing shells or gravel are interpreted as potential EWE deposits.

4.5.2. Conclusion

The new cores from the Sagara lowlands depict the Late Pleistocene to Holocene evolution of the Sagara coastal and fluvial system. Sporadic traces of event deposits are found in some cores of Site 1, although a marine origin of these event deposits is unclear. Core SGB-4 from Site 2 contains a series of potential EWE deposits. Further analysis (e.g. grain-size and micropaleontological analysis) and radiocarbon dating is required to ascertain the nature and age of these deposits.

4.6. Sedimentary records of past earthquakes in Lake Motosu during the last ca. 6000 years

The Fuji Five Lakes area is tectonically influenced by three subduction zones and a series of inland faults. The area is located at the triple junction where the North American Plate, the Eurasian plate and the Philippine Sea Plate meet.

The Philippine Sea Plate is subducting under the Eurasian Plate at a rate of 40-55 mm/yr in its central part (Seno et al., 1993; 1996; Mazzotti et al., 2000; DeMets et al., 2010; Loveless &

Meade, 2010) along the Nankai-Suruga Trough. Its inland extension constitutes the Fujikawa-kako Fault Zone (FKFZ) located southwest of the Fuji Five Lakes. The Nankai-Suruga Trough is divided into five segments (A to E; Figure 1), rupturing separately or in a range of multi-segment combinations (Ando, 1975a; Ishibashi, 2004). Recently, segments A and B ruptured during the 1946 CE Shōwa-Nankai earthquake (M_w 8.1) and the 1854 CE Ansei-Nankai earthquake (M_L 8.4) (Ando, 1975a; Ishibashi, 2004). Segments C and D ruptured during the 1944 CE Shōwa-Tōnankai earthquake (M_w 8.1) and the 1854 CE Ansei-Tōnankai earthquake (M_L 8.4) (Ando, 1975a; Ishibashi, 2004). The 1854 CE Ansei-Tōnankai earthquake also ruptured segment E. Since 1854 CE, segment E did not produce significant earthquakes.

The Sagami Trough is the locus of subduction of the Philippine Sea Plate beneath the North American Plate at an average rate of 20 mm/yr (Loveless & Meade, 2010). The Kozu-Matsuda Fault Zone (KMFZ), located to the east of the Fuji Five Lake area, is the onshore extension of the Sagami Trough (Figure 1). This fault branches from the plate boundary as an imbricate thrust (Sato et al., 2005). Over the last millennium, three major earthquakes occurred along the Sagami Trough: the 1923 CE Great Kanto earthquake (M_w 7.9-8.2), the 1703 CE Genroku earthquake and the 1293 CE Einin-Kamakura earthquake (Usami, 2003; Ishibashi, 1991). Trench excavations revealed that the Kozu-Matsuda Fault Zone did not rupture during the 1923 CE Great Kanto earthquake and the 1703 CE Genroku earthquake. The last rupture of this fault zone is inferred to have occurred during the 1293 CE Einin-Kamakura earthquake (Kanagawa Prefecture, 2003).

Along the Japan Trench, the Pacific Plate subducts under the North American Plate and Philippine Sea Plate with convergence rates ranging from 80 to 86 mm/yr (DeMets et al., 2010). After the 2011 Tōhoku-oki earthquake (M_w 9.0), fishermen reported water body oscillations (seiches) in two of the Fuji Five Lakes: Lake Sai (Suzuki, 2012) and Lake Motosu. This seiche left no trace in the lacustrine sediment of Lake Sai. Three days after the 2011 Tōhoku-oki earthquake, an aftershock was reported at the foot of Mount Fuji at 9 km depth, the 2011 Shizuoka-ken Tobu earthquake (M 6.4).

North of the Fuji Five Lakes area, the Itoigawa-Shizuoka Tectonic Line (ISTL) represents the present-day plate boundary between the North American Plate to the east and the Eurasian plate to the west (Nakamura, 1983; Wei and Seno, 1998; Taira, 2001). During the Late Quaternary, its average left-lateral slip rate is estimated between 5 to 14 mm/yr (Ikeda and Yonekura, 1986; Fujimori, 1991; Okumura et al., 1994). The last large magnitude earthquake occurred in AD 841 (Okumura, 2001).

In addition to megathrust or plate-boundary earthquakes, also intraplate earthquakes can cause severe seismic shaking in the Fuji Five Lakes area. A series of active faults are present to the north of the Fuji Five Lakes, at the southern margin of the Kofu Basin (Sone-kyuryo Fault Zone) (Active Fault Data Base of Japan, https://gbank.gsj.jp/activefault/index_e_gmap.html). On the Izu Peninsula, south of the Fuji Five Lakes area, active faults such as Tanna Fault may generate large magnitude earthquakes. The Tanna Fault triggered in 1930 CE the Kita-Izu earthquake (M_s 7.3) (Usami, 2003).

In this section we investigate the possible traces of past earthquakes as recorded by the sedimentary infill of Lake Motosu, one of the studied Fuji Five Lakes. This section contains *capita selecta* from Lamair (2018).

4.6.1. Results

4.6.1.1. Bathymetry/Morphology

Lake Motosu, located at the foot of the northwestern flank of Mount Fuji, is relatively small (4.7 km²) and deep (max. 125 m), with a catchment covering an area of 24.45 km². It is characterized by a restricted flat deep basin. This deep basin is surrounded to the east and southeast by steep slopes (between 18° and 26°), which are formed by the Aokigahara and Motosu lava flows, to the south and to the north by steep slopes (between 20° and 37°), which are formed by the Furusekigawa and Tokiwa Formations and to the northwest, southwest and northeast by shallow platforms with gentle slopes (between 1.5° and 7°) (Lamair et al., 2018). These shallow platforms are located downstream of the river valleys and have a stair-case morphology, suggesting that the lake's water level has increased through time. The following stages in platform development can be defined, based on their water depth position: platform stage 1 lies at ca. 120 m, platform stage 2 between 65 and 115 m, platform stage 3 between 27 and 55 m, and platform stage 4 at ca. 24 m. Platform stage 2 is the largest one and covers an area of ca. 0.65 km² (Lamair et al., 2018). The platforms show a decreasing sedimentary thickness, going from ca. 11 m for platform 2, to ca. 2 m for platform 4.

The deep basin lake floor morphology has been strongly affected by the presence two large mass-transport deposits (MTDs), dated at around ca. 8000 cal yr BP and ca. 2000 cal yr BP (Lamair et al., 2018). The expression of the ca. 2000 cal yr BP MTD (MTD 13) is still visible on the lake floor, as a hummocky relief in the eastern part of the deep basin.

4.6.1.2. Sedimentology

Analysis of the gravity cores (MOT14-01 up to MOT14-06) shows that the sedimentary succession on the platforms differs from that of the deep basin floor.

On the platforms, the sedimentary infill consists of clayey silt with very few mm-scale silty laminae. Magnetic susceptibility values are relatively stable with an average of 1×10^{-3} SI. The LOI at 550° (% OM) ranges from 8.5 % to 12.0 %. The crystalline fraction comprises on average 18 % of plagioclase, 5 % of muscovite, 22 % of quartz+cristobalite and 55 % of clay. The clay fraction consists of illite (75 %) and chlorite (25 %). The amorphous mineral fraction equals on average 48 % and is predominantly composed of diatom frustules. SEM observations show that diatoms are mostly intact and well preserved. These clayey silt deposits are interpreted as the background sedimentation, representing the steady-state sedimentary dynamics and resulting from primary productivity in the water column and the settling of river-supplied suspended matter. This background sediment is interbedded by a unit composed of 9 scoria layers, characterized by high magnetic susceptibility values (max. 5.6×10^{-3} SI). X-ray images show that 4 of these scoria layers consist of reworked scoria, embedded in the clayey silt deposits. These are probably derived from scoria fall-out deposited on the platforms. The other scoria layers may be related to direct fall-out from Mount Fuji. XRF analysis indicates that all of them have a similar composition: SiO₂ 51.2 % ± 1.0 %, TiO₂ 1.0 % ± 0.1 %, Al₂O₃ 17.5 % ± 0.8 %, Fe₂O₃ 10.3 % ± 0.5 %, MnO 0.2 % ± 0.01 %, MgO 9.6 % ± 0.5 %, CaO 9.6 % ± 0.5 %, Na₂O 2.1 % ± 0.07 %, K₂O 0.6 % ± 0.1 % and P₂O₅ 0.2 % ± 0.04 %. This geochemical signature is similar to that of the known Mount Fuji scoria (Ishizuka et al., 2007). Therefore, we infer that the scoria layers on the platform originated from Mount Fuji and could be represent either direct scoria fall-out or reworking processes.

On the basin floor, the same background sedimentation, consisting of clayey silt, rich in diatoms and with a small fraction of organic matter and terrigenous sediments, is present. It is interrupted by instantaneous (i.e. rapidly deposited) sedimentary event deposits (i.e. turbidites) that constitute more than 60 % of the sedimentary record. The turbidites were classified into three groups: Facies 2 (F2), Facies 3 (F3) and Facies 4 (F4) turbidites (Lamair et al., 2018).

- F2 turbidites consist of a thin coarse-grained base (sand) covered by a grey-brown siliceous clayey silt, with a fine-grained white layer at the top. The basal coarse sandy layer is characterized by high peaks of MS and Sr, and may contain scattered organic matter. The homogeneous grey-brown siliceous clayey silt deposit is characterized by uniform MS and LOI at 550°C (in average, 10 % of organic matter content). Also the Br, Sr and Zr content show little variability. Diatoms are heavily broken; in the upper part of F2 turbidites, smaller broken pieces of diatoms are abundant, while also some large diatoms with no damage are present.
- F3 turbidites are characterized by a thin coarse-grained basal layer (most of the time, organic matter) covered by grey-brown siliceous clayey silt. The fine-grained white cap is usually absent or not visible to the naked eye. MS values tend to be low at the base due to the presence of high concentrations of organic matter. The clayey silt deposits show stable MS values and LOI at 550°C (in average, 10 % of organic matter content). F3 turbidites have similar concentrations of Br and Zr, a lower Ti content and MS values and a higher concentration of S than F2 turbidites. Most diatoms are heavily damaged.

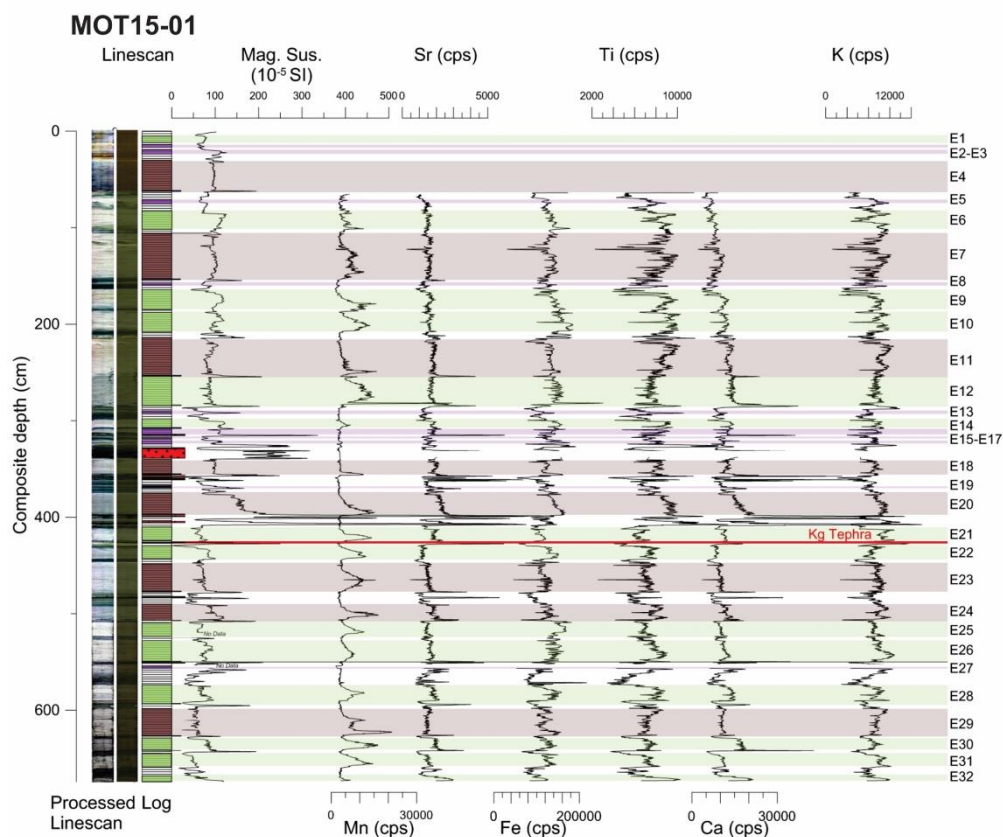


Figure 31: Geophysical and geochemical parameters of composite piston core MOT15-01. From left to right, processed linescan image, linescan image, sedimentary log, MS, Mn, Sr, Fe, Ti, Ca and K depth profile.

- F4 turbidites are a normally graded deposit characterized by a thin basal coarse-grained layer (sand and/or organic matter) covered by gray-brown siliceous clayey silt. In comparison with the other turbidites, F4 turbidites are usually very thin (2.5-4.0 cm thick). MS, Zr and Sr values increase within the sandy layer, and show a decreasing trend immediately in the overlying silty deposits. LOI at 550°C shows a similar pattern. F4 turbidites are composed of a mixture of broken diatoms and terrigenous material, but also contain well-preserved diatoms.

4.6.1.3. Background sedimentation versus sedimentary event deposits in the deep basin

The sedimentary log and the MS and XRF data of the master composite core MOT15-01 are presented in Figure 31. The background sedimentation in MOT15-01 consists of grey-brown clayey silt, rich in diatoms and containing small fractions of terrigenous material and organic matter. It is similar to the background sedimentation in the gravity cores (Lamair et al., 2018). As in the gravity cores, this background sedimentation is interrupted by a series of instantaneous sedimentary event deposits, interpreted as turbidites (i.e. F2, F3 and F4 turbidites). In total, 32 sedimentary event deposits were identified in MOT15-01: E1 to E32, comprising 8 F2 turbidites, 14 F3 turbidites and 10 F4 turbidites (Figure 31).

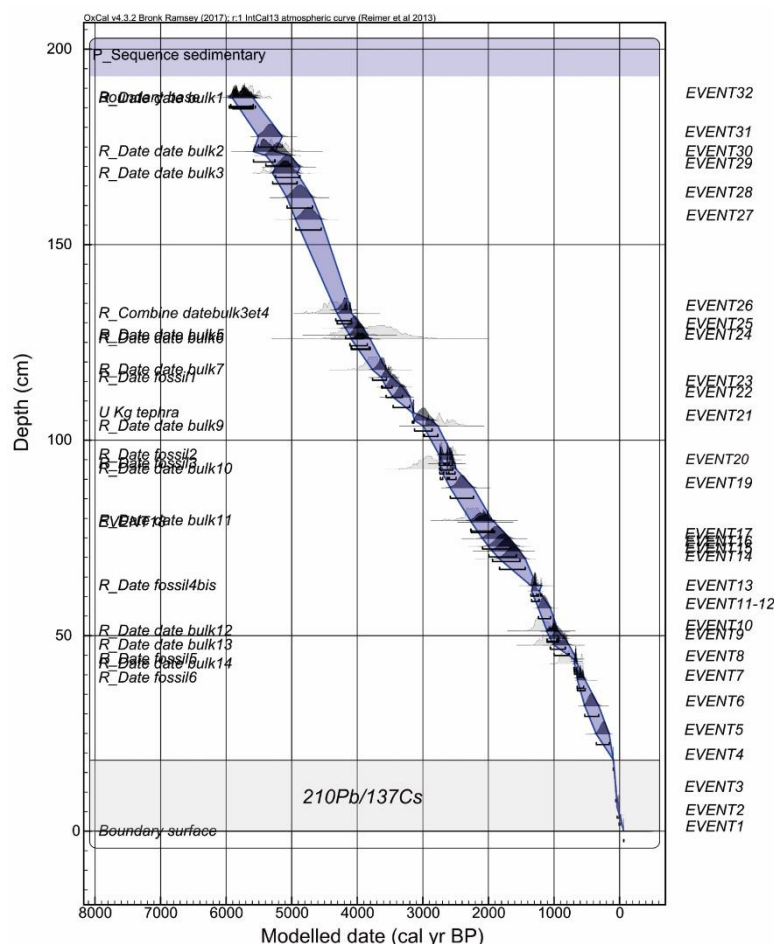


Figure 32: Age-depth model of the composite piston core MOT15-01.

4.6.1.4. Age of the event deposits

According to the age-depth model (Figure 32), the sedimentary record of the master composite core MOT15-1 covers the last ca. 5500-6000 cal yr BP, during which 32

sedimentary events were recorded. This implies a mean recurrence time of 184 ± 8 years.

The age of the last four events (E1 to E4) has been constrained by $^{137}\text{Cs}/^{210}\text{Pb}$ dating (Lamair et al., 2018); that of the older events by ^{14}C dating, combined with a tephra marker age (i.e. the Kawagodaira pumice (Kg), dated at 3160-3137 cal yr BP; Tani et al., 2013).

4.6.2. Discussion

4.6.2.1. Identifying trigger mechanisms for turbidites

The sedimentary sequence of Lake Motosu contains a succession of turbidites, as well as MTDs (Lamair et al., 2018). In high-seismicity regions, most sub-lacustrine slope failures, leading to the deposition of MTDs and/or turbidites, are generally linked to earthquake shaking (e.g. in Chilean lakes: Van Daele et al., 2015; in Alpine lakes: Schnellmann et al., 2006; Beck, 2009; in Alaskan lakes: Praet et al., 2017). A seismic trigger is normally ascertained by demonstrating that the three following criteria are respected: (i) sub-lacustrine slope failures are regionally synchronous (Adams, 1990; Beck et al., 2007; Goldfinger, 2011; Patton et al., 2013; Atwater et al., 2014; Howarth et al., 2016); (ii) historic ones are coeval with an historical earthquake (e.g. Chapron et al., 1999; Schnellmann et al., 2002; Monecke et al., 2004); (iii) alternative trigger mechanisms can be dismissed.

Multiple and synchronous slope failures

Earthquake shaking is a regional-scale process and therefore multiple slope failures are expected to be recorded simultaneously within the same lake, and even within multiple lakes in the same region. In Lake Motosu, only one large mass-transport deposit (MTD 13; Lamair et al., 2018) is recorded during the last ca. 6000 years, which is associated with one of the turbidites identified in piston core MOT15-01 (i.e. probably E18). All other turbidites in the record are not associated with an MTD and were likely not caused by sub-lacustrine slope failure, but rather by the remobilization of a surficial veneer of sediment covering the platforms. The remobilization of a surficial slope sediment layer of 4 to 15 cm on the platforms would be required to generate the thickest turbidites deposited on the basin floor. Moreover, the turbidites are rich in diatoms and their C/N ratio indicates that most of the organic matter was produced in-situ. Their geochemical composition close to that of the background sedimentation indicates that the source of the sediment is reworked background sediment. Similar observations have been described in Chile (Moernaut et al., 2017). Turbidites were identified in both gravity cores and piston cores taken in different depositional environments (i.e. on the basin floor close to the slopes versus on the deep flat basin floor). Core-to-core correlation highlights the synchronicity of the turbiditic flows, supporting a lake-scale process.

Correlation with recent earthquakes

The historical earthquake catalogue documents earthquakes since the 7th century (Ishibashi, 2004). Due to various reasons, such as civil wars, the amount of documents from the 14th-16th centuries is much smaller than in other periods (Ishibashi, 2004). Consequently, earthquakes that occurred during this time span might be missing in the catalogue. The ages of the upper four turbidites identified in piston core MOT15-01 (E1 to E4) are relatively well constrained. Based on the $^{210}\text{Pb}/^{137}\text{Cs}$ age-depth model and the historical earthquake catalogue, we correlate the sedimentary event deposits with recent historical earthquakes.

The absence of ^{137}Cs above E1 suggests that E1 has been deposited before 1955 CE and is likely related to the 1944 CE Shōwa-Tōnankai earthquake (M_w 8.1, 1223 casualties), which ruptured segments C and D of the Nankai-Suruga megathrust, but did not include segment E (NOAA, 2017). It is the most recent, large-magnitude earthquake that affected the Fuji Five Lakes area (JMA intensity 5; Usami, 2003).

According to the ^{210}Pb age-depth model, the age of E2 is estimated between 1930 CE and 1919 CE. During this period, two earthquakes impacted the Fuji Five Lakes area: the 1930 CE Kita-Izu (M 7.3) and the 1923 CE Great Kanto earthquake (M_w 7.9-8.2). The first one is an intraplate earthquake that ruptured the Tanna strike-slip Fault (Izu Peninsula) and killed 259 people (NOAA, 2017). A JMA seismic intensity of 4 was recorded in the Lake Motosu area (Usami, 2003). The second one, the 1923 CE Great Kanto earthquake, occurred along the Sagami Trough (> 100 000 casualties), affecting the Motosu area with a JMA intensity of 5 (Usami, 2003). Given that it was characterized by a higher JMA seismic intensity in the Lake Motosu area, it is more likely that the 1923 CE Great Kanto earthquake triggered turbidite E2.

E3 is dated around 1877 CE \pm 20. Based on the historical earthquake catalogue, this turbidite could correspond to the 1894 CE Meiji Tokyo (M 7.0) or the 1895 CE Ibaraki-ken Nanbu (M 7.2) earthquakes. Both earthquakes generated JMA seismic intensities higher than 4 around Lake Motosu (Usami, 2003). It is impossible to uncover which of the two earthquake is recorded in the lake as both of them occurred in a very short time span. The 1894 CE Meiji Tokyo earthquake (M 7.0) ruptured the Philippine subduction plate and affected mostly the eastern Tokyo and Tokyo Bay areas (31 casualties). The deeper (80 km) 1895 CE Ibaraki-ken Nanbu earthquake (M 7.2) occurred further east, rupturing the subducting Pacific plate.

E4 was deposited before 1877 CE \pm 20. In the 19th century, only the 1854 CE Ansei-Tōkai earthquake (M_l 8.4) generated a JMA seismic intensity higher than 4 in the Fuji Five Lakes area (Usami, 2003). It ruptured segments C, D and E of the Nankai-Suruga megathrust and the Fujikawa-kako Fault Zone. The 1854 CE Ansei-Tōkai earthquake seems a likely trigger for E4.

Correlation with historical earthquakes

Due to the uncertainties within the ^{14}C -based age-depth model, most of the older sedimentary event deposits (E5-E13) cannot be unambiguously associated with one specific historical earthquake. Most turbidite ages bracket ages of two or more historical earthquakes that occurred along the Nankai-Suruga Trough or the Sagami Trough.

Only three sedimentary event deposits can be attributed to one single seismic event:

- E7 (F2 turbidite): the 1361 CE Shōhei earthquake, along the Nankai-Suruga Trough (segments Z to E);
- E8 (F4 turbidite): the 1293 CE Einin-Kamakura earthquake, along the Sagami Trough and the Kozu-Matsuda Fault Zone;
- E9 (F3 turbidite): 1096 CE Eichō earthquake, along the Nankai-Suruga Trough (segments C and D).

All other turbidites can be associated with two or more earthquakes.

Based on these hypothetical correlations, some high-magnitude historical earthquakes are missing from the lacustrine record.

For example, the age of event deposit E5 (F4 turbidite) is estimated between 1596 CE and 1793 CE. During this period of time, at least three high-magnitude earthquakes occurred: the 1707 CE Hōei earthquake (Nankai-Suruga Trough), the 1703 CE Genroku earthquake (Sagami Trough) and the 1605 CE Keichō earthquake (Nankai-Suruga Trough). According to literature, the 1707 CE Hōei earthquake ruptured segments A to E of the Nankai-Suruga Trough, although there is only sparse evidence for the rupture of segment E (see chapter 4.1). Additional radiocarbon dates are needed to decipher which earthquake can be correlated with E5.

A second example is the E11-E12 doublet. The lack of background sedimentation between E11 (F2 turbidite) and E12 (F3 turbidite) suggests that either two earthquakes occurred in a very short time span, or that two turbiditic flows from different sources were recorded. Five earthquakes are historically documented during the time span covered by the E11-E12 doublet (between 713 CE and 896 CE), namely in 670-760 CE (Shishikura, 2003), 841 CE, 878 CE and in 887 CE (Usami, 2003). We infer that the 841 CE Izu Peninsula earthquake was probably not recorded, as also the 1930 CE Kita-Izu earthquake did not trigger a turbidity current in Lake Motosu. The 841 CE earthquake occurred along the northern and middle segment of the Itoigawa-Shizuoka Tectonic Line (Okumura, 2001) and was probably too remote (110 km) to be recorded in Lake Motosu. Based on the location of the surface rupture, we assume that the CE 887 Ninna earthquake (Nankai-Suruga Trough) is the most suitable candidate as trigger of E11-E12 (in the case of one seismic event). In the hypothesis of two earthquakes occurring in a short time span, the 887 CE Ninna earthquake (Nankai-Suruga Trough) and the 878 CE earthquake (Sagami Trough) might have triggered E11 and E12, respectively.

The last sedimentary event deposit that can be correlated with historical documents is E13 (F4 turbidite). E13 might correspond either to the 684 CE Tenmu earthquake or to a prehistorical earthquake occurring along the Sagami Trough between 670 CE and 760 CE (Shishikura, 2003).

In addition to synchronicity criteria, the correlation with recent and historical earthquakes supports earthquake shaking as a likely trigger for the turbidites. The correlation between hypothetical earthquakes and their associated deposits shows that the F2 and F3 turbidites are more likely triggered by earthquakes rupturing segments D and E of the Nankai-Suruga Trough. By contrast, F4 turbidites are in most cases generated by earthquakes from the Sagami Trough. Earthquakes occurring along the Nankai-Suruga Trough are characterized by a higher seismic magnitude than the ones rupturing along the Sagami Trough. NIED (2017) estimate that the Nankai-Suruga Trough is capable of generating an earthquake with a moment magnitude between 8.2 and 9, whereas the moment magnitude for earthquake rupturing the Sagami Trough is estimated between 7.9 and 8.6. Therefore, at Lake Motosu, the seismic intensity of the Nankai-Suruga Trough earthquakes is expected to be higher.

Discounting Alternative Trigger Mechanisms

Turbidites are not necessarily only triggered by earthquake shaking. Several other processes can generate turbidity currents as well, such as floods (Arnaud et al., 2002; Gilli et al., 2003; Moreno et al., 2008), volcanic processes (Trofimovs et al., 2013), lake level changes (Anselmetti et al., 2009) or spontaneous slope failure (Girardclos et al., 2007; Hilbe and Anselmetti, 2014). Each year, strong typhoons associated with heavy rains and floods hit Japan. Such storms and typhoons can provoke sub-aquatic slope failure in shallow water settings, mostly driven by wave loading. In Lake Motosu,

which has a restricted fetch, wind-driven wave generation is limited and the impact of wave loading is insufficient to produce large slope failures at greater depths. The last damaging typhoons hit the region in 1983 and in 1966. After Typhoon Ida (September 1966), several sub-aerial landslides and debris flows were reported close to Lake Sai, at a distance of 8 km from Lake Motosu (Herath et al., 1992). In Lake Sai, turbidites associated with Typhoon Ida have been recorded (see chapter 4.7). In gravity core MOT14-5B, supported ^{210}Pb concentrations show a lower value at 2.5 cm depth, suggesting the reworking of older sediment. The depth of the disturbance might correspond to a flood associated with the 1966 typhoon. Flood-generated turbidites are generally thinner and richer in terrigenous material than those triggered by earthquakes (Wilhelm et al., 2013; Revel-Rolland et al., 2005; Vandekerckhove et al., 2020; Praet et al., 2020).

Due to the proximity of Mount Fuji, it cannot be excluded that explosive volcanic eruptions may have caused slope destabilization inducing turbidites in the lake. The last major Plinian eruption of Mount Fuji occurred in 1707 CE (Hōei eruption). The sedimentary record does not contain a thick turbidite (F2 or F3 turbidite) of that age. Event deposit E5, a F4 turbidite, could potentially be attributed to the 1707 CE Hōei eruption, but could also have been triggered by the Hōei earthquake. Volcanic ejecta did not reach Lake Motosu due to the wind direction (Miyaji et al., 2011), so that there is no record of the 1707 CE tephra in the sediments of Lake Motosu. Consequently, it remains unclear whether E5 was triggered by the 1707 CE Hōei earthquake or by the 1707 CE Hōei eruption, but we assume that sub-lacustrine slope destabilization triggered by volcanic eruptions of Mount Fuji was of minor importance.

Concerning older volcanic eruptions, one turbidite (E20), recorded at 3.76 m depth, covers a scoria layer. X-Ray analysis indicates that the top of the scoria layer has been reworked and constitutes the base of the turbidite. The geochemical fingerprint of E20 is slightly different from that of the other turbidites in Lake Motosu: Ca, Ti and Sr contents are higher, suggesting a higher concentration of volcanic ejecta in E20. Turbidites triggered by volcanic eruptions of Mount Fuji are expected to be rich in volcanic ejecta and/or to be associated with scoria layer. However, as prehistorical volcanic eruptions are not well constrained in time, we cannot assess if the deposition of E20 occurred during/or after a volcanic eruption, or if its deposition was caused by another mechanism soon after the volcanic eruption.

Extreme lake-level variations may have caused the formation of turbidites in Lake Motosu. Four staircase platforms were identified in the lake and attributed to step-wise rises in lake level (Lamair et al., 2018). Based on the seismic reflection data (Lamair et al., 2018), the age of the sediments covering the platform 2 was estimated to be older than 13600 yr BP, which suggests that the increases in lake level occurred before 6000 cal yr BP. It therefore seems that if sub-lacustrine slope failure might have been produced by variations in lake level, it probably did not do so in the last 6000 years.

Spontaneous slope failure, from sediment loading on the platform, can be excluded as a possible turbidite trigger mechanism because of the relatively low sedimentation rates in Lake Motosu.

Based on the sedimentological evidence, the synchronicity of event deposits between coring sites and the correlation with recent and historical earthquakes, we conclude that most of the turbidites in Lake Motosu were triggered by seismic shaking. On the

high-resolution seismic reflection profiles, fluid-escape features are observed at the top of MTDs (Lamair et al., 2018). These can be the result of seismic shaking of un-compacted sediments with excess pore water pressure (Moernaut et al., 2009). Their presence suggests that Lake Motosu underwent significant earthquake shaking.

4.6.2.2. *Lake Motosu's sensitivity threshold*

Monecke et al. (2004), Van Daele et al. (2015) and Howarth et al. (2016) proposed, based on empirical data, that a minimal seismic intensity of VI on the Modified Mercalli Intensity Scale (MMI) is required to generate a sedimentary record of earthquake shaking in lakes. In Japan, seismic intensity is reported according to the Japan Meteorological Agency (JMA) seismic intensity scale, which is less accurate than MMI. For example, a JMA 4 intensity approximately corresponds to VI or VII on the MMI scale (e.g. Ishibashi, 2004). Since 1996, JMA intensities are calculated based on seismometer measurements. Sokolow and Furuma (2008) show that the new calculation method sometimes overestimates the intensity.

The sedimentary infill of Lake Motosu has recorded historical earthquakes with a JMA equal or higher than 4. However, when considering the last 200 years, some earthquakes with a inferred JMA equal or higher than 4 are missing from the sedimentary record. This is, for instance, the case for the 2011 CE Shizuoka-ken Tobu earthquake, the 2011 CE Tōhoku-oki earthquake and the 1930 Kita-Izu earthquake.

The 2011 CE Tōhoku-oki earthquake had a reported JMA intensity of 5- around Lake Motosu (Japan Meteorological Agency, 2011). With this intensity, rockfalls and slope failures, as well as damage to buildings would be expected. However, none of these were reported around Lake Motosu. We infer that the JMA intensity for this earthquake may indeed have been overestimated.

The absence of the 1930 CE Kita-Izu earthquake in the sedimentary record of Lake Motosu suggests that either other parameters are needed to define an adequate sensitivity threshold in Lake Motosu or that JMA intensities around Lake Motosu have also been overestimated for this earthquake.

4.6.2.3. *Prehistorical earthquakes and their implications for regional seismicity*

The correlation between the Lake Motosu turbidites and recent and historical earthquakes suggests that the Fuji Five Lakes area is mostly impacted by high-magnitude megathrust earthquakes from the Nankai-Suruga and Sagami Troughs. The absence of the 2011 CE Tōhoku-oki earthquake in the sedimentary record indicates that earthquakes rupturing the Japan Trench are likely not recorded. Over the last ca. 6000 years, the mean recurrence time of seismic events affecting the Fuji Five Lakes area is 184 ± 8 years. Based on documented historical records, the Nankai-Suruga Trough has ruptured twelve times between 684 CE and 1946 CE, with an average recurrence interval for high-magnitude earthquakes of 115 ± 89 years (see chapter 4.1). At the segment level, the A-B segments rupture on average every 193 ± 67 years, the C-D segments on average every 151 ± 64 years, and segment E (and the Fujikawa-Kako Fault Zone) has ruptured only five times during the last 1330 years (see chapter 4.1). The mean recurrence time for high-magnitude earthquakes along the Sagami Trough is estimated around 400 years (Shishikura et al., 2001; 2005).

Most of the prehistoric sedimentary event deposits recorded in Lake Motosu can be correlated with geological evidence of paleo-earthquakes along the Nankai-Suruga Trough or the Sagami Through. However, due to the high seismicity of the area, it is impossible to assess with 100 % certainty which earthquake has been recorded or not

in Lake Motosu. All F2 and F3 turbidites are correlated with published paleoseismological evidence. The correlation between the F4 turbidites and the inland geological evidence is more difficult to assess, as these F4 turbidites are likely related to more remote earthquakes or to earthquakes of smaller magnitude.

4.6.3. Conclusion

The lacustrine sediments of Lake Motosu constitute a good archive of the seismic history of the Fuji Five Lakes area. Due to its location, Lake Motosu can record earthquakes from both the Nankai-Suruga Trough and the Sagami Trough. Turbidites triggered by earthquakes generated along the C-D-E segments of the Nankai-Suruga Trough are thicker than those generated by other faults. This suggests that the Nankai-Suruga Trough earthquakes have a bigger impact on the Fuji Five Lakes area than those of the Sagami Trough. The recurrence time for high-magnitude earthquakes affecting the Fuji Five Lakes area is estimated around 184 ± 8 years.

In the future, more lacustrine paleoseismological studies need to be carried out in other lakes close to the Nankai-Suruga Trough and the Sagami Trough in order to refine our estimation of paleointensity of historical and prehistorical earthquakes.

4.7. Signature of earthquakes and extreme flood events in Lake Sai

In this section we discuss the sedimentary infill of Lake Sai, another one of the studied Fuji Five Lakes, and evaluate if it contains traces of past earthquakes. This section contains *capita selecta* from Lamair et al. (in preparation) and Lamair (2018).

4.7.1. Results

4.7.1.1. Bathymetry/Morphology

Lake Sai occupies an east-west elongated basin that can be divided into a relatively small perched western sub-basin (0.92 km² and 44.5 m max. depth) and a deep central basin (1.94 km² and 71.6 m max. depth) surrounded to the north and to the south by steep slopes. The two sub-basins are separated by a ridge created by the Aokigahara lava flow, which also delineates the western and the southwestern shorelines of the lake. The deep central basin is dominated by three prominent delta fans in the north, northeast and east. The northern and the northeastern delta fans present two platforms showing a stair-case morphology. The maximum thickness of the sediment covering the sub-lacustrine delta fans is about 8 m. The northern and the northeastern delta fans are separated by a channel, transferring sediments directly towards the deep basin. In the deep basin, the seismic reflection data image the sedimentary infill down to 3 m depth, below which acoustic blanking prevents deeper penetration of the seismic data. No recent large collapse of the fan deltas or sub-lacustrine slope failure can be observed.

4.7.1.2. Sedimentology

Sedimentation in the different depositional settings

Gravity core SAI14-3B is located in the deep central basin. Background sediments consist of diatomaceous ooze, containing a small fraction of terrigenous clays/silts and organic matter ($13 \pm 1.4\%$), and displaying irregular, mm-scale laminations. These background sediments are interrupted by 15 layers characterized by sharp contacts, higher MS, higher density and coarser grain size (silt to sand). They are labeled SED1 to SED15, from top to bottom (Figure 33). Most are less than 1.8 cm in thickness, except SED2, which is 3.8 cm thick, and SED5 and SED11, which reach anomalous

thicknesses of 13.6 cm and 16.8 cm, respectively. In all layers, the Si/Ti ratio is generally low and Sr is generally high compared to the background sedimentation (Figure 33). These 15 layers are interpreted as sedimentary event deposits.

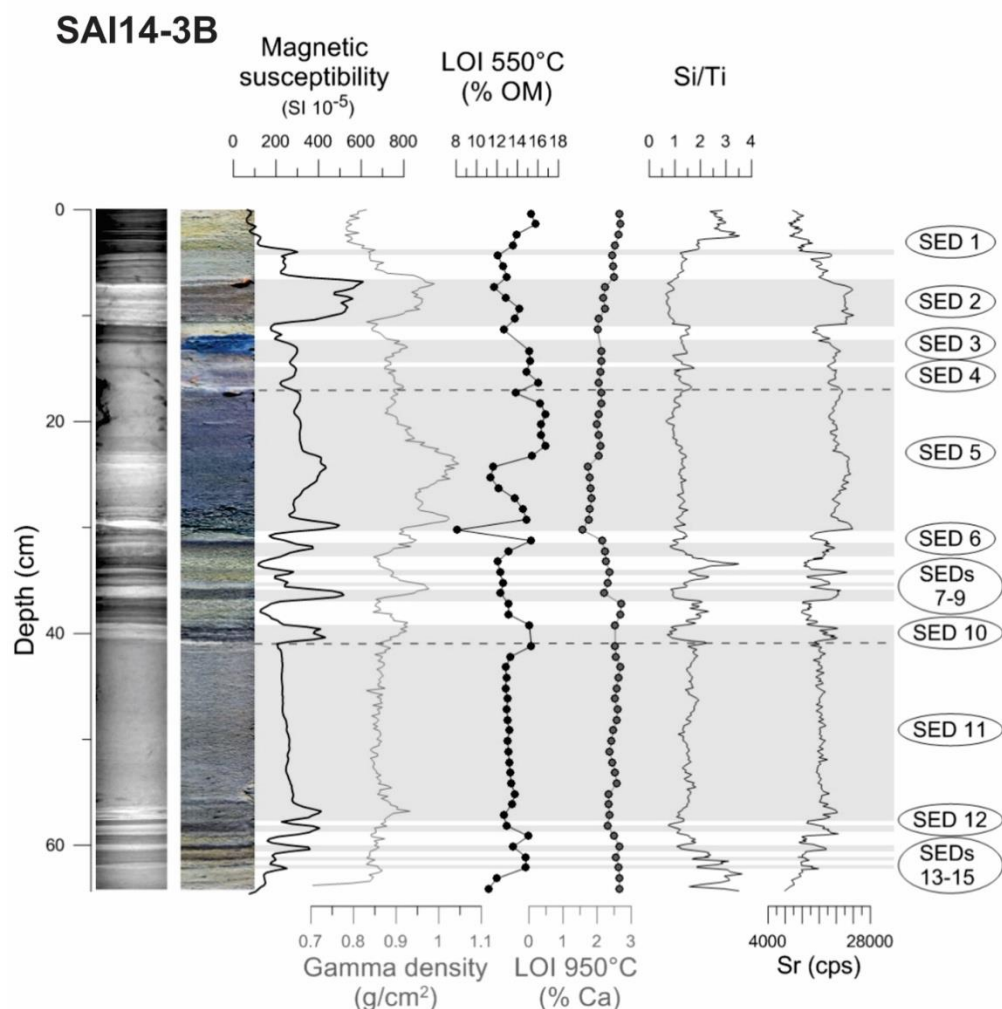


Figure 33: Piston core from the central deep basin (SAI14-3B). From left to right: X-ray radiography, processed linescan imagery, MS, gamma density, organic matter and carbonate content, XRF data (Si/Ti ratio and Sr).

Gravity core SAI14-1D, taken in the separate western perched sub-basin, shows an identical sedimentological pattern. Stratigraphic correlation between the two cores shows that sediment accumulation rate in the perched sub-basin is higher than that in the deep central basin. The background sediments in both locations have similar thickness, but the sedimentary event deposits are thicker in the small sub-basin.

Almost all sedimentary event deposits are present in the two locations, though they must have a different source as the two basins are separated by a shallow sill. SED4 and SED8 are absent from the sedimentary record of the western basin.

Also in gravity cores SAI14-6B and SAI14-4B, from the fan deltas, and SAI14-5C, from the channel, the background sediments are similar as those in the two basins. The organic content varies from 10.5 % to 14 % in the delta fans. Like in the basins, the background sedimentation is interrupted by a series of layers characterized by higher density, higher MS values and coarser-grained sediment.

As the thickness, grainsize and geochemical composition of the sedimentary event

deposits are different in different environments, correlation between of event deposits between the fan deltas and the basins is impossible. Only the two most recent event deposits (SED1 and SED2) can be correlated through the fan deltas, the channel, the deep basin (and the western sub-basin).

Characteristics of the sedimentary event deposits

The 15 sedimentary event deposits from the deep central basin and the western sub-basin were characterized based on their grain size. In the deep basin, the event deposits show a large diversity of grain size patterns: (i) normal graded beds (SED1, SED5, SED7, SED9 and SED10); (ii) normal-to-inverse graded bed (SED2); (iii) inversely graded beds (SED3, SED4 and SED6); and (iv) thick homogenous layer with a thin coarse base (SED11). SED8, SED12, SED13, SED14 and SED15 are too thin to determine the grading of the layer, but they are coarser grained than the background sedimentation. In the sub-basin, the grain size pattern of the event deposits is similar than that of their correlative counterparts in the deep basin, except for SED2 and SED6, which show a normal grading.

The normal graded beds in the deep basin are relatively thin (ranging from 1 cm to 1.7 cm), except for SED5 (13.6 cm). SED1, SED8, SED9 and SED10 consist of a thin (1 cm to 1.7 cm) fining-upward graded bed overlying a thin coarse base.

SED2 stands out from the other sedimentary deposit events. In the deep basin, it is composed of a series of dense layers. These stacked layers show a normal-to-inverse grading. The base and the top of SED2 consist of thin sandy layers. By contrast, in the western sub-basin, SED2 appears as homogenous interval. In the channel, SED2 is characterized by normal grading, with a base composed of coarse sand and terrestrial organic matter.

The thick homogenous layer, SED11, consists mostly of homogenous mud with a thin, laminated coarser base, and, at the top, a fine-grained whitish layer.

Each event deposit is characterized by a basal peak in MS or by higher MS values, and in general higher density.

Also the geochemical signatures of the event deposits thicker than 0.8 cm were compared. Based on their geochemical composition, they were classified in two groups. The first group (SED2, SED3, SED4, SED5, SED8, SED9, SED10 and SED12) is richer in terrigenous material (higher Sr, Zr and Ti) and has a higher Al and Ca content. The second group (SED1 and SED11) have a geochemical composition closer to that of the background sediments suggesting that they represent reworked background sediments. In SED11, Sr, Zr and Cu remain stable in the homogenous interval. SED6 has characteristics overlapping with groups 1 and 2.

SED2, SED5 and SED6 contain almost no diatom frustules in the western sub-basin, while in the central basin they contain a small proportion of broken diatoms. These observations are supported by their low Si/Ti content.

4.7.1.3. *Geochronology*

The $^{210}\text{Pb}_{\text{xs}}$ profile of gravity core SAI14-3B shows a rapid activity decrease from the surface down to a depth of 31-32 cm (Figure 34). The instantaneous event deposits were subtracted from the sedimentary sequence to produce a corrected $^{210}\text{Pb}_{\text{xs}}$ profile. The CF:CS model was used and this yielded an average background sedimentation rate of 0.19-0.22 cm/yr. A clear peak in the ^{137}Cs curve is in coherence with the ^{210}Pb model and suggests that SED5 was deposited shortly after 1963 CE (Figure 34). Assuming that the background sedimentation rate is constant over time, the bottom of SAI14-3B is dated between 1911 and 1925.

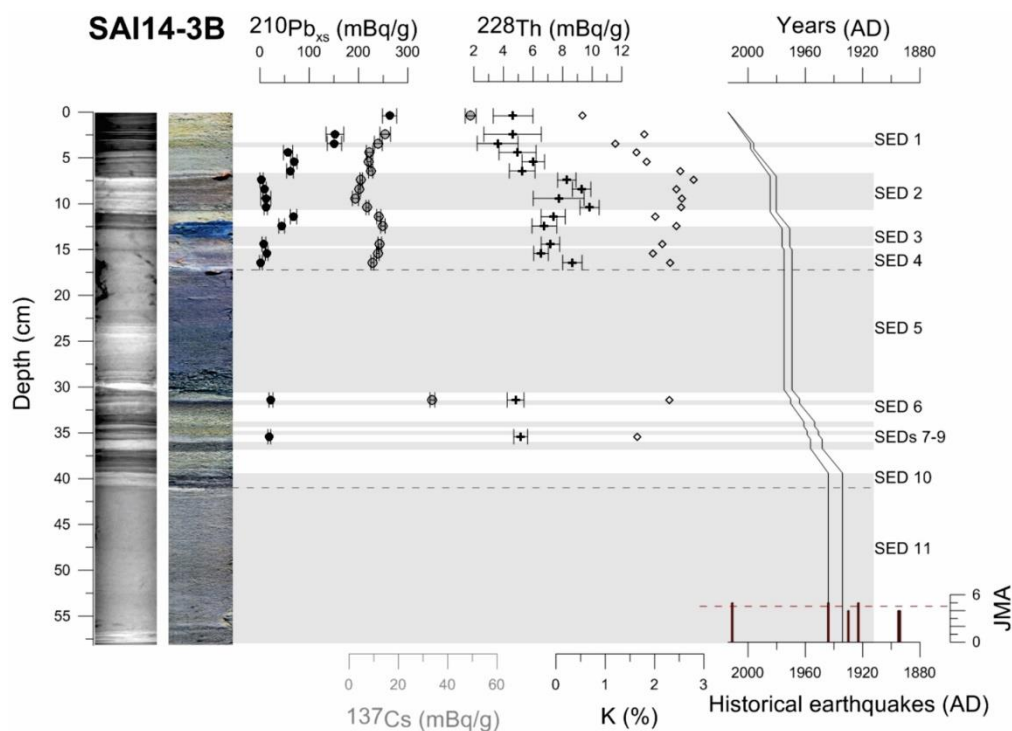


Figure 34: $^{210}\text{Pb}/^{137}\text{Cs}$ measurements on the upper part of piston core SAI14-3B. From left to right: X-ray radiography, processed linescan imagery, ^{210}Pb depth profile, ^{137}Cs depth profile, and the conversion in years.

4.7.2. Discussion

4.7.2.1. Interpretation of the sedimentary record

Through its history, the Fuji Five Lakes area has been impacted by three types of natural hazards: volcanic eruptions, earthquakes, and typhoons causing floods and landslides. All these natural hazards may leave an imprint the lakes' sedimentary records as instantaneous event deposits interrupting the background sedimentation. Below we will assess how floods and earthquakes have been recorded in the Lake Sai sediments; we will not discuss volcanic activity as the last eruption of Mount Fuji occurred in 1707 CE and thus predates the 90 years old sedimentary record contained in our gravity cores.

The 1966 CE Typhoon Ida and the origin of event deposits SED4 and SED5

Typhoon Ida hit the Fuji region severely in September 1966 causing severe damage and loss of life. Typhoon Ida was hydrologically characterized by short (4 h duration) and intense rainfall (max. 68.5 mm/h and a total precipitation of 145.9 mm²). Several deadly landslides and debris flows were triggered by the heavy rains in the catchment of Lake Sai. In total, 187 people were killed, and the damage was estimated around 3.9 million JPY (Herath et al., 1992). In the sedimentary record of Lake Sai, SED5 and SED4 are interpreted as the imprint of Typhoon Ida. The age of SED5 is well constrained by the ^{137}Cs peak related to 1963 nuclear fall-out at 1 cm below the deposit (Figure 34). We interpret SED5, which is characterized by a typical turbidite texture, as a "lacustrine turbidite type 2", in the sense of Van Daele et al. (2015). The turbidite source material is reworked sediment originating from the nearshore environment and/or from the catchment (e.g. onshore landslides and debris flows), as evidenced by the geochemical composition which indicates a higher terrigenous content than in the background sediments of the fan deltas. The absence of

background sediments between SED5 and SED4 indicates that SED4 was deposited shortly after SED5. SED4 shows an inversely graded bed, typical for a hyperpycnal flow (Mulder et al., 2001). This hyperpycnal flow was caused by the heavy rains that accompanied Typhoon Ida. The absence of SED4 in the western sub-basin suggests that the hyperpycnal flow affected only the central basin.

Origin of the small-scale event deposits

The small-scale event deposits, SED1, SED2, SED3, SED6, SED7, SED8, SED9, SED10, SED12, SED13, SED14 and SED15 are interpreted as sediment layers deposited by floods. Flood-deposited layers are generally characterized by: (i) high detrital content (Revel-Rolland et al., 2005); (ii) high MS values (Chapron et al., 2005), and (iii) a base showing high bulk density (Gilli et al., 2003). SED1, SED2, SED3, SED6, SED7, SED8, SED9, SED10, SED12, SED13, SED14 and SED15 fulfil all of these criteria. Additional evidence for a flood origin is given by the almost complete absence of diatom frustules within these event deposits supporting an external source scenario for their origin. A flood origin is also corroborated by grainsize analysis. In the deep basin, SED2 consists of a stacked graded interval (normal-to-inverse). These stacked deposits suggest either an interference between flows from adjacent sources or successive flows occurring during a short time span. In the western sub-basin, SED2 is characterized by a normal graded bed indicating that one single flow was recorded. In the deep basin, SED3 and SED6 present an inversely graded bed (like SED 4) and are interpreted as flood layers deposited by a hyperpycnal flow. SED1, SED7, SED9 and SED10 are characterized by normal graded bedding and can thus have been generated by various triggers: floods, lake water-level fluctuations (e.g. Anselmetti et al., 2009), spontaneous slope failures (e.g. Girardclos et al., 2007; Hilbe and Anselmetti, 2014) or slope failures induced by earthquake shaking (e.g. Waldmann et al., 2011). However, based on their thickness (from 1 cm to 1.7 cm), their geochemical composition and the absence of recent slope failures, we favor a flood origin for these events.

Origin of the mud turbidite SED 11

SED11 differs from the other sedimentary event deposits in terms of thickness, grainsize and geochemical composition, suggesting another trigger mechanism. Its composition is identical to that of the background sediments, and it can therefore be interpreted as resulting from a large in-lake remobilization of hemipelagic sediments, or as a “lacustrine turbidite type 1”, in the sense of Van Daele et al. (2015). Such turbidites are most likely seismically triggered (Van Daele et al., 2015). According to the ²¹⁰Pb age-depth model, SED11 occurred in 1939 CE ± 5. At least four high-magnitude earthquakes impacted the Fuji Five Lakes area over the last century. The largest earthquakes (with a JMA intensity of 5 in the area) were: (1) the 2011 CE Shizuoka-ken Tobu earthquake, of which the epicenter was located at the southwestern foot of Mount Fuji; (2) the 1944 CE Shōwa-Tōnankai earthquake that ruptured the eastern end of the Nankai-Suruga Trough, and (3) the 1923 CE Great Kanto earthquake, along the Sagami Trough. In addition, the 1930 CE Kita-Izu earthquake had a JMA intensity of 4 in the region. This earthquake ruptured the Tanna strike-slip Fault. According to the age-depth model, the 1944 CE Shōwa-Tōnankai earthquake is the most likely trigger of SED11.

4.7.2.2. Lake Sai’s sensitivity to earthquake shaking

Recent studies (Van Daele et al., 2015; Howarth et al., 2016) suggest that a minimum intensity of VI on the Modified Mercalli Intensity (MMI) scale is required to generate

a sedimentary record of earthquake shaking in a lacustrine environment. In Japan, the JMA seismic intensity scale is preferred to MMI scale. The JMA seismic intensity scale consists of 8 levels and has been updated to 10 levels for earthquakes occurring after 1996. The conversion between the JMA seismic intensity and MMI scales is not accurate. For example, a seismic intensity 4 on JMA scale is approximately equal to VI-VII on the MMI scale (Ishibashi, 2004). Moreover, since 1996, the JMA seismic intensity is calculated by converting instrumental ground-motion parameters into intensity values which does not reflect anymore the real damages but is closer to the concept of magnitude (Yamazaki et al., 1998).

During the time span covered by our sediment cores from Lake Sai, four earthquakes affected the Fuji Five Lakes area with a JMA higher than 4 and could thus have triggered a turbidity current. However, only one likely earthquake-triggered turbidite was identified in the cores. According to the age-depth model, the 1944 CE Shōwa-Tōnankai earthquake was the most likely trigger. This earthquake also triggered an event deposit in nearby Lake Motosu (see chapter 4.6).

The 2011 CE Shizuoka-ken Tobu earthquake, the 1930 CE Kita-Izu earthquake and the 1923 CE Great Kanto earthquake did not leave an imprint in the sediments of Lake Sai (although the latter did produce an event deposit in nearby Lake Motosu, see chapter 4.6). Of course, the 1930 CE and 1923 CE earthquakes occurred at the limit of the investigated age window. The absence of a turbidite related to the 2011 Shizuoka-ken Tobu earthquake can likely be explained by an overestimation of the JMA intensities in the Fuji Five Lakes area related to the new calculation method.

Based on the record retrieved by the gravity cores, we suggest that a JMA higher than 5 (calculated by the 'old' method) is required to produce a sedimentary imprint of earthquake shaking in Lake Sai.

4.7.3. Conclusion

Three types of imprints from natural hazards are present in the lacustrine sedimentary record of Lake Sai: earthquakes, floods triggered by heavy rains and debris flows triggered by typhoons. Each type generates a characteristic turbidite.

- The turbidite triggered by the 1944 CE Shōwa-Tōnankai earthquake was caused by the remobilization of hemipelagic sediments from the lacustrine slopes, and is significantly thicker than the other turbidites in the record. Based on the analysis of our short gravity cores, we suggest that a JMA seismic intensity higher than 5 is required to trigger turbidites in Lake Sai.
- In 1966, the destructive Typhoon Ida triggered onshore landslides and debris flows that were recorded in Lake Sai as thick turbidites, rich in terrigenous material.
- Flood turbidites are thinner and have a high terrigenous content.

Retrieval of longer cores, spanning a much longer time period, is required to assess the return period of flood and typhoon events, and high-magnitude earthquakes in this region of Japan.

4.8. The potential of the Fuji Five Lakes to record natural hazards: a general discussion

This section contains *capita selecta* from Lamair (2018).

4.8.1. Results

4.8.1.1. Morphology and seismic stratigraphy of Lakes Motosu, Sai, Kawaguchi and Yamanaka

The geomorphological characteristics of Lake Motosu, Lake Sai, Lake Kawaguchi and Lake Yamanaka are summarized in Table 2.

Table 2: Morphological parameters for Lakes Motosu, Sai, Kawaguchi and Yamanaka.

	Lake Motosu	Lake Sai	Lake Kawaguchi	Lake Yamanaka
Max. Depth (m)	12.5	71.6	12	14.3
Lake area	4.7 km ²	2.13 km ²	5.66 km ²	6.89 km ²
Catchment area	24.45 km ²	28.02 km ²	102.47 km ²	69.81 km ²
% Catchment area occupied by Misaka/Tanzawa Mts	36 % (9.02 km ²)	62 % (17.42 km ²)	43 % (44.95 km ²)	84 % (58.62 km ²)
Slope catchment	20-46° (in the north, west and south) 0.5-8° (east)	20-46° (in the north, east and south) 0.5-8° (west)	0-2° (in the northwest, northeast) 0-6° (south) 20-40° (in the north, east and southeast)	13-18° (in the North) 2-5° (E-N-E flank of Mt. Fuji)
Sublacustrine slope gradient	Platforms: 1.5-7° Lava flow edges: 18°-26° Other slopes: 20°-37°	Fan delta slopes: 4 - 10° Other slopes (central basin): 12.5 - 35.5° Other slopes (western basin): 7.5° - 38.5°	Slope of Unoshima island: 2 - 4.6° Slope alluvial fans: 2-3.5° Other slopes: 0.5 - 5.5°	N-W slopes to N-E slopes: 0.5 - 2.3° S-W slopes to S-E slopes: 0.6° - 0.8°
Sublacustrine slope area	4.27 km ² (91 %)	1.59 km ² (75 %)	2.22 km ² (40 %)	2.87 km ² (42 %)
River inflows	Yes	Yes	Yes	Yes
Sediment accumulation on sublacustrine slope	2 - 11 m (platforms)	Max. 8 m (delta fans)	Not imaged	Not imaged
Active alluvial fan	Yes	Yes	Yes	No
Coring distance from the present alluvial fans/delta fans	Between 800 m and 2100 m	Between 430 m and 1000 m	Between 570 m and 1700 m	Between 2770 m and 1700 m (East alluvial fan)
Distance between the central basin and the subaerial fans	Between 1270 m and 1850 m	Between 600 m and 1450 m	1000 m	Between 1000 m and 2800 m
Anthropogenic modification of the catchment	Yes	Yes	Yes	Yes

Based on these geomorphological parameters, two types of lakes can be defined:

- The first group consists of relatively large, flat and shallow (max. 14 m depth) lakes, dominated by acoustic blanking on seismic profiles and having a large catchment: Lake Yamanaka and Lake Kawaguchi. These lakes did not persist through the Holocene. At some stage, their basin was partially or completely occupied by a river. The main difference between the two lakes is the presence of large alluvial fans in Lake Kawaguchi and the size of the catchment. Lake Kawaguchi's catchment is ca. 1.5 times larger than Lake Yamanaka's one. In Lake Yamanaka, the alluvial fans are relatively reduced, which implies that sediment supply from the catchment and stream power of the ephemeral streams are

lower than in Lake Kawaguchi.

- The second group is defined by relatively small, but deep lakes with steep slopes, a large slope area and a restricted catchment: Lake Sai and Lake Motosu. Lakes Sai and Motosu present several similarities. Their catchment size is less than 30 km², both occupy a deep basin surrounded by steep slopes, and both also have gentle slopes (fan delta/platform) covered by sediments. Lake Motosu is the deepest with a maximum depth of 125 m, whereas Lake Sai has only a max. depth of 71.6 m. The deep basin of Lake Motosu is located farther away from the lake margins, where ephemeral streams provide temporary inflow, than the Sai deep basin.

4.8.1.2. Sedimentology of Lakes Motosu, Sai, Kawaguchi and Yamanaka

Background sediments

The characteristics of the background sedimentation in Lake Motosu, Lake Sai, Lake Kawaguchi and Lake Yamanaka are listed in Table 3.

Table 3: Sedimentological characteristics of Lakes Motosu, Sai, Kawaguchi and Yamanaka.

¹ Measurements performed in the background sedimentation. * without scoria layers.

	Lake Motosu	Lake Sai	Lake Kawaguchi	Lake Yamanaka
D50 (μm) ¹ (deep basin)	17.0 \pm 2.0	19.3 \pm 4.2	16.2 \pm 1.8	18.0 \pm 4.8
D90 (μm) ¹ (deep basin)	69 \pm 18	90 \pm 40	60 \pm 9	81.0 \pm 25.0
D90 (μm) (slope)	16.0 \pm 5.0*	13.2 \pm 1.8	/	/
D90 (μm) (slope)	64.0 \pm 34.2*	47.9 \pm 9.9	/	/
Amorphous material content				60-70% of amorphous material
Mineralogy content ¹	45 – 58 % of total clays 1 – 2 % of kaolinite 10-20 % of plagioclase 1 – 3 % of cristobalite 14 – 23 % of quartz 2 – 10 % of muscovite	No data	No data	24.3 – 36.5 % of total clays 37 – 52% of feldspars-K 13-19 % of plagioclase 4 – 9 % of cristobalite
Clay content ¹	Illite Chlorite Kaolinite	No data	Illite Chlorite Smectite	Illite Chlorite
Diatoms ¹	Centric diatoms	Pennate diatoms	Pennate diatoms and centric diatoms	Mostly centric diatoms
Sedimentation rate (cm/yr) ¹	0.08 cm/yr	0.22 cm/yr	Between 0.19 cm/yr to 0.25 cm/yr	Variable ranging from 0.08 cm/yr to 1 cm/yr
Water content	62.6 \pm 2.5 %	71.7 \pm 6.2 %	72.8 \pm 2.7 %	78.5 \pm 0.8 %
Organic content ¹	10.7 \pm 0.13 %	11-16 %	11-14 %	11-16 %
Carbonate content ¹	2.18 – 2 %	1.5 – 3 %	2 – 3.5 %	2 – 3 %
Water content (slope)	63.5 \pm 3.3 % ³	65.6 \pm 4.8 % ³ (northern delta fan)	/	/
Organic content (slope)	12.1 \pm 3.0 %	12.8 \pm 0.9 % (northern delta fan)	/	/
Carbonate content (slope)	1.4 \pm 0.6 %	2.18 \pm 0.13 % (northern delta fan)	/	/

Sedimentary event deposits

In Lake Motosu, 32 sedimentary event deposits were identified, interbedded within the background sediments, over the last ca. 6000 years, which is the period covered by long piston core MOT15-01. These 32 event deposits (E1 to E32), comprise 8 F2 turbidites, 14 F3 turbidites and 10 F4 turbidites (see chapter 4.6). Only one large mass-transport deposit (MTD 13; Lamair et al., 2018) is recorded during this period. It is associated with one of the turbidites (i.e. probably E18).

The four most recent event deposits (E1 to E4), the ages of which could be relatively well constrained based on the $^{210}\text{Pb}/^{137}\text{Cs}$ age-depth model, were attributed to:

- E1: 1944 CE Shōwa-Tōnankai earthquake;
- E2: 1923 CE Great Kanto earthquake;
- E3: 1894 CE Meiji Tokyo earthquake or 1895 CE Ibaraki-ken Nanbu earthquake;
- E4: 1854 CE Ansei-Tōkai earthquake.

Most of the older event deposits (E5-E13) cannot be unambiguously associated with one specific historical earthquake. Only for three of these events a tentative correlation can be proposed:

- E7: the 1361 CE Shōhei earthquake;
- E8: the 1293 CE Einin-Kamakura earthquake;
- E9: 1096 CE Eichō earthquake.

The other events (E14 to E32) are all older than the historical records.

In Lake Sai, 15 sedimentary event deposits were identified, over the last ca. 100 years, which is the period covered by short gravity core SAI14-3B. These 15 event deposits (SED1 to SED15) are characterized by a large diversity in thickness and grain size pattern (see chapter 4.7).

Of these 15 event deposits, only one could be associated with a known historical earthquake:

- SED11: the 1944 CE Shōwa-Tōnankai earthquake.

All other event deposits were in all likelihood caused either by floods, triggered by heavy rains, or by debris flows, triggered by typhoons.

In Lake Kawaguchi, the background sedimentation is interrupted by two sedimentary event deposits: SED1 and SED 2 (Lamair, 2018). SED 1 is only recorded in the central and eastern basins, while SED2 is present in all three basins. It is characterized by high-magnetic susceptibility values, a high terrigenous content (Fe, Ca, Ti, Sr) and a high density. The high terrigenous content indicates that the sediment is originating from the catchment. Based on the $^{210}\text{Pb}/^{137}\text{Cs}$ age-depth model established on KAW14-3A, the ages of SED1 (projected) and SED2 are estimated around 1935 CE \pm 15 and between 1730 CE and 1798 CE, respectively (Lamair, 2018).

In Lake Yamanaka, only one sedimentary event deposit was encountered, and in only one of the five gravity cores (i.e. YAM14-1A). It is 3 cm thick, coarse-grained and cross-laminated. According to the $^{210}\text{Pb}/^{137}\text{Cs}$ age-depth model established on YAM14-2A and projected to YAM14-1A, its age is estimated as ca. 1900 CE (Lamair et al., 2019).

Intra-lake correlation

The core-to-core correlation between the different lakes is presented in Figure 35 for the gravity cores and in Figure 36 for the piston cores.

4.8.2. Discussion

The comparison of the earthquake catalogue (i.e. of earthquakes potentially affecting

the Fuji Five Lake area) with the identified turbidites in the sedimentary record of the gravity cores, shows that the record of turbidites triggered by earthquake shaking strongly varies from lake to lake.

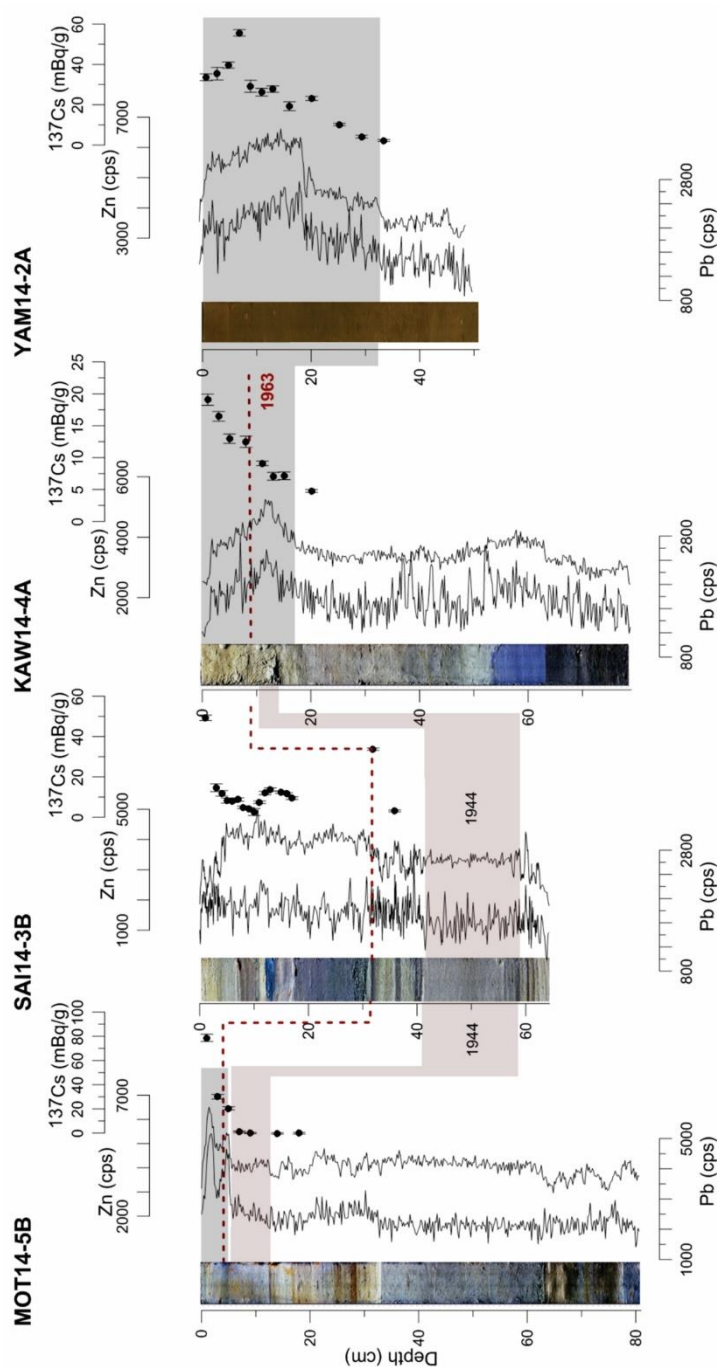


Figure 35: Correlation between short cores from Lake Motosu, Lake Sai, Lake Kawaguchi and Lake Yamanaka. The correlation is based on ^{210}Pb and ^{137}Cs measurements, as well as Pb (cps) and Zn (cps).

Since 1800 CE (i.e. the period for which the age-depth models are sufficiently reliable), Lake Motosu recorded four event deposits related to the 1854 CE Ansei-Tōkai, the 1923 CE Great Kanto, 1894 CE Meiji Tokyo or 1895 CE Ibaraki-ken Nanbu and the 1944 CE Shōwa-Tōnankai earthquakes. Located 8 km to the east, Lake Sai recorded only one event deposit, corresponding to the 1944 CE Shōwa-Tōnankai earthquake. In Lake

Kawaguchi, an event deposit was produced during a period overlapping the time of the 1944 CE Shōwa-Tōnankai earthquake. However, in absence of further analysis, the trigger of this event deposit remains uncertain. Lake Yamanaka is characterized by a lack of event deposits in its sedimentary record.

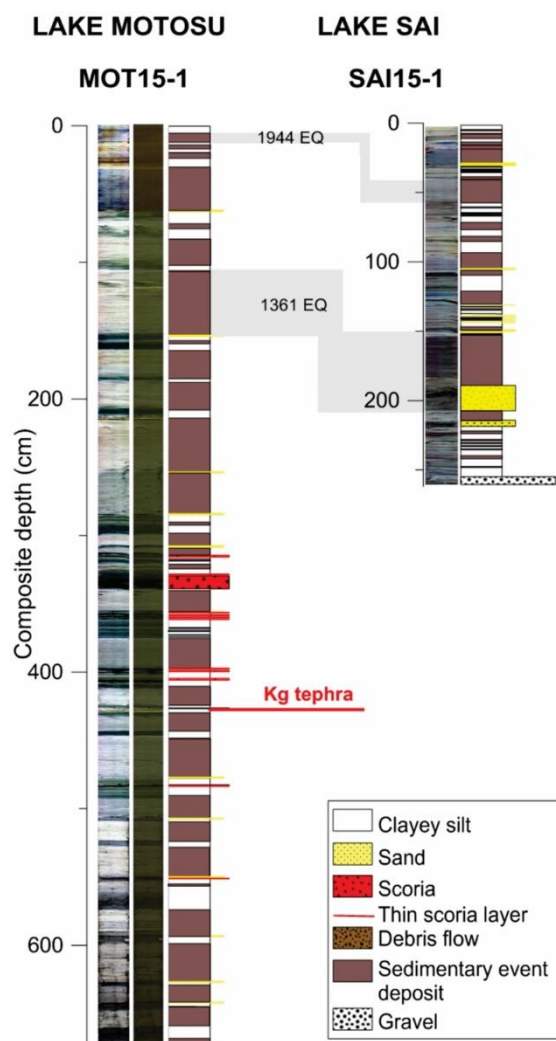


Figure 36: Correlation between the long cores from Lake Motosu (MOT15-1) and Lake Sai (SAI15-1).

Considering that high-magnitude earthquakes are expected to affect all Fuji Five Lakes equally, given that they are quite near to each other, we can conclude that the lakes have a different sensitivity to slope instability under the impact of earthquake shaking, and that Lake Motosu has the highest sensitivity for recording an earthquake. Such differences in sensitivity between lakes of a same region was also observed in Chile (e.g. Moernaut et al., 2014; Van Daele et al., 2015), in the Alps (e.g. Wilhem et al., 2016), and in New Zealand (e.g. Howarth et al., 2016). The variability in lake sensitivity depends on a series of factors (e.g. bathymetry of the lake, catchment, type of sediment, sedimentation rate, etc.). Depending on the sensitivity of the lake, a minimum local shaking intensity threshold of VI to VII on the Modified Mercalli scale is usually needed to trigger seismoturbidites (Moernaut et al., 2014; Van Daele et al., 2015; Howarth et al., 2016).

In Japan, seismic iso-intensity maps are only available for the most recent

earthquakes. We here compared the available physical parameters (magnitude, distance from the rupture plane, modelled max. slip) of the earthquakes that occurred over the last century in the region (i.e. it was impossible to do this also for the pre-1900 earthquakes due to a lack of data). Based on the small data set available, we suggest that a magnitude of 7.9-8.0 and a max. distance of ca. 150 km between Lake Motosu and the closest rupture zone are required to trigger a turbidite in Lake Motosu (Figure 37). The record of the 1894-1895 earthquakes in Lake Motosu suggests that smaller magnitude earthquakes are potentially also recorded. Not much information is, however, available about these two earthquakes. In the absence of more data, we assume that they may have been recorded in Lake Motosu as a result of favorable earthquake directivity. We assume that the seismic attenuation is similar in all of the Fuji Five Lakes as the study area is rather small.

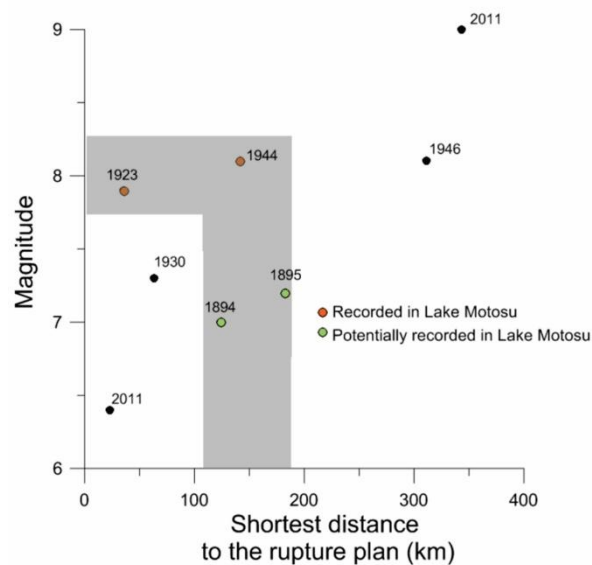


Figure 37: Plot of the magnitude vs the shortest distance to the rupture plan (km). The events recorded in the sedimentation of Lake Motosu are marked in orange.

Lake Motosu and Lake Sai have basins with a similar morphology (steep and gentle slope, thick sediment packages covering the delta fans, steep and small catchments). The basin of Lake Motosu consists of ca. 91 % of slope area (ca. 75 % for Lake Sai), making Lake Motosu more susceptible to fail under seismic loading. In addition to slope area, other parameters can also control the deposition of sedimentary events.

In Lake Sai and in Lake Motosu, the absence of recent large mass-transport deposits seems to indicate that the recorded turbidites might result from the remobilization of a thin surficial veneer of sediment (as also reported in Chilean lakes by Moernaut et al., 2017). This hypothesis is supported by the estimation of the remobilized surficial slope volume necessary to form the turbidites in Lake Motosu. We estimate that the remobilization of a surficial slope sediment layer of 4 to 15 cm is required to generate the thickest turbidites. The increase of the turbidite thicknesses in the upper part of the sedimentary infill of Lake Motosu is an indirect result of the emplacement of MTD13, which reduced the size of the deep basin. In Lake Sai, the absence of recent MTDs and the geochemical signature of the 1944 CE Shōwa-Tōnankai event deposit being almost identical to that of the background sediments are also supporting the mechanism of remobilization of a surficial veneer of sediment.

The initiation of a turbidity current by remobilization of surficial sediments differs from the classical slope failure mechanism triggering sub-lacustrine landslides (Moernaut et al., 2017). In Chilean lakes, Moernaut et al. (2017) observed that surficial slope destabilization occurred in sediments characterized by a high water content, low peak and remolded shear strengths. Due to their composition, the sediment disintegration and following turbulent transport require minor energy. Moernaut et al. (2017) propose that this mechanism occurs exclusively on the slopes. They suggest that during earthquake shaking the shearing provokes partial remolding and localized transient excess pore pressures in water-rich surficial sediments. Due to the reduction of the shear strength, the surficial sediments can lose their cohesion and move downslope. The sediments from Lake Motosu and Lake Sai are similar to the sediments in the Chilean lakes studied by Moernaut et al. (2017) and have a high water (> 60 %) and diatom content.

In absence of geotechnical measurements in the Fuji Five Lakes, the remobilization of the upper sedimentary layer and its potential shear-strength values are discussed by comparing the sediment gravity cores taken on the slope of Lake Motosu and Lake Sai. No large variation in grain-size parameters is observed in the sediments of Lake Motosu. The organic matter content is similar in both lakes. We assume that the variability in lake sensitivity is related to the diatom content in the lacustrine sediments. Diatomaceous sediments have unique geotechnical properties. Water content, void ratio, porosity, permeability, compressibility, and shear strength (confined, drained, cyclic undrained) increase with diatom content (Day, 1995; Diaz-Rodriguez et al., 1998; Diaz-Rodriguez, 2011; Shiwakoti et al., 2002; Tanaka et al., 2003; Wiemer & Kopf, 2017). The water content is slightly higher in the sediment from Lake Sai suggesting a slightly higher diatom content and therefore, a slightly higher shear strength. However, this minor difference in the water/diatoms content is insufficient to explain the sensitivity difference to earthquake shaking. The main difference between the sediments of the two lakes is the type of diatoms: centric in Lake Motosu and pennate in Lake Sai. Pennate diatoms are assimilated to elongated particles whereas centric diatoms are assimilated to rounded grains or discs. Particle angularity tends to increase the static and cyclic shear strength (Vaid et al., 1985; Wiemer & Kopf, 2015). Moreover, particle interlocking is stronger in elongated particles. Therefore, we assume that the lacustrine sediments of Lake Sai are characterized by higher shear-strength values than the sediment from Lake Motosu and are less susceptible to be remobilized under seismic loading.

In addition to the sediment shear strength, the correlation of Lake Motosu's record with more remote earthquakes (i.e. the 1894-1895 CE earthquakes) indicates that site effects can occur in Lake Motosu. The sedimentary infill is thicker in Lake Motosu and consists of unconsolidated sediments, potentially amplifying the seismic waves. To support this hypothesis, numerical modeling needs to be done.

The two shallow lakes, Lakes Kawaguchi and Yamanaka, are less sensitive to earthquake shaking. Lake Yamanaka is characterized by gentle slopes (on average 0.7° and max. 2.3°). In marine environments, sub-aqueous slopes of less than 1° are susceptible to fail (Talling et al., 2014). However, in Lake Yamanaka, no slope failure or turbidite has been recorded. By contrast, over the last 200 years, Lake Kawaguchi has recorded one (very localized) sedimentary event deposit possibly associated with the 1944 CE Shōwa-Tōnankai or to the 1923 CE Great Kanto earthquake. The bathymetric map shows that Lake Kawaguchi has short and gentle slopes (max. 5.5°)

that are prone to fail. Seismic reflection profiles reveal that the western slopes of the Unoshima island triggered mass-transport deposits. Clay content and the type of clay can affect slope stability. In sub-aerial environments, the frictional resistance of the soil decreases as the clay content increases (Shuzui, 2001). Smectite has a low frictional resistance (e.g. Lupini et al., 1981) and therefore, its presence can contribute to slope destabilization. However, to our knowledge, there is a lack of literature regarding the relation between clay content and sub-aqueous slope stability.

5. CONCLUSIONS AND RECOMMENDATIONS

The main goals of the QuakeRecNankai project were

- i) to reassess all existing historical and geological evidence of past earthquakes and tsunamis along the Nankai-Suruga Trough, and
- ii) to generate a series of new and reliable records of past earthquakes and tsunamis, from a number of key sites, in order to contribute to the production of an improved hazard assessment for the region.

5.1. Reassessment of all existing geological evidence of earthquakes and tsunamis

At the start of the QuakeRecNankai project, a critical examination was conducted of the available paleoseismic evidence from 72 sites along the Nankai-Suruga Trough, in order to reveal the current state of knowledge regarding geological evidence for past earthquakes and tsunamis along this subduction zone (Garrett et al., 2016). Sites included marine, coastal, lacustrine and terrestrial locations that have recorded evidence for intense shaking, coseismic deformation and/or tsunami inundation. **Of these 72 sites, only a minority provide compelling and well-dated evidence. For all other sites, important issues were identified with reliable differentiation between seismic and non-seismic evidence and with insufficient chronological control, severely limiting their contribution to understanding past fault behaviour.**

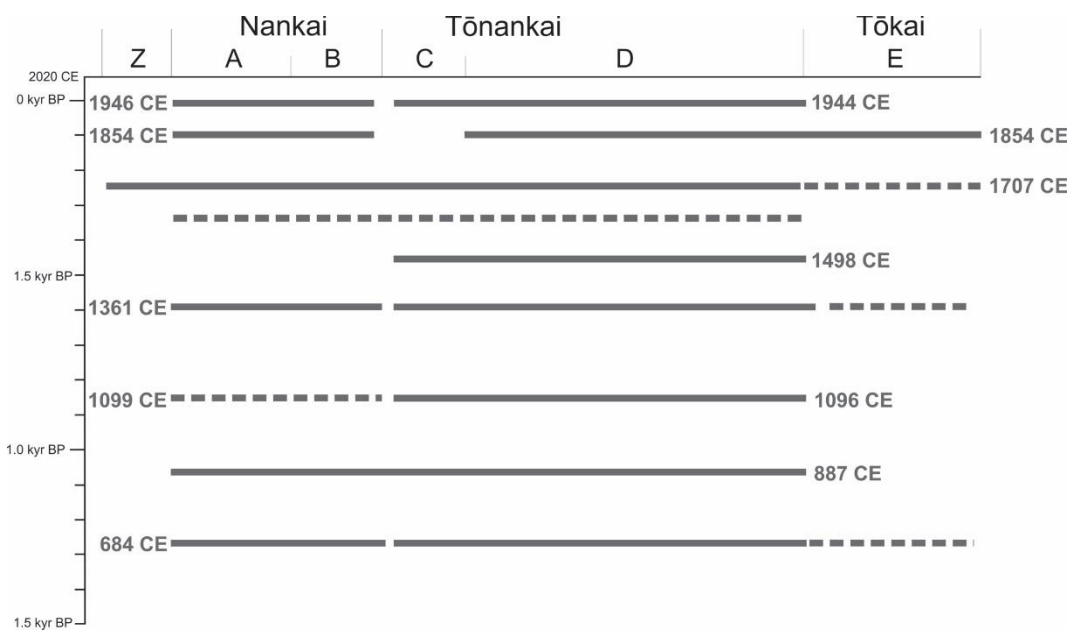


Figure 38: Spatiotemporal of 11 historical earthquakes of which the available geological evidence has been critically assessed (Modified from Fujiwara et al., 2020).

For eleven earthquakes, for which also historical records are available, the best available evidence was used to constrain their most likely rupture zones (Figure 38). This spatiotemporal compilation suggests the 1707 CE Hōei earthquake might have involved slip on at least five of six proposed seismic segments; an along-strike distance in excess of 600 km. The distribution of geological evidence suggests the 1361 CE Shōhei earthquake and the 684 CE Tenmu earthquake possibly ruptured all six segments, although further research is required to conclusively discount the possibility of temporally closely spaced ruptures of adjacent segments. Intervening earthquakes probably involved smaller areas of the subduction interface, including at least one rupture potentially confined to the area up-dip of the main seismogenic zone, highlighting a **high degree of variability in rupture mode**. We found insufficient geological evidence to consider the 1099 CE Kowa earthquake a great interplate event, but note that additional

previously undocumented subduction megathrust earthquakes may have occurred during the historical period.

The combined historical and geological record (Figure 38) suggests intervals between ruptures of the same seismic segment ranged from 90 to 474 years over the last ~1350 years. Over the longer timescales afforded by paleoseismic data, individual sites suggest intervals between earthquakes of 200 to 700 years. These figures do not just reflect the intervals between great earthquakes, however, and **future assessments must consider thresholds of evidence creation and preservation when assessing the intervals between earthquakes from paleoseismic data.**

While the Central Disaster Management Council of the Japanese Cabinet Office has called for historical and geological data to be used to define the largest magnitude of past earthquakes (Central Disaster Management Council, 2012), few attempts have yet been made to use paleoseismic data to compare relative sizes or quantify absolute magnitudes of past earthquakes along the Nankai-Suruga Trough. As such, **there is currently no evidence for the occurrence of a larger magnitude earthquake or greater tsunami inundation than that experienced in 1707 CE.**

Future research efforts should address **the question of maximum magnitude** through combined field and modelling efforts. Amongst the diverse range of paleoseismic evidence types available, **records of turbidite emplacement in marine and lacustrine settings and tsunami inundation from coastal lowlands and lakes**, offering combined records of both seismic shaking and deformation and extreme wave event inundation, appear best placed to provide new insights into the dimensions of past fault ruptures. These approaches and complementary methods will also be crucial to future attempts to answer a range of additional questions pertinent to probabilistic seismic hazard assessments. These include **uncertainties over the permanence of segment boundaries over time**, the **simultaneity of ruptures of the Nankai, Tōnankai and Tōkai regions** and the **occurrence, frequency and characteristics of tsunami earthquakes.**

5.2. Newly generated records of past earthquakes and tsunamis

In the course of the QuakeRecNankai project, new field data were collected and analyzed, and new sedimentary records of past earthquakes and/or tsunamis were generated from i) coastal Lake Hamana, ii) the Shirasuka coastal lowlands around Lake Hamana, iii) the coastal lowlands at the town of Sagara, and iv) the in-land Fuji Five Lakes.

5.2.1. Lake Hamana

The newly generated long sedimentary record from coastal Lake Hamana (Boes et al., submitted). represents one of the pieces to complete the existing data gaps regarding variability in megathrust event recurrence for the Tōnankai and Tōkai segments of the Nankai-Suruga Trough:

- The collected cores from the lake basin contain a **~7.5 kyr long sedimentary record** comprising a total of **≥ 22 possible event deposits**, interpreted as **products of extreme wave events (EWEs), such as tsunamis and typhoons, and megathrust earthquakes.**
- Detailed sedimentological analysis of these event deposits allow them to be divided in **type α deposits, inferred to have been triggered by marine inundation during a tsunami or typhoon**, and **type β deposits, inferred to have been triggered by earthquake shaking.**
- Nine of the 22 identified event deposits cover the period for which historical records exist. **A few of the event deposits can be attributed to historical megathrust events**, such as the 1707 CE Hōei earthquake and/or tsunami, and the 1498 CE Meiō

and 684 CE Tenmu tsunamis, **but others are more likely to be attributed to storm surges and/or typhoons**. The top surface sand sheet, for example, is attributed to the 2014 category 4 Phanfone Typhoon.

- **Diversity in lateral thickness distribution of event deposits in Lake Hamana might be key to differentiate between a tsunami or a typhoon/flood trigger**, which is still an ongoing issue in the paleo-tsunami community, as storm surges will also cause river flooding and form turbidites in northern sub-basins, while tsunamis will only affect sedimentation in the central basin.
- **Prehistorical event deposits show good agreement with other existing sources of megathrust evidence** from the region, and add complementary information when going back to 7.5 ka BP.

5.2.2. Coastal lowlands near Lake Hamana

In the Shirasuka coastal lowlands, new sedimentary records were generated from a site that had previously already been investigated by Fujiwara et al. (2006b) and Komatsubara et al. (2006b; 2008). These records contained **four sand layers, interpreted as event deposits reflecting inundation during tsunamis or typhoon-driven storm surges as well as terrestrial mass movements** (Garrett et al., 2018). In order to help constrain the ages of the sand layers, **infrared-stimulated luminescence dating of feldspar single grains** was applied (Riedesel et al., 2018):

- The oldest event deposit (Sand 4) is attributed to the 1361 CE Shōhei tsunami. This correlation is also supported by newly obtained single-grain infrared stimulated luminescence ages. The presence of this deposit and possible evidence for coeval shaking support the latest interpretation that the Tōkai and Nankai earthquakes occurred at short intervals in 1361 CE, rupturing the entire seismogenic zone of the Nankai Trough (Figure 38).
- The subsequent event deposit (Sand 3) is attributed to the 1498 CE Meiō tsunami, supported by a new age model that incorporates ¹⁴C dates from the previous (reanalyzed) and current studies, as well as newly obtained luminescence ages.
- While the previous studies identified four discrete sand layers associated with tsunamis in 1605 CE, 1707 CE and 1854 CE and a storm surge in 1680 CE or 1699 CE, our record contains a single 50-cm-thick sand layer (Sand 2). The probable overprinting of evidence previously attributed to multiple EWEs highlights both the **high degree of lateral variability in the deposits** and the **potential for geological records to underestimate the frequency of tsunami occurrence**.
- The youngest sand layer (Sand 1) is interpreted as being deposited by a sub-aerial landslide, triggered by the 1944 CE Shōwa-Tōnankai earthquake. The age of the sand layer is constrained by radionuclide data and newly obtained luminescence ages. This deposit constitutes a rare geological record of the most recent great earthquake in the region. The occurrence of earthquake-triggered failures of uplifted marine terraces supports the development of **terrestrial mass movement deposits as a complementary paleoseismic approach** in this and other regions.

5.2.3. Coastal lowlands in Sagara

In the lowlands at the town of Sagara, a series of cores were retrieved along several transects at both sides of the Hagima River. The new cores depict the Late Pleistocene to Holocene evolution of the Sagara coastal and fluvial system. Sporadic traces of event deposits are found in some cores on the northeastern side of the river, although a marine origin of these event deposits is unclear. A long core obtained from the southwestern side of the river contains a **series of potential extreme wave event (EWE) deposits**. Further analysis (e.g. grain-size analysis) and radiocarbon dating is, however,

required to ascertain the nature and age of these deposits. **This further analysis is still ongoing.**

5.2.4. The Fuji Five Lakes

New field data were collected on four of the five Fuji Five Lakes: i.e. Lake Motosu, Lake Sai, Lake Kawaguchi and Lake Yamanaka. For these lakes, the newly generated sedimentary records were analyzed for traces of –likely earthquake-induced– sedimentary event deposits. Of the four lakes, Lake Motosu and Lake Sai hold the most promising record of event deposits.

5.2.4.1. Lake Motosu

In Lake Motosu, **32 sedimentary event deposits** were identified, interbedded within the background sediments, in a **sedimentary record covering the last ca. 6000 years** (i.e. a record obtained by long piston coring). The ages of the four most recent of these 32 event deposits (E1 to E4) could be relatively well constrained based on a radionuclide-based age-depth model. They were attributed to:

- E1: 1944 CE Shōwa-Tōnankai earthquake;
- E2: 1923 CE Great Kanto earthquake;
- E3: 1894 CE Meiji Tokyo earthquake or 1895 CE Ibaraki-ken Nanbu earthquake;
- E4: 1854 CE Ansei-Tōkai earthquake.

Most of the older event deposits (E5-E13) cannot be unambiguously associated with one specific historical earthquake. Only for three of these events a tentative correlation can be proposed:

- E7: the 1361 CE Shōhei earthquake;
- E8: the 1293 CE Einin-Kamakura earthquake;
- E9: 1096 CE Eichō earthquake.

The other events (E14 to E32) are all older than the historical records.

The lacustrine sediments of Lake Motosu constitute a **good archive of the seismic history of the Fuji Five Lakes area**. Due to its location, Lake Motosu can record earthquakes from both the Nankai-Suruga Trough and the Sagami Trough. **Turbidites triggered by earthquakes generated along the C-D-E segments of the Nankai-Suruga Trough are thicker than those generated by other faults**. This suggests that the Nankai-Suruga Trough earthquakes have a bigger impact on the Fuji Five Lakes area than those of the Sagami Trough. The recurrence time for high-magnitude earthquakes affecting the Fuji Five Lakes area is estimated around 184 ± 8 years.

5.2.4.2. Lake Sai

In Lake Sai, **15 sedimentary event deposits** were identified in a **sedimentary record covering the last ca. 100 years** (i.e. a record obtained by short gravity coring). These 15 event deposits (SED1 to SED15) are characterized by a large diversity in thickness and grainsize pattern.

Of these 15 event deposits, **only one could be associated with a known historical earthquake**:

- SED11: the 1944 CE Shōwa-Tōnankai earthquake.

All other event deposits were in all likelihood caused either by floods, triggered by heavy rains, or by debris flows, triggered by typhoons.

The lacustrine sediments of Lake Sai contain **three types of imprints from natural hazards: earthquakes, floods triggered by heavy rains and debris flows triggered by typhoons**. Each type generates a characteristic turbidite. Our analysis suggests that a

JMA seismic intensity of > 5 is required to trigger seismoturbidites in Lake Sai. Retrieval of longer cores, spanning a much longer time period, is required to assess the return period of flood and typhoon events, as well as high-magnitude earthquakes in this region of Japan.

5.2.4.3. *Lake Kawaguchi and Lake Yamanaka*

In Lake Kawaguchi, only **two sedimentary event deposits** interrupt the background sediments in a sedimentary record covering the past ca. 250 years (i.e. a record obtained by short gravity coring). Of these two event deposits, **one could be associated with a known historical earthquake**:

- SED1: the 1944 CE Shōwa-Tōnankai earthquake.

The other event deposit was likely caused by an extreme rainfall/run-off event, dated between 1730 CE and 1798 CE.

Lake Yamanaka is characterized by a lack of convincing event deposits in its sedimentary record.

5.2.4.4. *The Fuji Five Lakes*

Comparison of the sedimentary records of the four Fuji Five Lakes shows that the number of sedimentary event deposits that can be attributed to earthquake shaking varies strongly from lake to lake, indicating that **the lakes have a different sensitivity to earthquake shaking**.

The two shallow lakes, Lakes Kawaguchi and Yamanaka, are not sensitive to earthquake shaking and therefore less suited as a paleo-earthquake archive. The two deep lakes, Lakes Motosu and Sai, are much better suited, and especially **Lake Motosu has a high sensitivity for recording earthquakes**.

The differences in sensitivity between Lake Motosu and Lake Sai can be due to a number of factors:

- Compared to Lake Sai, Lake Motosu has a larger **proportion of slope area**, which is **more susceptible to fail or to be affected by surficial sediment remobilization** under the impact of seismic shaking;
- In Lake Motosu and Lake Sai, the absence of large mass-transport deposits suggests that the **recorded turbidites result from the remobilization of a thin surficial veneer of sediment** on the lacustrine slopes, rather than from gravitational slope failure. The main **difference between the background sediments of the two lakes is the type of diatoms**: centric diatoms in Lake Motosu and pennate diatoms in Lake Sai. Pennate diatoms likely behave as elongated particles, for which it has been shown that particle angularity tends to increase the static and cyclic shear strength. The slope sediments of Lake Sai are therefore likely characterized by higher shear-strength values than those from Lake Motosu and are thus less susceptible to be remobilized under the influence of seismic shaking.

Future work needs to verify and quantify the exact role these factors play in determining the lakes' sensitivity for recording an earthquake.

The results of the QuakeRecNankai project have been incorporated in new risk and hazard assessments, have been used to support government policy updates, and have been the subject of active public outreach activities.

6. REFERENCES

- Abe, T., Goto, K. & Sugawara, D., 2012. Relationship between the maximum extent of tsunami sand and the inundation limit of the 2011 Tohoku-oki tsunami on the Sendai Plain, Japan. *Sedimentary Geology*, **282**, 142-150.
- Abe, K., 1979. Size of great earthquakes of 1837–1974 inferred from tsunami data. *Journal of Geophysical Research - Solid Earth*, **84**, 1561–1568.
- Adamiec, G. & Aitken, M.J., 1998. Dose-rate conversion factors: update. *Ancient TL*, **16(2)**, 37-50.
- Adams, J., 1990. Paleoseismicity of the Cascadia subduction zone: Evidence from turbidites off the Oregon-Washington Margin. *Tectonics*, **9**, 569-583.
- Aitken, M.J., 1985. *Thermoluminescence Dating*. Academic Press, 359 pp.
- Ambraseys, N.N., 1988. Engineering seismology. *Earthquake Engineering and Structural Dynamics*, **17**, 1–105.
- Ando, M., 1975a. Source mechanisms and tectonic significance of historical earthquakes along the Nankai Trough, Japan. *Tectonophysics*, **27**, 119-140.
- Ando, M., 1975b. Possibility of a major earthquake in the Tokai district, Japan and its pre-estimated seismotectonic effects. *Tectonophysics*, **25**, 69-85.
- Ando, M. & Nakamura, M., 2013. Seismological evidence for a tsunami earthquake recorded four centuries ago on historical documents. *Geophysical Journal International*, **195**, 1088-1101.
- Anselmetti, F.S., Ariztegui, D., De Batist, M., Gebhardt, C., Haberzettl, T., Niessen, F., Ohlendorf, C. & Zolitschka, B., 2009. Environmental history of southern Patagonia unraveled by the seismic stratigraphy of Laguna Potrok Aike. *Sedimentology*, **56(4)**, 873-892.
- Aoki, Y. & Scholz, C.H., 2003. Interseismic deformation at the Nankai subduction zone and the Median Tectonic Line, southwest Japan. *Journal of Geophysical Research - Solid Earth*, **108**, 2470.
- Appleby, P.G., 1998. Dating recent sediments by ^{210}Pb : problems and solutions. In: Illus, E. (ed.) *Dating of sediments and determination rate*. Vol STUK-A145. Helsinki: STUK, pp. 7-24.
- Appleby, P.G. & Oldfield, F., 1978. The calculation of lead-210 dates assuming a constant rate of supply of unsupported ^{210}Pb to the sediment. *Catena*, **5**, 1-8.
- Aramaki, S., Fujii, T., Nakada, S. & Miyaji, N., (eds.), 2007. *Fuji Volcano*. Yamanashi Institute of Environmental Sciences, Fuji-Yoshida, 485 pp.
- Arnaud, F., Lignier, V., Revel, M., Desmet, M., Beck, C., Pourchet, M., Charlet, F., Trentesaux, A. & Tribouvillard, N., 2002. Flood and earthquake disturbance of ^{210}Pb geochronology (Lake Anterne, NW Alps). *Terra Nova*, **14(4)**, 225-232.
- Atwater, B.F., Carson, B., Griggs, G.B., Johnson, H.P. & Salmi, M.S., 2014. Rethinking turbidite paleoseismology along the Cascadia subduction zone. *Geology*, **42**, 827-830.
- Atwater, B.F., Satoko, M.-R., Kenji, S., Yoshinobu, T., Kazue, U. & Yamaguchi, D.K., 2015. The Orphan Tsunami of 1700 - Japanese Clues to a Parent Earthquake in North America. University of Washington Press, 135 pp.
- Atwater, B.F. & Yamaguchi, D.K., 1991. Sudden, probably coseismic submergence of Holocene trees and grass in coastal Washington State. *Geology*, **19**, 706-709.
- Auclair, M., Lamothe, M. & Huot, S., 2003. Measurement of anomalous fading for feldspar IRSL using SAR. *Radiation Measurements*, **37**, 487-492.
- Azuma, T., Ota, Y., Ishikawa, M. & Taniguchi, K., 2005. Late Quaternary coastal tectonics and development of marine terraces in Omaezaki, Pacific coast of central Japan. *The Quaternary Research*, **44**, 169-176.
- Baba, T. & Cummins, P.R., 2005. Contiguous rupture areas of two Nankai Trough earthquakes revealed by high-resolution tsunami waveform inversion. *Geophysical Research Letters*, **32**, L08305.
- Baba, T., Tanioka, Y., Cummins, P.R. & Uhira, K., 2002. The slip distribution of the 1946 Nankai earthquake estimated from tsunami inversion using a new plate model. *Physics of the Earth and Planetary Interiors*, **132**, 59-73.

- Bangs, N.L., Shipley, T.H., Gulick, S.P.S., Moore, G.F., Kuromoto, S. & Nakamura, Y., 2004. Evolution of the Nankai Trough décollement from the trench into the seismogenic zone: inferences from three-dimensional seismic reflection imaging. *Geology*, **32**, 273–276.
- Beck, C., 2009. Late Quaternary lacustrine paleo-seismic archives in northwestern Alps: Examples of earthquake-origin assessment of sedimentary disturbances. *Earth-Science Reviews*, **96**, 327–344.
- Beck, C., Mercier de Lépinay, B., Schneider, J.-L., Cremer, M., Çağatay, N., Wendenbaum, E., Boutareaud, S., Ménot, G., Schmidt, S., Weber, O., Eris, K., Armijo, R., Meyer, B., Pondard, N., Gutscher, M.-A. & the MARMACORE Cruise Party (Turon, J.-L., Labeyrie, L., Cortijo, E., Gallet, Y., Bouquerel, H., Gorur, N., Gervais, A., Castera, M.-H., Londeix, L., de Ressaiguier, A., Jaouen, A.), 2007. Late Quaternary co-seismic sedimentation in the Sea of Marmara's deep basins. *Sedimentary Geology*, **199**, 65–89.
- Bell, W.T., 1980. Alpha attenuation in quartz grains for thermoluminescence dating. *Ancient TL*, **12**, 4–8.
- Beug, H.J., 2004. Leitfaden der Pollenbestimmung für Mitteleuropa und angrenzende Gebiete. Verlag Friedrich Pfeil, 542 pp.
- Blott, S.J. & Pye, K., 2001. Gradistat: A grain size distribution and statistics package for the analysis of unconsolidated sediments. *Earth Surface Processes and Landforms*, **26**, 1237–1248.
- Boes, E., Yokoyama, Y., Fujiwara, O., Miyairi, Y., Kempf, P., Schmidt, S., Nakamura, A., Heyvaert, V.M.A., Brückner, H., De Batist, M. & the QuakeRecNankai team, (submitted). An 8,000-year-long record of extreme wave event deposits and coastal evolution from tidal Lake Hamana, south-central Japan. *Quaternary Science Reviews*.
- Bondevik, S., Svendsen, J.I. & Mangerud, J., 1998. Distinction between the Storegga tsunami and the Holocene marine transgression in coastal basin deposits of western Norway. *Journal of Quaternary Science*, **13(6)**, 529–537.
- Brill, D., Klasen, N., Jankaew, K., Brückner, H., Kelletat, D., Scheffers, A. & Scheffers, S., 2012. Local inundation distances and regional tsunami recurrence in the Indian Ocean inferred from luminescence dating of sandy deposits in Thailand. *Natural Hazards and Earth System Science*, **12**, 2177–2192.
- Bronk Ramsey, C., 1995. Radiocarbon calibration and analysis of stratigraphy; the OxCal program. *Radiocarbon*, **37**, 425–430.
- Bronk Ramsey, C., 2008. Deposition models for chronological records. *Quaternary Science Reviews*, **27**, 42–60.
- Bronk Ramsey, C., 2009. Bayesian analysis of radiocarbon dates. *Radiocarbon*, **51**, 337–360.
- Buylaert, J.-P., Huot, S., Murray, A.S. & van den Haute, P., 2011. Infrared stimulated luminescence dating of an Eemian (MIS 5e) site in Denmark using K-feldspar. *Boreas*, **40**, 46–56.
- Central Disaster Management Council, 2011. Report of the Committee for Technical Investigation on Countermeasures for Earthquakes and Tsunamis Based on the Lessons Learned from the “2011 off the Pacific coast of Tohoku Earthquake.”
- Central Disaster Management Council, 2012. Final Report - Toward the reconstruction for sound and unwavering Japan.
- Chagué-Goff, C., Andrew, A., Szczuciński, W., Goff, J. & Nishimura, Y., 2012. Geochemical signatures up to the maximum inundation of the 2011 Tohoku-oki tsunami - Implications for the 869 AD Jogan and other palaeotsunamis. *Sedimentary Geology*, **282**, 65–77.
- Chagué-Goff, C., Chan, J.C.H., Goff, J. & Gadd, P., 2016. Late Holocene records of environmental changes, cyclones and tsunamis in a coastal lake, Mangaia, Cook Islands. *Island Arc*, **25(5)**, 333–349.
- Chagué-Goff, C., Schneider, J.-L., Goff, J.R., Dominey-Howes, D., Strotz, L., 2011. Expanding the proxy toolkit to help identify past events - lessons from the 2004 Indian Ocean tsunami and the 2009 South Pacific tsunami. *Earth-Science Reviews*, **107**, 107–122.

- Chagué-Goff, C., Szczuciński, W. & Shinozaki, T., 2017. Applications of geochemistry in tsunami research: A review. *Earth-Science Reviews*, **165**, 203-244.
- Chapron, E., Arnaud, F., Noel, H., Revel, M., Desmet, M. & Perdereau, L. 2005. Rhone River flood deposits in Lake Le Bourget: a proxy for Holocene environmental changes in the NW Alps, France. *Boreas*, **34**, 404-416.
- Chapron, E., Beck, C., Pourchet, M. & Deconinck, J.F., 1999. 1822 earthquake-triggered homogenite in Lake Le Bourget (NW Alps). *Terra Nova*, **11**, 86-92.
- Chen, C.-T. & Millero, F.J., 1977. Speed of sound in seawater at high pressures. *Journal of the Acoustical Society of America*, **62(5)**, 1129-1135.
- Chiba, T., Sugihara, S., Matsushima, Y., Arai, Y. & Endo, K., 2016. Reconstruction of Holocene relative sea-level change and residual uplift in the Lake Inba area, Japan. *Palaeogeography, Palaeoclimatology, Palaeoecology*, **441(4)**, 982-996.
- Chorley, R.J., 1962. *Geomorphology and General Systems Theory*. US Government Printing Office, Washington DC.
- Cisternas, M., Atwater, B.F., Torrejón, F., Sawai, Y., Machuca, G., Lagos, M., Eipert, A., Youlton, C., Salgado, I. & Kamataki, T., 2005. Predecessors of the giant 1960 Chile earthquake. *Nature*, **437**, 404-407.
- Cummins, P.R., Baba, T., Kodaira, S. & Kaneda, Y., 2002. The 1946 Nankai earthquake and segmentation of the Nankai Trough. *Physics of the Earth and Planetary Interiors*, **132**, 75-87.
- Cummins, P.R., Hori, T. & Kaneda, Y., 2001. Splay fault and megathrust earthquake slip in the Nankai Trough. *Earth, Planets and Space*, **53**, 243-248.
- Dawson, A.G., Foster, I.D.L., Shi, S., Smith, D.E. & Long, D., 1991. The identification of tsunami deposits in coastal sediment sequences. *Science of Tsunami Hazards*, **9(1)**, 73-82.
- Day, R.W., 1995. Engineering properties of diatomaceous fill. *Journal of Geotechnical and Geoenvironmental Engineering*, **121(12)**, 908-910.
- DeMets, C., Gordon, R.G. & Argus, D.F., 2010. Geologically current plate motions. *Geophysical Journal International*, **181**, 1-80.
- Demske, D., Tarasov, P.E. & Nakagawa, T., 2013 Atlas of pollen, spores and further non-pollen palynomorphs recorded in the glacial-interglacial late Quaternary sediments of Lake Suigetsu, central Japan. *Quaternary International*, **290**, 164-238.
- Diaz-Rodriguez, J.A., 2011. Diatomaceous soils: Monotonic behavior. Paper presented at the International Symposium on Deformation Characteristics of Geomaterials, Seoul.
- Diaz-Rodriguez, J., Cruz, R.L.-S., Davila-Alcocer, V., Vallejo, E. & Giron, P., 1998. Physical, chemical, and mineralogical properties of Mexico City sediments: A geotechnical perspective. *Canadian Geotechnical Journal*, **35(4)**, 600-610.
- Durcan, J.A., King, G.E. & Duller, G.A.T., 2015. DRAC: dose rate and age calculator for trapped charge dating. *Quaternary Geochronology*, **28**, 54-61.
- Engel, M. & Brückner, H., 2011. The identification of palaeo-tsunami deposits - a major challenge in coastal sedimentary research. *Coastline Reports*, **17**, 65-80.
- Engel, M., Brückner, H., Fürstenberg, S., Frenzel, P., Konopczak, A.M., Scheffers, A., Kelleat, D., May, S.M., Schäbitz, F. & Daut, G., 2013. A prehistoric tsunami induced long-lasting ecosystem changes on a semi-arid tropical island - the case of Boka Bartol (Bonaire, Leeward Antilles). *Naturwissenschaften*, **100(1)**, 51-67.
- Folk, R.L. & Ward, W.C., 1957. Brazos River bar: a study in the significance of grain size parameters. *Journal of Sedimentary Petrology*, **27**, 3-26.
- Fujimori, T., 1991. Active faults in the Suwa basin, and its evolution as a pull-apart basin on the Itoigawa-Shizuoka tectonic line, Central Japan. *Geographical Review of Japan*, **64**, 665-696.
- Fujino, S., Kimura, H., Komatsubara, J., Matsumoto, D., Namegaya, Y., Sawai, Y. & Shishikura, M., 2018. Stratigraphic evidence of historical and prehistorical tsunamis on the Pacific coast of central Japan: Implications for the variable recurrence of tsunamis in the Nankai Trough. *Quaternary Science Reviews*, **201**, 147-161.

- Fujino, S., Komatsubara, J., Shishikura, M., Kimura, H. & Namegaya, Y., 2008. Preliminary results on paleotsunami study by hand coring in Shima Peninsula, Mie Prefecture, central Japan. *Annual Report on Active Fault and Paleoearthquake Researches*, **8**, 255-265.
- Fujiwara, O., 2013. Earthquake and tsunamis along the Nankai Trough, inferred from geology and geomorphology — examples in Tokai region. *Geological Survey of Japan Chishitsu News*, **2**, 197-200.
- Fujiwara, O., Fujino, S., Komatsubara, J., Morita, Y. & Namegaya, Y., 2016. Paleocological evidence for coastal subsidence during five great earthquakes in the past 1500 years along the northern onshore continuation of the Nankai subduction zone. *Quaternary International*, **397**, 523-540.
- Fujiwara, O., Hirakawa, K., Irizuki, T., Hasegawa, S., Hase, Y., Uchida, J. & Abe, K., 2010a. Millennium-scale recurrent uplift inferred from beach deposits bordering the eastern Nankai Trough, Omaezaki area, central Japan. *Island Arc*, **19**, 374-388.
- Fujiwara, O., Komatsubara, J. & Sawai, Y., 2006a. Holocene earthquakes along the Nankai Trough and sedimentary facies of the Ukishima-ga-hara lowland beside Suruga Bay, Shizuoka Prefecture, central Japan: a preliminary report. *Annual Report on Active Fault and Paleoearthquake Researches*, **6**, 89-106.
- Fujiwara, O., Komatsubara, J., Takada, K., Shishikura, M. & Kamataki, T., 2006b. Temporal development of a late Holocene strand plain system in the Shirasuka area along western Shizuoka Prefecture on the Pacific coast of central Japan. *Journal of Geography*, **115(5)**, 569-581.
- Fujiwara, O., Ono, E., Satake, K., Sawai, Y., Umitsu, M., Yata, T., Abe, K., Ikeda, T., Okamura, Y., Sato, Y., Aung, T.T. & Uchida, J., 2007a. Trace of the AD1707 Hoei earthquake from the coastal lowland, Shizuoka Prefecture, central Japan. *Annual Report on Active Fault and Paleoearthquake Researches*, **7**, 157-171.
- Fujiwara, O., Ono, E., Yata, T., Umitsu, M., Kamataki, T. & Uchida, J., 2008. Late Holocene environmental change and tsunami deposits in the southwestern part of Otagawa lowland, central Japan. *Annual Report on Active Fault and Paleoearthquake Researches*, **8**, 187-202.
- Fujiwara, O., Ono, E., Yata, T., Umitsu, M., Sato, Y. & Heyvaert, V.M.A., 2010b. Geomorphic impact by the 1498 Meio earthquake along the Hamana River on the Enshu-nada coast, Central Japan: Evidence from the cored sediments. *Historical Earthquakes*, **25**, 29-38.
- Fujiwara, O., Ono, E., Yata, T., Umitsu, M., Sato, Y. & Heyvaert, V.M.A., 2013a. Assessing the impact of 1498 Meio earthquake and tsunami along the Enshu-nada coast, central Japan using coastal geology. *Quaternary International*, **308**, 4-12.
- Fujiwara, O., Sato, Y., Ono, E. & Umitsu, M., 2013b. Researches on tsunami deposits using sediment cores: 3.4 ka tsunami deposit in the Rokken-gawa lowland near Lake Hamana, Pacific coast of central Japan. *Journal of Geography*, **122(2)**, 308-322.
- Fujiwara, O., Sawai, Y., Morita, Y., Komatsubara, J. & Abe, K., 2007b. Coseismic subsidence recorded in the Holocene sequence in the Ukishima-ga-hara lowland, Shizuoka Prefecture, central Japan. *Annual Report on Active Fault and Paleoearthquake Researches*, **7**, 91-118.
- Fujiwara, O. & Tanigawa, K., 2014. Bedforms record the flow conditions of the 2011 Tohoku-Oki tsunami on the Sendai Plain, northeast Japan. *Marine Geology*, **358**, 79-88.
- Furumura, T., Imai, K. & Maeda, T., 2011. A revised tsunami source model for the 1707 Hoei earthquake and simulation of tsunami inundation of Ryujin Lake, Kyushu, Japan. *Journal of Geophysical Research - Solid Earth*, **116**, B02308.
- Garrett, E., Fujiwara, O., Garrett, P., Heyvaert, V.M.A., Shishikura, M., Yokoyama, Y., Hubert-Ferrari, A., Brückner, H., Nakamura, A., De Batist, M. & the QuakeRecNankai team, 2016. A systematic review of geological evidence for Holocene earthquakes and tsunamis along the Nankai-Suruga Trough, Japan. *Earth-Science Reviews*, **159**, 337-357.
- Garrett, E., Fujiwara, O., Riedesel, S., Walstra, J., Deforce, K., Yokoyama, Y., Schmidt, S., Brückner, H., De Batist, M., Heyvaert, V.M.A. & the QuakeRecNankai team, 2018. Historical Nankai-Suruga megathrust earthquakes recorded by tsunami and terrestrial mass movement deposits on the Shirasuka coastal Lowlands, Shizuoka Prefecture, Japan. *The Holocene*, **28(6)**, 968-983.

- Gilli, A., Anselmetti, F.S., Ariztegui, D. & McKenzie, J.A., 2003. A 600-year sedimentary record of flood events from two sub-alpine lakes (Schwendiseen, Northeastern Switzerland). *Eclogae Geologicae Helveticae*, **96** (Supplement 1), S49-S58.
- Girardclos, S., Schmidt, O.T., Sturm, M., Ariztegui, D., Pugin, A. & Anselmetti, F.S., 2007. The 1996 AD delta collapse and large turbidite in Lake Brienz. *Marine Geology*, **241(1-4)**, 137-154.
- Goff, J., Chagué-Goff, C., Nichol, S., Jaffe, B. & Dominey-Howes, D., 2012. Progress in palaeotsunami research. *Sedimentary Geology*, **243**, 70–88.
- Goldfinger, C., Ikeda, Y., Yeats, R.S. & Ren, J., 2013. Superquakes and supercycles. *Seismological Research Letters*, **84**, 24-32.
- Goldfinger, C., Nelson, C.H. & Johnson, J.E., 2003. Holocene earthquake records from the Cascadia subduction zone and northern San Andreas fault based on precise dating of offshore turbidites. *Annual Review of Earth and Planetary Sciences*, **31**, 555-577.
- Goldfinger, C., Nelson, C.H., Morey, A.E., Johnson, J.E., Patton, J.R., Karabanov, E., Gutierrez-Pastor, J., Eriksson, A.T., Gracia, E. & Dunhill, G., 2012. Turbidite Event History: Methods and Implications for Holocene Paleoseismicity of the Cascadia Subduction Zone. US Department of the Interior, US Geological Survey.
- Goldfinger, C., 2011. Submarine Paleoseismology Based on Turbidite Records. *Annual Reviews of Marine Science*, **3**, 35-66.
- Goto, K., Chagué-Goff, C., Fujino, S., Goff, J., Jaffe, B., Nishimura, Y., Richmond, B., Sugawara, D., Szczuciński, W. & Tappin, D.R., 2011. New insights of tsunami hazard from the 2011 Tohoku-oki event. *Marine Geology*, **290**, 46-50.
- Goto, K., Fujino, S., Sugawara, D. & Nishimura, Y., 2014. The current situation of tsunami geology under new policies for disaster countermeasures in Japan. *Episodes*, **37**, 258-264.
- Goto, T., Satake, K., Sugai, T., Ishibe, T., Harada, T. & Murotani, S., 2015. Historical tsunami and storm deposits during the last five centuries on the Sanriku coast, Japan. *Marine Geology*, **367**, 105-117.
- Green, R.A., Obermeier, S.F. & Olson, S.M., 2005. Engineering geologic and geotechnical analysis of paleoseismic shaking using liquefaction effects: field examples. *Engineering Geology*, **76**, 263–293.
- Guérin, G., Mercier, N., Nathan, R., Adamiec, G. & Lefrais, Y., 2012. On the use of the infinite matrix assumption and associated concepts: a critical review. *Radiation Measurements*, **47**, 778-785.
- Habe, T., 1977. *Systematics of Mollusca in Japan. Bivalvia and Scaphopoda*. Zukan-no-Hokuryukan, 372 pp.
- Hansom, J.D., Pile, J. & Switzer, A.D., 2015. Chapter 11: Extreme waves: Causes, characteristics and impact on coastal environments and society. In: Shroder, J.F. (ed.) *Coastal and marine hazards, risks, and disasters*. Elsevier, pp. 307-334.
- Hartley, B., Barber, H. & Carter, J., 1996. *An Atlas of British Diatoms*. Biopress, 601 pp.
- Hashimoto, C., Fukui, K. & Matsu'ura, M., 2004. 3-D modelling of plate interfaces and numerical simulation of long-term crustal deformation in and around Japan. *Pure and Applied Geophysics*, **161**, 2053–2068.
- Hatori, T., 1975. Sources of large tsunamis generated in the Boso, Tōkai and Nankai regions in 1498 and 1605. *Bulletin of the Earthquake Research Institute, University of Tokyo*, **50**, 171-185.
- Hawkes, A.D. & Horton, B.P., 2012. Sedimentary record of storm deposits from Hurricane Ike, Galveston and San Luis Islands, Texas. *Geomorphology*, **171**, 180–189.
- Herath, S., Meguro, K., Oki, T. & Miura, K., 1992. Saiko high water: A preliminary report. *Seisan-Kenkyu*, **44**, 132-136.
- Herrendörfer, R., van Dinther, Y., Gerya, T. & Dalguer, L.A., 2015. Earthquake supercycle in subduction zones controlled by the width of the seismogenic zone. *Nature Geoscience*, **8**, 471–474.

- Hideshima, S., Matsumoto, E., Abe, O. & Kitagawa, H., 2001. Northwest Pacific marine reservoir correction estimated from annually banded coral from Ishigaki Island, southern Japan. *Radiocarbon*, **43**, 473-476.
- Hilbe, M. & Anselmetti, F.S., 2014. Signatures of slope failures and river-delta collapses in a perialpine lake (Lake Lucerne, Switzerland). *Sedimentology*, **61**, 1883-1907.
- Hirose, F., Nakajima, J. & Hasegawa, A., 2008. Three-dimensional seismic velocity structure and configuration of the Philippine Sea slab in southwestern Japan estimated by double-difference tomography. *Journal of Geophysical Research - Solid Earth*, **113**, B09315.
- History of Asaba town editing committee (ed.), 2000. *History of Asaba town: Part of the overview of town history*, 1133 pp.
- Honda, S. & Kashima, K., 1997. Paleo-environmental changes during the last 1,000 years from a lake deposit at Lake Hamana, central Japan. *Laguna*, **4**, 69-76.
- Hovland, M. & Judd, A.G., 1988. *Seabed pockmarks and seepages: Impact on geology, biology and the marine environment*. Graham and Trotman, 293 pp.
- Howarth, J.D., Fitzsimons, S.J., Norris, R.J. & Jacobsen, G.E., 2014. Lake sediments record high intensity shaking that provides insight into the location and rupture length of large earthquakes on the Alpine Fault, New Zealand. *Earth and Planetary Science Letters*, **403**, 340-351.
- Howarth, J.D., Fitzsimons, S.J., Norris, R.J., Langridge, R. & Vandergoes, M.J., 2016. A 2000 yr rupture history for the Alpine fault derived from Lake Ellery, South Island, New Zealand. *Geological Society of America Bulletin*, **128**, 627-643.
- Huntley, D.J. & Lamothe, M., 2001. Ubiquity of anomalous fading in K-feldspars and the measurement and correction for it in optical dating. *Canadian Journal of Earth Sciences*, **38**, 1093-1106.
- Hyndman, R.D., Wang, K. & Yamano, M., 1995. Thermal constraints on the seismogenic portion of the southwestern Japan subduction thrust. *Journal of Geophysical Research - Solid Earth*, **100**, 373-392.
- Hyodo, M. & Hori, T., 2013. Re-examination of possible great interplate earthquake scenarios in the Nankai Trough, southwest Japan, based on recent findings and numerical simulations. *Tectonophysics*, **600**, 175-186.
- Ikeda, Y. & Yonekura, N., 1986. Determination of late Quaternary rates of net slip on two major fault zones in central Japan. *Bulletin of the Department of Geography, University of Tokyo*, **18**, 49-63.
- Ikeya, N., Wada, H. & Ohmori, M., 1987. On the boring core sediments from Hamana Lake. *Geoscience Reports Shizuoka University*, **13**, 67-111.
- Inouchi, Y., Kinugasa, Y., Kumon, F., Nakano, S., Yasumatsu, S. & Shiki, T., 1996. Turbidites as records of intense palaeoearthquakes in Lake Biwa, Japan. *Sedimentary Geology*, **104**, 117-125.
- Ishibashi, K., 1976. Re-examination of estimated Tōkai region great earthquakes – regarding Suruga Bay great earthquakes. *Earthquake Study Association Preliminary Draft Collection*, **2**, pp. 30-34.
- Ishibashi, K., 1981. Specification of a soon-to-occur seismic faulting in the Tokai district, central Japan, based upon seismotectonics. In: Simpson, D.W. & Richards, P.G. (eds.) *Earthquake Prediction: An international review*, Maurice Ewing Series Vol. 4, 297-332.
- Ishibashi, K., 1991. The 1293 Einin Kamakura earthquake and the recurrence time of great interplate earthquakes along the Sagami Trough, central Japan. Abstract of 1991 Fall Meeting Seismological Society of Japan, Tokyo.
- Ishibashi, K., 1998. No great Nankai earthquake occurred on March 17, 1233. *Journal of the Seismological Society of Japan*, **51**, 335-338.
- Ishibashi, K., 1999. Great Tokai and Nankai, Japan, earthquakes as revealed by historical seismology: 1. Review of the events until the mid-14th century. *Journal of Geography*, **108(4)**, 399-423.
- Ishibashi, K., 2004. Status of historical seismology in Japan. *Annals of Geophysics*, **47**, 339-368.
- Ishibashi, K., 2014. *Nankai Trough great earthquake, History, Science and Society*. Iwanami Shoten Publishers, 205 pp.

- Ishibashi, K. & Satake, K., 1998. Problems on forecasting great earthquakes in the subduction zones around Japan by means of paleoseismology. *Journal of the Seismological Society of Japan*, **50**, 1-21.
- Ishiwa, T., Yokoyama, Y., Miyairi, Y., Ikehara, M. & Obrochta, S., 2016. Sedimentary environmental change induced from late Quaternary sea-level change in the Bonaparte Gulf, northwestern Australia. *Geoscience Letters*, **3**, 33.
- Ishizuka, Y., Takada, A., Suzuki, Y., Kobayashi, M. & Nakano, S., 2007. Eruption ages and whole-rock chemistries of scoria cones on the northern to western slope of Fuji Volcano based on trenching surveys. *Bulletin of the Geological Survey of Japan*, **57**, 357-376.
- Itoh, N., Tani, Y., Nagatani, T. & Soma, M., 2003a. Phototrophic activity and redox condition in Lake Hamana, Japan, indicated by sedimentary photosynthetic pigments and molybdenum over the last ~250 years. *Journal of Paleolimnology*, **29**, 403-422.
- Itoh, N., Tani, Y. & Soma, M., 2003b. Sedimentary photosynthetic pigments of algae and phototrophic bacteria in Lake Hamana, Japan: temporal changes of anoxia in its five basins. *Limnology*, **4**, 139-148.
- Iwai, M., Fujiwara, O., Momma, H., Iwasaki, N., Kano, H., Oda, M., Matsuoka, H. & Okamura, M., 2004. Holocene seismoturbidites from the Tosabae Trough a landward slope basin of Nankai Trough off Muroto: Core KR9750P1. *Memoirs of the Geological Society of Japan*, **58**, 137-152.
- Japan Meteorological Agency, 2011. Information on the 2011 Great East Japan Earthquake. http://www.jma.go.jp/jma/en/2011_Earthquake/Information_on_2011_Earthquake.html, Consulted on 6 January 2018.
- Kai, A. & Ikeya, M., 1989. ESR study of fossil shells in sediments at Hamana Lake. *Applied Radiation and Isotopes*, **40**, 1139-1142.
- Kanagawa Prefecture, 2003. *Survey result report of the Kannawa/Kozu-Matsuda Fault Zone*.
- Kashima, K., Honda, S. & Morita, H., 1997. Paleoenvironmental changes of Lake Hamana, a semienclosed brackish lake at the central Japan, during the last 6000 years presumed by the diatom assemblages from core samples of lake deposits. *Diatom*, **13**, 185-191.
- Keefer, D.K., 1984. Landslides caused by earthquakes. *Geological Society of America Bulletin*, **95**, 406-421.
- Keefer, D.K., 2002. Investigating landslides caused by earthquakes - A historical review. *Surveys in Geophysics*, **23**, 473-510.
- Kempf, P., Moernaut, J., Van Daele, M., Vandoorne, W., Pino, M., Urrutia, R. & De Batist, M., 2017. Coastal lake sediments reveal 5500 years of tsunami history in south central Chile. *Quaternary Science Reviews*, **161**, 99-116.
- Kitamura, A., Fujiwara, O. & Kobayashi, K., 2011. Preliminary study on drill cores for evidence of run-up tsunami deposits from Holocene sediments in the southeast Shizuoka Plain, Shizuoka Prefecture. *Geoscience Reports Shizuoka University*, **38**, 3-19.
- Kitamura, A., Fujiwara, O., Shinohara, K., Akaike, S., Masuda, T., Ogura, K., Urano, Y., Kobayashi, K., Tamaki, C. & Mori, H., 2013. Identifying possible tsunami deposits on the Shizuoka Plain, Japan and their correlation with earthquake activity over the past 4000 years. *The Holocene*, **23**, 1684-1698.
- Kitamura, A. & Kawate, S., 2015. Tsunami deposits from the coastal lowland of Minami-Izu and Kisami, Shizuoka Prefecture, Japan. *Geoscience Reports Shizuoka University*, **42**, 15-23.
- Kitamura, A. & Kobayashi, K., 2014. Geologic evidence for prehistoric tsunamis and coseismic uplift during the ad 1854 Ansei-Tokai earthquake in Holocene sediments on the Shimizu Plain, central Japan. *The Holocene*, **24(7)**, 814-827.
- Kitamura, A., Ohashi, Y., Ishibashi, H., Miyairi, Y., Yokoyama, Y., Ikuta, R., Ito, Y., Ikeda, M. & Shimano, T., 2016. Holocene geohazard events on the southern Izu Peninsula, central Japan. *Quaternary International*, **397**, 541-554.
- Kobayasi, H., 2006. *Atlas of Japanese Diatoms Based on Electron Microscopy*. Uchida Rokakuho, 533 pp.

- Kodaira, S., Kurashimo, E., Park, J.-O., Takahashi, N., Nakanishi, A., Miura, S., Iwasaki, T., Hirata, N., Ito, K. & Kaneda, Y., 2002. Structural factors controlling the rupture process of a megathrust earthquake at the Nankai trough seismogenic zone. *Geophysical Journal International*, **149**, 815–835.
- Kodaira, S., Takahashi, N., Park, J., Mochizuki, K., Shinohara, M. & Kimura, S., 2000. Western Nankai Trough seismogenic zone: results from a wide-angle ocean bottom seismic survey. *Journal of Geophysical Research - Solid Earth*, **105**, 5887–5905.
- Koike, K. & Machida, H., 2001. *Atlas of Quaternary Marine Terraces in the Japanese Islands*. University of Tokyo Press, 105 pp.
- Komatsubara, J. & Fujiwara, O., 2007. Overview of Holocene tsunami deposits along the Nankai, Suruga, and Sagami Troughs, southwest Japan. *Pure and Applied Geophysics*, **164**, 493-507.
- Komatsubara, J. & Okamura, Y., 2007. Preliminary research of tsunami deposits in the Shijima Lowland, Shima Peninsula, central Japan. *Annual Report on Active Fault and Paleearthquake Researches*, **7**, 209-217.
- Komatsubara, J., Fujiwara, O., Kamataki, T., 2006a. Tsunami deposits along the Nankai, Suruga and Sagami Troughs. *Historical Earthquakes*, **21**, 93-109.
- Komatsubara, J., Fujiwara, O., Takada, K., Sawai, Y., Aung, T.T. & Kamataki, T., 2006b. Historical tsunamis and storms recorded in a coastal lowland deposit, along the Nankai Trough, southwestern Japan. *Annual Report on Active Fault and Paleearthquake Researches*, **6**, 107-122.
- Komatsubara, J., Fujiwara, O., Takada, K., Sawai, Y., Aung, T.T. & Kamataki, T., 2008. Historical tsunamis and storms recorded in a coastal lowland, Shizuoka Prefecture, along the Pacific Coast of Japan. *Sedimentology*, **55**, 1703-1716.
- Kortekaas, S. & Dawson, A.G., 2007. Distinguishing tsunami and storm deposits: an example from Martinhal, SW Portugal. *Sedimentary Geology*, **200**, 208-221.
- Kouli, K., 2012. Vegetation development and human activities in Attiki (SE Greece) during the last 5,000 years. *Vegetation History and Archaeobotany*, **21(4-5)**, 267-278.
- Kreutzer, S., 2016. calc_FadingCorr(): apply a fading correction according to Huntley & Lamothe (2001) for a given g-value and a given tc. Function version 0.4.2. In: Kreutzer, S., Dietze, M., Burow, C., Fuchs, M.C., Schmidt, C., Fischer, M. & Friedrich, J. (eds.) *Luminescence: Comprehensive Luminescence Dating Data Analysis*, R package version 0.6.4. <https://CRAN.R-project.org/package=Luminescence>.
- Kreutzer, S., Schmidt, C., Fuchs, M.C., Dietze, M., Fischer, M. & Fuchs, M., 2012. Introducing an R package for luminescence dating analysis. *Ancient TL*, **30(1)**, 1-8.
- Kumagai, H., 1999. Tsunami deposits of large earthquakes along the Nankai Trough: Investigation around Hamana Lake in central Japan. *Journal of Geography*, **108(4)**, 424-432.
- Lamair, L., 2018. *Holocene history of natural hazards in central Japan (Fuji Five Lake): imprints of earthquakes, typhoons and volcanic events in lacustrine sediments*. PhD thesis, University of Liège - Belgium.
- Lamair, L., Hubert-Ferrari, A., El Ouahabi, M., Yamamoto, S., Schmidt, S., Vander Auwera, J., Lepoint, G., Boes, E., Fujiwara, O., Yokoyama, Y., De Batist, M. & Heyvaert, V.M.A., 2019. Late Holocene changes on erosion pattern on a lacustrine environment: landscape stabilization by volcanic activity versus human activity. *Geochemistry, Geophysics, Geosystems*, **20(4)**, 1720-1733.
- Lamair, L., Hubert-Ferrari, A., Schmidt, S., Yamamoto, S., Fujiwara, O., Yokoyama, Y., De Batist, M., Heyvaert, V.M.A. & the QuakeRecNankai Team, (in preparation). Signature of extreme flood events and earthquakes in Lake Sai, Fuji Five Lakes, Central Japan. *Natural Hazards and Earth System Sciences*.
- Lamair, L., Hubert-Ferrari, A., Yamamoto, S., El Ouahabi, M., Vander Auwera, J., Obrochta, S., Boes, E., Nakamura, A., Fujiwara, O., Shishikura, M., Schmidt, S., Siani, G., Miyairi, Y., Yokoyama, Y., De Batist, M., Heyvaert, V.M.A. & the QuakeRecNankai Team, 2018. Volcanic influence of Mt. Fuji

- on the watershed of Lake Motosu and its impact on the lacustrine sedimentary record. *Sedimentary Geology*, **363**, 200-220.
- Leri, A.C., Hakala, J.A., Marcus, M.A., Lanzirotti, A., Reddy, C.M. & Myneni, S.C.B., 2010. Natural organobromine in marine sediments: New evidence of biogeochemical Br cycling. *Global Biogeochemical Cycles*, **24(4)**, GB4017.
- Li, Y., Tsukamoto, S., Hu, K. & Frechen, M., 2017. Quartz OSL and K-feldspar post-IR IRSL dating of sand accumulation in the lower Liao Plain (Liaoning, NE China). *Geochronometria*, **44**, 1-15.
- Lienkaemper, J.J. & Ramsey, C.B., 2009. OxCal: Versatile tool for developing paleoearthquake chronologies—A primer. *Seismological Research Letters*, **80**, 431-434.
- Lin, A., Iida, K. & Tanaka, H., 2013. On-land active thrust faults of the Nankai-Suruga subduction zone: The Fujikawa-kako Fault Zone, central Japan. *Tectonophysics*, **601**, 1-19.
- Liu, X. & Zhao, D., 2014. Structural control on the nucleation of megathrust earthquakes in the Nankai subduction zone. *Geophysical Research Letters*, **41**, 8288–8293.
- Loveless, J.P. & Meade, B.J., 2010. Geodetic imaging of plate motions, slip rates, and partitioning of deformation in Japan. *Journal of Geophysical Research - Solid Earth*, **115**, B09315.
- Lupini, J.F., Skinner, A.E. & Vaughan, P.R. 1981. The drained residual strength of cohesive soils. *Géotechnique*, **31(2)**, 181-213.
- Machida, H. & Arai, F., 2003. *Atlas of tephra in and around Japan* (revised edition). University of Tokyo Press, 336 pp.
- Matsubara, A., 2005. Processes in the Holocene development of coastal ridges in Japan. *Hiyoshi Review of Natural Science*, **15**, 73-90.
- May, S.M., Brill, D., Engel, M., Scheffers, A., Pint, A., Opitz, S., Wennrich, V., Squire, P., Kelletat, D. & Brückner, H., 2015a. Traces of historical tropical cyclones and tsunamis in the Ashburton Delta (north-west Australia). *Sedimentology*, **62(6)**, 1546–1572.
- May, S.M., Engel, M., Brill, D., Cuadra, C., Lagmay, A.M.F., Santiago, J., Suarez, J.K., Reyes, M. & Brückner, H., 2015b. Block and boulder transport in Eastern Samar (Philippines) during Supertyphoon Haiyan. *Earth Surface Dynamics*, **3**, 543–558.
- May, S.M., Falvard, S., Norpoth, M., Pint, A., Brill, D., Engel, M., Scheffers, A., Dierick, M., Paris, R., Squire, P. & Brückner, H., 2016. A mid-Holocene candidate tsunami deposit from the NW Cape (Western Australia). *Sedimentary Geology*, **332**, 40-50.
- Mazda, Y., 1984. Year-to-year change in water exchange characteristics in a semi-enclosed bay, Lake Hamana. *Journal of Oceanographical Society of Japan*, **40**, 199-206.
- Mazzotti, S., Le Pichon, X., Henry, P. & Miyazaki, S., 2000. Full interseismic locking of the Nankai and Japan-west Kurile subduction zones: An analysis of uniform elastic strain accumulation in Japan constrained by permanent GPS. *Journal of Geophysical Research - Solid Earth*, **105**, 13159-13177.
- McCalpin, J.P. & Nelson, A.R., 2009. Introduction to Paleoseismology. In: McCalpin, J.P. (ed.) *Paleoseismology*. Elsevier, pp. 1-27.
- Miyaji, N., Kan'no, A., Kanamaru T. & Mannen, K., 2011. High-resolution reconstruction of the Hoei eruption (AD 1707) of Fuji volcano, Japan. *Journal of Volcanology and Geothermal Research*, **207**, 113-129.
- Moernaut, J., De Batist, M., Heirman, K., Van Daele, M., Pino, M., Brümmer, R. & Urrutia, R., 2009. Fluidization of buried mass-wasting deposits in lake sediments and its relevance for paleoseismology: Results from a reflection seismic study of lakes Villarrica and Calafquén (South-Central Chile). *Sedimentary Geology*, **213**, 121-135.
- Moernaut, J., Van Daele, M., Heirman, K., Fontijn, K., Strasser, M., Pino, M., Urrutia, R. & De Batist, M., 2014. Lacustrine turbidites as a tool for quantitative earthquake reconstruction: New evidence for a variable rupture mode in south central Chile. *Journal of Geophysical Research - Solid Earth*, **119**, 1607-1633.
- Moernaut, J., Van Daele, M., Strasser, M., Heirman, K., Viel, M., Cardenas, J., Ladròn de Guevara, B., Pino, M., Urrutia, R. & De Batist, M., 2017. Lacustrine turbidites produced by surficial slope

- sediment remobilization: A mechanism for continuous and sensitive turbidite paleoseismic records. *Marine Geology*, **384**, 159-176.
- Monecke, K., Anselmetti, F.S., Becker, A., Sturm, M. & Giardini, D., 2004. The record of historic earthquakes in lake sediments of Central Switzerland. *Tectonophysics*, **394**, 21-40.
- Moore, G.F., Bangs, N.L., Taira, A., Kuramoto, S., Pangborn, E. & Tobin, H.J., 2007. Threedimensional splay fault geometry and implications for tsunami generation. *Science*, **318**, 1128–1131.
- Moore, P., Webb, J. & Collinson, M., 1991. *Pollen Analysis*. Blackwell, 216 pp.
- Moreno, A., Valero-Garcés, B.L., González-Sampériz, P. & Rico, M., 2008. Flood response to rainfall variability during the last 2000 years inferred from the Taravilla Lake record (Central Iberian Range, Spain). *Journal of Paleolimnology*, **40(3)**, 943-961.
- Morita, H., Kashima, K. & Takayasu, K., 1998. Paleoenvironmental changes of Lake Hamana and Lake Shinji during the last 10,000 years, inferred by diatom assemblages from lake core sediments. *Laguna*, **5**, 47-53.
- Morton, R.A., Gelfenbaum, G. & Jaffe, B.E., 2007. Physical criteria for distinguishing sandy tsunami and storm deposits using modern examples. *Sedimentary Geology*, **200**, 184-207.
- Mulder, T., Migeon, S., Savoye, B. & Faugères, J.-C., 2001. Inversely graded turbidite sequences in the deep Mediterranean: a record of deposits from flood-generated turbidity currents? *Geo-Marine Letters*, **21**, 86-93.
- Nagasaka, M., Yoshizawa, K. & Hirabayashi, K., 2002. Temporal changes and vertical distribution of macrophytes in Lake Kawaguchi. *The Japanese Society of Limnology*, **3**, 107–114.
- Nakajima, J. & Hasegawa, A., 2007. Subduction of the Philippine Sea plate beneath southwestern Japan: Slab geometry and its relationship to arc magmatism. *Journal of Geophysical Research - Solid Earth*, **112**, B08306,
- Nakamura, A., Yokoyama, Y., Maemoku, H., Yagi, H., Okamura, M., Matsuoka, H., Miyake, N., Osada, T., Teramura, H., Pani Adhikari, D., Dangol, V., Miyairi, Y., Obrochta, S. & Matsuzaki, H., 2012. Late-Holocene Asian monsoon variations recorded in Lake Rara sediment, western Nepal. *Journal of Quaternary Science*, **27(2)**, 125-128.
- Nakamura, K., 1983. Possibility of a nascent plate boundary at the eastern margin of the Japan Sea. *Bulletin of the Earthquake Research Institute, University of Tokyo*, **58**, 711-722.
- Nakamura, T., Masuda, K., Miyake, F., Hakozaiki, M., Kimura, K., Nishimoto, H. & Hitoki, E., 2016. High-precision age determination of Holocene samples by radiocarbon dating with accelerator mass spectrometry at Nagoya University. *Quaternary International*, **397**, 250-257.
- Nakamura, T., Nishida, I., Takada, H., Okuno, M., Minami, M. & Oda, H., 2007. Marine reservoir effect deduced from 14 C dates on marine shells and terrestrial remains at archeological sites in Japan. *Nuclear Instruments and Methods in Physics Research Section B: Beam Interactions with Materials and Atoms*, **259**, 453-459.
- Nakanishi, A., Takahashi, N., Park, J., Miura, S., Kodaira, S., Kaneda, Y., Hirata, N., Iwasaki, T. & Nakamura, M., 2002. Crustal structure across the coseismic rupture zone of the 1944 Tonankai earthquake, the central Nankai Trough seismogenic zone. *Journal of Geophysical Research - Solid Earth*, **107**, 10.1029/2001JB000424.
- Naruse, H., Fujino, S., Suphawajraksakul, A. & Jarupongsakul, T., 2010. Features and formation processes of multiple deposition layers from the 2004 Indian Ocean Tsunami at Ban Nam Kem, southern Thailand. *Island Arc*, **19(3)**, 399-411.
- Nelson, A.R., Atwater, B.F., Bobrowsky, P.T., Bradley, L.-A., Clague, J.J., Carver, G.A., Darienzo, M.E., Grant, W.C., Krueger, H.W. & Sparks, R., 1995. Radiocarbon evidence for extensive plate-boundary rupture about 300 years ago at the Cascadia subduction zone. *Nature*, **378**, 371-374.
- Nelson, A.R., Kelsey, H.M. & Witter, R.C., 2006. Great earthquakes of variable magnitude at the Cascadia subduction zone. *Quaternary Research*, **65**, 354-365.
- Nichol, S.L., Chagué-Goff, C., Goff, J.R., Horrocks, M., McFadgen, B.G. & Strotz, L.C., 2010. Geomorphology and accommodation space as limiting factors on tsunami deposition: Chatham Island, southwest Pacific Ocean. *Sedimentary Geology*, **229(1-2)**, 41-52.

- NIED (National Research Institute for Earth Science and Disaster Resilience), 2017. *Japan Seismic Hazard information*. <http://www.j-shis.bosai.go.jp/map/?lang=en>, Consulted on 5 January 2018.
- NOAA (National Oceanic and Atmospheric Administration), 2017. Global Significant Earthquake Database, 2150 B.C. to present. <https://www.ngdc.noaa.gov/hazard/earthqk.shtml>, Consulted on 6 December 2017.
- Obata, S. & Umino, S., 1999. Morphology of A.D. 864 Aokigahara Lava Flow Exposed on the Coast of Motosuko Lake, Fuji Volcano. *Bulletin of the Volcanological Society of Japan*, **44**(4), 201-216.
- Obermeier, S.F., 1996. Use of liquefaction-induced features for paleoseismic analysis – an overview of how seismic liquefaction features can be distinguished from other features and how their regional distribution and properties of source sediment can be used to infer the location and strength of Holocene paleoearthquakes. *Engineering Geology*, **44**, 1–76.
- Obermeier, S., 2009. Using liquefaction-induced and other soft-sediment features for paleoseismic analysis. In: McCalpin, J.P. (ed.) *Paleoseismology*. Elsevier, pp. 497–564.
- Ohta, K. & Ide, S., 2011. Precise hypocenter distribution of deep low-frequency earthquakes and its relationship to the local geometry of the subducting plate in the Nankai subduction zone, Japan. *Journal of Geophysical Research - Solid Earth*, **116**, B01308.
- Okahashi, H., Yasuhara, M., Mitamura, M., Hirose, K. & Yoshikawa, S., 2005. Event deposits associated with tsunamis and their sedimentary structure in Holocene marsh deposits on the east coast of the Shima Peninsula, central Japan. *Journal of Geosciences Osaka City University*, **48**, 143.
- Okamura, M. & Matsuoka, H., 2012. Nankai Earthquake recurrences from tsunami sediment. *Kagaku*, **82**, 182-194.
- Okamura, M., Matsuoka, H., Tsukuda, E. & Tsuji, Y., 2000. Tectonic movements of recent 10000 years and observations of historical tsunamis based on coastal lake deposits. *Chikyu Monthly*, 162-168.
- Okumura, K., 2001. Paleoseismology of the Itoigawa-Shizuoka tectonic line in central Japan. *Journal of Seismology*, **5**, 411-431.
- Okumura, K., Shimokawa, K., Yamazaki, H. & Tsukuda, E., 1994. Recent surface faulting events along the middle section of the Itoigawa-Shizuoka tectonic line - Trenching Survey of the Gofukuji Fault near Matsumoto, Central Japan. *Journal of the Seismological Society of Japan*, **46**, 425-438.
- Okutani, T. (ed.), 2000. *Marine Mollusks in Japan*. Tokai University Press, 1173 pp.
- Oldfield, F. & Appleby, P.G., 1984. A combined radiometric and mineral magnetic approach to recent geochronology in lakes affected by catchment disturbance and sediment redistribution. *Chemical Geology*, **44**, 67-83.
- Olson, S.M., Green, R.A. & Obermeier, S.F., 2005. Geotechnical analysis of paleoseismic shaking using liquefaction features: a major updating. *Engineering Geology*, **76**, 235–261.
- Ozawa, T., Tabei, T. & Miyazaki, S., 1999. Interplate coupling along the Nankai Trough off southwest Japan derived from GPS measurements. *Geophysical Research Letters*, **26**, 927-930.
- Palmer, A.J.M. & Abbott, W.H., 1986. Diatoms as indicators of sealevel change. In: van de Plassche, O. (ed.) *Sea-Level Research*. Springer, pp. 457-487.
- Park, J.-O., Fujie, G., Wijerathne, L., Hori, T., Kodaira, S., Fukao, Y., Moore, G.F., Bangs, N.L., Kuramoto, S. & Taira, A., 2010. A low-velocity zone with weak reflectivity along the Nankai subduction zone. *Geology*, **38**, 283–286.
- Park, J.O., Naruse, H. & Bangs, N.L., 2014. Along-strike variations in the Nankai shallow décollement properties and their implications for tsunami earthquake generation. *Geophysical Research Letters*, **41**, 7057–7064.
- Park, J.-O., Tsuru, T., Kodaira, S., Cummins, P.R. & Kaneda, Y., 2002. Splay fault branching along the Nankai Subduction Zone. *Science*, **297**, 1157–1160.
- Patton, J.R., Goldfinger, C., Morey, A., Romsos, C., Black, B., Djadjadihardja, Y. & Udrek, 2013. Seismoturbidite record as preserved at core sites at the Cascadia and Sumatra-Andaman subduction zones. *Natural Hazards and Earth System Sciences*, **13**, 833-867.

- Pouderoux, H., Proust, J.-N. & Lamarche, G., 2014. Submarine paleoseismology of the northern Hikurangi subduction margin of New Zealand as deduced from Turbidite record since 16 ka. *Quaternary Science Reviews*, **84**, 116–131.
- Praet, N., Moernaut, J., Van Daele, M., Boes, E., Haeussler, P.J., Strupler, M., Schmidt, S., Loso, M.G. & De Batist, M., 2017. Paleoseismic potential of sublacustrine landslide records in a high-seismicity setting (south-central Alaska). *Marine Geology*, **384**, 103-119.
- Praet, N., Van Daele, M., Collart, T., Moernaut, J., Vandekerckhove, E., Kempf, P., Haeussler, P.J. & De Batist, M., 2020. Turbidite stratigraphy in proglacial lakes: Deciphering trigger mechanisms using a statistical approach. *Sedimentology*, **67(5)**, 2332-2359.
- Prescott, J.R. & Hutton, J.T., 1994. Cosmic ray contributions to dose rates for luminescence and ESR dating: large depths and long-term time variations. *Radiation Measurements*, **23**, 497-500.
- Reimer, P.J., Bard, E., Bayliss, A., Beck, J.W., Blackwell, P.G., Bronk Ramsey, C., Buck, C.E., Cheng, H., Edwards, R.L. & Friedrich, M., 2013. IntCal13 and Marine13 radiocarbon age calibration curves 0-50,000 years cal BP. *Radiocarbon*, **55**, 1869-1887.
- Revel-Rolland, M., Arnaud, F., Chapron, E., Desmet, M., Givelet, N., Alibert, C. & McCulloch, M., 2005. Sr and Nd isotopes as tracers of clastic sources in Lake Le Bourget sediment (NW Alps, France) during the Little Ice Age: palaeohydrology implications. *Chemical Geology*, **224**, 183-200.
- Riedesel, S., Brill, D., Roberts, H.M., Duller, G.A.T., Garrett, E., Zander, A.M., King, G.E., Tamura, T., Burow, C., Cunningham, A., Seeliger, M., De Batist, M., Heyvaert, V.M.A., Fujiwara, O. & Brückner, H., 2018. Single-grain feldspar luminescence chronology of historical extreme wave event deposits recorded in a coastal lowland, Pacific coast of central Japan. *Quaternary Geochronology*, **45**, 37-49.
- Rikitake, T., 1979. The large-scale earthquake countermeasures act and the earthquake prediction council in Japan. *EOS Transactions*, **60**, 553–555.
- Sagiya, T., 1999. Interplate coupling in the Tokai district, central Japan, deduced from continuous GPS data. *Geophysical Research Letters*, **26**, 2315-2318.
- Saito, H., Nanayama, D. & Matsuyama, H., 2010. Relationship between the initiation of a shallow landslide and rainfall intensity - Duration thresholds in Japan. *Geomorphology*, **118**, 167-175.
- Sakaguchi, A., Kimura, G., Strasser, M., Sreaton, E.J., Curewitz, D. & Murayama, M., 2011. Episodic seafloor mud brecciation due to great subduction zone earthquakes. *Geology*, **39**, 919-922.
- Sangawa, A., 2001. Recent results of paleoseismological study based on earthquake traces excavated at archaeological sites. *Annual Report on Active Fault and Paleoearthquake Researches*, **1**, 287-300.
- Sangawa, A., 2009. A study of paleoearthquakes at archeological sites - A new interdisciplinary area between paleoseismology and archeology. *Synthesiology*, **2(2)**, 91-100.
- Sangawa, A., 2013. Research results of earthquake-archaeology. *The Quaternary Research*, **52**, 191-202.
- Sanukida, S., Okamoto, H. & Hitomi, M., 1985. Bottom environments causing the extinction of macrobenthic fauna in the stagnant period in Lake Hamana on the Pacific coast of central Japan. *Bulletin of the Japanese Society of Scientific Fisheries*, **51(9)**, 1407-1417.
- Satake, K., 2015. Geological and historical evidence of irregular recurrent earthquakes in Japan. *Philosophical Transactions of the Royal Society A*, **373(2053)**, 20140375.
- Sato, H., Hirata, H., Koketsu, K., Okaya, D., Abe, S., Kobayashi, R., Matsubara, M., Iwasaki, T., Ito, T., Ikawa, T., Kawanaka, T., Kasahara, K. & Harder, S., 2005. Earthquake source fault beneath Tokyo. *Science*, **309**, 462-464.
- Sato, Y., 2012. Reconstruction of geo-environment in alluvial lowlands around the lake Hamana inferred from diatom fossil analysis. In: Umitsu, M. (ed.) *Geo-environment of Alluvial and Coastal Lowlands*. Kokon-Shoin Publishers, Tokyo, 119-131.
- Sato, Y. & Fujiwara, O., 2017. Microfossil evidence for recurrent coseismic subsidence around Lake Hamana, near the Nankai-Suruga trough, central Japan. *Quaternary International*, **456**, 39-52.

- Sato, Y., Fujiwara, O., Ono, E. & Umitsu, M., 2011. Environmental change in coastal lowlands around the Lake Hamana during the Middle to Late Holocene. *Geographical Review of Japan*, **84**, 258-273.
- Sato, Y., Fujiwara, O. & Ono, E., 2016a. Late Holocene geomorphological development of beach ridges in western Hamamatsu strand plain, central Japan. *The Quaternary Research*, **55(1)**, 17-35.
- Sato, Y., Matsuoka, H., Okamura, M. & Kashima, K., 2016b. Late Holocene environmental changes of coastal lagoon inferred from a fossil diatom analysis of sediment core from lake Hamana, central Japan. *Quaternary International*, **397**, 317-329.
- Sawai, Y., 2012. Study on paleotsunami deposits in geologic stratum. *Journal of the Geological Society of Japan*, **118(9)**, 535-558.
- Sawai, Y. & Nagumo, T., 2003. Diatom (Bacillariophyceae) flora of salt marshes along the Pacific coast of eastern Hokkaido, northern Japan. *Bulletin of the Nippon Dental University*, **32**, 93-108.
- Schmidt, S. & De Deckker, P., 2015. Present-day sedimentation rates on the southern and southeastern Australian continental margins. *Australian Journal of Earth Sciences*, **62**, 143-150.
- Schneider, J.-L., Chagué-Goff, C., Bouchez, J.-L., Goff, J., Sugawara, D., Goto, K., Jaffe, B. & Richmond, B., 2014. Using magnetic fabric to reconstruct the dynamics of tsunami deposition on the Sendai Plain, Japan—the 2011 Tohoku-oki tsunami. *Marine Geology*, **358**, 89–106.
- Schnellmann, M., Anselmetti, F.S., Giardini, D. & McKenzie, J.A., 2006. 15,000 Years of mass-movement history in Lake Lucerne: Implications for seismic and tsunami hazards. *Eclogae Geologicae Helveticae*, **99(3)**, 409-428.
- Schnellmann, M., Anselmetti, F.S., Giardini, D., McKenzie, J.A. & Ward, S.N., 2002. Prehistoric earthquake history revealed by lacustrine slump deposits. *Geology*, **30**, 1131-1134.
- Seno, T., Sakurai, T. & Stein, S., 1996. Can the Okhotsk plate be discriminated from the North American plate? *Journal of Geophysical Research - Solid Earth*, **101**, 11305-11315.
- Seno, T., Stein, S. & Gripp, A.E., 1993. A model for the motion of the Philippine Sea plate consistent with NUVEL-1 and geological data. *Journal of Geophysical Research - Solid Earth*, **98**, 17941-17948.
- Seno, T., 2012. Great earthquakes along the Nankai Trough -A new idea for their rupture mode and time series. *Journal of the Seismological Society of Japan*, **64**, 97-116.
- Shanmugam, G., 2012. Process-sedimentological challenges in distinguishing paleo-tsunami deposits. *Natural Hazards*, **63**, 5-30.
- Shennan, I., Barlow, N., Carver, G., Davies, F., Garrett, E. & Hocking, E., 2014a. Great tsunamigenic earthquakes during the past 1000 yr on the Alaska megathrust. *Geology*, **42**, 687–690.
- Shennan, I., Bruhn, R., Barlow, N., Good, K. & Hocking, E., 2014b. Late Holocene great earthquakes in the eastern part of the Aleutian megathrust. *Quaternary Science Reviews*, **84**, 86–97.
- Shi, S., Dawson, A.G. & Smith, D.E., 1995. Coastal sedimentation associated with the December 12th, 1992 tsunami in Flores, Indonesia. In: *Tsunamis: 1992-1994*. Springer, pp. 525-536.
- Shiki, T., Tsuji, Y., Yamazaki, T. & Minoura, K. (Eds.), 2008. *Tsunamiites: Features and implications*. Elsevier, 432 pp.
- Shinozaki, T., Goto, K., Fujino, S., Sugawara, D. & Chiba, T., 2015. Erosion of a paleo-tsunami record by the 2011 Tohoku-oki tsunami along the southern Sendai Plain. *Marine Geology*, **369**, 127-136.
- Shiomi, K., Matsubara, M., Ito, Y. & Obara, K., 2008. Simple relationship between seismic activity along Philippine Sea slab and geometry of oceanic Moho beneath southwest Japan. *Geophysical Journal International*, **173**, 1018–1029.
- Shirai, M., Omura, A., Wakabayashi, T., Uchida, J. & Ogami, T., 2010. Depositional age and triggering event of turbidites in the western Kumano Trough, central Japan during the last ca. 100 years. *Marine Geology*, **271**, 225-235.
- Shishikura, M., 2003. Cycle of Interplate Earthquake Along the Sagami Trough, Deduced from Tectonic Geomorphology. *Bulletin of the Earthquake Research Institute*, **78**, 245-254.

- Shishikura, M., 2013. Earthquake and tsunamis along the Nankai Trough, inferred from geology and geomorphology — examples in Nankai region. *Geological Survey of Japan Chishitsu News*, **2**, 201-204.
- Shishikura, M., Echigo, T. & Kaneda, H., 2007. Marine reservoir correction for the Pacific coast of central Japan using 14 C ages of marine mollusks uplifted during historical earthquakes. *Quaternary Research*, **67**, 286-291.
- Shishikura, M., Echigo, T., Maemoku, H. & Ishiyama, T., 2008. Height and ages of uplifted sessile assemblage distributed along the southern coast of the Kii Peninsula, south-central Japan - Reconstruction of multi-segment earthquake history along the Nankai Trough. *Annual Report on Active Fault and Paleoseismicity Researches*, **8**, 267-280.
- Shishikura, M., Haraguchi, T. & Miyauchi, T., 2001. Timing and recurrence interval of the Taisho-type Kanto Earthquake, analyzing Holocene emerged shoreline topography in the Iwai Lowland, the southwestern part of the Boso Peninsula, central Japan. *Journal of the Seismological Society of Japan*, **53**, 357-372.
- Shishikura, M., Kamataki, T., Takada, K., Suzuki, K. & Okamura, Y., 2005. Survey report of emerged beach ridges in the southwestern part of Boso Peninsula-Timing of the Taisho-type Kanto earthquake. *Annual Report on Active Fault and Paleoseismicity Researches*, **5**, 51-68.
- Shiwakoti, D.R., Tanaka, H. & Tanaka, M., 2002. Influences of diatom microfossils on engineering properties of soils. *Soils and Foundations*, **42(3)**, 1-17.
- Shizuoka Prefecture, 2016. Shizuoka Prefecture Fourth Earthquake Damage Estimate; Related Materials. Available at <http://www.pref.shizuoka.jp/bousai/4higaisoutei/shiryou.html>
- Shuzui, H., 2001. Process of slip-surface development and formation of slip-surface clay in landslides in Tertiary volcanic rocks, Japan. *Engineering Geology*, **61**, 199-219.
- Sieh, K., Natawidjaja, D.H., Meltzner, A.J., Shen, C.-C., Cheng, H., Li, K.-S., Suwargadi, B.W., Galetzka, J., Philibosian, B. & Edwards, R.L., 2008. Earthquake supercycles inferred from sea-level changes recorded in the corals of west Sumatra. *Science*, **322**, 1674-1678.
- Silva-Sánchez, N., Martínez Cortizas, A. & López-Merino, L., 2014. Linking forest cover, soil erosion and mire hydrology to late-Holocene human activity and climate in NW Spain. *The Holocene*, **24(6)**, 714-725.
- Sokolov, V. & Furumura, T., 2008. Comparative analysis of two methods for instrumental intensity estimations using the database accumulated during recent large earthquakes in Japan. *Earthquake Spectra*, **24(2)**, 513-532.
- Sugawara, D., 2014. Extracting magnitude information from tsunami deposits. *Journal of Geography*, **123(6)**, 797-812.
- Sugawara, D. & Goff, J., 2014. Seismic-driving of sand beach ridge formation in northern Honshu, Japan? *Marine Geology*, **358**, 138-149.
- Suzuki, S., 2012. Seismic Seiche occurred at Lake Saiko due to the 2011 off the Pacific coast of Tohoku Earthquake. Paper presented at 15 WCEE, Lisboa.
- Switzer, A.D., Pucillo, K., Haredy, R.A., Jones, B.G. & Bryant, E.A., 2005. Sea level, storm, or tsunami: Enigmatic sand sheet deposits in a sheltered coastal embayment from southeastern New South Wales, Australia. *Journal of Coastal Research*, **21(4)**, 655-663.
- Synal, H.-A., Stocker, M. & Suter, M., 2007. MICADAS: A new compact radiocarbon AMS system. *Nuclear Instruments and Methods in Physics Research Section B: Beam Interactions with Materials and Atoms*, **259(1)**, 7-13.
- Szczuciński, W., Kokociński, M., Rzeszewski, M., Chagué-Goff, C., Cachão, M., Goto, K. & Sugawara, D., 2012. Sediment sources and sedimentation processes of 2011 Tohoku-oki tsunami deposits on the Sendai Plain, Japan - Insights from diatoms, nannoliths and grain size distribution. *Sedimentary Geology*, **282**, 40-56.
- Taguchi, K. & Nakata, K., 1998. Analysis of water quality in Lake Hamana using a coupled physical and biochemical model. *Journal of Marine Systems*, **16**, 107-132.

- Taira, A., 2001. Tectonic evolution of the Japanese island arc system. *Annual Review of Earth and Planetary Sciences*, **29**, 109-134.
- Takada, K., Satake, K., Sangawa, A., Shimokawa, K., Kumagai, H., Goto, K., Haraguchi, T. & Aoshima, A., 2002. Survey of tsunami deposits at an archaeological site along the eastern Nankai trough. *Chikyu Monthly*, **24**, 736-742.
- Takahashi, N., Kodaira, S., Nakanishi, A., Park, J., Miura, S., Tsuru, T., Kaneda, Y., Suyehiro, K., Kinoshita, H. & Hirata, N., 2002. Seismic structure of western end of the Nankai trough seismicogenic zone. *Journal of Geophysical Research - Solid Earth*, **107**, 2212.
- Talling, P.J., 2014. On the triggers, resulting flow types and frequencies of subaqueous sediment density flows in different settings. *Marine Geology*, **352**, 155-182.
- Tamura, T., Sawai, Y. & Ito, K., 2015. OSL dating of the AD 869 Jogan tsunami deposit, northeastern Japan. *Quaternary Geochronology*, **30**, 294-298.
- Tanaka, M., Tanaka, H., Kamei, T. & Hayashi, S., 2003. Effects of diatom microfossil contents on engineering properties of soils. Paper presented at the Thirteenth International Offshore and Polar Engineering Conference, Honolulu, Hawaii.
- Tani, S., Kitagawa, H., Hong, W. & Par, J.H., 2013. Age determination of the Kawagodaira volcanic eruption in Japan by ^{14}C wiggle-matching. *Radiocarbon*, **55**, 748-752.
- Tanioka, Y. & Satake, K., 2001a. Coseismic slip distribution of the 1946 Nankai earthquake and aseismic slips caused by the earthquake. *Earth, Planets and Space*, **53**, 235-241.
- Tanioka, Y. & Satake, K., 2001b. Detailed coseismic slip distribution of the 1944 Tonankai earthquake estimated from tsunami waveforms. *Geophysical Research Letters*, **28**, 1075-1078.
- Tappin, D., 2007. Sedimentary features of tsunami deposits - Their origin, recognition and discrimination: An introduction. *Sedimentary Geology*, **200(3)**, 151-154.
- Thompson, R., Battarbee, R.W., O'Sullivan, P.E. & Oldfield, F., 1975. Magnetic susceptibility of lake sediments. *Limnology and Oceanography*, **20(5)**, 687-698.
- Törnqvist, T.E., De Jong, A.F.M., Oosterbaan, W.A. & Van Der Borg, K., 1992. Accurate dating of organic deposits by AMS ^{14}C measurement of macrofossils. *Radiocarbon*, **34(3)**, 566-577.
- Trofimovs, J., Talling, P.J., Fisher, J.K., Sparks, R.S.J., Watt, S.F.L., Hart, M.B., Smart, C.W., Le Friant, A., Cassidy, M., Moreton, S.G. & Leng, M.J., 2013. Timing, origin, and emplacement dynamics of mass flows offshore SE Montserrat in the last 110 ka: Implications for landslide and tsunami hazards, eruption history, and volcanic island evolution. *Geochemistry Geophysics Geosystems*, **14**, 385-406.
- Tsuji, Y., Okamura, M., Matsuoka, H., Goto, T. & Han, S.S., 2002. Prehistorical and historical tsunami traces in lake floor deposits, Oike Lake, Owase City and Suwaike Lake, Kii-Nagashima City, Mie Prefecture, central Japan. *Chikyu Monthly*, **24**, 743-747.
- Tsuji, Y., Okamura, M., Matsuoka, H. & Murakami, Y., 1998. Study of tsunami traces in lake floor sediment of the Lake Hamanako. *Historical Earthquakes*, **14**, 101-113.
- Tsukamoto, S., Rink, W.J. & Watanuki, T., 2003. OSL of tephric loess and volcanic quartz in Japan and an alternative procedure for estimating De from a fast OSL component. *Radiation Measurements*, **37**, 459-465.
- Uchida, J., Fujiwara, O., Hasegawa, S. & Kamataki, T., 2010. Sources and depositional processes of tsunami deposits: Analysis using foraminiferal tests and hydrodynamic verification. *Island Arc*, **19**, 427-442.
- Usami, T., 1996. Materials for comprehensive list of destructive earthquakes in Japan. *Bulletin of the Earthquake Research Institute, University of Tokyo*, 416995.
- Usami, T., 2003. *Materials for Comprehensive List of Destructive Earthquakes in Japan*. University of Tokyo Press, 605 pp.
- Vaid, Y., Chern, J. & Tumi, H., 1985. Confining pressure, grain angularity, and liquefaction. *Journal of Geotechnical and Geoenvironmental Engineering*, **111(10)**, 1229-1235.
- Van Daele, M., Moernaut, J., Doom, L., Boes, E., Fontijn, K., Heirman, K., Vandoorne, W., Hebbeln, D., Pino, M., Urrutia, R., Brümmer, R. & De Batist, M. 2015. A comparison of the sedimentary

- records of the 1960 and 2010 great Chilean earthquakes in 17 lakes: Implications for quantitative lacustrine palaeoseismology. *Sedimentology*, **62**, 1466-1496.
- Van Geel, B., 1978. A palaeoecological study of Holocene peat bog sections in Germany and the Netherlands, based on the analysis of pollen, spores and macro-and microscopic remains of fungi, algae, cormophytes and animals. *Review of Palaeobotany and Palynology*, **25(1)**, 1-120.
- Van Geel, B., 2001. Non-pollen palynomorphs. In: Smol, J., Birks, H.J.B. & Last, W. (eds.) *Tracking Environmental Change Using Lake Sediments, Volume 3: Terrestrial, Algal, and Siliceous Indicators*. Kluwer, pp. 99-109.
- Van Geel, B., Coope, G.R. & van der Hammen, T., 1989. Palaeoecology and stratigraphy of the lateglacial type section at Usselo (the Netherlands). *Review of Palaeobotany and Palynology*, **60(1-2)**, 25-129.
- Vandekerckhove, E., Van Daele, M., Praet, N., Cnudde, V., Haeussler, P. & De Batist, M., 2020. Flood-triggered versus earthquake-triggered turbidites: A sedimentological study in clastic lake sediments (Eklutna Lake, Alaska). *Sedimentology*, **67(1)**, 364-389.
- Waldmann, N., Anselmetti, F.S., Ariztegui, D., Austin, Jr. J.A., Pirouz, M., Moy, C.M. & Dunbark R., 2011. Holocene mass-wasting events in Lago Fagnano, Tierra del Fuego (54°S): implications for paleoseismicity of the Magallanes-Fagnano transform fault. *Basin Research*, **23**, 171-190.
- Wassmer, P., Schneider, J.-L., Fonfrege, A.-V., Lavigne, F., Paris, R. & Gomez, C., 2010. Use of anisotropy of magnetic susceptibility (AMS) in the study of tsunami deposits: application to the 2004 deposits on the eastern coast of Banda Aceh, North Sumatra, Indonesia. *Marine Geology*, **275**, 255-272.
- Watanabe, H., 1998. *Comprehensive list of tsunamis to hit the Japanese Islands* (Second Edition). University of Tokyo Press, 238 pp.
- Wei, D. & Seno, T., 1998. Determination of the Amurian plate motion. In: Flower, M., Chung, S.-L., Lo, C.-H. & Lee, T.-Y. (eds.) *Mantle dynamics and plate interactions in East Asia*. Geodynamics Series 27, AGU, pp. 337-346.
- Wiemer, G. & Kopf, A., 2015. Altered marine tephra deposits as potential slope failure planes? *Geo-Marine Letters*, **35(4)**, 305-314.
- Wiemer, G. & Kopf, A., 2017. Influence of diatom microfossils on sediment shear strength and slope stability. *Geochemistry, Geophysics, Geosystems*, **18**, 333-345.
- Wilhelm, B., Arnaud, F., Sabatier, P., Magand, O., Chapron, E., Courp, T., Tachikawa, K., Fanget, B., Malet, E., Pignol, C., Bard, E. & Delannoy, J.J., 2013. Palaeoflood activity and climate change over the last 1400 years recorded by lake sediments in the north-west European Alps. *Journal of Quaternary Science*, **28(2)**, 189-199.
- Wilhelm, B., Nomade, J., Crouzet, C., Litty, C., Sabatier, P., Belle, S., Rolland, Y., Revel, M., Courboulex, F., Arnaud, F. & Anselmetti, F.S., 2016. Quantified sensitivity of small lake sediments to record historic earthquakes: Implications for paleoseismology. *Journal of Geophysical Research - Earth Surface*, **121**, 2-16.
- Williams, H.F.L., 2009. Stratigraphy, sedimentology, and microfossil content of Hurricane Rita storm surge deposits in southwest Louisiana. *Journal of Coastal Research*, **25**, 1041-1051.
- Witter, R.C., Zhang, Y., Wang, K., Goldfinger, C., Priest, G.R. & Allan, J.C., 2012. Coseismic slip on the southern Cascadia megathrust implied by tsunami deposits in an Oregon lake and earthquake-triggered marine turbidites. *Journal of Geophysical Research - Solid Earth*, **117**, B10303.
- Yamamoto, T. & Hagiwara, T., 1995. On the earthquake of 16 December Keicho era (1605): a tsunami earthquake off Tokai and Nankai? In: Hagiwara, T. (ed.) *Search for Paleo-Earthquakes: Approach to Offshore Earthquakes*. University of Tokyo Press, pp. 160-260.
- Yamazaki, F., Noda, S. & Meguro, K., 1998. Developments of early earthquake damage assessment systems in Japan. 7th international conference on structural safety and reliability, 1573-1580.
- Yata, T., 2005. The damages by tsunami in Meiou-Toukai earthquake in 1498 and the suffering in Anotsu in the Middle Ages. *Historical Earthquakes*, **20**, 9-12.

- Yokoyama, T., Danhara, T. & Yamashita, T., 1986. A new refractometer for volcanic glass. *The Quaternary Research*, **25(1)**, 21-30.
- Yokoyama, Y., Anderson, J.B., Yamane, M., Simkins, L.M., Miyairi, Y., Yamazaki, T., Koizumi, M., Suga, H., Kusahara, K., Prothro, L., Hasumi, H., Southon, J.R. & Ohkouchi, N., 2016. Widespread collapse of the Ross Ice Shelf during the late-Holocene. *Proceedings of the National Academy of Sciences*, **113(9)**, 2354–2359.
- Yoneda, M., Kitagawa, H., van der Plicht, J., Uchida, M., Tanaka, A., Uehiro, T., Shibata, Y., Morita, M. & Ohno, T., 2000. Pre-bomb marine reservoir ages in the western north Pacific: Preliminary result on Kyoto University collection. *Nuclear Instruments and Methods in Physics Research Section B: Beam Interactions with Materials and Atoms*, **172**, 377-381.
- Yoneda, M., Uno, H., Shibata, Y., Suzuki, R., Kumamoto, Y., Yoshida, K., Sasaki, T., Suzuki, A. & Kawahata, H., 2007. Radiocarbon marine reservoir ages in the western Pacific estimated by pre-bomb molluscan shells. *Nuclear Instruments and Methods in Physics Research Section B: Beam Interactions with Materials and Atoms*, **259**, 432-437.
- Yuk, J.H. & Aoki, S., 2007. Impact of jetty construction on the current and ecological systems in an estuary with a narrow inlet. *Journal of Coastal Research*, **50**, 784-788.

7. DISSEMINATION AND VALORISATION

7.1. Communication to the scientific community - presentations at conferences

- 4th International Tsunami Field Symposium - Science, Technology, and Disaster Mitigation (23.03.2015-27.03.2015, Phuket - Thailand)
- EGU General Assembly 2015 (12.04.2015-17.04.2015, Vienna - Austria)
- Pan Pacific Palaeoseismology symposium (20.04.2015-21.04.2015, Durham - UK)
- XIX INQUA Congress (27.07.2015-02.08.2015, Nagoya - Japan)
- Arthur Holmes Meeting 2015 on "Tsunami Hazards and Risks: Using the Geological Record" (25.09.2015, London - UK)
- Multidisciplinaire themadag "Vulnerable Coastal Areas" (10.12.2015, Brussels - Belgium)
- 2015 AGU Fall Meeting (14.12.2015-18.12.2015, San Francisco - USA)
- 5th International Geologica Belgica Congress (26.01.2016-29.01.2016, Mons - Belgium)
- BELQUA Scientific Workshop 2016 (04.03.2016, Brussels - Belgium)
- EGU General Assembly 2016 (17.04.2016-22.04.2016, Vienna - Austria)
- Japan Geoscience Union Meeting 2016 (22.05.2016-26.05.2016, Chiba - Japan)
- UK Luminescence and ESR meeting 2016 (11.07.2016-13.07.2016, Liverpool - UK)
- German LED 2016 (04.11.2016-06.11.2016, Freiburg - Germany)
- Mount Fuji Research Institute International Symposium (21.01.2017-23.01.2017, Fujiyoshida - Japan)
- BELQUA Scientific Workshop 2017 (09.03.2017, Brussels - Belgium)
- EGU General Assembly 2017 (23.04.2017-28.04.2017, Vienna - Austria)
- 5th International Tsunami Field Symposium (03.09.2017-07.09.2017, Lisbon - Portugal)
- Multidisciplinary workshop on "Disasters and resilience in the 21st century" (11.12.2017, Brussels - Belgium)
- 2017 AGU Fall Meeting (11.12.2017-15.12.2017, New Orleans - USA)
- EGU General Assembly 2018 (08.04.2018-13.04.2018, Vienna - Austria)
- Japan Geoscience Union Meeting 2018 (20.05.2018-24.05.2018, Chiba - Japan)
- 20th International Sedimentological Congress (13.08.2018-17.08.2018, Quebec - Canada)
- 6th International Geologica Belgica Meeting 2018 (13.09.2018-14.09.2018, Leuven - Belgium)
- XX INQUA Congress (25.07.2019-31.07.2019, Dublin - Ireland)

7.2. Communication to the scientific community - organization of sessions/conferences

- Organization of a session at the 2016 EGU General Assembly on "Geological records of extreme wave events", with linked special issue of Marine Geology
- Organization of a session at the 2017 EGU General Assembly on "Geological records of extreme wave events"
- Organization of a session at the 2018 EGU General Assembly on "Geological records of extreme wave events"
- Participation in the organization of the 1st Pan Pacific Palaeoseismology symposium (Durham, UK)

7.3. Outreach and awareness

- Project website = <http://www.quakerecnankai.ugent.be/>
Is used a.o. to share project-related documents (e.g. reports, conference presentations) with the Follow-Up Committee
- Project blog = <http://quakerecnankai.blogspot.be/>
Is regularly updated with reports from the field and laboratory. Approximately 600 page views per month
- Project twitter account = <https://twitter.com/QuakeRecNankai>

- Media coverage:
 - Major Japanese newspapers (including web version): Yomiuri, Asahi, Mainichi, Sankei, Nihon Keizai Shimbun;
 - Local newspapers (including web version): Yamagata, Tohoku, Kanagawa, Yamanashi;
 - Tabloid (including web version): Yūkanfuji, Zaikei
 - Web news: TEAM (Cabinet Office Japan Disaster Management in Japan – <https://bosaijapan.jp/news/>), 47News (joint web site of 52 newspaper companies in Japan and Kyodo News Service), Tsukuba Science News (<http://www.tsukuba-sci.com/?p=5223>), Goo news, Wikipedia (Japanese version), Hazard lab (<https://www.hazardlab.jp/know/topics/detail/2/6/26839.html>)

8. PUBLICATIONS

8.1. Publications in SCI Journals

- Boes, E., Yokoyama, Y., Fujiwara, O., Miyairi, Y., Kempf, P., Schmidt, S., Nakamura, A., Heyvaert, V.M.A., Brückner, H., De Batist, M. & the QuakeRecNankai team, (submitted). An 8,000-year-long record of extreme wave event deposits and coastal evolution from tidal Lake Hamana, south-central Japan. *Quaternary Science Reviews*.
- Brill, D., Reimann, T., Wallinga, J., May, S.M., Engel, M., Riedesel, S. & Brückner, H., 2018. Testing the accuracy of feldspar single grains to date late Holocene cyclone and tsunami deposits. *Quaternary Geochronology*, **48**, 91-103.
- Fujiwara, O., Goto, K., Ando, R. & Garrett, E., 2020. Paleotsunami research along the Nankai Trough and Ryukyu Trench subduction zones - Current achievements and future challenges. *Earth-Science Reviews*, **210**, 103333.
- Garrett, E., Fujiwara, O., Garrett, P., Heyvaert, V.M.A., Shishikura, M., Yokoyama, Y., Hubert-Ferrari, A., Bruckner, H., Nakamura, A., De Batist, M. & the QuakeRecNankai team, 2016. A systematic review of geological evidence for Holocene earthquakes and tsunamis along the Nankai-Suruga Trough, Japan. *Earth-Science Reviews*, **159**, 337-357.
- Garrett, E., Fujiwara, O., Riedesel, S., Walstra, J., Deforce, K., Yokoyama, Y., Schmidt, S., Brückner, H., De Batist, M., Heyvaert, V.M.A. & the QuakeRecNankai team, 2018. Historical Nankai-Suruga megathrust earthquakes recorded by tsunami and terrestrial mass movement deposits on the Shirasuka coastal Lowlands, Shizuoka Prefecture, Japan. *The Holocene*, **28(6)**, 968-983.
- Kempf, P., Garrett, E., Fujiwara, O., Yokoyama, Y., Heyvaert, V.M.A., De Batist, M. & the QuakeRecNankai Team, (in preparation). Holocene sedimentary evolution of the Sagara floodplain and its potential to record extreme wave events, Tokai Region, Japan. *The Holocene*.
- Lamair, L., Hubert-Ferrari, A., El Ouahabi, M., Yamamoto, S., Schmidt, S., Vander Auwera, J., Lepoint, G., Boes, E., Fujiwara, O., Yokoyama, Y., De Batist, M. & Heyvaert, V.M.A., 2019. Late Holocene changes on erosion pattern on a lacustrine environment: landscape stabilization by volcanic activity versus human activity. *Geochemistry, Geophysics, Geosystems*, **20(4)**, 1720-1733.
- Lamair, L., Hubert-Ferrari, A., Schmidt, S., Yamamoto, S., Fujiwara, O., Yokoyama, Y., De Batist, M., Heyvaert, V.M.A. & the QuakeRecNankai Team, (in preparation). Signature of extreme flood events and earthquakes in Lake Sai, Fuji Five Lakes, Central Japan. *Natural Hazards and Earth System Sciences*.
- Lamair, L., Hubert-Ferrari, A., Yamamoto, S., El Ouahabi, M., Vander Auwera, J., Obrochta, S., Boes, E., Nakamura, A., Fujiwara, O., Shishikura, M., Schmidt, S., Siani, G., Miyairi, Y., Yokoyama, Y., De Batist, M., Heyvaert, V.M.A. & the QuakeRecNankai Team, 2018. Volcanic influence of Mt. Fuji on the watershed of Lake Motosu and its impact on the lacustrine sedimentary record. *Sedimentary Geology*, **363**, 200-220.
- Lamair, L., Hubert-Ferrari, A., Yamamoto, S., Fujiwara, O., Yokoyama, Y., Garrett, E., De Batist, M., Heyvaert, V.M.A. & the QuakeRecNankai Team, 2019. Use of high-resolution seismic reflection data for paleogeographical reconstruction of shallow Lake Yamanaka (Fuji Five Lakes, Japan). *Palaeogeography, Palaeoclimatology, Palaeoecology*, **514**, 233-250.
- Lougheed, B.C. & Obrochta, S.P., 2019. A Rapid, deterministic age-depth modeling routine for

geological sequences with inherent depth uncertainty. *Paleoceanography and Paleoclimatology*, **34(1)**, 122-133.

Obrochta, S.P., Yokoyama, Y., Yoshimoto, M., Yamamoto, S., Miyairi, Y., Nagano, G., Nakamura, A., Tsunematsu, K., Lamair, L., Hubert-Ferrari, A., Loughheed, B.C, Hokanishi, A., Yasuda, A., Heyvaert, V.M.A., De Batist, M., Fujiwara, O. & the QuakeRecNankai Team, 2018. Mt. Fuji Holocene eruption history reconstructed from proximal lake sediments and high-density radiocarbon dating. *Quaternary Science Reviews*, **200**, 395-405.

Riedesel, S., Bell, A.M.T., Duller, G.A.T., Finch, A.A., Jain, M., King, G.E., Pearce, N.J. & Roberts, H.M., (submitted). Exploring sources of variation in thermoluminescence emissions and anomalous fading in alkali feldspars. *Radiation Measurements*.

Riedesel, S., Brill, D., Roberts, H.M., Duller, G.A.T., Garrett, E., Zander, A.M., King, G.E., Tamura, T., Burow, C., Cunningham, A., Seeliger, M., De Batist, M., Heyvaert, V.M.A., Fujiwara, O., Brückner, H. & the QuakeRecNankai team, 2018. Single-grain feldspar luminescence chronology of historical extreme wave event deposits recorded in a coastal lowland, Pacific coast of central Japan. *Quaternary Geochronology*, **45**, 37-49.

Riedesel, S., King, G. E., Prasad, A. K., Kumar, R., Finch, A. A. & Jain, M., 2018. Optical determination of the width of the band-tail states, and the excited and ground state energies of the principal dosimetric trap in feldspar. *Radiation Measurements*, **125**, 40-51.

Yamamoto, S., Hubert-Ferrari, A., Lamair, L., Miyata, Y., Ochiai, S., Nagao, S., Miyauchi, N., Yoshida, K., Fujiwara, O., Yokoyama, Y., Heyvaert, V.M.A., De Batist, M. & the QuakeRecNankai Team, 2020. Organic carbon accumulation and productivity over the past 130 years in Lake Kawaguchi (central Japan) reconstructed using organic geochemical proxies. *Journal of Palaeolimnology*, **64(4)**, 365-377.

8.2. Publications as Abstracts or Proceedings

Boes, E., Fujiwara, O., Garrett, E., Lamair, L., De Batist, M., Heyvaert, V., Yokoyama, Y., Miyairi, Y., Irizuki, T., Riedesel, S., Brückner, H., Hubert-Ferrari, A. & the QuakeRecNankai Team, 2015. Exploring the potential of Lake Hamana (Shizuoka Prefecture, Japan) to hold a long and reliable sedimentary record of paleo-earthquakes and -tsunami along the Nankai-Suruga Trough. Abstract of the XIX INQUA Congress (27.07.2015-02.08.2015, Nagoya - Japan).

Boes, E., Fujiwara, O., Garrett, E., Lamair, L., De Batist, M., Heyvaert, V.M.A., Yokoyama, Y., Miyairi, Y., Irizuki, T., Riedesel, S., Brückner, H., Hubert-Ferrari, A. & the QuakeRecNankai team, 2015. Exploring the potential of Lake Hamana (Japan) to hold a long and reliable sedimentary record of paleotsunamis along the Nankai-Suruga Trough. Abstract of the Arthur Holmes Meeting 2015 on "Tsunami Hazards and Risks: Using the Geological Record" (25.09.2015, London - UK).

Boes, E., Fujiwara, O., Garrett, E., Lamair, L., De Batist, M., Heyvaert, V.M.A., Yokoyama, Y., Miyairi, Y., Irizuki, T., Riedesel, S., Brückner, H., Hubert-Ferrari, A. & the QuakeRecNankai team, 2016. Exploring the potential of Lake Hamana to hold a long and reliable sedimentary record of paleotsunamis along the Nankai-Suruga Trough. Abstract of the 5th International Geologica Belgica Congress (26.01.2016-29.01.2016, Mons - Belgium).

Boes, E., Fujiwara, O., Nakamura, A., De Batist, M., Garrett, E., Heyvaert, V.M.A., Yokoyama, Y., Miyairi, Y. & the QuakeRecNankai team, 2016. Extreme wave deposits in coastal Lake Hamana, Shizuoka Prefecture, Japan: a first step towards the extraction of a continuous tsunami inundation history. Abstract of the BELQUA Scientific Workshop 2016 (04.03.2016, Brussels - Belgium).

- Boes, E., Kempf, P., De Batist, M., Van Daele, M., Vandoorne, W., Fujiwara, O., Garrett, E., Heyvaert, V., Yokoyama, Y., Miyairi, Y., Irizuki, T., Moernaut, J., Pino, M., Urrutia, R. & the QuakeRecNankai Team, 2015. On how to extract the paleotsunami history from a coastal lake record. Abstract of the 4th International Tsunami Field Symposium - Science, Technology, and Disaster Mitigation (23.03.2015-27.03.2015, Phuket - Thailand).
- Boes, E., Yokoyama, Y., Schmidt, S., Riedesel, S., Fujiwara, O., Nakamura, A., Garrett, E., Heyvaert, V.M.A., De Batist, M. & the QuakeRecNankai team, 2017. A long record of extreme wave events in coastal Lake Hamana, Japan. Abstract of the EGU General Assembly 2017 (23.04.2017-28.04.2017, Vienna - Austria).
- Boes, E., Yokoyama, Y., Schmidt, S., Riedesel, S., Fujiwara, O., Nakamura, A., Heyvaert, V.M.A., Brückner, H. & De Batist, M., 2017. A long record of extreme wave events in coastal Lake Hamana, Japan. Abstract of the 5th International Tsunami Field Symposium (03.09.2017-07.09.2017, Lisbon - Portugal).
- Boes, E., Yokoyama, Y., Schmidt, S., Riedesel, S., Kempf, P., Fujiwara, O., Nakamura, A., Heyvaert, V.M.A., Brückner, H., De Batist, M. & the QuakeRecNankai Team, 2018. A 7-8 ka long record of extreme wave events in coastal Lake Hamana, Japan. Abstract of the Japan Geoscience Union Meeting 2018 (20.05.2018-24.05.2018, Chiba - Japan).
- Boes, E., Yokoyama, Y., Schmidt, S., Riedesel, S., Kempf, P., Miyairi, Y., Fujiwara, O., Nakamura, A., Heyvaert, V.M.A., Brückner, H., De Batist, M. & the QuakeRecNankai Team, 2018. A 7-8 kyr long record of extreme wave events in coastal Lake Hamana, Japan. Abstract of the 20th International Sedimentological Congress (13.08.2018-17.08.2018, Quebec - Canada).
- De Batist, M., Heyvaert, V., Hubert-Ferrari, A., Fujiwara, O., Shishikura, M., Yokoyama, Y., Brueckner, H., Garrett, E., Boes, E., Lamair, L., Nakamura, A., Miyairi, Y., Yamamoto, S. & the QuakeRecNankai Project Team, 2015. New Geological Evidence of Past Earthquakes and Tsunami Along the Nankai Trough, Japan. Abstract of the 2015 AGU Fall Meeting (14.12.2015-18.12.2015, San Francisco - USA)
- De Batist, M., Heyvaert, V., Hubert-Ferrari, A., Fujiwara, O., Shishikura, M., Yokoyama, Y., Brückner, H., Garrett, E., Boes, E., Lamair, L., Nakamura, A., Miyairi, Y., Yamamoto, S. & the QuakeRecNankai Project Team, 2016. New Geological Evidence of Past Earthquakes and Tsunami Along the Nankai Trough, Japan. Abstract of the 5th International Geologica Belgica Congress (26.01.2016-29.01.2016, Mons - Belgium).
- Garrett, E., De Batist, M., Boes, E., Brückner, H., Fujiwara, O., Garrett, P., Heyvaert, V., Hubert-Ferrari, A., Lamair, L., Riedesel, S., Walstra, J., Yokoyama, Y. & the QuakeRecNankai team, 2015. The QuakeRecNankai project: palaeoseismic data for improved seismic hazard assessment along the Nankai Trough, Japan. Abstract of the Pan Pacific Palaeoseismology symposium (20.04.2015-21.04.2015, Durham - UK)
- Garrett, E., De Batist, M., Heyvaert, V., Hubert-Ferrari, A., Fujiwara, O., Yokoyama, Y., Bruckner, H., Miyairi, Y., Garrett, P. & the QuakeRecNankai Team, 2015. Geological evidence for historical and older earthquakes and tsunamis along the Nankai Trough, Japan. Abstract of the EGU General Assembly 2015 (12.04.2015-17.04.2015, Vienna - Austria)
- Garrett, E., Fujiwara, O., Garrett, P., Heyvaert, V.M.A., Shishikura, M., Yokoyama, Y., Hubert-Ferrari, A., Brückner, H., Nakamura, A., De Batist, M. & the QuakeRecNankai Team, 2016. Geological evidence for Holocene earthquakes and tsunamis along the Nankai-Suruga Trough, Japan. Abstract of the EGU General Assembly 2016 (17.04.2016-22.04.2016, Vienna - Austria).

- Garrett, E., Fujiwara, O., Heyvaert, V., De Batist, M., Yokoyama, Y., Brückner, H., Garrett, P., Boes, E., Miyairi, Y. & the QuakeRecNankai Team, 2015. Progress in paleoearthquake and paleotsunami research along the Nankai Trough following the 2011 Tōhoku earthquake. Abstract of the XIX INQUA Congress (27.07.2015-02.08.2015, Nagoya - Japan).
- Garrett, E., Fujiwara, O., Riedesel, S., Walstra, J., Deforce, K., Yokoyama, Y., Schmidt, S., Brückner, H., De Batist, M., Heyvaert, V.M.A. & the QuakeRecNankai team, 2018. Historical Nankai-Suruga megathrust earthquakes recorded by tsunami and landslide deposits on the Shirasuka coastal lowlands, Shizuoka Prefecture. Abstract of the Japan Geoscience Union Meeting 2018 (20.05.2018-24.05.2018, Chiba - Japan).
- Garrett, E., Garrett, P., Fujiwara, O., Heyvaert, V., Shishikura, M., De Batist, M. & Yokoyama, Y., 2015. Current status of palaeoseismic research along the Nankai Trough, Japan. Abstract of the Arthur Holmes Meeting 2015 on "Tsunami Hazards and Risks: Using the Geological Record" (25.09.2015, London - UK).
- Garrett, E., Heyvaert, V.M.A., Brückner, H., Fujiwara, O., Hubert-Ferrari, A., Shishikura, M., Yokoyama, Y., De Batist, M. & the QuakeRecNankai team, 2015. Using coastal geology to improve hazard assessments along tectonically active coasts: Current progress along the Nankai Trough, Japan. Abstract of the Multidisciplinaire themadag "Vulnerable Coastal Areas" (10.12.2015, Brussels - Belgium).
- Garrett, E., Heyvaert, V.M.A., De Batist, M., Boes, E., Brückner, H., Fujiwara, O., Hubert-Ferrari, A., Lamair, L., Riedesel, S., Walstra, J. & Yokoyama, Y., 2015. The QuakeRecNankai project: reconstructing past earthquakes and tsunamis along the Nankai Trough, south central Japan. Abstract of the 4th International Tsunami Field Symposium - Science, Technology, and Disaster Mitigation (23.03.2015-27.03.2015, Phuket - Thailand).
- Garrett, E., Heyvaert, V.M.A., Fujiwara, O., Brückner, H., Yokoyama, Y., Riedesel, S., Miyairi, Y., Shishikura, M. & De Batist, M., 2016. Sedimentary imprints of tsunami and storm deposits on the Shizuoka coastline, south central Japan. Abstract of the EGU General Assembly 2016 (17.04.2016-22.04.2016, Vienna - Austria).
- Garrett, E., Heyvaert, V., Fujiwara, O., De Batist, M., Brückner, H., Yokoyama, Y., Walstra, J., Riedesel, S., Brill, D., Miyairi, Y., Obrochta, S. & the QuakeRecNankai Team, 2015. Radiometric and luminescence dating of historical tsunamis and storm deposits from Shirasuka, south central Japan. Abstract of the XIX INQUA Congress (27.07.2015-02.08.2015, Nagoya - Japan).
- Garrett, E., Heyvaert, V.M.A., Fujiwara, O., De Batist, M., Garrett, P., Shishikura, M., Hubert-Ferrari, A., Brückner, H., Nakamura, A., Yokoyama, Y. & the QuakeRecNankai team, 2016. Nankai Trough (Japan) palaeoseismology: progress since the 2011 Tōhoku earthquake. Abstract of the 5th International Geologica Belgica Congress (26.01.2016-29.01.2016, Mons - Belgium).
- Garrett, E., Riedesel, S., Fujiwara, O., Walstra, J., Deforce, K., Yokoyama, Y., Schmidt, S., Brill, D., Roberts, H.M., Duller, G.A T., Brückner, H., De Batist, M., Heyvaert, V.M.A. & the QuakeRecNankai team, 2017. Historical extreme wave and landslide deposits on the Shirasuka coastal lowlands, Shizuoka Prefecture, Japan. Abstract of the EGU General Assembly 2017 (23.04.2017-28.04.2017, Vienna - Austria).
- Garrett, E., Riedesel, S., Fujiwara, O., Walstra, J., Deforce, K., Yokoyama, Y., Schmidt, S., Brill, D., Roberts, H., Duller, G., Brückner, H., De Batist, M., Heyvaert, V.M.A & The QuakeRecNankai Team, 2017. Historical extreme wave and landslide deposits on the Shirasuka coastal

lowlands, Shizuoka Prefecture, Japan. Abstract of the 5th International Tsunami Field Symposium (03.09.2017-07.09.2017, Lisbon - Portugal).

Heyvaert, V.M.A., De Batist, M., Brueckner, H., Hubert-Ferrari, A., Fujiwara, O., Shishikura, M., Yokoyama, Y., Boes, E., Garrett, E., Lamair, L., Miyairi, Y., Nakamura, A., Yamamoto, S. & the QuakeRecNankai Project Team, 2015. The QuakeRecNankai project: Towards New Geological Evidence of Past Earthquakes and Tsunami Along the Nankai Trough, Japan. Abstract of the Arthur Holmes Meeting 2015 on "Tsunami Hazards and Risks: Using the Geological Record" (25.09.2015, London - UK).

Hubert-Ferrari, A., Lamair, L., Yamamoto, S., Fujiwara, O., Yokoyama, Y., Obrochta, S., Miyairi, Y., Nakamura, A., De Batist, M., Heyvaert, V.M.A. & the QuakeRecNankai Team, 2018. Natural hazards recorded in the Fuji Five Lakes: earthquake shaking, typhoon induced flooding and volcanic eruptions. Abstract of the Japan Geoscience Union Meeting 2018 (20.05.2018-24.05.2018, Chiba - Japan).

Kempf, P., Fujiwara, O., Miyairi, Y., Yokoyama, Y., Nakamura, A., Garrett, E., De Batist, M., Heyvaert, V.M.A. & the QuakeRecNankai team, 2018. Geological evidence for extreme wave events on the Sagara coastal lowland facing the Tōkai segment of the Nankai-Suruga Trough. Abstract of the Japan Geoscience Union Meeting 2018 (20.05.2018-24.05.2018, Chiba - Japan).

Kempf, P., Garrett, E., Fujiwara, O., Shishikura, M., Nakamura, A., Heyvaert, V.M.A. & the QuakeRecNankai Team, 2017. Geological evidence for extreme wave events on a coastal lowland facing the Tokai segment of the Nankai-Suruga Trough. Abstract of the 5th International Tsunami Field Symposium (03.09.2017-07.09.2017, Lisbon - Portugal).

Kempf, P., Garrett, E., Fujiwara, O., Yokoyama, Y., Heyvaert, V.M.A., De Batist, M. & the QuakeRecNankai team, 2018. Sedimentary evolution of the Sagara coastal area in Japan and its potential to preserve extreme wave deposits. Abstract of the EGU General Assembly 2018 (08.04.2018-13.04.2018, Vienna - Austria).

Kempf, P., Garrett, E., Fujiwara, O., Yokoyama, Y., Heyvaert, V.M.A., De Batist, M. & the QuakeRecNankai Team, 2018. Sedimentary evolution of the Sagara coastal area in Japan and its potential to preserve extreme wave deposits. Abstract of the 6th International Geologica Belgica Meeting 2018 (13.09.2018-14.09.2018, Leuven - Belgium).

Lamair, L., Hubert-Ferrari, A., Boes, E., Schmidt, S., Yamamoto, S., Fujiwara, O., Garrett, E., Heyvaert, V., Miyairi, Y., Yokoyama, Y., De Batist, M., Brückner, H. & the QuakeRecNankai Team, 2015. The last 300 years of sedimentation in the Fuji lakes: the impact of natural disasters with a special focus on earthquakes. Abstract of the XIX INQUA Congress (27.07.2015-02.08.2015, Nagoya - Japan).

Lamair, L., Hubert-Ferrari, A., Boes, E., Yamamoto, S., Garrett, E., Heyvaert, V.M.A., Fujiwara, O., Yokoyama, Y., De Batist, M. & the QuakeRecNankai Team, 2015. Investigation of the Five Fuji Lakes, Japan, and their potential for recording paleoearthquakes. Abstract of the BELQUA Scientific Workshop 2015 (03.03.2015, Brussels - Belgium).

Lamair, L., Hubert-Ferrari, A., Boes, E., Yamamoto, S., Garrett, E., Heyvaert, V., Fujiwara, O., Yokoyama, Y., De Batist, M. & the QuakeRecNankai Team, 2015. Late Holocene History of the Fuji lakes (Japan). Abstract of the XIX INQUA Congress (27.07.2015-02.08.2015, Nagoya - Japan).

Lamair, L., Hubert-Ferrari, A., Boes, E., Yamamoto, S., Garrett, E., Heyvaert, V.M.A., Nakamura,

- A., Miyairi, Y., Yokoyama, Y., De Batist, M. & the QuakeRecNankai Project Team, 2016. A history of mass transport complexes related to earthquake shaking: the case of Lake Motosu (Japan). Abstract of the 5th International Geologica Belgica Congress (26.01.2016-29.01.2016, Mons - Belgium).
- Lamair, L., Hubert-Ferrari, A., El Ouahabi, M., Boes, E., Garrett, E., Heyvaert, V.M.A., Yamamoto, S., Nakamura, A., Miyairi, Y., Yokoyama, Y., De Batist, M. & the QuakeRecNankai Team, 2016. A history of mass transport complexes related to eruptions and earthquake shaking: the case of Lake Motosu (Japan). Abstract of the BELQUA Scientific Workshop 2016 (04.03.2016, Brussels - Belgium).
- Lamair, L., Hubert-Ferrari, A., El Ouahabi, M., Yamamoto, S., Develle, A.L., Schmidt, S., Lepoint, G., Boes, E., Fujiwara, O., Yokoyama, Y., De Batist, M. Heyvaert, V.M.A. & the QuakeRecNankai Team, 2017. The role of natural hazards and human activities on change of sedimentation patterns: The case of Lake Yamanaka (Fuji Five Lakes, Japan). Abstract of the BELQUA Scientific Workshop 2017 (09.03.2017, Brussels - Belgium).
- Lamair, L., Hubert-Ferrari, A., Yamamoto, S., El Ouahabi, M., Garrett, E., Shishikura, M., Schmidt, S., Boes, E., Obrochta, S., Nakamura, A., Miyairi, Y., Yokoyama, Y., De Batist, M., Heyvaert, V.M.A. & the QuakeRecNankai Team, 2017. Sedimentation influx and volcanic interactions in the Fuji Five Lakes: implications for paleoseismological records. Abstract of the EGU General Assembly 2017 (23.04.2017-28.04.2017, Vienna - Austria).
- Lamair, L., Hubert-Ferrari, A., Yamamoto, S., Shishikura, M., Fujiwara, O., Boes, E., Obrochta, S., Nakamura, A., Miyairi, Y., Yokoyama, Y., De Batist, M., Heyvaert, V.M.A. & the QuakeRecNankai Team, 2017. The natural paleohazard history of Fuji Five Lakes (Mt. Fuji, Japan) over the last ca. 6000 years. Abstract of the Multidisciplinary workshop on "Disasters and resilience in the 21st century" (11.12.2017, Brussels - Belgium).
- Lamair, L., Hubert-Ferrari, A., Yamamoto, S., Yokoyama, Y., Miyairi, Y., Garrett, E., Fujiwara, O., Obrochta, S., Nakamura, A., De Batist, M., Heyvaert, V. & the QuakeRecNankai Team, 2018. A 6000-year sedimentary record of earthquakes from the Fuji Five Lakes, Japan. Abstract of the EGU General Assembly 2018 (08.04.2018-13.04.2018, Vienna - Austria).
- Lamair, L., Hubert-Ferrari, A., Yamamoto, S., Yokoyama, Y., Miyairi, Y., Garrett, E., Fujiwara, O., Obrochta, S., Nakamura, A., De Batist, M., Heyvaert, V.M.A. & the QuakeRecNankai Team, 2018. Paleoearthquakes recorded in the Fuji Five Lakes during the last ca. 6000 years (Fuji Five Lakes, Japan). Abstract of the Japan Geoscience Union Meeting 2018 (20.05.2018-24.05.2018, Chiba - Japan).
- McDonald, S., Tyler, J., Obrochta, S.P., Yokoyama, Y., Miyairi, Y. & Ota, K., 2019. An 8,000-year climate record from Lake Motosu, Japan: Implications for the East Asian Monsoon. Abstract of the Japan Geoscience Union Meeting 2019 (26.05.2019-30.05.2019, Chiba - Japan).
- Nagano, G., Yokoyama, Y., Obrochta, S.P., Miyairi, Y., Yoshimoto, M. & Yamamoto, Y., 2017. High-precision multipoint radiocarbon dating and reconstruction of the eruption history of the Mt. Fuji during the last 8,000 years using sediment cores obtained from the Fuji Five Lakes. Abstract of the Japan Geoscience Union Meeting 2017 (20.05.2017-25.05.2017, Chiba - Japan).
- Nakamura, A., Boes, E., Brückner, H., De Batist, M., Fujiwara, O., Garrett, E., Heyvaert, V., Hubert-Ferrari, A., Lamair, L., Miyairi, Y., Obrochta, S., Shishikura, M., Yamamoto, S., Yokoyama, Y. & the QuakeRecNankai team, 2016. Geological evidence for tsunamis and earthquakes from Lake Hamana and Fuji Five Lakes. Abstract of the Japan Geoscience Union Meeting 2016

(22.05.2016-26.05.2016, Chiba - Japan).

Obrochta, S.P. & Lougheed, B.C., 2018. A rapid, deterministic age-depth modelling routine for geological sequences with inherent depth uncertainty. Abstract of the 2018 AGU Fall Meeting (10.12.2018-14.12.2018, Washington DC - USA).

Obrochta, S.P. & Lougheed, B.C., 2019. A rapid, deterministic age-depth modelling routine for geological sequences with inherent depth uncertainty. Abstract of the XX INQUA Congress (25.07.2019-31.07.2019, Dublin - Ireland).

Obrochta, S.P. & Lougheed, B.C., 2019. A rapid, deterministic age-depth modelling routine for geological sequences with inherent depth uncertainty. Abstract of the ICP13 (02.09.2019-06.09.2019, Sydney - Australia).

Obrochta, S.P., Lougheed, B.C., Muscheler, R., Yokoyama, Y. & Miyairi, Y., 2018. An age-depth modeling method for improved treatment of uncertainty. Abstract of the Japan Geoscience Union Meeting 2018 (20.05.2018-24.05.2018, Chiba - Japan).

Obrochta, S., Yokoyama, Y., Yoshimoto, M., Yamamoto, S., Miyairi, Y., Nagano, G., Nakamura, A., Tsunematsu, K., Lamair, L., Hubert-Ferrari, A., Heyvaert, V., De Batist, M., Fujiwara, O. & The QuakeRecNankai Team, 2017. Mt. Fuji Holocene eruption history reconstructed from proximal lake sediments and high-density radiocarbon dating. Abstract of the 2017 AGU Fall Meeting (11.12.2017-15.12.2017, New Orleans - USA).

Riedesel, S., Brill, D., Brückner, H., De Batist, M., Fujiwara, O., Garrett, E., Heyvaert, V.M.A., Miyairi, Y., Opitz, S., Seeliger, M., Shishikura, M., Yokoyama, Y., Zander, A. & the QuakeRecNankai Team, 2016. Constraining timing and origin of extreme wave events, Shirazuka Lowlands, Japan. Abstract of the EGU General Assembly 2016 (17.04.2016-22.04.2016, Vienna - Austria).

Riedesel, S., Brill, D., Burow, C., Duller, G., Fujiwara, O., Garrett, E., King, G., Roberts, H., Tamura, T., Zander, A., Brückner, H. & The QuakeRecNankai Team, 2016. Feldspar dating of historical extreme wave event deposits recorded at Shirazuka lowlands, Pacific coast of Japan. Abstract of the UK Luminescence and ESR meeting 2016 (11.07.2016-13.07.2016, Liverpool - UK).

Riedesel, S., Brill, D., Duller, G.A.T., Fujiwara, O., Garrett, E., King, G.E., Roberts, H.M., Tamura, T., Zander, A.M., Brückner, H. & the QuakeRecNankai Team, 2017. Luminescence characteristics and IRSL-chronology of extreme-wave event deposits recorded at the Shirazuka lowlands, Japan. Abstract of the Japan Geoscience Union Meeting 2017 (20.05.2017-25.05.2017, Chiba - Japan).

Riedesel, S., Brill, D., Roberts, H.M., Duller, G.A.T., Zander, A., King, G.E., Boes, E., Garrett, E., De Batist, M., Brückner, H. & The QuakeRecNankai Team, 2016. The potential of using feldspars to date on- and offshore recorded extreme wave event deposits. Abstract of the German LED 2016 (04.11.2016-06.11.2016, Freiburg - Germany).

8.3. Theses

Boes, E., in preparation. *Exploring the potential of coastal lakes and lagoons as palaeotsunami records*. PhD thesis, Ghent University - Belgium.

Lamair, L., 2018. *Holocene history of natural hazards in central Japan (Fuji Five Lake): imprints of earthquakes, typhoons and volcanic events in lacustrine sediments*. PhD thesis, University of Liège - Belgium.

- McDonald, S.A., 2018. *Maritime controls on coastal East Asian climate during the Holocene: evidence from the sediments of Lake Motosu, Japan*. MSc thesis, University of Adelaide - Australia.
- Nagano, G., 2017. *Paleoenvironmental reconstruction during the last 8,000 years using sediment cores obtained from the Fuji Five Lakes*. MSc thesis, University of Tokyo – Japan.
- Potums, L., 2017. *InSAR insights: Land surface deformation around coastal lakes along the Nankai Trough subduction zone, Japan*. MSc thesis, Ghent University - Belgium.
- Riedesel, S., 2017. *Characterisation and optical dating of extreme event deposits recorded at the Shirasuka lowlands, Japan*. MSc thesis, University of Cologne - Germany.

9. ACKNOWLEDGEMENTS

In terms of funding:

- This project was funded by the Belgian Science Policy Office, as part of the BRAIN-be program (Belgian Research Action through Interdisciplinary Networks 2012-2017).
- Additional financial support for specific associated activities was provided by the University of Tokyo, the Deutschlandstipendium program of BMBF (German Federal Ministry of Education and Research), the PROMOS student mobility scholarship program of DAAD (German Academic Exchange Service), the Camille Hela foundation, the Marie-Louise Léonard price and Swiss National Science Foundation grant PZ00P2_167960.

In terms of fieldwork:

- We thank local authorities and land-owners in the study areas for allowing us to conduct fieldwork and for providing access to their land and paddy fields.
- We also thank the University of Tokyo Fisheries Laboratory, the Suzuki marina in Washizu and the Mount Fuji Research Institute for invaluable logistical support during fieldwork, Akita University, UTokyo and AIST for invaluable assistance in the organization and planning of the fieldwork.
- And we are indebted to H. Brückner, K. De Rycker, E. Garrett, T. Ishiwa, L. Lamair, D. Matsumoto, T. Mestdagh, Y. Miyairi, G. Nagano, A. Nakamura, Y. Namegaya, S. Obrochta, E. Ono, S. Riedesel, Y. Sato, Y. Sawai, M. Seeliger, K. Shimokawa, M. Shishikura, K. Tanigawa, R. Tsunekawa, K. Tsunematsu, T. Uchiyama, E. Vandekerkhove, J. Walstra, S. Yamamoto, M. Yoshimoto for their help with the fieldwork, during one or more of the field expeditions in 2014, 2015 and 2016.

Last, but not least, in terms of research facilities, we are grateful to:

- R. Achten (UGent) for access to the CT scanner of UZ Ghent;
- I. Bailiff (UDurham) for help with OSL data processing;
- A. Beckers (ULiège) for extra help;
- E. Bertemes (ULiège) for lab work;
- H. Cieszynski (UCologne) for the REM images;
- A.-L. Develle (University Savoie-Mont-Blanc) for access to the Avaatech scanner;
- T. Govaerts (GSB) for preparing samples and XRD analysis;
- F. Hatert (ULiège) for tephrostratigraphic analysis;
- D. Hodgson and S. Roberts (BAS) for use of their UWITEC coring platform;
- M. Van Daele (UGent) for providing CT scanning expertise;
- J. Jurceka, R. Dasseville and A.-E. Debeer (UGent) for preparing microscopic slides;
- U. Röhl and V. Lukies (MARUM) for access to the XRF Core Scanning Lab;
- Y. Sato, Y. Sawai and T. Naya (AIST) for helpful discussions on diatom taxonomy and geomorphic development of Lake Hamana region;
- S. Schmidt (UBordeaux) for Pb/Cs dating;
- H. Wynne (UAberystwyth) for her help in the OSL lab.

ANNEX I: LAKE HAMANA GRAVITY AND PISTON CORES

Lake Hamana: gravity cores								
Core name	Short name	Date	Latitude (N)	Longitude (E)	Water depth (m)	Length (cm)	Remarks	Archived at
HAM14-02A-1G-1	HAM2A/2A	29/10/2014	34°46'43.45"	137°33'23.84"	6,67	100,5		AIST
HAM14-02B-1G-1	HAM2B/2B	29/10/2014	34°46'43.84"	137°33'23.61"	6,67	106,5		UGent
HAM14-03A-1G-1	HAM3A/3A	27/10/2014	34°45'40.29"	137°32'16.23"	11,63	48,0		AIST
HAM14-03B-1G-1	HAM3B/3B	27/10/2014	34°45'40.29"	137°32'16.23"	11,63	59,0		UGent
HAM14-04A-1G-1	HAM4A/4A	27/10/2014	34°45'12.34"	137°32'59.77"	9,64	93,0		UGent
HAM14-04B-1G-1	HAM4B/4B	27/10/2014	34°45'12.73"	137°33'00.23"	9,72	85,0		AIST
HAM14-05A-1G-1	HAM5A/5A	27/10/2014	34°44'37.30"	137°34'06.14"	8,99	55,0		UGent
HAM14-05B-1G-1	HAM5B/5B	27/10/2014	34°44'37.49"	137°34'06.14"	8,99	48,5	No cc	AIST
HAM14-07A-1G-1	HAM7A/7A	27/10/2014	34°45'21.58"	137°34'46.33"	10,59	92,0		UGent
HAM14-07B-1G-1	HAM7B/7B	27/10/2014	34°45'21.58"	137°34'46.09"	10,59	84,5		AIST
HAM14-08A-1G-1	HAM8A/8A	27/10/2014	34°45'59.86"	137°35'33.26"	11,96	82,0		UGent
HAM14-08B-1G-1	HAM8B/8B	27/10/2014	34°45'59.67"	137°35'33.03"	11,96	80,0		AIST
HAM14-09A-1G-1	HAM9A/9A	29/10/2014	34°46'46.28"	137°35'09.46"	10,15	89,5		UGent
HAM14-09B-1G-1	HAM9B/9B	29/10/2014	34°46'46.67"	137°35'09.46"	10,15	110,5		UGent
HAM14-09C-1G-1	HAM9C/9C	29/10/2014	34°46'46.28"	137°35'09.46"	10,15	100,5		AIST
HAM14-10A-1G-1	HAM10A/10A	27/10/2014	34°46'50.27"	137°37'03.97"	9,57	67,0		UGent
HAM14-10B-1G-1	HAM10B/10B	27/10/2014	34°46'50.07"	137°37'03.97"	9,57	108,0		AIST
HAM14-10C-1G-1	HAM10C/10C	27/10/2014	34°46'50.27"	137°37'03.97"	9,57	108,5		UGent
HAM14-11A-1G-1	HAM11A/11A	27/10/2014	34°47'22.54"	137°37'53.70"	5,80	94,5		AIST
HAM14-11B-1G-1	HAM11B/11B	27/10/2014	34°47'21.77"	137°37'53.70"	5,73	112,0		UGent
HAM14-11C-1G-1	HAM11C/11C	27/10/2014	34°47'22.15"	137°37'53.00"	5,80	83,5		UGent
HAM14-12A-1G-1	HAM12A/12A	29/10/2014	34°47'08.30"	137°37'12.73"	7,61	104,5		AIST
HAM14-12B-1G-1	HAM12B/12B	29/10/2014	34°47'08.30"	137°37'12.73"	7,61	49,5		UGent
HAM14-12C-1G-1	HAM12C/12C	29/10/2014	34°47'08.30"	137°37'12.73"	7,61	114,5		UGent
HAM14-13A-1G-1	HAM13A/13A	29/10/2014	34°47'13.53"	137°37'2014.39"	7,18	84,0		UGent
HAM14-13B-1G-1	HAM13B/13B	29/10/2014	34°47'13.15"	137°37'2014.39"	7,18	108,5		AIST
HAM14-14A-1G-1	HAM14A/14A	29/10/2014	34°46'53.63"	137°37'32.26"	6,53	100,0		AIST
HAM14-14B-1G-1	HAM14B/14B	29/10/2014	34°46'53.83"	137°37'32.03"	6,53	96,0		UGent
HAM14-15A-1G-1	HAM15A/15A	29/10/2014	34°45'30.07"	137°31'31.09"	6,24	85,0		UGent
HAM14-15B-1G-1	HAM15B/15B	29/10/2014	34°45'30.07"	137°31'30.63"	6,24	75,5		AIST
HAM14-16A-1G-1	HAM16A/16A	29/10/2014	34°47'27.77"	137°33'13.09"	4,86	96,5		UGent
HAM14-16B-1G-1	HAM16B/16B	29/10/2014	34°46'46.67"	137°33'13.09"	4,93	66,0	No cc	UGent
HAM14-16C-1G-1	HAM16C/16C	29/10/2014	34°46'46.28"	137°33'13.09"	4,93	73,5		AIST

Lake Hamana: piston cores									
Core name	Date	Latitude (N)	Longitude (E)	Water depth (m)	Depth (m)	Length (cm)	Type	Archived at	
HAM15-01A-1G-1	15/10/2015	34°44.664'	137°34.037'	9,00	Top	60,0	Gravity	UGent	
HAM15-01A-1P-1/2	15/10/2015	34°44.664'	137°34.037'	9,00	0-2	177,0	Piston	UGent	
HAM15-01A-2P-1/2	15/10/2015	34°44.664'	137°34.037'	9,00	2-4	177,0	Piston	UGent	
HAM15-01A-3P-1/2	16/10/2015	34°44.662'	137°34.021'	9,00	4-6	172,0	Piston	UGent	
HAM15-01A-4P-1/2	16/10/2015	34°44.662'	137°34.021'	9,00	6-8	192,0	Piston	UGent	
HAM15-01B-1P-1/2	15/10/2015	34°44.664'	137°34.037'	9,00	1-3	149,0	Piston	UGent	
HAM15-01B-2P-1/2	16/10/2015	34°44.662'	137°34.021'	9,00	3-5	172,0	Piston	UGent	
HAM15-01B-3P-1/2	19/10/2015	34°44.668'	137°34.039'	9,00	5-7	191,0	Piston	UGent	
HAM15-01B-4P-1/2	19/10/2015	34°44.668'	137°34.039'	9,00	7-9	191,0	Piston	UGent	
HAM15-02A-1G-1	5/10/2015	34°45.068'	137°34.347'	10,50	Top	64,0	Gravity	UGent	
HAM15-02A-1P-1/2	5/10/2015	34°45.068'	137°34.347'	10,50	0-2	200,0	Piston	UGent	
HAM15-02A-1P-1/02bis	7/10/2015	34°45.076'	137°34.377'	10,50	0-2	148,0	Piston	UGent	
HAM15-02A-2P-1/2	7/10/2015	34°45.079'	137°34.361'	10,50	2-4	152,0	Piston	UGent	
HAM15-02A-3P-1/2	9/10/2015	34°45.055'	137°34.361'	10,50	4-6	166,0	Piston	UGent	
HAM15-02A-4P-1/2	9/10/2015	34°45.055'	137°34.361'	10,50	6-8	175,0	Piston	UGent	
HAM15-02B-1P-1/2	14/10/2015	34°45.071'	137°34.312'	10,50	1-3	176,0	Piston	UGent	
HAM15-02B-2P-1/2	14/10/2015	34°45.071'	137°34.312'	10,50	3-5	147,0	Piston	UGent	
HAM15-02B-2P-1/02bis	14/10/2015	34°45.071'	137°34.312'	10,50	3-5	166,0	Piston	UGent	
HAM15-02B-3P-1/2	14/10/2015	34°45.071'	137°34.312'	10,50	5-7	169,0	Piston	UGent	
HAM15-02B-4P-1/2	15/10/2015	34°45.068'	137°34.329'	10,50	7-9	193,0	Piston	UGent	
HAM15-03A-1G-1	21/10/2015	34°45.483'	137°34.652'	11,00	Top	64,0	Gravity	UGent	
HAM15-03A-1P-1/2	21/10/2015	34°45.483'	137°34.652'	11,00	0-2	170,0	Piston	UGent	
HAM15-03A-2P-1/2	21/10/2015	34°45.483'	137°34.652'	11,00	2-4	159,0	Piston	UGent	
HAM15-03A-3P-1/2	22/10/2015	34°45.478'	137°34.638'	11,00	4-6	172,0	Piston	UGent	
HAM15-03A-4P-1/2	22/10/2015	34°45.478'	137°34.638'	11,00	6-8	174,0	Piston	UGent	
HAM15-03B-1P-1/2	21/10/2015	34°45.502'	137°34.670'	11,00	1-3	177,0	Piston	UGent	
HAM15-03B-2P-1/2	22/10/2015	34°45.478'	137°34.638'	11,00	3-5	158,0	Piston	UGent	
HAM15-03B-3P-1/2		Not Collected			5-7				
HAM15-03B-4P-1/2		Not Collected			7-9				
HAM15-04A-1G-1	23/10/2015	34°45.911'	137°34.906'	12,00	Top	66,0	Gravity	UGent	
HAM15-04A-1P-1/2	23/10/2015	34°45.911'	137°34.906'	12,00	0-2	176,0	Piston	UGent	
HAM15-04A-2P-1/2	23/10/2015	34°45.911'	137°34.906'	12,00	2-4	163,0	Piston	UGent	
HAM15-04A-3P-1/2	23/10/2015	34°45.911'	137°34.906'	12,00	4-6	184,0	Piston	UGent	
HAM15-04A-4P-1/2	26/10/2015	34°45.916'	137°34.902'	12,00	6-8	167,0	Piston	UGent	
HAM15-04B-1P-1/2	23/10/2015	34°45.911'	137°34.906'	12,00	1-3	173,0	Piston	UGent	
HAM15-04B-2P-1/2		Not Collected			3-5				
HAM15-04B-3P-1/2	26/10/2015	34°45.916'	137°34.902'	12,00	5-7	191,0	Piston	UGent	
HAM15-04B-4P-1/2	26/10/2015	34°45.916'	137°34.902'	12,00	7-9	189,0	Piston	UGent	

ANNEX II: FUJI FIVE LAKES GRAVITY AND PISTON CORES

Lake Motosu: gravity cores								
Core name	Short name	Date	Latitude (N)	Longitude (E)	Depth (m)	Length (cm)	Remarks	Archived at
MOT14-01A-1G-1	MOT14-1A	12/10/2014	35°27'36,71"	138°34'30,45"	92,0	80,0		ULiège
MOT14-01B-1G-1	MOT14-1B	12/10/2014	35°27'36,71"	138°34'30,45"	92,0	70,0		MFRI
MOT14-02A-1G-1	MOT14-2A	12/10/2014	35°27'35,42"	138°35'03,64"	117,2	79,0		MFRI
MOT14-02B-1G-1	MOT14-2B	12/10/2014	35°27'35,08"	138°35'03,06"	117,2	79,5		ULiège
MOT14-02C-1G-1	MOT14-2C	12/10/2014	35°27'35,90"	138°35'07,69"	117,2	82,0		MFRI
MOT14-03A-1G-1	MOT14-3A	12/10/2014	35°27'35,63"	138°35'17,65"	123,2	68,0		ULiège
MOT14-03B-1G-1	MOT14-3B	12/10/2014	35°27'35,97"	138°35'17,53"	123,2	44,0	No cc	MFRI
MOT14-03C-1G-1	MOT14-3C	12/10/2014	35°27'36,29"	138°35'17,79"	123,2	50,0		MFRI
MOT14-04A-1G-1	MOT14-4A	12/10/2014	35°27'58,21"	138°34'58,78"	126,1	62,0		MFRI
MOT14-04B-1G-1	MOT14-4B	12/10/2014	35°27'58,43"	138°34'58,77"	126,1	88,5		ULiège
MOT14-04C-1G-1	MOT14-4C	12/10/2014	35°27'58,56"	138°34'59,10"	126,1	97,0		MFRI
MOT14-05A-1G-1	MOT14-5A	12/10/2014	35°28'10,75"	138°34'58,43"	126,1	81,0		MFRI
MOT14-05B-1G-1	MOT14-5B	12/10/2014	35°28'11,20"	138°34'58,19"	126,1	97,0		ULiège
MOT14-06A-1G-1	MOT14-6A	12/10/2014	35°27'51,92"	138°35'25,94"	124,6	77,0	No cc	ULiège
MOT14-06B-1G-1	MOT14-6B	12/10/2014	35°27'51,99"	138°35'25,62"	124,6	85,0		MFRI

Lake Sai: gravity cores								
Core name	Short name	Date	Latitude (N)	Longitude (E)	Depth (m)	Length (cm)	Remarks	Archived at
SAI14-01A-1G-1	SAI14-1A	15/10/2014	35,4989925	138,6683855	47,5	38,0		MFRI
SAI14-01B-1G-1	SAI14-1B	15/10/2014	35,4989829	138,6684792	47,5	87,0		MFRI
SAI14-01C-1G-1	SAI14-1C	15/10/2014	35,4990921	138,6684119	47,5	68,0	No cc	MFRI
SAI14-01D-1G-1	SAI14-1D	15/10/2014	35,4989894	138,6684012	47,5	103,0		ULiège
SAI14-02A-1G-1	SAI14-2A	15/10/2014	35,4999363	138,6760761	70,5	81,0		MFRI
SAI14-02B-1G-2	SAI14-2B	15/10/2014	35,4999911	138,6760191	70,5	90,0		ULiège
SAI14-03A-1G-1	SAI14-3A	15/10/2014	35,4951373	138,684042	73,5	77,0		MFRI
SAI14-03B-1G-1	SAI14-3B	15/10/2014	35,4951249	138,6840859	73,5	78,0		ULiège
SAI14-04A-1G-1	SAI14-4A	15/10/2014	35,4987563	138,693773	48,2	59,0	No cc	ULiège
SAI14-04B-1G-1	SAI14-4B	15/10/2014	35,4987657	138,6937199	48,2	40,0		MFRI
SAI14-05A-1G-1	SAI14-5A	15/10/2014	35,4988195	138,688525	69,8	51,0		MFRI
SAI14-05B-1G-1	SAI14-5B	15/10/2014	35,4990352	138,6883343	69,8	64,0		MFRI
SAI14-05C-1G-1	SAI14-5C	15/10/2014	35,4990977	138,6884829	69,8	72,0		ULiège
SAI14-06A-1G-1	SAI14-6A	15/10/2014	35,4988975	138,685244	50,4	64,5		ULiège
SAI14-06B-1G-1	SAI14-6B	15/10/2014	35,4988672	138,6852538	50,4	64,5		MFRI

Lake Kawaguchi: gravity cores								
Core name	Short name	Date	Latitude (N)	Longitude (E)	Depth (m)	Length (cm)	Remarks	Archived at
KAW14-01A-1G-1	KAW14-1A	18/10/2014	35°30'47.89"	138°45'05.28"	9,7			MFRI
KAW14-01B-1G-1	KAW14-1B	18/10/2014	35°30'47.93"	138°45'05.34"	9,7	92,0		ULiège
KAW14-02A-1G-1	KAW14-2A	18/10/2014	35°31'00.68"	138°45'14.64"	10,4	86,5		ULiège
KAW14-02B-1G-1	KAW14-2B	18/10/2014	35°31'00.73"	138°45'14.52"	10,4			MFRI
KAW14-03A-1G-1	KAW14-3A	18/10/2014	35°30'27.66"	138°43'46.00"	14,1	91,0		ULiège
KAW14-03B-1G-1	KAW14-3B	18/10/2014	35°30'27.69"	138°43'45.90"	14,1			MFRI
KAW14-04A-1G-1	KAW14-4A	18/10/2014	35°30'34.03"	138°44'04.14"	14,1	90,0		ULiège
KAW14-04B-1G-1	KAW14-4B	18/10/2014	35°30'33.91"	138°44'04.24"	14,1			MFRI
KAW14-05A-1G-1	KAW14-5A	18/10/2014	35°30'32.60"	138°43'44.24"	14,1			MFRI
KAW14-05B-1G-1	KAW14-5B	18/10/2014	35°30'32.69"	138°43'44.43"	14,1	92,5		ULiège
KAW14-06A-1G-1	KAW14-6A	18/10/2014	35°30'34.38"	138°46'00.78"	4,4			MFRI
KAW14-06B-1G-1	KAW14-6B	18/10/2014	35°30'34.42"	138°46'00.84"	4,4	43,0		ULiège
KAW14-07A-1G-1	KAW14-7A	18/10/2014	35°30'23.85"	138°46'10.50"	11,1			MFRI
KAW14-07B-1G-1	KAW14-7B	18/10/2014	35°30'24.09"	138°46'10.81"	11,1	90,0		ULiège

Lake Yamanaka: gravity cores

Core name	Short name	Date	Latitude (N)	Longitude (E)	Depth (m)	Length (cm)	Remarks	Archived at
YAM14-01A-1G-1	YAM14-1A	9/10/2014	35°25'37,26"	138°51'16,61"	10,4	85,0	No cc	MFRI
YAM14-02A-1G-1	YAM14-2A	9/10/2014	35°25'20,60"	138°52'18,80"	14,8	70,0	No cc	ULiège
YAM14-02B-1G-1	YAM14-2B	9/10/2014	35°25'23,34"	138°52'11,46"	14,8	79,0	No cc	MFRI
YAM14-03A-1G-1	YAM14-3A	9/10/2014	35°25'25,87"	138°51'46,64"	14,1	75,0		MFRI
YAM14-03B-1G-1	YAM14-3B	9/10/2014	35°25'27,00"	138°51'41,39"	14,1	78,0		ULiège
YAM14-04A-1G-1	YAM14-4A	9/10/2014	35°25'02,87"	138°51'51,65"	11,9	58,0		MFRI
YAM14-04B-1G-1	YAM14-4B	9/10/2014	35°25'02,87"	138°51'51,65"	11,9	64,0		ULiège
YAM14-05A-1G-1	YAM14-5A	9/10/2014	35°24'48,36"	138°52'17,32"	11,9	56,0		ULiège
YAM14-05B-1G-1	YAM14-5B	9/10/2014	35°24'50,27"	138°52'21,02"	11,9	59,0		MFRI

Lake Motosu: piston cores

Core name	Date	Latitude (N)	Longitude (E)	Water depth (m)	Depth (m)	Length (cm)	Type	Archived at
MOT15-1A-1G-1	9/11/2015	35°28.080'	138°35.047'	126,00	Top	48,0	Gravity	UGent
MOT15-1I-1G-1	17/11/2015	35°28.087'	138°35.046'	126,00	Top	44,0	Gravity	MFRI
MOT15-1A-1P-1/2	12/11/2015	35°28.084'	138°35.047'	126,00	0-2	159,0	Piston	UGent
MOT15-1A-2P-1/2*	12/11/2015	35°28.079'	138°35.042'	126,00	2-4	157,0	Piston	Split
MOT15-1B-1P-1/2	13/11/2015	35°28.083'	138°35.053'	126,00	1-3	174,0	Piston	UGent
MOT15-1B-2P-1/2	13/11/2015	35°28.082'	138°35.053'	126,00	3-5	181,0	Piston	UGent
MOT15-1C-1P-1/2	13/11/2015	35°28.083'	138°35.055'	126,00	4-6	162,0	Piston	Split
MOT15-1D-1P-1/2	16/11/2015	35°28.080'	138°35.053'	126,00	5-7	174,0	Piston	Split
MOT15-1E-1P-1/2	16/11/2015	35°28.081'	138°35.053'	126,00	2-4	174,0	Piston	UGent
MOT15-1F-1P-1/2	16/11/2015	35°28.084'	138°35.037'	126,00	0-2	147,0	Piston	MFRI
MOT15-1G-1P-1/2	17/11/2015	35°28.085'	138°35.038'	126,00	2-4	184,0	Piston	MFRI
MOT15-1H-1P-1/2	17/11/2015	35°28.085'	138°35.041'	126,00	3-5	180,0	Piston	MFRI
MOT15-1J-1P-1/2	17/11/2015	35°28.087'	138°35.039'	126,00	1-3	186,0	Piston	MFRI
MOT15-2A-1G-1	18/11/2015	35°27.690'	138°35.156'	124,00	Top	27,0	Gravity	UGent
MOT15-2B-1G-1	18/11/2015	35°27.690'	138°35.156'	124,00	Top	34,0	Gravity	MFRI
MOT15-2A-1P-1/2	19/11/2015	35°27.683'	138°35.154'	124,00	0-2	185,0	Piston	UGent
MOT15-2B-1P-1/2	19/11/2015	35°27.684'	138°35.154'	124,00	2-4	155,0	Piston	Split
MOT15-2C-1P-1/2	19/11/2015	35°27.683'	138°35.156'	124,00	1-3	187,0	Piston	UGent
MOT15-2D-1P-1/2	19/11/2015	35°27.684'	138°35.155'	124,00	0-2	186,0	Piston	MFRI
MOT15-2E-1P-1/2	20/11/2015	35°27.686'	138°35.159'	124,00	1-3	188,0	Piston	MFRI

Lake Sai: piston cores

Core name	Date	Latitude (N)	Longitude (E)	Water depth (m)	Depth (m)	Length (cm)	Type	Archived at
SAI15-1A-1G-1	24/11/2015	35°29.690'	138°41.039'	73,00	Top		Gravity	UGent
SAI15-1B-1G-1	24/11/2015	35°29.689'	138°41.039'	73,00	Top		Gravity	MFRI
SAI15-1A-1P-1/2	24/11/2015	35°29.690'	138°41.041'	73,00	0-2	176,0	Piston	UGent
SAI15-1B-1P-1/2	24/11/2015	35°29.692°	138°41.043'	73,00	1-3	161,0	Piston	UGent
SAI15-1C-1P-1/2	24/11/2015	35°29.692°	138°41.040'	73,00	0-2	190,0	Piston	MFRI
SAI15-1D-1P-1/2	26/11/2015	35°29.690°	138°41.038'	73,00	1-3	190,0	Piston	MFRI
SAI15-2A-1G-1	25/11/2015	35°29.980'	138°41.362'	65,00	Top		Gravity	UGent
SAI15-2B-1G-1	25/11/2015	35°29.980'	138°41.361'	65,00	Top		Gravity	MFRI
SAI15-2A-1P-1/2*	25/11/2015	35°29.988'	138°41.362'	65,00	0-2	188,0	Piston	UGent
SAI15-2B-1P-1/2	25/11/2015	35°29.980'	138°41.359'	65,00	1-3	178,0	Piston	UGent
SAI15-2C-1P-1/2	25/11/2015	35°29.982'	138°41.361'	65,00	0-2	173,0	Piston	MFRI
SAI15-2D-1P-1/2	25/11/2015	35°29.981'	138°41.360'	65,00	1-3	182,0	Piston	MFRI
SAI15-2E-1P-1/2	26/11/2015	35°29.981'	138°41.361'	65,00	0-2	155,0	Piston	MFRI

Lake Kawaguchi: piston cores

Core name	Date	Latitude (N)	Longitude (E)	Water depth (m)	Depth (m)	Length (cm)	Type	Archived at
KAW15-1A-1G-1	4/11/2015	35°30.784'	138°44.366'	12,00	Top	50,0	Gravity	UGent
KAW15-1B-1G-1	4/11/2015	35°30.784'	138°44.366'	12,00	Top	51,0	Gravity	MFRI
KAW15-1A-1P-1/2	4/11/2015	35°30.784'	138°44.366'	12,00	0-2	166,0	Piston	UGent
KAW15-1A-2P-1/2	4/11/2015	35°30.784'	138°44.366'	12,00	2-4	157,0	Piston	Split
KAW15-1B-1P-1/2	4/11/2015	35°30.784'	138°44.366'	12,00	1-3	168,0	Piston	Split
KAW15-1B-2P-1/2	4/11/2015	35°30.784'	138°44.366'	12,00	3-5	130,0	Piston	Split
KAW15-1C-1P-1/2	4/11/2015	35°30.784'	138°44.366'	12,00	0-2	130,0	Piston	MFRI
KAW15-2A-1G-1	5/11/2015	35°30.842'	138°44.974'	10,00	Top	50,0	Gravity	MFRI
KAW15-2B-1G-1	5/11/2015	35°30.842'	138°44.974'	10,00	Top	52,0	Gravity	UGent
KAW15-2A-1P-1/2	5/11/2015	35°30.842'	138°44.974'	10,00	0-2	172,0	Piston	UGent
KAW15-2A-2P-1/2	5/11/2015	35°30.842'	138°44.974'	10,00	2-4	172,0	Piston	UGent
KAW15-2A-3P-1/2	5/11/2015	35°30.842'	138°44.974'	10,00	4-6	154,0	Piston	UGent
KAW15-2B-1P-1/2	5/11/2015	35°30.842'	138°44.974'	10,00	1-3	169,0	Piston	UGent
KAW15-2B-2P-1/2	6/11/2015	35°30.842'	138°44.974'	10,00	3-5	169,0	Piston	Split
KAW15-2C-1P-1/2	6/11/2015	35°30.842'	138°44.974'	10,00	0-2	174,0	Piston	MFRI
KAW15-2C-2P-1/2	6/11/2015	35°30.842'	138°44.974'	10,00	5-7	158,0	Piston	Split
KAW15-2D-1P-1/2	6/11/2015	35°30.842'	138°44.974'	10,00	6-8	169,0	Piston	Split
KAW15-2E-1P-1/2	6/11/2015	35°30.842'	138°44.974'	10,00	2-4	176,0	Piston	MFRI
KAW15-2E-2P-1/2	6/11/2015	35°30.842'	138°44.974'	10,00	4-6	162,0	Piston	MFRI
KAW15-2F-1P-1/2	6/11/2015	35°30.842'	138°44.974'	10,00	1-3	176,0	Piston	MFRI

ANNEX III: FULL CORE ANALYSES/FULL CORE SCANS

Lake Hamana: full core analyses/scans					
Core	Visual description	MSCL	X-ray radiography	CT	XRF
HAM14-01	gravity/short	UGent; continuous; 2mm	-	Med CT UZGent; continuous	-
HAM14-02	gravity/short	UGent; continuous; 2mm	-	Med CT UZGent; continuous	-
HAM14-03	gravity/short	UGent; continuous; 2mm	-	Med CT UZGent; continuous	-
HAM14-04	gravity/short	UGent; continuous; 2mm	-	Med CT UZGent; continuous	-
HAM14-05	gravity/short	UGent; continuous; 2mm	-	Med CT UZGent; continuous	-
HAM14-06	gravity/short	UGent; continuous; 2mm	-	Med CT UZGent; continuous	-
HAM14-07	gravity/short	UGent; continuous; 2mm	-	Med CT UZGent; continuous	-
HAM14-08	gravity/short	UGent; continuous; 2mm	-	Med CT UZGent; continuous	-
HAM14-09	gravity/short	UGent; continuous; 2mm	-	Med CT UZGent; continuous	-
HAM14-10	gravity/short	UGent; continuous; 2mm	-	Med CT UZGent; continuous	-
HAM14-11	gravity/short	UGent; continuous; 2mm	-	Med CT UZGent; continuous	-
HAM14-12	gravity/short	UGent; continuous; 2mm	-	Med CT UZGent; continuous	-
HAM14-13	gravity/short	UGent; continuous; 2mm	-	Med CT UZGent; continuous	-
HAM14-14	gravity/short	UGent; continuous; 2mm	-	Med CT UZGent; continuous	-
HAM15-01	piston/long	UGent; continuous; 2mm	-	Med CT UZGent; continuous	MARUM; Avaatech; continuous; 10 mm
HAM15-02	piston/long	UGent; continuous; 2mm	-	Med CT UZGent; continuous	MARUM; Avaatech; continuous; 10 mm
HAM15-03	piston/long	UGent; continuous; 2mm	-	Med CT UZGent; continuous	-
HAM15-04	piston/long	UGent; continuous; 2mm	-	Med CT UZGent; continuous	-

Lake Motosu: full core analyses/scans					
Core	Visual description	MSCL	X-ray radiography	CT	XRF
MOT14-01	gravity/short	ULiège	ULiège	-	-
MOT14-02	gravity/short	ULiège	ULiège	-	-
MOT14-03	gravity/short	ULiège	ULiège	-	-
MOT14-04	gravity/short	ULiège	ULiège	-	USavoie; Avaatech; continuous; 2 mm
MOT14-05	gravity/short	ULiège	ULiège	-	USavoie; Avaatech; continuous; 2 mm
MOT14-06	gravity/short	ULiège	ULiège	-	-
MOT15-01	piston/long	ULiège	ULiège	-	MARUM; Avaatech; continuous; 2 mm
MOT15-02	piston/long	ULiège	ULiège	-	MARUM; Avaatech; continuous; 2 mm

Lake Sai: full core analyses/scans					
Core	Visual description	MSCL	X-ray radiography	CT	XRF
SAI14-01	gravity/short	ULiège	ULiège	-	-
SAI14-02	gravity/short	ULiège	ULiège	-	-
SAI14-03	gravity/short	ULiège	ULiège	-	USavoie; Avaatech; continuous; 2 mm
SAI14-04	gravity/short	ULiège	ULiège	-	-
SAI14-05	gravity/short	ULiège	ULiège	-	-
SAI14-06	gravity/short	ULiège	ULiège	-	USavoie; Avaatech; continuous; 2 mm
SAI15-01	piston/long	ULiège	ULiège	-	USavoie; Avaatech; continuous; 2 mm
SAI15-02	piston/long	ULiège	ULiège	-	USavoie; Avaatech; continuous; 2 mm

Lake Yamanaka: full core analyses/scans					
Core	Visual description	MSCL	X-ray radiography	CT	XRF
YAM14-01	gravity/short	UGent; continuous; 2mm	Ullège	-	USavoie; Avaatech; continuous; 2 mm
YAM14-02	gravity/short	UGent; continuous; 2mm	Ullège	-	USavoie; Avaatech; continuous; 2 mm
YAM14-03	gravity/short	UGent; continuous; 2mm	Ullège	-	USavoie; Avaatech; continuous; 2 mm
YAM14-04	gravity/short	UGent; continuous; 2mm	Ullège	-	USavoie; Avaatech; continuous; 2 mm
YAM14-05	gravity/short	UGent; continuous; 2mm	Ullège	-	USavoie; Avaatech; continuous; 2 mm

Lake Kawaguchi: full core analyses/scans					
Core	Visual description	MSCL	X-ray radiography	CT	XRF
KAW14-01	gravity/short	UGent; continuous; 2mm	Ullège	-	USavoie; Avaatech; continuous; 2 mm
KAW14-02	gravity/short	UGent; continuous; 2mm	Ullège	-	USavoie; Avaatech; continuous; 2 mm
KAW14-03	gravity/short	UGent; continuous; 2mm	Ullège	-	USavoie; Avaatech; continuous; 2 mm
KAW14-04	gravity/short	UGent; continuous; 2mm	Ullège	-	USavoie; Avaatech; continuous; 2 mm
KAW14-05	gravity/short	UGent; continuous; 2mm	Ullège	-	USavoie; Avaatech; continuous; 2 mm
KAW14-06	gravity/short	UGent; continuous; 2mm	Ullège	-	USavoie; Avaatech; continuous; 2 mm
KAW14-07	gravity/short	UGent; continuous; 2mm	Ullège	-	USavoie; Avaatech; continuous; 2 mm
KAW15-01	piston/long	UGent; continuous; 2mm	Ullège	-	USavoie; Avaatech; continuous; 2 mm
KAW15-02	piston/long	UGent; continuous; 2mm	Ullège	-	USavoie; Avaatech; continuous; 2 mm

Shirasuka lowlands: full core analyses/scans					
Core	Visual description	MSCL	X-ray radiography	CT	XRF
JSH1/Full	Vibrocore	-	-	-	-
JSH1b/Full	Vibrocore	-	-	-	-
JSH1/Overlap	Vibrocore	-	-	-	-
JSH2/Full	Vibrocore	-	-	-	-
JSH3/Full	Vibrocore	-	-	Med CT UZGent; selected sections	-
JSH3/Overlap	Vibrocore	-	-	Med CT UZGent; selected sections	-
	surface samples	-	-	-	-

Sagara: full core analyses/scans					
Core	Visual description	MISCL	X-ray radiography	CT	XRF
SGL-1	Vibrocore	G58	UGent; continuous	Med CT UZGent; selected sections	-
SGL-2	Vibrocore	G58	UGent; continuous	Med CT UZGent; selected sections	-
SGL-3	Vibrocore	G58	UGent; continuous	Med CT UZGent; continuous	-
SGL-4	Vibrocore	G58	UGent; continuous	Med CT UZGent; continuous	-
SGL-5	Vibrocore	G58	UGent; continuous	Med CT UZGent; continuous	-
SGL-6	Vibrocore	G58	UGent; continuous	Med CT UZGent; continuous	-
SGL-7	Vibrocore	G58	UGent; continuous	Med CT UZGent; continuous	-
SGL-8	Vibrocore	G58	UGent; continuous	Med CT UZGent; continuous	-
SGL-9	Vibrocore	G58	UGent; continuous	Med CT UZGent; continuous	-
SGL-10	Vibrocore	G58	UGent; continuous	Med CT UZGent; continuous	-
SGL-11	Vibrocore	G58	UGent; continuous	Med CT UZGent; continuous	-
SGL-12	Vibrocore	G58	UGent; continuous	Med CT UZGent; continuous	-
SGL-13	Vibrocore	G58	UGent; continuous	Med CT UZGent; continuous	-
SGL-14	Vibrocore	G58	UGent; continuous	Med CT UZGent; continuous	-
SGL-15	Vibrocore	G58	UGent; continuous	Med CT UZGent; continuous	-
SGL-17	Vibrocore	G58	UGent; continuous	Med CT UZGent; continuous	-
SGL-18	Vibrocore	G58	UGent; continuous	Med CT UZGent; continuous	-
SGL-19	Vibrocore	G58	UGent; continuous	Med CT UZGent; continuous	-
SGL-20	Vibrocore	G58	UGent; continuous	Med CT UZGent; continuous	-
SGL-21	Vibrocore	G58	UGent; continuous	Med CT UZGent; continuous	-
SGL-22	Vibrocore	G58	UGent; continuous	Med CT UZGent; continuous	-
SGL-23	Vibrocore	G58	UGent; continuous	Med CT UZGent; continuous	-
SGL-24	Vibrocore	G58	UGent; continuous	Med CT UZGent; continuous	-
SGL-25	Vibrocore	G58	UGent; continuous	Med CT UZGent; continuous	-
SGL-26	Vibrocore	G58	UGent; continuous	Med CT UZGent; continuous	UCologue; Itrax; selected intervals; 2 mm
SGL-27	Vibrocore	G58	UGent; continuous	Med CT UZGent; continuous	UCologue; Itrax; selected intervals; 2 mm
SGL-28	Vibrocore	G58	UGent; continuous	Med CT UZGent; continuous	-
SGB-1	Vibrocore	G58	UGent; continuous	Med CT UZGent; continuous	-
SGB-2	Vibrocore	G58	UGent; continuous	Med CT UZGent; continuous	-
SGB-3	Vibrocore	G58	UGent; continuous	Med CT UZGent; continuous	-
SGB-4	Vibrocore	G58	-	AIST	-
SGB-4'	Vibrocore	G58	-	AIST	-

ANNEX IV: SEDIMENTOLOGICAL-GEOCHEMICAL ANALYSES

Lake Hamana: sedimentological-geochemical analyses									
Core	Smear slides	Grain size	LO (105/550/950)	C/N	XRF	XRD	SEM	EMP	
HAMI14-01	gravity/short	-	-	-	-	-	-	-	-
HAMI14-02	gravity/short	-	-	-	-	-	-	-	-
HAMI14-03	gravity/short	-	-	-	-	-	-	-	-
HAMI14-04	gravity/short	-	-	-	-	-	-	-	-
HAMI14-05	gravity/short	-	-	-	-	-	-	-	-
HAMI14-06	gravity/short	-	-	-	-	-	-	-	-
HAMI14-07	gravity/short	-	-	-	-	-	-	-	-
HAMI14-08	gravity/short	-	-	-	-	-	-	-	-
HAMI14-09	gravity/short	-	-	-	-	-	-	-	-
HAMI14-10	gravity/short	-	-	-	-	-	-	-	-
HAMI14-11	gravity/short	-	-	-	-	-	-	-	-
HAMI14-12	gravity/short	-	-	-	-	-	-	-	-
HAMI14-13	gravity/short	-	-	-	-	-	-	-	-
HAMI14-14	gravity/short	-	-	-	-	-	-	-	-
HAMI15-01	piston/long	UGent; continuous; 50-100 mm and 10-20 mm	-	-	-	-	-	-	-
HAMI15-02	piston/long	-	-	-	-	-	-	-	-
HAMI15-03	piston/long	-	-	-	-	-	-	-	-
HAMI15-04	piston/long	-	-	-	-	-	-	-	-

Lake Motosu: sedimentological-geochemical analyses									
Core	Smear slides	Grain size	LO (105/550/950)	C/N	XRF	XRD	SEM	EMP	
MOT14-01	gravity/short	-	Uliège; continuous; 10 mm	-	Uliège; 8 samples	-	-	-	-
MOT14-02	gravity/short	-	Uliège; continuous; 5 mm	-	-	-	-	-	-
MOT14-03	gravity/short	-	-	-	-	-	-	-	-
MOT14-04	gravity/short	-	-	Uliège; 45 samples	-	GSB; 6 samples + Uliège; 7 samples	Uliège/GSB; 35 samples	-	-
MOT14-05	gravity/short	Uliège; continuous; 5 mm	Uliège; continuous; 10 mm	-	-	-	-	-	-
MOT14-06	gravity/short	-	-	-	-	-	-	-	-
MOT15-01	piston/long	-	-	-	-	-	-	-	UParisVI; 1 sample
MOT15-02	piston/long	-	-	-	-	-	-	-	-

Lake Sai: sedimentological-geochemical analyses									
Core	Smear slides	Grain size	LO (105/550/950)	C/N	XRF	XRD	SEM	EMP	
SAI14-01	gravity/short	Uliège; selected samples	Uliège; continuous; 10 mm	-	Uliège; selected samples	-	Uliège/GSB; selected samples	-	-
SAI14-02	gravity/short	-	Uliège; continuous; 10 mm	-	Uliège; selected samples	-	-	-	-
SAI14-03	gravity/short	Uliège; continuous; 5 mm	Uliège; continuous; 10 mm	-	Uliège; selected samples	-	Uliège/GSB; selected samples	-	-
SAI14-04	gravity/short	-	Uliège; continuous; 10 mm	-	Uliège; selected samples	GSB; 17 samples	-	-	-
SAI14-05	gravity/short	Uliège; continuous; 5 mm	Uliège; continuous; 10 mm	-	Uliège; selected samples	-	-	-	-
SAI14-06	gravity/short	-	Uliège; continuous; 10 mm	-	Uliège; selected samples	-	-	-	-
SAI15-01	piston/long	Uliège; continuous; between 5 and 20 mm	Uliège; continuous; 10 mm	-	Uliège; selected samples	-	-	-	-
SAI15-02	piston/long	-	Uliège; continuous; 10 mm	-	Uliège; selected samples	-	-	-	-

Lake Yamanaka: sedimentological-geochemical analyses									
Core	Smear slides	Grain size	LOI (105/550/950)	C/N	XRF	XRD	SEM	EMP	
YAMI14-01	gravity/short	Ulège, continuous; 5 mm	Ulège, continuous; 10 mm						
YAMI14-02	gravity/short	Ulège, continuous; 5 mm	Ulège, continuous; 10 mm		Ulège; 10 samples				
YAMI14-03	gravity/short	Ulège, continuous; 5 mm	Ulège, continuous; 10 mm	Ulège; 43 samples					
YAMI14-04	gravity/short	Ulège, continuous; 5 mm	Ulège, continuous; 10 mm						GSB; 46 samples + Ulège; 1 samples
YAMI14-05	gravity/short	Ulège, continuous; 5 mm	Ulège, continuous; 10 mm						
Lake Kawaguchi: sedimentological-geochemical analyses									
Core	Smear slides	Grain size	LOI (105/550/950)	C/N	XRF	XRD	SEM	EMP	
KAW14-01	gravity/short				Ulège; selected samples				
KAW14-02	gravity/short				Ulège; selected samples				
KAW14-03	gravity/short				Ulège; selected samples				
KAW14-04	gravity/short	Ulège, continuous; 5 mm			Ulège; selected samples				Ulège/GSB; 4 samples
KAW14-05	gravity/short				Ulège; selected samples				
KAW14-06	gravity/short				Ulège; selected samples				
KAW14-07	gravity/short				Ulège; selected samples				
KAW15-01	piston/long				Ulège; selected samples				
KAW15-02	piston/long				Ulège; selected samples				
Shirasuka lowlands: sedimentological-geochemical analyses									
Core	Smear slides	Grain size	LOI (105/550/950)	C/N	XRF	XRD	SEM	EMP	
JSH1/Full									
JSH1b/Full		UDurham; sandy intervals							
JSH1/Overlap									
JSH2/Full									
JSH3/Full		UDurham; sandy intervals							
JSH3/Overlap		UDurham; sandy intervals							
	surface samples	UDurham; bulk							UCologne

Sagara: sedimentological-geochemical analyses										
Core	Smear slides	Grain size	LOI (105/550/950)	C/N	XRF	XRD	SEM	EMP		
SGL-1	Vibrocore	-	-	-	-	-	-	-	-	-
SGL-2	Vibrocore	-	-	-	-	-	-	-	-	-
SGL-3	Vibrocore	-	-	-	-	-	-	-	-	-
SGL-4	Vibrocore	-	-	-	-	-	-	-	-	-
SGL-5	Vibrocore	-	-	-	-	-	-	-	-	-
SGL-6	Vibrocore	GSB, selected facies	-	-	-	-	-	-	-	-
SGL-7	Vibrocore	-	-	-	-	-	-	-	-	-
SGL-8	Vibrocore	-	-	-	-	-	-	-	-	-
SGL-9	Vibrocore	GSB, selected facies	-	-	-	-	-	-	-	-
SGL-10	Vibrocore	GSB, selected facies	-	-	-	-	-	-	-	-
SGL-11	Vibrocore	-	-	-	-	-	-	-	-	-
SGL-12	Vibrocore	GSB, selected facies	-	-	-	-	-	-	-	-
SGL-13	Vibrocore	-	-	-	-	-	-	-	-	-
SGL-14	Vibrocore	-	-	-	-	-	-	-	-	-
SGL-15	Vibrocore	-	-	-	-	-	-	-	-	-
SGL-17	Vibrocore	GSB, selected facies	-	-	-	-	-	-	-	-
SGL-18	Vibrocore	-	-	-	-	-	-	-	-	-
SGL-19	Vibrocore	-	-	-	-	-	-	-	-	-
SGL-20	Vibrocore	GSB, selected facies	-	-	-	-	-	-	-	-
SGL-21	Vibrocore	-	-	-	-	-	-	-	-	-
SGL-22	Vibrocore	GSB, selected facies	-	-	-	-	-	-	-	-
SGL-23	Vibrocore	GSB, selected facies	-	-	-	-	-	-	-	-
SGL-24	Vibrocore	GSB, selected facies	-	-	-	-	-	-	-	-
SGL-25	Vibrocore	-	-	-	-	-	-	-	-	-
SGL-26	Vibrocore	-	-	-	-	-	-	-	-	-
SGL-27	Vibrocore	-	-	-	-	-	-	-	-	-
SGL-28	Vibrocore	-	-	-	-	-	-	-	-	-
SGB-1	Vibrocore	GSB, selected facies	-	-	-	-	-	-	-	-
SGB-2	Vibrocore	-	-	-	-	-	-	-	-	-
SGB-3	Vibrocore	-	-	-	-	-	-	-	-	-
SGB-4	Vibrocore	-	-	-	-	-	-	-	-	-
SGB-4'	Vibrocore	-	-	-	-	-	-	-	-	-

ANNEX V: GEOCHRONOLOGICAL AND PALEO-ECOLOGICAL ANALYSES

Lake Hamana: geochronological analyses					
Core	²¹⁰ Pb/ ¹³⁷ Cs	¹⁴ C	Tephro	OSL	
HAM14-01	gravity/short	-	-	-	
HAM14-02	gravity/short	-	-	-	
HAM14-03	gravity/short	-	-	-	
HAM14-04	gravity/short	-	-	-	
HAM14-05	gravity/short	-	-	-	
HAM14-06	gravity/short	-	-	-	
HAM14-07	gravity/short	-	-	-	
HAM14-08	gravity/short	-	-	-	
HAM14-09	gravity/short	Ubordeaux	-	-	
HAM14-10	gravity/short	ETH; 2 samples	-	-	
HAM14-11	gravity/short	-	-	-	
HAM14-12	gravity/short	-	-	-	
HAM14-13	gravity/short	-	-	-	
HAM14-14	gravity/short	-	-	-	
HAM15-01	piston/long	UTokyo; 15 samples	-	-	
HAM15-02	piston/long	UTokyo; 7 samples	-	-	
HAM15-03	piston/long	UTokyo; 8 samples	-	-	Paleo Labo; 2 samples
HAM15-04	piston/long	UTokyo; 4 samples	-	-	

Lake Motosu: geochronological analyses					
Core	²¹⁰ Pb/ ¹³⁷ Cs	¹⁴ C	Tephro	OSL	
MOT14-01	gravity/short	UTokyo; 1 sample	-	-	
MOT14-02	gravity/short	-	-	-	
MOT14-03	gravity/short	-	-	-	
MOT14-04	gravity/short	-	-	-	
MOT14-05	gravity/short	Ubordeaux	-	-	
MOT14-06	gravity/short	-	-	-	
MOT15-01	piston/long	UTokyo; 2 samples	-	-	
MOT15-02	piston/long	UTokyo; 1 sample	-	-	

Lake Hamana: paleo-ecological analyses					
Core	Diatoms	Pollen/Palynomorphs			
HAM14-01	gravity/short	-	-	-	
HAM14-02	gravity/short	-	-	-	
HAM14-03	gravity/short	-	-	-	
HAM14-04	gravity/short	-	-	-	
HAM14-05	gravity/short	-	-	-	
HAM14-06	gravity/short	-	-	-	
HAM14-07	gravity/short	-	-	-	
HAM14-08	gravity/short	-	-	-	
HAM14-09	gravity/short	-	-	-	
HAM14-10	gravity/short	-	-	-	
HAM14-11	gravity/short	-	-	-	
HAM14-12	gravity/short	-	-	-	
HAM14-13	gravity/short	-	-	-	
HAM14-14	gravity/short	-	-	-	
HAM15-01	piston/long	-	-	-	
HAM15-02	piston/long	-	-	-	
HAM15-03	piston/long	-	-	-	
HAM15-04	piston/long	-	-	-	

Lake Motosu: paleo-ecological analyses					
Core	Diatoms	Pollen/Palynomorphs			
MOT14-01	gravity/short	-	-	-	
MOT14-02	gravity/short	-	-	-	
MOT14-03	gravity/short	-	-	-	
MOT14-04	gravity/short	-	-	-	
MOT14-05	gravity/short	-	-	-	
MOT14-06	gravity/short	-	-	-	
MOT15-01	piston/long	-	-	-	
MOT15-02	piston/long	-	-	-	

Lake Sai: geochronological analyses					
Core	²¹⁰ Pb/ ¹³⁷ Cs	¹⁴ C	Tephro	OSL	
SAI14-01	gravity/short	-	-	-	
SAI14-02	gravity/short	-	-	-	
SAI14-03	gravity/short	Ubordeaux	-	-	
SAI14-04	gravity/short	-	-	-	
SAI14-05	gravity/short	-	-	-	
SAI14-06	gravity/short	-	-	-	
SAI15-01	piston/long	UTokyo; 4 samples	-	-	
SAI15-02	piston/long	-	-	-	

Lake Sai: paleo-ecological analyses					
Core	Diatoms	Pollen/Palynomorphs			
SAI14-01	gravity/short	-	-	-	
SAI14-02	gravity/short	-	-	-	
SAI14-03	gravity/short	-	-	-	
SAI14-04	gravity/short	-	-	-	
SAI14-05	gravity/short	-	-	-	
SAI14-06	gravity/short	-	-	-	
SAI15-01	piston/long	-	-	-	
SAI15-02	piston/long	-	-	-	

Lake Yamanaka: paleo-ecological analyses			
Core	Core	Diatoms	Pollen/Palynomorphs
YAM14-01	gravity/short	-	-
YAM14-02	gravity/short	-	-
YAM14-03	gravity/short	-	-
YAM14-04	gravity/short	-	-
YAM14-05	gravity/short	-	-

Lake Kawaguchi: paleo-ecological analyses			
Core	Core	Diatoms	Pollen/Palynomorphs
KAW14-01	gravity/short	-	-
KAW14-02	gravity/short	-	-
KAW14-03	gravity/short	-	-
KAW14-04	gravity/short	-	-
KAW14-05	gravity/short	-	-
KAW14-06	gravity/short	-	-
KAW14-07	gravity/short	-	-
KAW15-01	piston/long	-	-
KAW15-02	piston/long	-	-

Shirasuka lowlands: paleo-ecological analyses			
Core	Core	Diatoms	Pollen/Palynomorphs
JSH1/Full	Vibrocore	-	-
JSH1b/Full	Vibrocore	-	-
JSH1/Overlap	Vibrocore	-	-
JSH2/Full	Vibrocore	-	-
JSH3/Full	Vibrocore	-	-
JSH3/Overlap	Vibrocore	GSB; sandy intervals; 2-5 cm	GSB; sandy intervals
surface samples			
		GSB; sandy intervals; 2-5 cm	GSB; sandy intervals
		-	GSB

Lake Yamanaka: geochronological analyses				
Core	$^{210}\text{Pb}/^{137}\text{Cs}$	^{14}C	Tephro	OSL
YAM14-01	gravity/short	-	-	-
YAM14-02	gravity/short	UBordeaux	-	-
YAM14-03	gravity/short	-	-	-
YAM14-04	gravity/short	-	-	-
YAM14-05	gravity/short	-	-	-

Lake Kawaguchi: geochronological analyses				
Core	$^{210}\text{Pb}/^{137}\text{Cs}$	^{14}C	Tephro	OSL
KAW14-01	gravity/short	-	-	-
KAW14-02	gravity/short	-	-	-
KAW14-03	gravity/short	UBordeaux	-	-
KAW14-04	gravity/short	-	-	-
KAW14-05	gravity/short	-	-	-
KAW14-06	gravity/short	-	-	-
KAW14-07	gravity/short	-	-	-
KAW15-01	piston/long	-	-	-
KAW15-02	piston/long	-	-	-

Shirasuka lowlands: geochronological analyses				
Core	$^{210}\text{Pb}/^{137}\text{Cs}$	^{14}C	Tephro	OSL
JSH1/Full	Vibrocore	-	-	-
JSH1b/Full	Vibrocore	UTokyo; 6 samples	-	UCologne; sandy intervals
JSH1/Overlap	Vibrocore	UTokyo; 2 samples	-	UCologne; sandy intervals
JSH2/Full	Vibrocore	-	-	-
JSH3/Full	Vibrocore	UTokyo; 10 samples	-	-
JSH3/Overlap	Vibrocore	UTokyo; 10 samples	-	-
surface samples				
		-	-	-

Sagara: paleo-ecological analyses			
Core	Diatoms	Pollen/Palynomorphs	
SGL-1	Vibrocare	-	-
SGL-2	Vibrocare	-	-
SGL-3	Vibrocare	-	-
SGL-4	Vibrocare	-	-
SGL-5	Vibrocare	-	-
SGL-6	Vibrocare	-	-
SGL-7	Vibrocare	-	-
SGL-8	Vibrocare	-	-
SGL-9	Vibrocare	-	-
SGL-10	Vibrocare	-	-
SGL-11	Vibrocare	-	-
SGL-12	Vibrocare	-	-
SGL-13	Vibrocare	-	-
SGL-14	Vibrocare	-	-
SGL-15	Vibrocare	-	-
SGL-17	Vibrocare	-	-
SGL-18	Vibrocare	-	-
SGL-19	Vibrocare	-	-
SGL-20	Vibrocare	-	-
SGL-21	Vibrocare	-	-
SGL-22	Vibrocare	-	-
SGL-23	Vibrocare	-	-
SGL-24	Vibrocare	-	-
SGL-25	Vibrocare	-	-
SGL-26	Vibrocare	-	-
SGL-27	Vibrocare	-	-
SGL-28	Vibrocare	-	-
SGB-1	Vibrocare	-	-
SGB-2	Vibrocare	-	-
SGB-3	Vibrocare	-	-
SGB-4	Vibrocare	-	-
SGB-4'	Vibrocare	-	-

Sagara: geochronological analyses				
Core	²¹⁰ Pb/ ¹³⁷ Cs	¹⁴ C	Tephro	OSL
SGL-1	Vibrocare	-	-	-
SGL-2	Vibrocare	UTokyo; 2 samples	-	-
SGL-3	Vibrocare	-	-	-
SGL-4	Vibrocare	-	-	-
SGL-5	Vibrocare	-	-	-
SGL-6	Vibrocare	-	-	-
SGL-7	Vibrocare	-	-	-
SGL-8	Vibrocare	-	-	-
SGL-9	Vibrocare	-	-	-
SGL-10	Vibrocare	-	-	-
SGL-11	Vibrocare	-	-	-
SGL-12	Vibrocare	-	-	-
SGL-13	Vibrocare	-	-	-
SGL-14	Vibrocare	-	-	-
SGL-15	Vibrocare	-	-	-
SGL-17	Vibrocare	-	-	-
SGL-18	Vibrocare	RIC; 1 sample	-	-
SGL-19	Vibrocare	-	-	-
SGL-20	Vibrocare	UTokyo; 2 samples	-	-
SGL-21	Vibrocare	-	-	-
SGL-22	Vibrocare	-	-	-
SGL-23	Vibrocare	-	-	-
SGL-24	Vibrocare	-	-	-
SGL-25	Vibrocare	-	-	-
SGL-26	Vibrocare	UTokyo; 1 samples + RIC; 1 sample	-	-
SGL-27	Vibrocare	UTokyo; 4 samples + RIC; 1 sample	-	-
SGL-28	Vibrocare	-	-	-
SGB-1	Vibrocare	UTokyo; 2 samples + Paleo Labo; 6 samples + RIC; 1 sample	-	-
SGB-2	Vibrocare	Paleo Labo; 3 samples	-	-
SGB-3	Vibrocare	Paleo Labo; 5 samples	-	-
SGB-4	Vibrocare	-	-	-
SGB-4'	Vibrocare	-	-	-